Doctorate Program in Molecular Oncology and Endocrinology
Doctorate School in Molecular Medicine

XXV cycle - 2009–2012
Coordinator: Prof. Massimo Santoro

"Role of *PATZ1* as a potential tumor suppressor gene in thyroid cancer"

Teresa Valentino

Università degli Studi di Napoli Federico II
Dipartimento di Medicina Molecolare e Biotecnologie Mediche

Administrative Location

Università degli Studi di Napoli Federico II
Dipartimento di Medicina Molecolare e Biotecnologie Mediche

Partner Institutions

Italian Institutions
Università degli Studi di Napoli "Federico II", Naples, Italy
Istituto di Endocrinologia ed Oncologia Sperimentale "G. Salvatore", CNR, Naples, Italy
Seconda Università di Napoli, Naples, Italy
Università degli Studi di Napoli "Parthenope", Naples, Italy
Università degli Studi del Sannio, Benevento, Italy
Università degli Studi di Genova, Genova, Italy
Università degli Studi di Padova, Padova, Italy
Università degli Studi "Magna Graecia", Catanzaro, Italy
Università degli Studi di Udine, Udine, Italy

Foreign Institutions
Université Libre de Bruxelles, Bruxelles, Belgium
Universidade Federal de Sao Paulo, Brazil
University of Turku, Turku, Finland
Université Paris Sud XI, Paris, France
University of Madras, Chennai, India
University Pavol Jozef Šafàrik, Kosice, Slovakia
Universidad Autonoma de Madrid, Centro de Investigaciones Oncologicas (CNIO), Spain
Johns Hopkins School of Medicine, Baltimore, MD, USA
Johns Hopkins Krieger School of Arts and Sciences, Baltimore, MD, USA
National Institutes of Health, Bethesda, MD, USA
Ohio State University, Columbus, OH, USA
Albert Einstein College of Medicine of Yeshiwa University, N.Y., USA

Supporting Institutions
Dipartimento di Biologia e Patologia Cellulare e Molecolare "L. Califano", Università degli Studi di Napoli "Federico II", Naples, Italy
Istituto di Endocrinologia ed Oncologia Sperimentale "G. Salvatore", CNR, Naples, Italy
Istituto Superiore di Oncologia, Italy

Italian Faculty

Salvatore Maria Aloj
Francesco Saverio Ambesi
Impiombato
Francesco Beguinot
Maria Teresa Berlingieri
Bernadette Biondi
Francesca Carlomagno
Gabriella Castoria
Maria Domenica Castellone
Angela Celetti
Lorenzo Chiariotti
Annamaria Cirafici
Annamaria Colao
Sabino De Placido
Gabriella De Vita
Monica Fedele
Pietro Formisano
Alfredo Fusco
Domenico Grieco
Michele Grieco
Maddalena Illario
Paolo Laccetti
Antonio Leonardi
Paolo Emidio Macchia
Barbara Majello
Rosa Marina Melillo
Claudia Miele
Nunzia Montuori
Roberto Pacelli
Giuseppe Palumbo
Maria Giovanna Pierantoni
Rosario Pivonello
Giuseppe Portella
Maria Fiammetta Romano
Giuliana Salvatore
Massimo Santoro
Giampaolo Tortora
Donatella Tramontano
Giancarlo Troncone
Giancarlo Vecchio,
Giuseppe Viglietto
Mario Vitale

“Role of *PATZ1* as a potential tumor suppressor gene in thyroid cancer”

TABLE OF CONTENTS

LIST OF PUBLICATIONS

This dissertation refers to the following publications and manuscripts in preparation:

1. **Valentino T**, Chiappetta G, Vitiello M, Monaco M, Pasquinelli R, Palmieri D, Palma G, Luciano A, Arra C, Fusco A, Fedele M. **PATZ1 sensitizes anaplastic thyroid cancer cells to apoptosis and regulates their migration, invasion and *in vivo* tumorigenicity.** Manuscript in preparation. (The main body of dissertation)

2. Pero R, Palmieri D, Angrisano T, **Valentino T**, Federico A, Franco R, Lembo F, Klein-Szanto AJ, Del Vecchio L, Montanaro D, Keller S, Arra C, Papadopoulou V, Wagner SD, Croce CM, Fusco A, Chiaretti L, Fedele M. **POZ-, AT-HOOK-, and zinc finger containing protein (PATZ) interacts with human oncogene B cell lymphoma 6 (BCL6) and is required for its negative autoregulation**. J Biol Chem 2012; 287(22):18308-17. (Attached at the end)

3. **Valentino T**, Palmieri D, Vitiello M, Simeone A, Palma G, Arra C, Chieffi P, Chiariotti L, Fusco A, Fedele M. **Embryonic defects and growth alteration in mice with homozygous disruption of the Patz1 gene**. J Cell Physiol 2013;228(3):646-53. (Attached at the end)

4. Fedele M, Palmieri D, Chiappetta G, Pasquinelli R, De Martino I, Arra C, Palma G, **Valentino T**, Pierantoni GM, Viglietto G, Rothstein JL, Santoro M, Fusco A. **Impairment of the p27kip1 function enhances thyroid carcinogenesis in TRK-T1 transgenic mice.** Endocr Relat Cancer. 2009;16(2):483-90. (Attached at the end)

5. Fedele M, Visone R, De Martino I, Palmieri D, **Valentino T**, Esposito F, Klein-Szanto A, Arra C, Ciarmiello A, Croce CM, Fusco A. **Expression of a truncated Hmga1b gene induces gigantism, lipomatosis and B-cell lymphomas in mice**. Eur J Cancer. 2011;47(3):470-8. (Attached at the end)

6. Palmieri D, **Valentino T**, D'Angelo D, De Martino I, Postiglione I, Pacelli R, Croce CM, Fedele M, Fusco A. **HMGA proteins promote ATM expression and enhance cancer cell resistance to genotoxic agents.** Oncogene. 2011;30(27):3024-35. (Attached at the end)

7. Palmieri D, D'Angelo D, **Valentino T**, De Martino I, Ferraro A, Wierinckx A, Fedele M, Trouillas J, Fusco A. **Downregulation of HMGA-targeting microRNAs has a critical role in human pituitary tumorigenesis.** Oncogene. 2012;31(34):3857-65. (Attached at the end)

8. Palmieri D, **Valentino T**, De Martino I, Esposito F, Cappabianca P, Wierinckx A, Vitiello M, Lombardi G, Colao A, Trouillas J, Pierantoni GM, Fusco A, Fedele M. **PIT1 upregulation by HMGA proteins has a role in pituitary tumorigenesis.** Endocr Relat Cancer. 2012;19(2):123-35. (Attached at the end)

ABSTRACT

The POZ/BTB and AT-hook-containing zinc finger protein 1 (PATZ1), is a transcriptional regulatory factor that belongs to the POZ and Zinc Finger (POK) family of transcriptional factors involved in chromatin remodeling, protein-protein interaction, transcriptional regulation and targeting of proteins to distinct nuclear substructures. PATZ1 has been shown to regulate expression of different genes and its transcriptional activity, as for other POK proteins, depends on the POZ domain, which mediates oligomers formation. Therefore, it has been suggested that it may not be a typical transactivator but an architectural transcription factor, thus functioning either as activator or repressor depending on the presence of proteins able to interact with it, which could be different depending on the cellular context. The physiological role of PATZ1 is still not completely known, but it has been demonstrated that PATZ1 is important in testis development, in spermatogenesis and it plays a key role in the development of the central nervous system (CNS), and cardiac out-flow tract (OFT). Several studies suggest a role for PATZ1 in cancer but its cancer-related function is still debated between being a tumor suppressor or an oncogene. To better understand the role of PATZ1 in human cancer we focused on thyroid tumors, which represent a useful model to study the multi-step carcinogenesis. In this study quantitative real-time PCR (qRT-PCR) analysis showed that PATZ1 is down-regulated in human thyroid tumors with respect to normal thyroid gland, with the expression levels being inversely correlated with the degree of de-differentiation and malignancy. Immunohistochemical analysis confirmed this result showing the reduction of PATZ1 nuclear expression and its cellular delocalization from the nucleus to the cytoplasm proceeding from the normal to malignant human thyroid tissues. Subsequently, we conducted functional studies on two cell lines derived from human papillary thyroid carcinomas (TPC-1 and BC-PAP) and one cell line derived from a human anaplastic thyroid tumor (FRO), in which PATZ1 was strongly down-regulated compared to normal thyroid tissue, and the same cells in which the presence of PATZ1 has been restored by stable transfection. The comparative analysis of cells expressing or not PATZ1 allowed us to identify noticeable differences associated with the neoplastic phenotype. Indeed, the restoration of PATZ1 expression impaired the proliferation capacity of BC-PAP and FRO cells and induced apoptosis in FRO cells. Moreover, PATZ1 expression inhibited cell migration and invasiveness in all the three cells lines analyzed and suppressed the tumorigenicity of FRO cells both *in vitro* and *in vivo*. Furthermore, as PATZ is essentially a transcriptional regulator, we looked for the genes specifically regulated by it, which could explain its role in counteracting thyroid cell transformation. For this purpose we focused our attention on *BAX*, *PUMA* and

PERP genes, that are all targets of p53 and have a role in cellular migration and/or apoptosis induction. We found that the expression of all three of them was up-regulated in thyroid cell lines re-expressing PATZ1 compared to the parental control cells. Moreover, ChIP or EMSA assays demonstrated that PATZ1 is able to bind their promoters. Taken together these findings support the hypothesis that PATZ1 may act as a tumor-suppressor in thyroid cancer, likely inhibiting cellular migration and/or enhancing apoptosis through the up-regulation of *BAX*, *PUMA* and *PERP* expression. These studies open a road to investigate the diagnostic value and the prognostic impact of PATZ1 in thyroid neoplasia, as well as the efficacy of a thyroid cancer therapy based on the re-expression of the *PATZ1* gene.

1.BACKGROUND

1.1 The POK protein family

Transcription factors (TF) play a key role in certain mechanisms by which specific genes are expressed in a temporal and tissue-specific manner, and, as modular proteins, they can be classified mainly based on the structure of their DNA binding or protein-protein interacting domains. One of these domains, designated as a zinc finger motif on the base of its requirement for zinc, is the large C2H2 *Krüppel*-type zinc finger group, nickname due to the fact that it resembles the Drosophila segmentation protein *Krüppel*. It represents one of the most common types of DNA binding domains. There are approximately more than 600 genes in the human genome encoding C2H2 motifs (Venter et al. 2001), suggesting that this class of TF represents a substantial portion of the genes in the human genome. The Broad complex, Tramtrack, and Bric a` brac (BTB), also known as Poxviruses and Zinc-finger (POZ) domain is an evolutionary conserved protein–protein interaction domain. In most cases this domain is associated with C2H2 zinc finger motifs in TF involved in transcriptional regulation through chromatin re-modeling (Kelly and Daniel 2006). Although the number of proteins harboring this motif is lower than the ones including C2H2 zinc fingers, more than 100 proteins has been identified so far. In fact, it is estimated that 5–10% of the zinc finger proteins in humans also share this domain (Stogios et al. 2005). The proteins showing this combination of motifs are defined as members of the POK (POZ and *Krüppel*) family of transcriptional repressors. Therefore, the POK (Poxviruses and Zinc-finger (POZ) and *Krüppel*) family of transcription repressors is characterized by the presence, in their structures, of an amino-terminal POZ/Broad Complex, Tramtrack, and Bric a' brac (BTB) domain and several *Krüppel*-type zinc fingers at the carboxyterminal side (Costoya 2007) (Fig. 1). Interestingly, both in human and mouse genomes, more than 40 genes are associated with those domains (Stogios et al. 2005). The biological functions of POK proteins are defined on the base of the homo- and hetero-dimerization as well as protein-protein interactions properties conferred by the BTB/POZ domain, while the *Krüppel*-like C2H2 zinc fingers mediate the specific binding to DNA sequences located within gene-regulatory regions. Thus, the BTB/POZ domain promotes homo- and hetero-dimerization and exerts its transcriptional role through its interaction with transcriptional co-factors, including SIN3A, SMRT, NCOR1 and other co-repressors, which in turn recruit HDACs (Histone DeACetylases). Transcription is highly dependent on how DNA is packaged. DNA can be tightly compacted, thus preventing accessibility of TF, or can be available to TF via

modification of the nucleosome, fundamental subunit of chromatin. This architecture of chromatin is strongly influenced by post-translational modifications of the histones. POK proteins are able to act as a molecular switch opening or closing the chromatin through the deacetylation of the histones, and therefore regulating the transcription of their target genes (Costoya 2007). Most POK proteins studied so far have displayed a consistent trans-repressive activity in a variety of cell types and on various promoters although it remains possible that the transcriptional activity of POK proteins may be dependent on the cellular environment and may include the ability to trans-activate (Kobayashi et al. 2000). There are many proteins belonging to the POK family, some of them involved in cancer, development and stem cell biology (Fig. 1). Among these proteins family there is the POZ/BTB and AT-hook-containing Zinc finger protein 1 (PATZ1).

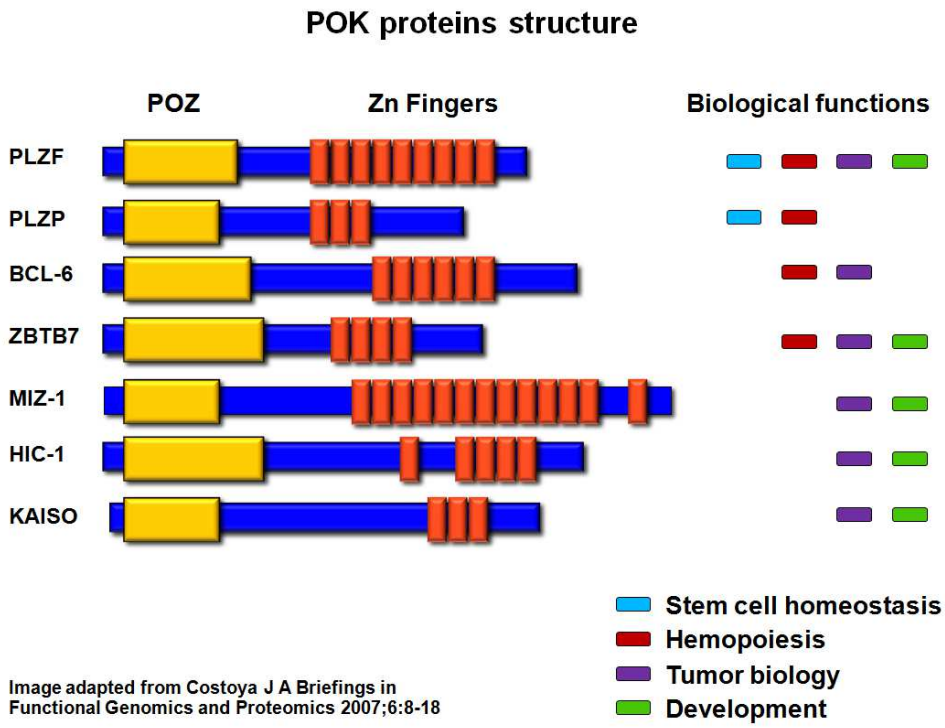

Figure 1. Structure of selected POK transcription factors. These proteins characteristically have an amino-terminal POZ/BTB domain and several carboxy-terminal *Krüppel*-type zinc fingers. These TF have been shown to play important roles in cancer, development and stem cell biology.

1.2 *PATZ1* gene and protein structure

The POZ/BTB and AT-hook-containing Zinc finger protein 1 (PATZ1), is a transcriptional regulatory factor also known as Zinc finger Sarcoma Gene (ZSG), MAZ-Related factor (MAZR) or Zinc Finger Protein 278 (ZNF278/Zfp278). The human *PATZ1* gene is located on chromosome 22 at the position 22q12 and was originally cloned in the 2000 by three independent groups (Fedele et al. 2000; Kobayashi et al. 2000; Mastrangelo et al. 2000). Mastrangelo and coworkers described a submicroscopic inversion of chromosome 22q in a small round cell sarcoma with a t(1;22)(p36.1;q12) translocation. The resultant chimeric transcript contained exon 8 of the Ewing sarcoma gene fused in-frame to exon 1 of the *PATZ1* gene, creating a protein with the transactivation domain of EWS fused to the zinc finger domains of PATZ1. Subsequently, the same group found that this paracentric inversion of chromosome 22q12 interrupted the *UQCRH* gene, with the breakpoint in intron 3, and created fusion genes with both *EWS* on der(22) and *PATZ1* on der(1). Kobayashi and coworkers, as well as our group, isolated PATZ1 by yeast 2-hybrid screenings with the POZ domain of Bach2 or the RING finger protein-4 (RNF4) as baits, respectively (Fedele et al. 2000; Kobayashi et al. 2000). *PATZ1* gene consists of 6 exons and encodes four alternatively expressed isoforms (ranging from 537 to 687 amino acids) that share a common modular structure consisting of a N-terminal BTB/POZ (Bric-a-brac-Tramtrack-Broad complex/Poxvirus Zinc finger) domain, one AT-hook (in the central region) and four to seven C2H2 Zinc fingers at the C-terminus (Fedele et al. 2012) (Fig. 2). Although such motifs are common to factors involved in transcriptional regulation, the presence of all these domains in the same protein appears to be an unique feature of PATZ1. The AT-hook motif is a small AT-rich DNA binding domain that was first described in the high mobility group non-histone chromosomal protein HMGI(Y) and then identified in a few other proteins such as HMGI-C and ALL-1, and is involved in the binding to the minor groove in correspondence of AT-rich regions (Fedele et al. 2000). The BTB/POZ and zinc finger domains makes PATZ1 a member of the POK family of transcriptional repressors (Costoya 2007). Consistent with its protein structure and with the presence of typical features of nuclear proteins, including two nuclear localization signals, PATZ1 localizes in the nucleus (Fedele et al. 2000).

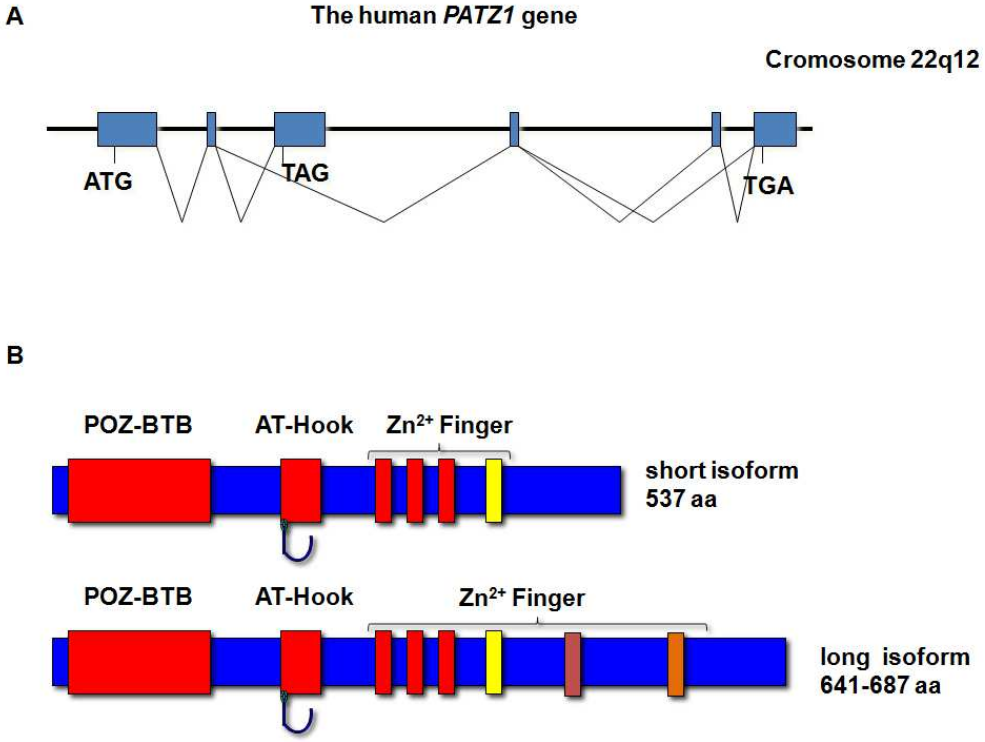

Figure 2. Schematic representation of human *PATZ1* gene and its encoded protein isoforms. A, The human PATZ1 gene consists of 6 exons, which give rice to 4 different proteins through alternative splicings (depicted by exons-connecting lines). B, The two short isoforms of 537 aa and the two long isoforms of 641 and 687 aa are represented by their characteristic domains.

1.3 Transcriptional activity of the *PATZ1* gene

Similarly to the other BTB/POZ proteins, the transcriptional activity of PATZ1 requires the POZ domain (Fedele et al. 2000). However, the mechanisms by which transcriptional regulation by PATZ1 occurs remain to be elucidated. The POZ domain of the POK proteins BCL6 and PLZF, as well as other POZ domain containg proteins, associates with the SMRT-mSin3AHDAC-1 complex and forms a multimeric repressor complex involving histone deacetylation activity (Huynh and Bardwell 1998). PATZ1 may also be involved in the formation of such a complex, since we have demonstrated that its binding to gene promoters is influenced by HDACs inhibitors (unpublished data). Moreover, it is likely that the

zinc finger motifs could target the PATZ1 protein to specific DNA sequences. PATZ1 has been shown to regulate expression of different genes in either a positive or negative manner (Tab. 1). This dual behavior is in the nature of POZ-containing TFs, because their transcriptional activity is due to the POZ-mediated oligomers formation, and therefore they may function either as activators or repressors depending on the presence of proteins able to interact with them, which may be different depending on the cellular context. PATZ1 also contains an AT-hook, a motif characteristic of architectural transcriptional factors, such as the HMGA proteins, whose activity in gene transcription depends on the cellular context (Fedele and Fusco 2010). It has been reported that PATZ1 can function as a transcriptional repressor of basal transcription or as a co-repressor of RNF4 RING finger protein-mediated transcription on the *c-myc*, *CDC6*, *galectin-1* and *SV40* promoters (Fedele et al. 2000). Moreover, PATZ1 acts as a transcriptional activator of the c-myc promoter in B cells and the c-myc transcriptional activation by BACH2 is enhanced by its interaction with the BTB/POZ domain of PATZ1 (Kobayashi et al. 2000). PATZ1 is also able to activate mast cell protease 6 (Morii et al. 2002) and FGF4 (Kobayashi et al. 2000), and to repress androgen receptor (Pero et al. 2002), *CD8* (Bilic et al. 2006) and *BCL-6* genes (Pero et al. 2012). Consistent with the CD8 regulation, it has been shown that PATZ1 is an important part of the transcription factor network that controls the CD4 *versus* CD8 lineage fate of double-positive thymocytes (Sakaguchi et al. 2010) (Tab. 1).

Table 1. Genes regulated by PATZ1

Positive regulation	**Negative regulation**
c-myc (Kobayashi et al. 2000)	c-myc (Fedele et al. 2000)
BACH2 (Fedele et al. 2000)	Galectin-1 (Fedele et al. 2000)
Mast cell protease 6 (Morii et al. 2002)	SV 40 (Fedele et al. 2000)
FGF4 (Kobayashi et al. 2000)	Androgen receptor (Pero et al. 2002)
	CD-8 (Bilic et al. 2006)
	BCL-6 (Pero et al. 2012)

1.4 PATZ1 expression and role in development

The physiological role of PATZ1 is still not completely known, but our group described an important role in testis development and spermatogenesis. Indeed, PATZ1 is expressed in spermatogonia and its lack led to increased apoptosis of the spermatocytes and total absence of spermatids and spermatozoa with subsequent male infertility (Fedele et al. 2008).

PATZ1 is strongly and widely expressed during the early steps of the embryogenesis especially in the central nervous system (CNS), where it is clearly restricted to the actively proliferating neuroblasts in the periventricular neocortical neuroepithelium, in the telencephalic cortical plate, in the hippocampus, and in the striatal neuroepithelium and subventricular zone; then, even though it keeps to be ubiquitously expressed, it is still abundant in restricted organs during the medium and late developmental stages (Valentino et al. 2012). Its ubiquitous expression is also kept in the adult life, but it is generally lower than in embryonic tissues and is still abundant in selected tissues, including skeletal muscle, spinal cord and thyroid (Fedele unpublished data). In order to understand the role of PATZ1 in development, adult life and cancer, a PATZ1 knock-out mouse model has been generated in our laboratory. The analysis of Patz1 -/- mouse embryos suggests that this gene plays an important role in the development of the CNS, and the cardiac out-flow tract (OFT). In fact, they showed defects in the CNS with a clear reduction of periventricular cells, and altered positioning of the cardiac OFT. Moreover, most Patz1 -/- embryos dye in utero: homozygous mutant pups totaled only 4% of the newborn offspring from heterozygous intercrosses, instead of the expected 25%, indicating that most PATZ1-null mice died during embryogenesis, probably because of the defects accumulated during CNS and cardiac OFT development. The few Patz1 -/- mice that survived showed defects in spermatogenesis (i.e. increased apoptosis of the spermatocytes and total absence of spermatids and spermatozoa) and a general growth retardation (Fedele et al. 2008; Valentino et al. 2012). The growth defects may be due, at least in part, to alterations in cell cycle progression and premature senescence. In fact, Patz1 -/- mouse embryonic fibroblasts (MEFs) showed arrest at or beyond the restriction point in either G1 or G2 phase and enter into premature cellular senescence (Fedele et al. 2008; Valentino et al. 2012). The results obtained on the Patz1-null MEFs are consistent with recent data showing growth inhibition and accelerated senescence in human umbilical vascular endothelial cells (HUVECs) interfered for PATZ1 expression (Cho et al. 2011).

1.5 *PATZ1* and cancer

Several studies suggest a role for PATZ1 in cancer but its cancer-related function is still debated between a tumor suppressor or an oncogenic one. The *PATZ1* gene maps on the FRA22B fragile site (on chromosome 22) which suffers loss of heterozygosity in several solid tumors and it has been found rearranged with Ewing sarcoma (EWS) gene in a small round cell sarcoma, with the loss of heterozygosis of the wild-type *PATZ1* allele, suggesting a potential tumor suppressor role (Mastrangelo et al. 2000; Burrow et al. 2009). In addition, our research group showed that in some cell lines PATZ1 is able to reduce the promoter activity of the proto-oncogene c-myc and may cooperate with the oncoprotein BCL6 in the inhibition of its own promoter. In particular we demonstrated that PATZ1 can bind *BCL6* exon 1 and negatively modulate *BCL6* promoter activity in GC-derived lymphoma B cells, thus acting as a tumor suppressor in lymphomagenesis (Fedele et al. 2000, Pero et al. 2012).

On the other hand, an oncogenic role for PATZ1 has also been suggested. Other groups showed that PATZ1 is capable to activate c-myc in other cellular contexts (Kobayashi et al. 2000), is overexpressed in some human malignant neoplasias, including colon and breast tumors (Tian et al. 2008; Yang et al. 2010) and its down-regulation by siRNA either blocks the growth or induces apoptosis of cell lines derived from colorectal cancer or gliomas, respectively (Tian et al. 2008; Tritz et al. 2008). Moreover, we demonstrated that in testicular seminomas, teratomas and embryonal carcinomas there is a significant overexpression of PATZ1 (Fedele et al. 2008). However, the PATZ1 protein localized in cytoplasm rather than nucleus, suggesting that this altered localization could lead to a reduction in the putative anti-oncogenic activity of PATZ1, but the molecular mechanisms that, because of the mis-localization of PATZ1, can lead to tumor development, have not been clarified yet. Similarly, our group recently demostrated mislocalization of PATZ protein to the cytoplasm in a group of human Diffuse large B-cell lymphoma (DLBCL) (unpublished data). Interestingly, it has been also shown that the delocalization of PATZ1 in testicular seminomas depends on estrogen receptor-β levels and the translocation from cytoplasm to the nucleus is mediated by cAMP (Esposito et al. 2011), as it was previously demonstrated in other cell systems, such as PC3M prostate carcinoma cells and normal fibroblasts (Yang et al. 2010). Yang and co-workers demonstrated that PATZ1 binds the RIα subunit of the cAMP-dependent protein kinase in the cytoplasm, and it is known that alteration of RIα expression, and then of the cAMP signaling, may confer cell growth advantage. Therefore, the sequestration of PATZ1 in the cytoplasm through its interaction with RIα would enable PATZ1 to translocate into nucleus and transactivate/repress its target genes upon activation of the cAMP pathway (Yang et al. 2009).

The analysis of PATZ1 knock-out mice carried out in our laboratory provided a strong effort to the tumor-suppressor hypothesis, since both heterozygous and homozygous Patz1 knock-out mice spontaneously develop tumors, including BCL6-expressing Non-Hodgkin lymphomas, sarcomas, hepatocellular carcinomas and rare lung adenocarcinomas (Pero et al. 2012). In particular, at the age of 4-24 months (average of 19 months), pathological analysis demonstrated that 9 out 63 *Patz1* +/+ mice, 50 out of 75 *Patz1* +/- mice, and 9 out of 11 *Patz1* -/- mice developed multiple neoplastic lesions, including both malignant tumors and benign lymphoproliferative diseases. All the tumors raised in heterozygous animals do not lose or mutate the second wild-type allele, and express the wild-type PATZ1 protein, thus excluding loss of heterozygosity as an explanation for the increased occurrence of tumors in *Patz1* +/- mice compared to *Patz1* +/+ mice and suggesting an haploinsufficient tumor suppressor role for PATZ1. Consistent with the role of PATZ in BCL6 autoregulation, *Patz1*-knock-out mice developed thymus hyperplasias or lymphomas and showed increased levels of BCL6, thus suggesting that PATZ causes up-regulation of BCL6 expression, which in turn could be responsible for the thymus pathological phenotype. This hypothesis was validated crossing *Patz1* +/- mice with *Bcl6* +/- mice to generate double mutants that had shown a normal phenotype rescue, indicating a key role for Bcl6 expression in its pathologic development (Pero et al. 2012). The controversial role of PATZ1 in tumorigenesis could be easily explained considering that its transcriptional modulation is highly dependent on specific molecular partners of a particular cellular context. Moreover, as for other well known architectural factors, it is possible an involvement in the development of neoplastic disease either if hyper- or hypo-expressed, stressing the great importance of the correct gene dosage for these factors. It is noteworthy in this regard that PATZ1 interacts with the HMGA proteins, which are architectural transcriptional factors that act as both oncogenes or tumor suppressors depending on the cellular context (Fedele et al. 2012).

1.6 Thyroid cancer

Carcinoma of the thyroid gland is an uncommon cancer, but one of the most frequent malignancies of the endocrine system and its incidence has been steadily increasing in many regions of the world. The thyroid carcinoma is a good multi-step carcinogenesis model because it differs in malignant potential as a result of different genetic alterations (Fig. 3). The vast majority of thyroid tumors (over 95%) arises from thyroid follicular epithelial cells, while a minority (3-5%), named medullary thyroid carcinomas, originates from para-follicular or C-cells

(Carcangiu et al. 1984; DeLellis et al. 2004; Kondo et al. 2006). Thyroid tumors are divided into benign and malignant tumors. Benign tumors are represented by goiters and follicular adenomas (FTA). Malignant tumors are, in the great majority of cases, carcinomas. Carcinomas derived from follicular cells are commonly divided into several subtypes characterized by different morphology, etiology and clinical behavior and they are sub-divided into well-differentiated thyroid carcinomas (WDTCs), poorly differentiated thyroid carcinomas (PDTCs) and anaplastic or undifferentiated thyroid carcinomas (ATC) (De Lellis et al. 2004; Nikiforov et al. 2009). WDTCs include two types: papillary thyroid carcinomas (PTCs) and follicular thyroid carcinomas (FTCs). The PTC is the most common thyroid carcinoma (about 80% of cases). It is characterized by the classic papillary architecture and cells with typical nuclear alterations (ground-glass nuclei). It is often multifocal and tends to metastasize to regional lymph nodes (DeLellis et al. 2004). The FTC is a relatively rare cancer (about 10% of thyroid cancers) that may develop from a pre-existing benign adenoma (FTA) or directly from the normal tissue "bypassing" the stage of adenoma. It is well differentiated, usually unifocal, encapsulated, and may be of conventional type or oncocityc type (Hurthle cells). Less-differentiated thyroid cancers, namely PDTCs and ATCs, can develop *de novo* although many of them arise through the process of stepwise dedifferentiation of PTCs and FTCs (Nikiforov et al. 2011). In particular, the ATC is a very rare (2-5% of thyroid cancers), highly aggressive and lethal tumor characterized by very undifferentiated cells, mostly insensitive to radiotherapy and conventional chemotherapy (Ain, 1999; Yau et al. 2008). The PDTC (also known as insular carcinoma) has an intermediate behavior between WDTC and ATC (Tallini 2011). The theory of sequential progression of well-differentiated thyroid carcinoma trough the spectrum of poorly differentiated to undifferentiated thyroid carcinomas is supported by the presence of pre- or co- existing well-differentiated thyroid carcinoma with less differentiated types and the common core of genetic loci with identical allelic imbalances in co-existing well-differentiated components (van der Laan et al. 1993). Similar to other cancer types, thyroid cancer initiation and progression occurs through gradual accumulation of various genetic (rearrangements that activate proto-oncogenes, point mutations and loss of tumor suppressor function) and epigenetic alterations, including activating and inactivating somatic mutations, alteration in gene expression patterns, micro-RNA dysregulation and aberrant gene methylation. A substantial fraction of PTCs (30%) shows a typical large alteration involving a rearrangement of the RET proto-oncogene. The rearrangement consists in the fusion of the tyrosine kinase domain (TK) of RET with other genes that provide the chimeric gene of promoter and 5' coding region. In about 10% of PTC cases rearrangements of the gene coding for TRK, another tyrosine kinase protein, which determines its fusion to partner genes similarly to RET/PTC

rearrangements, were identified. At least ten different types of RET/PTC rearrangements have been reported (Nikiforov 2002). RET/PTC1 and RET/PTC3 are the most frequent rearrangement found in PTCs. RET/PTC1 was generated by the fusion of RET TK domain with the 5' terminal region of the gene CCD6 (Grieco et al. 1990), whereas in RET/PTC3 the TK domain of RET is fused to the RFG gene (Santoro et al. 2004). In most cases of PTCs (40%) a point mutation of the BRAF gene was recovered, while in 10-20% of cases mutations of RAS genes (RAS K-RAS, H-ras and N-RAS) are observed. BRAF mutations are found in 29-69% of papillary carcinomas but not in thyroid follicular carcinomas and in up to 13% of poorly differentiated thyroid carcinomas and 35% of undifferentiated thyroid carcinomas (Kondo et al. 2006). In PTCs, BRAF mutation and RET/PTC rearrangements are mutually exclusive and cannot be found simultaneously in the same patients, yet they are not completely equivalent, since it has been shown that PTCs positive for BRAF are more aggressive than those positive for RET/PTC (Kimura e al. 2003; Soares et al. 2003). BRAF point mutation are not a significant event in post Chernobyl thyroid carcinomas; instead a chromosomal rearrangement (AKAP9-BRAF), that represents a paracentric inversion, has been identified in radiation-associated thyroid cancer (Ciampi et al. 2005). Mutation of RAS genes (K-RAS, H-RAS, and N-RAS), present in codons 12, 13 and 61, are observed in 10-20% of PTCs (Namba et al. 1990; Vasko et al. 2004). RAS gene mutations represent early molecular lesions since they are also frequently found in FTAs, which are considered FTC precursors. Mutations of RAS genes are also observed in 40-50% of conventional FTCs and in 20-40% of FTAs, while another group of FTCs (35%) presents a rearrangement PAX8/PPAR (Pallante et al. 2010). The PAX8/PPARγ rearrangement leads to the fusion between a portion of the PAX8 gene, which encodes a paired domain transcription factor, and PPARγ gene (Kroll et al. 2000); this fusion results in strong overexpression of the chimeric PAX8/PPARγ protein (Kroll et al. 2000; Powell et al. 2004) although the mechanism of its transforming activity remains to be fully understood. The PDTCs and ATCs can come from the WDTC. Therefore, the mutations that occur in the early stages of WDTCs are also reported in PDTCs and ATCs: in PDTCs RET/PTC rearrangements (13%) and mutations in the RAS (46-55%) and BRAF (12-17%) genes were identified, while in the ATC only mutations of RAS (6-52%) and BRAF (25-29%) genes were reported. In more advanced stages of thyroid carcinogenesis, alterations of PI3K and PTEN were also found (Paes & Ringel 2008). The molecular alteration that characterizes the ATC compared with differentiated thyroid carcinomas is the mutation of the p53 tumor suppressor gene. Almost all ATCs show inactivation of p53 and is therefore highly probable that it is the deficiency of p53, combined with mutations of oncogenes such as RAS and BRAF, to determine the high proliferative index and high aggressiveness of this tumor. Indeed, p53 mutations are common in both PDTCs (17-38%) and

ATCs (67-88%), but rare or absent (0-9%) in WDTCs (Ito et al. 1992; Donghi et al. 1993; Fagin et al. 1993). Other genes have been implicated in thyroid neoplasias. Even though critical molecular mechanisms of thyroid carcinogenesis have been clarified, other molecular steps of neoplastic progression still need to be investigated.

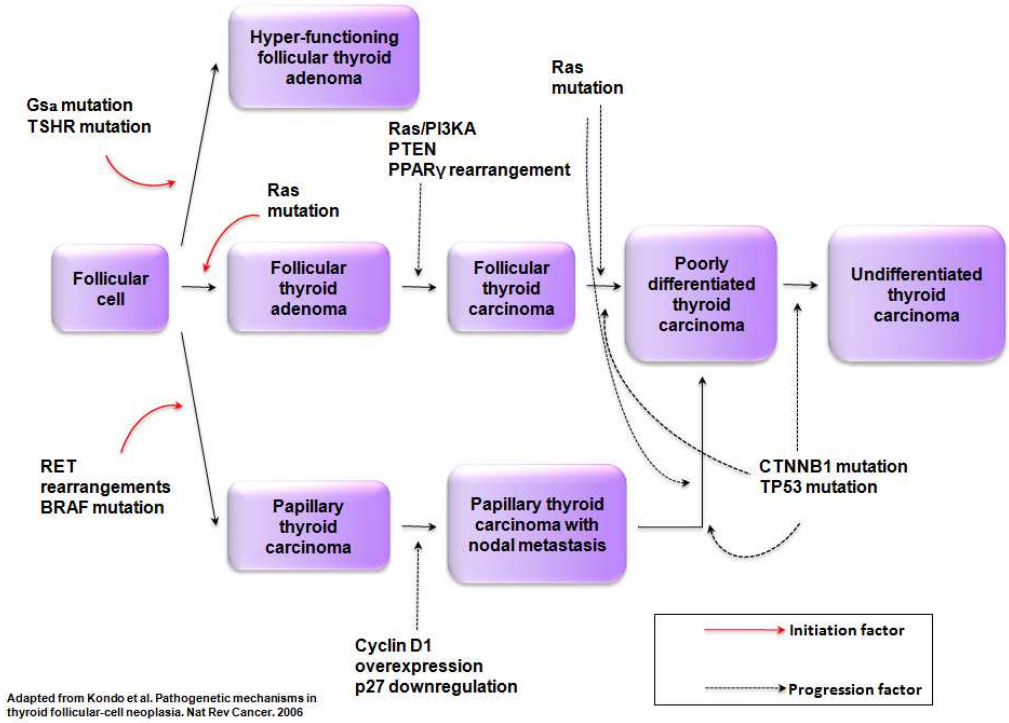

Figure 3. Model of multi-step carcinogenesis of thyroid tumors. Three distinct pathways have been proposed for the initiation of thyroid tumors including hyper-functioning follicular thyroid adenoma, FTC and PTC. Genetic defects that result in activation of RET or BRAF represent frequent early initiating events associated with radiation exposure that leads to PTC development. RAS mutations represent frequent early initiating events, associated with iodine deficiency, that lead to FTC development. By contrast, most PDTCs and ATCs are considered to derive from pre-existing well-differentiated thyroid carcinoma through the accumulation of additional genetic events that include nuclear accumulation of β-catenin (encoded by CTNNB1) and p53 inactivation.

1.7 p53 in thyroid cancer

Dubbed as the "guardian of the genome" and the "cellular gatekeeper", the p53 protein is a transcription factor that acts to transmit a variety of stress-inducing signals to different anti-proliferative cellular responses. Following various intracellular and extracellular stimuli such as DNA damage, heat shock, hypoxia, and oncogene overexpression, p53 is activated and emerged as a pivotal regulatory protein which triggers diverse biological responses (Levine 1997; Vousden and Lu 2002). Most of the biological effects elicited by p53 can be attributed to its ability to act as a sequence-specific transcription factor, which regulates expression of different cellular genes to modulate various cellular processes (Farmer et al. 1992), although protein-protein interactions may also play a role. In response to various types of stress, p53 is accumulated in the nucleus and binds specific promoters that, in turn, activate the transcription of specific genes. p53 downstream target genes are differentially regulated depending on the cell type, extent of the damage which has influenced p53 activation, and various other factors (Oren 2003). The product of the downstream target genes of p53 regulate cell cycle arrest, DNA repair, epithelial-mesemchymal transition (Zilfou et al. 2009). Among them there are $p21^{Waf/Cip1}$ (which mediates G1 cell growth arrest), *Gadd45* (which mediates DNA repair), *BAX* and *PUMA* (which mediate apoptosis) and *PERP* (which mediates apoptosis and cell-cell adhesion). Another p53 major target gene is *MDM2*, coding for an ubiquitin ligase that binds to the N-terminus of the p53 protein and causes p53 inactivation by its nuclear export and degradation. p53 is also a major regulator of cell senescence (Hofseth et al. 2004). Indeed, telomere shortening caused by cell replication triggers p53 activation, thereby blocking cell cycle and favoring cell entry into senescence. As a consequence, *p53* inactivation may contribute to the increased number of cell replications and, eventually, to the accumulation of further genetic abnormalities and the acquisition of the immortalized phenotype in cultured cells. Finally, the *p53* gene can use different internal promoters and\or internal translation start sites to produce a variety of N-terminally truncated isoforms with a variable degree of dominant negative activity (Malaguarnera et al. 2007). The p53 protein has three major functional domains, the N-terminal transactivation domain (TAD), the C-terminal oligomerization domain (OD), and a core domain (DBD), which has DNA-binding activity. The vast majority of p53 mutations occurs within the DBD domain (Murray-Zmijewski et al. 2006). Approximately half of all human tumors have a mutation or loss in the *p53* gene leading to inactivation of its function (Soussi and Beroud 2001). At variance with other human malignancies, *p53* mutations are not frequent in thyroid cancer and are believed to be responsible mainly for cancer progression to poorly differentiated and aggressive phenotype (Olivier *et al.* 2002). Studies on p53 protein expression in a large series of thyroid

tumor specimens suggest that, although not mutated, p53 activity may be inhibited in thyroid cancer by other mechanisms (Pollina et al. 1996). Indeed, increased p53 protein levels were observed by immunohistochemistry not only in anaplastic and poorly differentiated thyroid cancer, where p53 mutations are frequent, but also in well-differentiated cancers, in the absence of any p53 mutations (Soares et al. 1994). Non functioning p53 cannot induce Mdm2, its major degrading protein, and consequently accumulates in the cell nucleus. A strong p53 staining in paraffin-embedded specimens, therefore, is considered indirect evidence of nonfunctioning p53 (Dobashy et al. 1993). Thyroid cancers are also characterized by the loss of function of p63 and p73, two members of the p53 protein family (Malaguarnera et al. 2007). In general, the tumor suppressor activity of these proteins is kept latent by several mechanisms, including interaction with p53 mutants, dominant negative isoform overexpression, and impaired activation mechanisms. The overexpression of the High Mobility Group A (HMGA) oncogenes in thyroid cancers is one of the causes of the p53 family members loss of function. HMGA proteins are non-histone proteins, with several different functions, including gene transcription, malignant transformation promotion, and metastatic progression. The expression level of HMGA genes is maximal during the embryonic development, while it is very low in well-differentiated and adult cells (Reeves et al. 2001). In thyroid cancer, as in several human cancers, the HMGA1 protein level is high and correlates with the increasing degree of malignancy and metastatic potential. HMGA1 protein has an inhibitory effect on both ectopic and endogenous p53 family member activity. In particular, HMGA1 interacts with p53, p63 and p73 and it is able to inhibit p53 activity on G1 cell cycle arrest and apoptosis (Frasca et al. 2006). Moreover, HMGA1 overexpression promotes cytoplasmic relocalization of the p53 activator homeodomain-interacting protein kinase 2 (HIPK2), thus disabling the p53 phosphorylation at S46, which is required for its apoptotic function (Pierantoni et al. 2007). Interestingly, p53 may be used as a diagnostic and/or prognostic marker in thyroid cancer and as a predictive factor of chemioresistance. Indeed, since a consistent series of thyroid malignant tissues displays a positive immunostaining for at least one of the p53 family members (p53, p63 and p73), it is reasonable to hypothesize a possible use of these proteins in thyroid nodules differential diagnosis (Nishida et al. 1996). Moreover, several reports indicate that wild-type *p53* gene delivery into anaplastic thyroid cancer cells induces a partial differentiation, with re-expression of thyroid specific-genes, and makes cells more vulnerable to the effect of chemotherapy (Moretti et al. 1997).

1.8 BAX

The Bax (Bcl-2 Associated protein X) protein is one of the principal targets of p53 which activates an apoptotic program after DNA damage, irradiation, or in response to the activity of oncogenes and other stress factors. Apoptosis, the main and more studied form of programmed cell death, plays a central role in tissue homeostasis during development and all along the life of multicellular organisms. Alterations of apoptosis are involved in tumorigenesis, as well as in the cellular response to anti-tumor treatments (Hickman et al. 2002). Bax is a central regulator of the mitochondria-dependent apoptotic pathway. It is a member of the Bcl-2 protein family that includes proteins involved in apoptosis regulation characterized by the presence of one or more of the so-called "Bcl-2 Homology" domains (BH1 to BH4). The BH domains are involved in protein-protein interactions and their presence is fundamental for the function of the Bcl-2 family proteins. The main function of these proteins is to regulate the permeability of the outer mitochondrial membrane to different apoptogenic factors, namely cytochrome c, Smac/Diablo, Omi/HtrA2, endonuclease G, and apoptosis-inducing factor (AIF). Among the Bcl-2 family members there are both pro-apoptotic factors (like Bax, Bak and PUMA) and antiapoptotic factors (like Bcl-2 and Bcl-Xl) (Renault et al. 2011). In non-apoptotic cells, Bax remains under a closed conformation, making it poorly able to interact with other partners. It has been suggested that several proteins are able to retain Bax under this conformation (for example Ku70, humanin and 14-3-3) (Amsel et al. 2008; Nomura et al. 2003). Following a death signal, cytosolic BAX translocates to the mitochondria where it becomes an integral membrane protein. BAX overexpression induces mitochondrial permeability transition, which leads to the release of cytochrome c. Released cytochrome c binds to and activates APAF-1, which in turn recruits procaspase-9. This leads to the activation of the downstream caspase cascade and execution of the cell death (Lindsten et al. 2000). This p53-dependent apoptotic program is based both on the transcriptional activation of pro-apoptotic factors (Bax, PIG3, CD95, Perp, Noxa and PUMA) and on some transcription-independent p53 activities. Indeed, p53 is able to induce the mitochondrial outer membrane permeabilization and to activate some BH containing proteins interacting with them (Zilfou et al. 2009). Finally, it is important to underline that *BAX* gene plays an important role in human tumorigenesis: it is often mutated or downregulated in tumor tissues and it may be considered a tumor-suppressor. In thyroid tumorigenesis and tumor biology, the role of the pro-apoptotic BAX is controversially discussed. Hermann and co-workers showed elevated BAX expression in patients with thyroid carcinoma associated with p53 wild-type overexpression, suggesting that the increased BAX expression might be the consequence of dysregulation of wild-type p53 in these tumors (Hermann et al. 2001).

1.9 PUMA

PUMA (p53 upregulated modulator of apoptosis) belongs to the BH3-only subgroup of Bcl-2 family proteins, which share sequence similarity only within the BH3 domain. PUMA is a critical mediator of p53-dependent and -independent apoptosis induced by a wide variety of stimuli, including genotoxic stress, deregulated oncogene expression, toxins, altered redox status, growth factor/cytokine withdrawal and infection. In response to genotoxic stress, such as DNA damage, *PUMA* is transactivated by p53 (Vogelstein and Kinzler, 2004 ; J Yu and L Zhang 2008). Along with another BH3-only protein, Noxa, which in most cases has a minor function, PUMA accounts for virtually all of the proapoptotic activity of p53. PUMA is also activated by other transcription factors to initiate p53-independent apoptotic responses to nongenotoxic stimuli, including growth factor/cytokine deprivation, endoplasmic reticulum (ER) stress and ischemia/reperfusion. Similar to other BH3-only proteins, PUMA serves as a proximal signaling molecule that transduces death signals to the mitochondria where it acts through multidomain Bcl-2 family members to induce mitochondrial dysfunction and caspase activation. The BH3 domain of PUMA is required for its interactions with Bcl-2- like proteins, such as Bcl-2 and Bcl-XL (Nakano and Vousden 2001). PUMA primarily acts to indirectly activate *Bax* and/or *Bak* by relieving the inhibition of these proteins by antiapoptotic Bcl-2 family members, including Bcl-2, Bcl-XL, Mcl-1, Bcl-w and A1. It has also been suggested that PUMA can trigger apoptosis by directly activating Bax, or through cytoplasmic p53 in some cells. In contrast to its prominent function in p53-dependent apoptosis, the function of PUMA in p53-independent apoptosis remains to be fully appreciated. In addition to p53, a number of other transcription factors are implicated in *PUMA* induction. The oncoproteins E2F1 and c-myc can induce PUMA through their respective binding sites in the *PUMA* promoter (Fernandez et al. 2003; Hershko and Ginsberg, 2004). Moreover, general transcription factors, including C/EBPβ, CREB, c-Jun and Sp1 have been implicated in *PUMA* induction, some of which may do so by cooperating with p53 or p73 (Qiao et al. 2003; Hayakawa et al. 2004). On the other hand, *PUMA* transcription is subject to negative regulation by transcriptional repressors, including Slug (Wu et al. 2005), some alternative splice products of *p73* (ΔNp73 and p73α) (Melino et al. 2004) or *p63* (ΔNp63) (Rocco et al. 2006) and microRNA (Choy et al. 2008). Until now the activity of PUMA seems to be exclusively controlled by transcription, whereas other BH3-only proteins are often activated through multiple mechanisms including post-translational modifications. With such versatile functions, it is perhaps not surprising that PUMA has been implicated in many pathological and physiological processes including cancer, tissue injury, neurodegenerative diseases, immune response and bacterial or viral infection. Several lines of evidence suggest that the function of PUMA is compromised in cancer cells. First,

more than half of human tumors contain *p53* mutations (Vogelstein and Kinzler, 2004), which abrogate the induction of PUMA by irradiation and many chemotherapeutic drugs (Yu and Zhang, 2005). Second, frequent overexpression of antiapoptotic Bcl-2 family proteins and other antiapoptotic oncoproteins in tumors antagonizes PUMA-induced apoptosis. Third, PUMA expression was found to be reduced in malignant cutaneous melanoma, and PUMA expression appears to be an independent predictor of poor prognosis in patients. In addition, approximately 40% of primary human Burkitt's lymphomas do not express detectable levels of PUMA, which is attributable, in part, to DNA methylation. However, *PUMA* does not appear to be a direct target of genetic inactivation in human cancer (Yu and Zhang 2008). Finally, PUMA may be an excellent therapeutic target, as activating PUMA inhibits tumor growth by restoring apoptosis in cancer cells, whereas inhibiting PUMA curbs excessive apoptosis associated with tissue injury and neurodegeneration (Yu and Zhang 2008).

1.10 PERP

PERP (p53 apoptosis effector related to PMP-22) gene was discovered as a p53 target gene, involved in DNA damage-induced apoptosis, whose expression was high in apoptotic cells. However, in addition to this apoptotic function downstream of p53, PERP plays a role in development (Beaudry et al. 2010). PERP is a member of the claudin/PMP-22/EMP family of fourpass membrane proteins which participate in a variety of cellular processes including ion channel function, receptor trafficking, tight junction formation, and myelination. In particular, PERP is a component of the desmosomes which are cell-cell junctions important for tissue integrity. The dynamic regulation of cell-cell adhesion junctions, including desmosomes, is thought to be an important facet of wound healing. Desmosomes are multiprotein cell-cell adhesion complexes essential for maintaining the structural integrity of tissues through connection to the intermediate filament network. Desmosomal adhesion junctions are initially destabilized at the wound front, presumably to facilitate proliferation and migration, and are reassembled later during the sealing of the epithelium. Desmosome complexes form when the desmosomal cadherins, desmogleins and desmocollins, participate in heterotypic interactions that bring the plasma membranes of adjacent cells in close apposition. The cytoplasmatic tails of these cadherins interact with plakoglobin and plakophilins, which connect to the intermediate filament cytoskeleton via desmoplakin (Attardi et al. 2000). Several studies have shown that PERP has an important role in promoting cell adhesion and is essential for wound healing.

PERP's critical role in desmosomal adhesion was evidenced by the presence of dramatic blisters observed in the epidermis and oral mucosa of mice lacking *Perp* as well as by the ultrastructural abnormalities observed in desmosomes of these mice. Moreover, the analysis of conditional *Perp* knock-out mice (in which *Perp* expression is selectively ablated in stratified epithelia) suggests that this gene has a tumor-suppressor function. In particular, it has been demonstrated that *PERP* ablation predisposes mice to UVB induced squamous cell carcinoma (SCC) development by enhancing tumor initiation and progression. These effects are elicited at multiple levels, leading both to compromised apoptosis in response to ultraviolet light and loss of desmosomal adhesion. The defective apoptosis could allow the inappropriate survival of damaged cells, which could help initiate tumors. Interestingly, the loss of cell-cell and cell-matrix adhesion is a common feature of tumor progression and in particular of the epithelial-mesenchymal transition (EMT) (Beaudry et al. 2010). The EMT is a process characterized by loss of cell adhesion, repression of E-cadherin expression and increased cell motility. EMT is essential for numerous developmental processes and it is a typical step of the transformation process of epithelial cells (Muller et al. 2011). The absence of PERP in mice induces the expression of some genes involved in promoting inflammation, which is a well-established causative factor in tumorigenesis. The hypothesis that PERP has a tumor-suppressor function is confirmed also by the fact that its locus (in human chromosome 6q24) is mutated in a variety of cancers, including melanoma, cervical cancer, ovarian cancer, and breast cancer. Moreover, it has been recently discovered that PERP loss affects mammary epithelial homeostasis by causing the accumulation of inflammatory cells around mature mammary epithelium (Millikin et al. 1991; Foulkes et al. 1993; Noviello et al. 1996). Finally, PERP expression is reduced in many breast cancer cell lines compared with untransformed cells and PERP deficiency also promotes the development of mouse mammary cancer (Dusek et al. 2012).

2. AIM OF THE STUDY

The POZ/BTB and AT-hook-containing zinc finger protein 1 (PATZ1) is a transcription factor whose expression is frequently de-regulated in human cancer. It is still debated if PATZ1 is a tumor suppressor or an oncogene. To better understand the role of PATZ1 in human cancer we focused on thyroid tumors, which include a wide spectrum of lesions with different phenotypic characteristics and biological behaviors, thus representing a useful model to study the multi-step carcinogenesis. Furthermore, thyroid cancer is one of the most frequent malignancies of the endocrine system, whose mechanisms of pathogenesis are still far from being completely elucidated. Therefore, the aim of my study has been to elucidate PATZ1 function in thyroid cell transformation.

Beside the study of PATZ1 role in thyroid cancer, projects developed during my PhD program regarded:

1. Pero R, Palmieri D, Angrisano T, **Valentino T**, Federico A, Franco R, Lembo F, Klein-Szanto AJ, Del Vecchio L, Montanaro D, Keller S, Arra C, Papadopoulou V, Wagner SD, Croce CM, Fusco A, Chiaretti L, Fedele M. **POZ-, AT-HOOK-, and zinc finger containing protein (PATZ) interacts with human oncogene B cell lymphoma 6 (BCL6) and is required for its negative autoregulation**. J Biol Chem 2012; 287(22):18308-17. (Attached at the end)

2. **Valentino T**, Palmieri D, Vitiello M, Simeone A, Palma G, Arra C, Chieffi P, Chiariotti L, Fusco A, Fedele M. **Embryonic defects and growth alteration in mice with homozygous disruption of the Patz1 gene**. J Cell Physiol 2013;228(3):646-53. (Attached at the end)

3. Fedele M, Palmieri D, Chiappetta G, Pasquinelli R, De Martino I, Arra C, Palma G, **Valentino** T, Pierantoni GM, Viglietto G, Rothstein JL, Santoro M, Fusco A. **Impairment of the p27kip1 function enhances thyroid carcinogenesis in TRK-T1 transgenic mice.** Endocr Relat Cancer. 2009 Jun;16(2):483-90. (Attached at the end)

4. Fedele M, Visone R, De Martino I, Palmieri D, **Valentino T**, Esposito F, Klein-Szanto A, Arra C, Ciarmiello A, Croce CM, Fusco A. **Expression of a truncated Hmga1b gene induces gigantism, lipomatosis and B-cell lymphomas in mice**. Eur J Cancer. 2011 Feb;47(3):470-8. (Attached at the end)

5. Palmieri D, **Valentino T**, D'Angelo D, De Martino I, Postiglione I, Pacelli R, Croce CM, Fedele M, Fusco A. **HMGA proteins promote ATM expression and enhance cancer cell resistance to genotoxic agents.** Oncogene. 2011 Jul 7;30(27):3024-35. (Attached at the end)

6. Palmieri D, D'Angelo D, **Valentino T**, De Martino I, Ferraro A, Wierinckx A, Fedele M, Trouillas J, Fusco A. **Downregulation of HMGA-targeting microRNAs has a critical role in human pituitary tumorigenesis.** Oncogene. 2012 Aug 23;31(34):3857-65. (Attached at the end)

7. Palmieri D, **Valentino T**, De Martino I, Esposito F, Cappabianca P, Wierinckx A, Vitiello M, Lombardi G, Colao A, Trouillas J, Pierantoni GM, Fusco A, Fedele M. **PIT1 upregulation by HMGA proteins has a role in pituitary tumorigenesis.** Endocr Relat Cancer. 2012 Apr 10;19(2):123-35. (Attached at the end)

3. MATERIALS AND METHODS

3.1 Cell cultures, transfections and plasmids

Continuos human carcinoma thyroid cell lines TPC-1 and BC-PAP, derived from papillary thyroid cancer, FRO and FB1 derived from anaplastic thyroid cancer, and human embryonic kidney HEK293 cells were cultured in DMEM supplemented with 10% FBS, L-glutamine, and penicillin/streptomycin (GIBCO-BRL) in a 5% CO2 atmosphere. For transient transfection TPC-1 and FRO cells were transfected using Neon Electroporation System (Invitrogen), according to manufacturer's instruction. FB1 and BC-PAP cells were transfected using Arrest-in reagent (Open Biosystems, Huntsville USA). HEK293 transfection were performed by Lipofectamine 2000 (Invitrogen) according to manufacturer's instruction. All the cell lines were transfected with HA-PATZ1 plasmid encoding for PATZ1 variant 4 or the empty vector pCEFL-HA. For the stable transfection of TPC-1, BC-PAP, FRO and FB1 cell lines the same transfecting agent and the same protocol as the transient transfection were used. The cells were transfected with PATZ1-eGFP-C2 plasmid encoding for the human of PATZ1 variant 4 or with the empty vector eGFP-C2, both expressing the gene for the resistance to neomycin. Stable transfectants were clonally selected in medium with 1μg/ml neomycin (G418) (Life Technologies) for 10 days, and cell clones were screened for PATZ1 expression by qRT-PCR and Western blot analysis. The selected cell clones of TPC-1/PATZ1, BC-PAP/PATZ1, FRO/PATZ1, FB1/PATZ1 and the control cells were cultured in DMEM supplemented by 10% FBS, L-glutamine, penicillin/streptomycin (GIBCO-BRL) and neomycin (G418) 0,5 μg/ml in a 5% CO2 atmosphere.

3.2 Human thyroid tissue samples and immunohistochemistry

Neoplastic and normal human thyroid tissues and RNA samples were collected by the research group of Doctor G. Chiappetta at the Istituto dei Tumori di Napoli or by the research group of Professor A. Fusco at the Istituto di Endocrinologia ed Oncologia Sperimentale of Naples and derived from the Service d'Anatomo-Pathologie, Centre Hospitalier Lyon Sud, Pierre Benite, France. For immunohistochemistry, 6 μm paraffin sections were deparaffinised and then placed in a solution of absolute methanol and 0.3% hydrogen peroxide for 30 min

and then washed in PBS before immunoperoxidase staining. The slides were then incubated overnight at 4 °C in a humidified chamber with the antibodies diluted 1 : 100 in PBS. The slides were subsequently incubated with biotinylated goat anti-rabbit IgG for 20 min (Vectostain ABC kits, Vector Laboratories, Burlingame, CA, USA) and then with premixed reagent ABC (Vector) for 20 min. The immunostaining was performed by incubating the slides in diaminobenzidine (DAB-DAKO) solution containing 0.06 mM DAB and 2 mM hydrogen peroxide in 0.05% PBS, pH 7.6, for 5 min, and, after chromogen development, the slides were washed, dehydrated with alcohol and xylene and mounted with cover slips using a permanent mounting medium (Permount). The antibodies used are an home-made rabbit polyclonal anti-PATZ1 which reacts against the amino-terminal portion of the protein and anti-PERP (ab48032, Abcam). Tissue samples were scored as positive for immunohistochemistry when tissue immunoreactivity was detected in at least 10% of the cells. Negative controls were performed by omitting the first antibody. No staining was observed when normal thyroid gland was stained with antibodies pre-incubated with the peptide against which the antibodies were raised or without the primary antibodies (data not shown).

3.3 Protein extraction, Western blotting and antibodies

Cells were lysed in buffer containing 1% Nonidet P-40, 1 mmol/liter EDTA, 50 mmol/liter Tris-HCl (pH 7.5), and 150 mmol/liter NaCl supplemented with Complete protease inhibitors (Roche Applied Science). Total proteins were resolved in a 8% polyacrylamide gel under denaturing conditions and transferred to nitrocellulose filters for Western blot analyses. Membranes were blocked with 5% BSA in TBS and incubated with the primary antibodies. Membranes were then incubated with the horseradish peroxidase–conjugated secondary antibody (1:3.000) and the reaction was detected with a Western blotting detection system (enhanced chemiluminescence; GE Healthcare). The primary antibodies used are anti-PATZ1 antibody (polyclonal antibody raised against a conserved peptide recognizing all PATZ1 isoforms of mouse and human origin) and anti-E-cadherin (610181) (BD Transduction Laboratories). To ascertain that equal amounts of protein were loaded, the membranes were incubated with antibodies against the anti-vinculin protein (sc-7649) (Santa Cruz Biotechnology, Santa Cruz, CA).

3.4 Co-immunoprecipitation assay

For co-immunoprecipitation experiments, antigens and antibodies were incubated for 3 hours and then supplemented with protein A-sepharose or G sepharose beads. After 1 h, the beads were collected and washed five times with lysis buffer and boiled in Laemmli sample buffer for western blotting analysis. The antibodies used are antip53 (sc-126) (Santa Cruz Biotechnology, Santa Cruz, CA), anti-PATZ1 (polyclonal antibody raised against a conserved peptide recognizing all PATZ1 isoforms of mouse and human origin), and non-specific IgG (Santa Cruz Biotechnology, Santa Cruz, CA).

3.5 RNA extraction and qRT-PCR analysis

Total RNA was isolated using TRI-reagent solution (Sigma, St Louis, MO, USA) and treated with DNase (Invitrogen). Reverse transcription was performed according to standard procedures (Qiagen, Valencia, CA). qRT-PCR analysis was performed using the Power SYBR Green PCR Master Mix (Applied Biosystems) according to manufacters's instructions with the following primer sequences to amplify the indicated genes:

hPATZ1all-variants-Fw: 5'-TACATCTGCCAGAGCTGTGG-3'
hPATZ1all-variants-Rev: 5'-TGCACCTGCTTGATATGTCC-3'
hPATZ1short-variant-Fw: 5'-CTGAGCGGCCTCACAAGT-3'
hPATZ1short-variant-Rev: 5'-GTCGCTAGGAAGAGGTTCCA-3'
mPATZ-Fw: 5'-GAGCTTCCCCGAGCTCAT- 3'
mPATZ –Rv:e 5' -CAGATCTCGATGACCGACCT- 3'
hBAX-Fw: 5'-ATGTTTTCTGACGGCAACTTC-3'
hBAX-Rev: 5'-ATCAGTTCCGGCACCTTG-3'
hPERP-Fw: 5'-GACCCCAGATGCTTGTCTTC-3'
hPERP-Rev: 5'-ACCAGGGAGATGATCTGGAA-3'
hPUMA-Fw: 5'-TTCTCCGGAGTGTTCATGC-3'
hPUMA-Rev: 5'-TACAGCGGAGGGCATCAG-3'
mBAX-Fw: 5'-GTGAGCGGCTGCTTGTCT-3'
mBAX-Rev: 5'-GGTCCCGAAGTAGGAGAGGA-3'
mPERP-Fw: 5'-GACCCCAGATGCTTGTTTTC-3'
mPERP-Rev: 5'-ACCAGGGAGATGATCTGGAA-3'
mPUMA-Fw: 5'-GACCTCAACGCACAGTACGA-3'
mPUMA-Rev: 5'-GAGATTGTACAGGACCCTCCA-3'
hG6PD-Fw: 5'-GATCTACCGCATCGACCACT-3'

hG6PD-Rev: 5'-AGATCCTGTTGGCAAATCTCA-3'
mG6PD-Fw: 5'-GAAAGCAGAGTGAGCCCTTC-3'
mG6PD-Rev: 5'-CATAGGAATTACGGGCAAAGA-3'
To calculate the relative expression levels we used the 2-ΔΔCT method (Livak and Schmittgen, 2001). Primers specific for the glucose-6-phosphate dehydrogenase (G6PD) were used for normalization of Real-Time quantitative PCR data.

3.6 Proliferation assay

For colony assay the cells were plated at a density of 90% in 100-mm dishes, transfected with 5 μg of HA-PATZ1 plasmid encoding for the short isoform of PATZ1 or the empty vector pCEFL-HA, and supplemented with neomycin (G418) 24 h later. Two weeks after the onset of drug selection, the cells were fixed and stained with crystal violet (0.1% crystal violet in 20% methanol, SIGMA). After an incubation of 30 min, crystal violet has been removed, the plates were washed with PBS (137 mM NaCl, 2.7 mM KCl, 4.3 mM NaH2PO4), photographed and the cells were counted. For the growth curves the cells (4×10^4 cells/dish) were plated in a series of 6-cm culture dishes and counted daily for 10 consecutive days through the Bürker chamber. The count was performed in the presence of trypan blue, a dye that penetrate in cells that have lost membrane integrity and which shows, therefore, dying cells.

3.7 DNA ladder assay

Cells were plated ($2{,}5\times 10^5$ cells) in 100-mm dishes and 7 days later the assay was performed. The cells were harvested, washed with PBS 1X (137 mM NaCl, 2.7 mM KCl, 4.3 mM NaH2PO4) and lysed in buffer containing 0,5% TRITON, 5mM Tris pH 7.4, 20 mM EDTA) for 20 min in ice. Then cells were centrifugated at 13.200 rpm for 30 min and the supernatant containing DNA fragments was obtained. DNA was precipitated and the pellet was resospended and incubated for 30 min at 37 °C with 20 μL of buffer TE (10 mmol/L Tris-HCl, 1 mmol/L EDTA) and RNase 0,4 mg/ml. 12 μL of each samples was loaded on minigel for electrophoresis. Doxorubicin treatment (10 μg/ml) was used as a positive control.

3.8 SA–β-gal assay

Cells, plated (1×10^5 cells/dish) in a series of 6-cm culture dishes 24 hours before the assay, were washed twice with PBS and immersed in fixation buffer (2% [w/v] formaldehyde, 0.2% [w/v] glutaraldehyde in PBS) for 7 min. After 3 additional PBS washes, the cells were allowed to stain overnight in staining solution (40 mM citric acid/sodium phosphate, pH 6.0; 150 mM NaCl; 2.0 mM MgCl2; 1 mg/ml X-gal) at 37°C without CO2 to avoid changes in pH. The next day, the staining solution was replaced with PBS, and the stained and unstained cells were counted under light microscopy (at least 24 fields).

3.9 Migration and invasion assay

The migration assay was conducted in triplicate using plates transwell cell culture chambers according to described procedures (Corning Costar Corp., Cambridge, MA). Briefly, confluent cell monolayers were harvested with trypsin/EDTA , centrifuged at 1.200 rpm for 5 min, resuspended in medium without serum and plated (5×10^4 cells) to the upper chamber of a polycarbonate membrane filter of 8 μM pore size. The lower chamber was filled with complete medium. The cells were then incubated at 37°C in a humidified incubator in 5% CO2 for 24h and 48h. Non migrating cells on the upper side of the filter were wiped off and migrating cells on the reverse side of the filter were stained with 0.1% crystal violet in 20% methanol for 30 min, washed in PBS 7.4 (137 mM NaCl; 2.7 mM KCl, 4.3 mM NaH2PO4), photographed and counted. The rate of invasion was carried out, again by using plates transwell cell culture chambers in the presence of a Matrigel (BD Biosciences). The plate has been appropriately pretreated with a cold solution containing serum-free medium and Matrigel (diluted 1:4) and was left 45 min in the incubator at a temperature of 37 ° C, temperature at which the Matrigel polymerizes to produce a matrix biologically active that resembles the basement membrane of mammalian cells. Then the assay was performed as the migratory assay.

3.10 Soft agar colony forming assay

For soft agar assays 7 ml of mixture of serum supplemented medium and 0.5% agar were added in a 60-mm culture dish and allowed to solidify (base agar). Next, on top of the base layer was added a mixture of serum supplemented medium and 0.35% agar (total of 2 mL) containing $2x10^4$ of FRO cells expressing

PATZ1 or control cells (obtained as described before) and allowed to solidify (top agar). Subsequently, the dishes were kept in culture incubator maintained at 37^0C and 5% CO^2 for 14 days to allow for colony growth. After 14 days the colonies were counted.

3.11 Tumorigenesis *in vivo*

The tumorigenicity of the FRO cells expressing PATZ1 or control cells was tested by subcutaneous injections of $2x10^6$ cells into athymic mice. Severe combined immunodeficient mice (7 weeks old) Foxn1 nu/nu female mice (Harlan Laboratories) were s.c. injected in the right flank with 2×10^6 of FRO cells expressing PATZ1 and in the left flank with 2×10^6 of control cells suspended in 0.1 mL PBS. Tumor growth was assessed every day by measuring with calipers. Tumor volume was calculated using the following formula: (length × width)/2. Excised tumor sections were weighed, snapfrozen for protein analysis and fixed in formalin for immunohistochemical analysis. Staining with hematoxylin and eosin was performed for histologic confirmation of tumor cell growth. The humane care and use of the mice were in accordance with institutional guidelines.

3.12 Chromatin immunoprecipitation (ChIP) assays

For ChIP analysis $5x10^6$ HEK293 cells after transfection were cross-linked using formaldehyde 1% for 10 min at room temperature. The reaction was stopped with Glycine 0,125 M for 5 min. The cells were washed twice with cold PBS, harvested and lysed sequentially by 10 min in ice and 5 minute centrifugation at 3000 X *g* at 4°C with 1 mL buffer A (10 mM HEPES pH 8, 10 mM EDTA pH 8, 0,5 mM EGTA pH 8, 0,25% Triton X-100 and protease inhibitors), and then with 1 mL buffer B (10 mM HEPES pH 8, 200 mM NaCl, 1 mM EDTA pH 8, 0,5 mM EGTA pH 8, 0,01% Triton X-100 and protease inhibitors). The pellets were then resuspended in 200 µl of lysis buffer (10mM EDTA, 50 mM Tris-HCl pH 8, 1% SDS and protease inhibitors), and sonicated 5 times for 30 s at maximum settings obtaining fragments between 0,3 and 1,0 kbp. The samples were cleared by centrifugation at 14000 rpm for 15 min. After centrifugation 20 µl of the surnatants were used as imputs, and the other parts of the samples diluted 2,5-fold in Ip buffer (100 mM NaCl, 2 mM EDTA pH 8, 20 mM Tris-HCl ph 8, 0,5% Triton X-100 and protease inhibitors). The samples were subjected to immunoprecipitation with specific antibody anti-HA or non-specific IgG, after 2

hours preclearing at 4°C with Protein A Sepharose SA/Salmon Sperm (Upstate). Precipitates were washed sequentially with 1 mL Ip buffer (150 mM NaCl, 2 mM EDTA pH 8, 25 mM Tris-HCl ph 8, 1% Triton X-100 and SDS 0,1%), 1 ml Wash buffer 1 (500 mM NaCl, 2 mM EDTA pH 8, 20 mM Tris-HCl ph 8, 0,5% Triton X-100 and SDS 0,1%), 1 ml Wash Buffer 2 (0,25 M LiCl, 1% NP40, 1% Na deoxycholate, 1 mM EDTA and 10 mM Tris-HCl ph 8), and then twice with 1 mM EDTA, 10 mM Tris-HCl pH 8. Precipitated chromatin complexes were removed from the beads through 15 min incubation with 250 µl of 1% SDS, 0,1 M NaHCO3. This step was repeated twice. For qRT-PCR analysis, 1µl out of 30µl immunoprecipitated DNA was used with primers described below.

Primers used were:
BAX-prom -250/-530-Fw 5'-TAATCCCAGCGCTTTGGAA -3'
BAX-prom-250/-530 -Re 5'-GTCCAATCGCAGCTCTAATG -3'
PERP-prom -950/-700 -Fw 5'-CCACCCTTCCTGTCACATCT-3'
PERP-prom -950/-700 -Re 5'-GCAGTCCACTTCCTATCACGA-3'

3.13 Electrophoretic mobility shift assay (EMSA)

DNA binding assay with the recombinant proteins were performed as previously described (Thanos and Maniatis 1995). Briefly, 5 ng of human PATZ1 recombinant protein spanning from aa 259 to aa 367 (H00023598-Q01) (Abnova) were incubated with radio-labelled double-strand oligonucleotide, corresponding to region spanning bases -50 to -24 of the human PUMA promoter region. PATZ1 recombinant protein was incubated in a solution made of 20 mM HEPES pH 7.9, 40 mM KCl, 0,1 mM EDTA, 0,5 mM MgCl2, 0,5 mM DTT, 0,1 mM PMSF, 0,5 mg poly (dC-dG), 2 mg BSA and 10% glycerol, to a final volume of 20 ml, for 10 min at room temperature. The samples were incubated for 15 min after addition of 2,5 fmol of a ^{32}P-end-labelled oligonucleotide. A 200-fold molar excess of unlabelled oligonucleotide was addes as specific competitor. The DNA-protein complexes were resolved on 6% nondenaturing acrylamide gels and visualized by exposure to autoradiographic films.

3.14 Statistical analysis.

Student's t-test was used to determine the significance for all the quantitative experiments. Error bars represent the standard deviation (s.d.) of the average. Statistical significance for all the tests, assessed by calculating the p-value, was <0.05.

4. RESULTS

4.1 *PATZ1* gene expression is down-regulated in thyroid cancer

In order to evaluate a possible involvement of PATZ1 in neoplastic transformation of the thyroid gland, the expression of *PATZ1* gene has been analyzed, by quantitative RT-PCR (qRT-PCR), in two panels of human thyroid tumors representative of different histological types and different degrees of differentiation compared to normal thyroids. The first qRT-PCR was carried out on RNAs of 9 normal thyroids, 9 papillary carcinomas (PTC), 4 follicular carcinomas (FTC) and 8 anaplastic carcinomas (ATC) collected by the research group of Dr. Gennaro Chiappetta at the Istituto dei Tumori di Napoli. The experiment showed down-regulation of *PATZ1* in all tumor samples compared with normal thyroids with an inverse correlation with both malignancy and degree of de-differentiation. Indeed, as reported in Fig. 4 (Panel A), there was a negative fold change in *PATZ1* expression in PTC (up to -3,85) compared to the normal tissue; this down-regulation was stronger in FTC (up to -20) and is even more pronounced in ATC (up to -33,3). The second qRT-PCR was performed on RNAs of 3 normal thyroids, 19 PTC and 4 ATC collected by the research group of Professor Alfredo Fusco at the Istituto di Endocrinologia ed Oncologia Sperimentale of Naples and derived from the Service d'Anatomo-Pathologie, Centre Hospitalier Lyon Sud, Pierre Benite, France. This experiment confirmed that in all thyroid tumors the expression of *PATZ1* is reduced compared to normal thyroid. Indeed, as shown in Fig. 4 (Panel B), there was a negative fold change in *PATZ1* expression from -1,5 to -12,6 in the PTC samples and from -5,4 to -20 in ATC samples. These results suggest that PATZ1 can play a tumor suppressor role in thyroid cancer, mainly involved in the late stages of carcinogenesis.

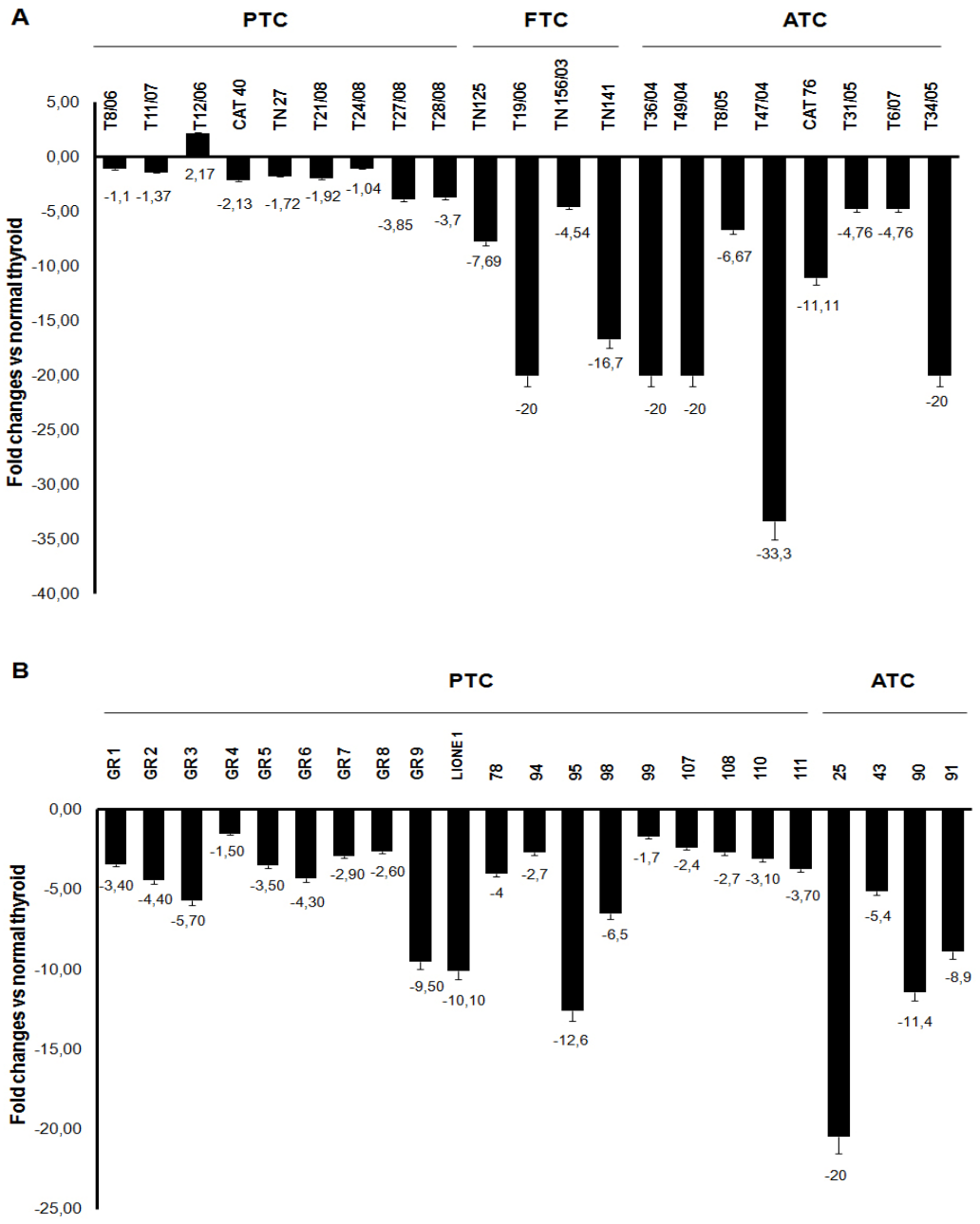

Figure 4. PATZ1 expression in Thyroid Cancer. A, qRT-PCR analysis of *PATZ1* in a panel of 9 PTC, 4 FTC and 8 ATC in comparison with a pool of 9 wild-type normal thyroid samples. B, qRT-PCR analysis of *PATZ1* in a panel of 19 PTC and 4 ATC in comparison with a pool of 3 wild-type normal thyroid samples. The fold change indicates the relative change in expression levels between tumor samples and normal samples, assuming that the value of each normal sample is equal to 1. The results shown are the mean $\pm$ SE of three analyses for each sample.

4.2 PATZ1 protein is delocalized in thyroid cancer

Subsequently, we analyzed PATZ1 protein expression and localization by immunohistochemistry (IHC). The experiment was performed in collaboration with the research group of Doctor G. Chiappetta at the Istituto dei Tumori di Napoli on a panel of human paraffin embedded normal and neoplastic thyroid samples, including 27 normal thyroids, 2 goiters, 11 adenomas, 26 PTC, 9 FTC, 16 ATC and 5 poorly differentiated thyroid carcinoma (PDTC). The analysis was performed using an anti-PATZ1 polyclonal antibody, which reacts against the amino-terminal portion of the protein and that recognizes all the isoforms of PATZ1. All samples of normal thyroid parenchyma and goiters expressed PATZ1 at a high level in the nucleus, which coincides with the strong PATZ1 staining in all follicles (Fig. 5). Conversely, compared to normal samples, PATZ1 expression in the nucleus was found to be weaker in adenoma (55%, 6/11 samples), in PTC (42%, 11/26 samples) and FTC (45%, 4/9 samples), and completely negative in most of poorly differentiated (80%, 4/5 samples) and anaplastic (75%, 12/16 samples) carcinomas (Table 2). Interestingly, PATZ1 protein showed a progressive displacement from the nucleus to the cytoplasm with a direct correlation with the undifferentiated and malignant phenotype. Indeed, in all normal thyroid tissues (100%, 27/27) and goiters (100%, 2/2) analyzed, PATZ1 is expressed and is present only in the nucleus, while in most adenoma samples (54% , 6/11), PTCs (73%, 19/26) and FTCs (89%, 8/9), PATZ1 protein was localized also in the cytoplasm. In 60% (3/5) of PDTCs PATZ1 protein was localized only in the cytoplasm as in 12,5% (2/16) of ATCs. Moreover, in 20% (1/5) of PDTCs and in 62% (10/16) of ATCs, PATZ1 expression was completely absent (Table 3). These results confirmed the inverse correlation between PATZ1 expression and the thyroid malignant phenotype.

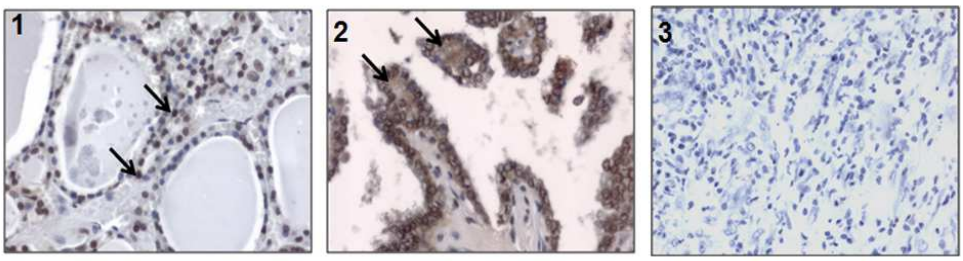

Figure 5. Normal and neoplastic thyroid tissues analyzed for PATZ1 protein expression by immunohistochemistry. PATZ1 staining was intense in the nucleus of normal thyroid tissue (1) and its localization moves to the cytoplasm proceeding from the normal to malignant samples such as in the PTC sample shown here (2), whereas it was absent in ATC (3).

Table 2. Nuclear anti-PATZ1 reactivity

Hystotype	N.	Negative (< 10%)	Weak (11-75%)	Strong (76-100%)
Normal	27		6 (22%)	21 (78%)
Goiter	2			2 (100%)
Adenoma	11		6 (55 %)	5 (45%)
Papillary carcinoma	26		11 (42%)	15 (58%)
Follicular carcinoma	9		4 (45 %)	5 (55%)
Poorly differentiated carcinoma	5	4 (80%)	1 (20 %)	
Anaplastic carcinoma	16	12 (75%)	3 (31,5%)	1 (6,25%)

Table 3. PATZ1 localization

Hystotype	N.	Nucleus	Nucleus/Cytosol	Cytosol	Negative
Normal	27	27 (100%)			
Goiter	2	2 (100%)			
Adenoma	11	3 (27%)	6 (54%)	1 (9%)	1 (9%)
Papillary carcinoma	26	7 (27%)	19 (73%)		
Follicular carcinoma	9	1 (11%)	8 (89%)		
Poorly differentiated carcinoma	5		1 (20%)	3 (60%)	1 (20%)
Anaplastic carcinoma	16		4 (25%)	2 (12,5%)	10 (62,5%)

Table 2 and 3. Summary of IHC results showing the expression and the sub-cellular localization of PATZ1. The subcellular localization of PATZ1 moves from the nucleus to the cytoplasm as they proceed from the normal to malignant samples, with an inverse correlation to the degree of de-differentiation, up to be completely absent in ATC.

4.3 Characterization of *PATZ1* gene expression in human cell lines of thyroid carcinoma and restoration of *PATZ1* expression in TPC-1, BC-PAP and FRO cells.

In order to investigate a causal role of PATZ1 in thyroid carcinogenesis and choose a suitable cellular system to work, we evaluated the expression of *PATZ1* gene in a series of human cell lines derived from thyroid carcinomas. This series includes cells derived from papillary (TPC-1, FB2, BC-PAP), follicular (WRO) and anaplastic (FRO, FB1, ACT1, 8505c) thyroid carcinomas compared to 3 normal thyroids. The analysis was carried out by qRT-PCR using primers able to amplify all transcript variants of PATZ1. As shown in Fig. 6, in all tumor cell lines the expression of *PATZ1* is reduced compared to normal control, represented by normal thyroid tissue.

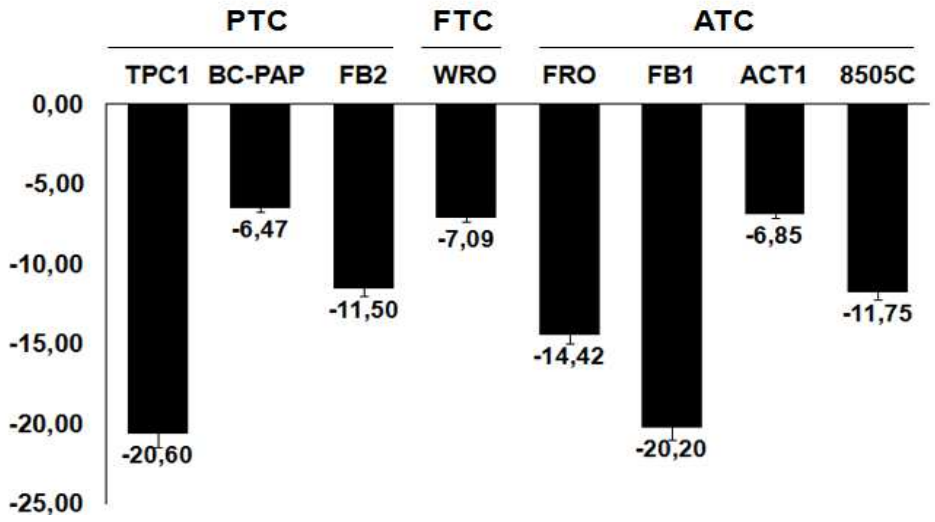

Figure 6. PATZ1 expression in human thyroid cancer cell lines. qRT-PCR analysis of PATZ1 in 3 PTC-derived cell lines (TPC-1, BC-PAP and FB2), 1 FTC-derived cell line (WRO) and 4 ATC-derived cell lines (FRO, FB1, ACT1, 8505C) in comparison with a pool of 3 normal thyroid glands. The fold change indicates the relative change in expression levels between thyroid cancer cell lines and the pool of normal thyroid glands, assuming that the value of each normal sample is equal to 1. The results shown are the mean ± SE of three analyses for each sample.

Subsequently, two cell lines representative of papillary thyroid carcinoma (TPC-1 and BC-PAP) and two representative of anaplastic thyroid carcinoma (FB1 and FRO) were selected to restore PATZ1 expression by stable transfecting a vector encoding for *PATZ1* variant 4. Cells transfected with the correspondent

empty vector have been used as negative controls. Following the transfection, PATZ1 expressing clones, called TPC1/PATZ1, BC-PAP/PATZ1, FB1/PATZ1 and FRO/PATZ1, were selected and the restoration of PATZ1 expression has been confirmed by qRT-PCR and Western-Blot analysis compared to clones transfected with the empty vector (CTRL). For qRT-PCR analysis we used primers able to amplify the short transcript variant of PATZ1 and for Western Blot analysis we used an anti-PATZ1 polyclonal antibody that recognizes all the isoforms of PATZ1. We also carefully observed the morphology of the clones at the optical microscope, and found some differences compared to control clones; indeed, some clones of TPC-1 re-expressing PATZ1 showed a shift toward an epithelial-like phenotype retaining a packed cuboidal and organized morphology compared to control cells that, instead, exhibited a spindle-shaped morphology (Fig. 7, panel A). Moreover, most FB1/PATZ1 clones showed features of a suffering phenotype with condensed nuclei and vacuolated cytoplasm (Fig. 7, panel B). Based on the data of Western-Blot, qRT-PCR analysis and morphological changes, we selected specific clones of TPC-1/PATZ1 (PA 1, PA 5, PA6) (Fig. 8, panel A-B), BC-PAP/PATZ1 (PA 3, PA7, PA10) (Fig. 8, panel C-D) and FRO/PATZ1 (PA11, PA16, PA17) (Fig. 8 panel E-F) in order to characterize growth and malignant properties in terms of proliferation, death, aging, migration, invasion and tumorigenicity. The TPC-1, BC-PAP and FRO cells transfected with the empty vector, were used as controls (CTRL). We were not able to keep FB1/PATZ1 clones in culture, because they stop to grow and die after few passages, thus suggesting a toxic role for PATZ1 expression in this cancer cell line.

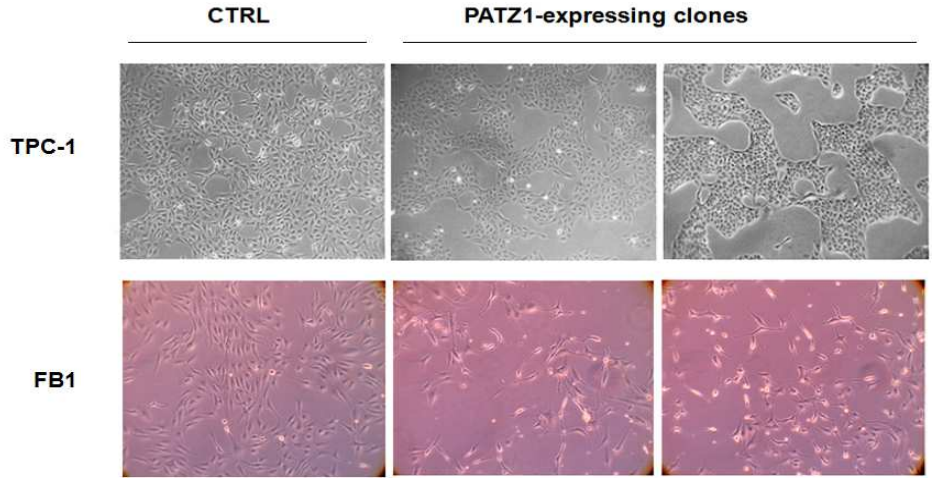

Figure 7. Effect of restoration of PATZ1 expression in TPC-1 and FB1 cells. Representative optical microscope images showing morphological changes of 2 cell clones of TPC-1 re-expressing PATZ1 and 2 cell clones of FB1 re-expressing PATZ1 compared to their CTRL.

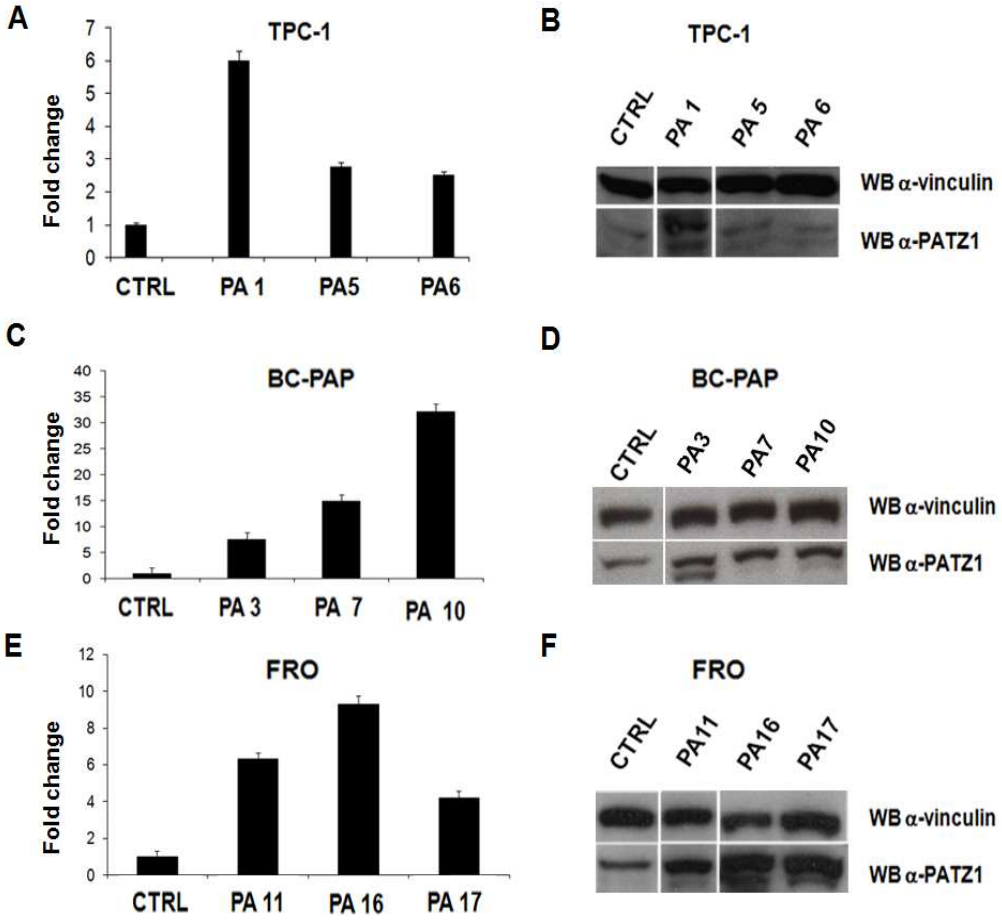

Figure 8. Restoration of PATZ1 expression in TPC-1, BC-PAP and FRO cells. qRT-PCR and Western Blot analysis of PATZ1 in 3 selected cell clones of TPC-1 (PA1, PA5, PA6) (A-B), BC-PAP (PA3, PA7, PA10) (C-D) and FRO (PA11, PA16, PA17) (E-F) transfected with a vector encoding for the short isoform of the PATZ1 gene compared to a clone transfected with the empty vector (CTRL).

4.4 PATZ1 inhibits growth rate in BC-PAP and FRO cells and induces apoptotic cell death in FRO cells

To determine whether the loss of *PATZ1* gene expression affects thyroid carcinogenesis, we first analyzed the properties of proliferation and survival carrying out a colony-forming assays in TPC-1, BC-PAP and FRO cells transfected with the empty vector (pCEFL-HA) or with the vector encoding for

PATZ1 (HA-PATZ). The colonies were scored after 10 days. All the assays carried out on TPC-1 showed no difference in the number of colonies expressing or not PATZ1, while BC-PAP and FRO cells transfected with PATZ1 showed a reduced number of colonies compared to controls: the inhibition was about the 40% for the BC-PAP cells and about 80% for the FRO cells (Fig. 9).

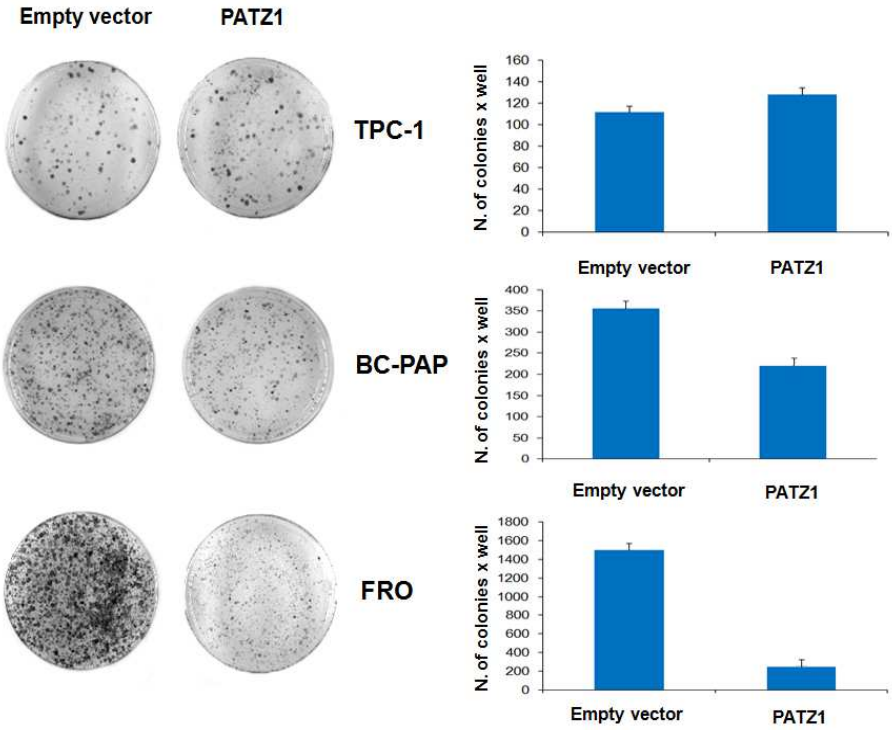

Figure 9. Colony-forming assay with PATZ1 transfection in TPC-1, BC-PAP and FRO cells. TPC-1, BC-PAP and FRO cells were transfected with a vector expressing PATZ1 cDNA and its corresponding empty vector. Cells were cultured for 10 days, selected for resistance to G418 and stained with crystal violet. The assays were quantified by counting the number of colonies formed.

To confirm these results and deeper investigate the cause of growth inhibition, we performed growth curves and cell viability assays on selected clones of TPC-1/PATZ1, BC-PAP/PATZ1 and FRO/PATZ1 compared to their respective controls (Fig. 10, panel A-C). In agreement with results from the colony assays, the growth rate of TPC-1/PATZ1 clones did not show any difference compared to control. Indeed, both the slope of the straight lines and the saturation density were similar in the different clones and controls. Furthermore, the absence of differences in the incorporation of trypan blue by the cells, showed a similar cell viability in all TPC-1/PATZ1 clones compared to controls (data not shown). Conversely, BC-PAP/PATZ1 clones, and especially FRO/PATZ1 clones, showed a significant decreased proliferation capacity that in FRO/PATZ1 clones is accompanied by a significant increase in cell death compared to their respective controls (Fig. 10, panel D). To analyze the mechanism of death in these cells, DNA-laddering analysis have been performed. This assay showed a strong DNA-laddering in FRO/PATZ1 cells compared to their control, whereas no differences of a DNA ladder-like pattern were observed in TPC1/PATZ1 and BC-PAP/PATZ1 clones compared to controls. These results suggest that a mechanism of apoptosis is responsible of the low survival of PATZ-expressing FRO cells (Fig. 10, panel E).

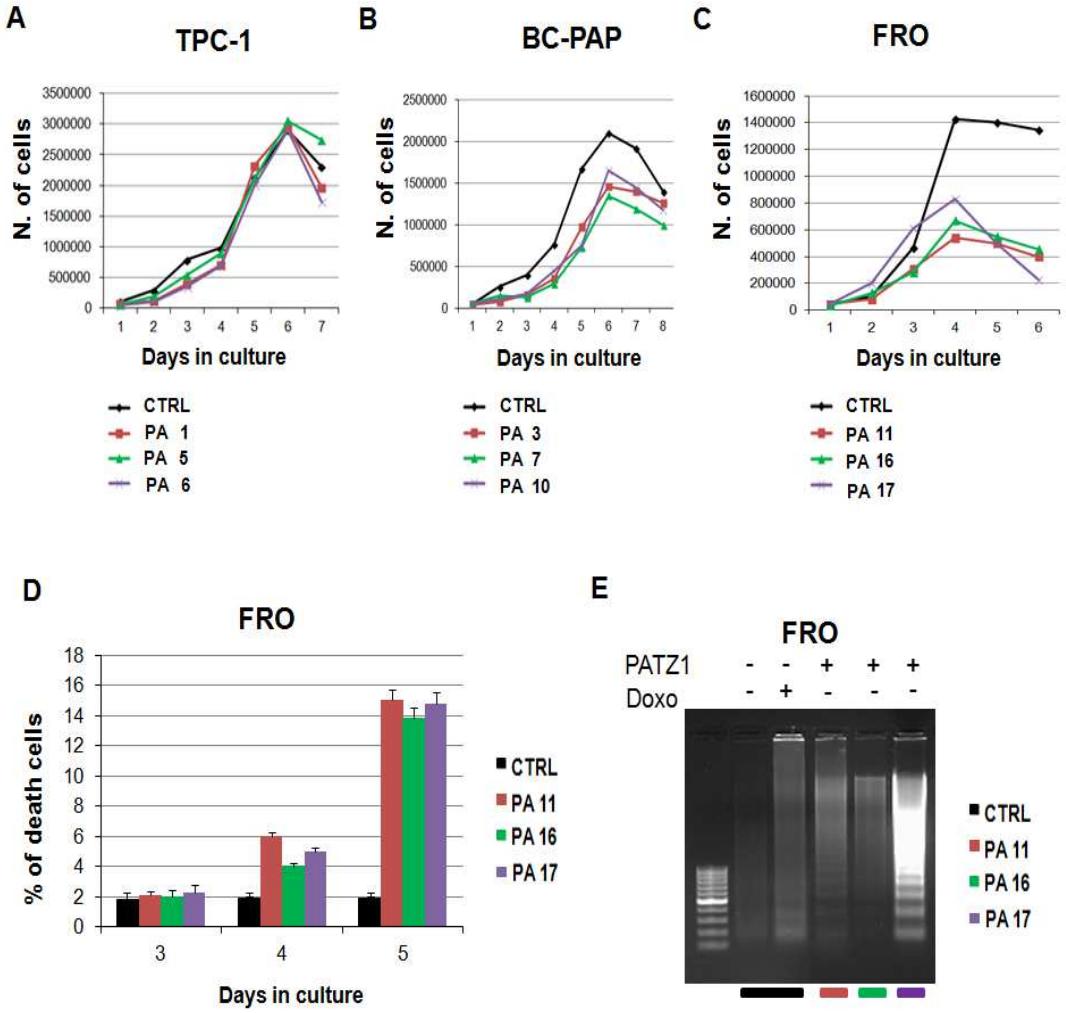

Figure 10. PATZ1 effects on the growth rate and apoptosis. A, B, C Growth curves performed on different stably expressing PATZ1 cell clones of TPC1 (PA 1, PA 5, PA 6), BC-PAP (PA 3, PA 7, PA 10) and FRO (PA 11, PA 16, PA 17) compared to control cells expressing the empty vector (CTRL). Representative curves of 3 independent experiments are reported. D, Tripan Blue staining assay in FRO/PATZ1 cells at different time points in culture. Mean values ± SD of 3 different cell clones expressing PATZ1 (PA 11, PA 16, PA17) are reported. E, DNA ladder assay in FRO/PATZ1 (PA 11, PA 16, PA 17) cells performed after 5 days in culture, when the percentage of dead cells was highest, to investigate whether death observed was due to apoptosis. Doxorubicin (Doxo) treatment was used as a positive control.

4.5 PATZ1 inhibits cellular senescence in TPC-1 and FRO cells

Cellular senescence is an irreversible state of cell proliferation arrest, which can be caused by diverse factors, such as telomere shortening or dysfunction, oncogenic activation, chromatin perturbation, DNA damage, oxidative or inflammatory stresses, irradiation and so on (Collado et al. 2006). A large body of evidence suggests that cellular senescence may be an underlying mechanism for protection against cancer development due to uncontrolled proliferation (Campisi et al. 2007). To analyze weather induced cellular senescence in thyroid cancer is impaired by PATZ1 expression, we conducted senescence-associated β-galactosidase (β-SA) staining assays on the selected clones of TPC1/PATZ1, BC-PAP/PATZ1 and FRO/PATZ1 compared to their controls. The cells were plated with only one medium change to induce a mild culture stress. Seven days later the assay was performed. As shown in Fig. 11, β-galactosidase activity was positive in controls cells, as evidenced by the presence of green cells. Conversely, a significant reduction in the number of senescent cells in the clones TPC1/PATZ1 and FRO/PATZ1 compared to their controls was found. This result was even more striking in the FRO/PATZ1 clones, where we could easily appreciate a drastic reduction of senescent cells in clone FRO/PA11 and a total absence of positivity in clones FRO/PA16 and FRO/PA17. We could not evaluate the cellular senescence in BC-PAP cells because control cells not showed positive β-galactosidase staining (data not shown). The anti-senescence effect of PATZ expression in TPC1 and FRO cells is consistent with our recent data, showing that *PATZ1* (-/-) embryonic fibroblasts (MEFs) enter into premature cellular senescence (Valentino et al. 2012), and with other recent data showing growth inhibition and accelerated senescence in human umbilical vascular endothelial cells (HUVECs) interfered for PATZ1 expression (Cho et al. 2011). These data suggest a role for PATZ1 in protecting these tumor cells from going to stress-induced senescence. This role is apparently in contrast with its tumor suppressor function, since senescence is one of the main barriers to tumor progression. However, previous data showed that a tumor suppressor gene can inhibit senescence and simultaneously block other functions related to the development and/or progression of the tumor (Pan et al. 2011).

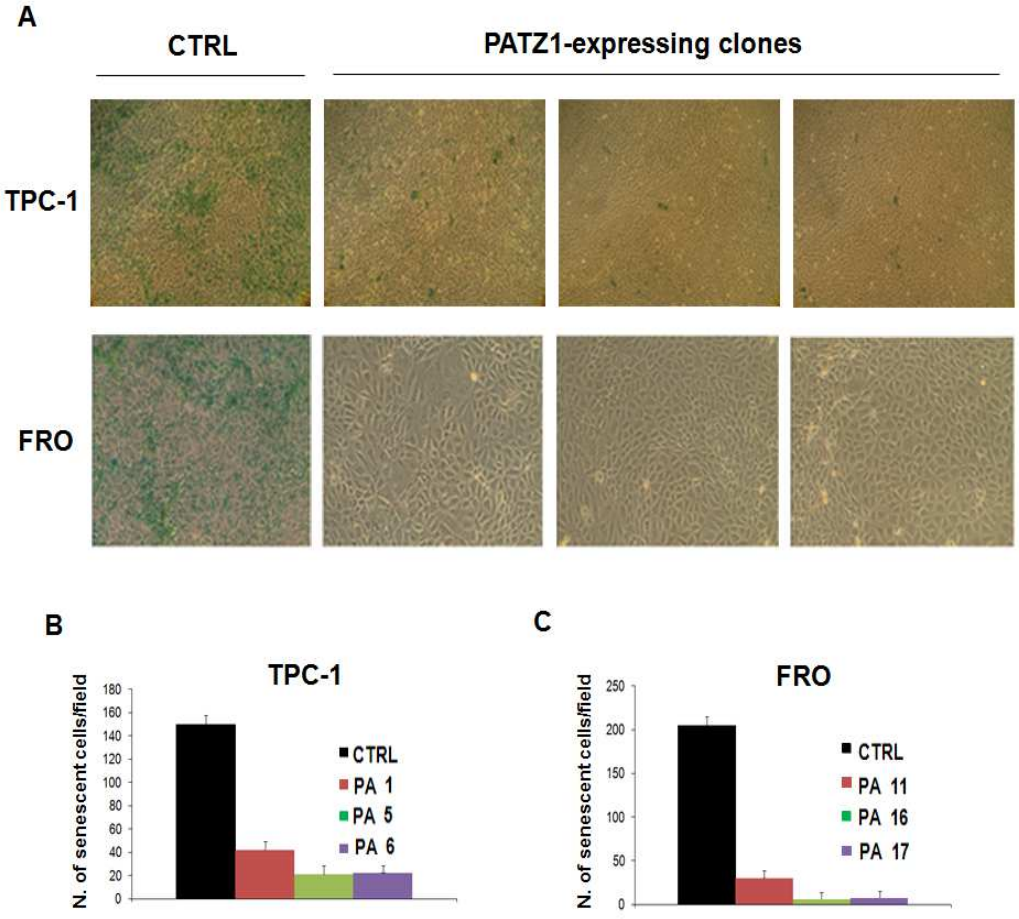

Figure 11. *PATZ1* inhibits cellular senescence in TPC-1 and FRO cells. A, senescence-associated β-galactosidase (SA-beta-gal)-staining performed on different stably expressing PATZ1 cell clones of TPC1 (PA 1, PA 5, PA 6) and FRO (PA 11, PA 16, PA 17) compared to control cells expressing the empty vector (CTRL). Representative images are reported. B, Quantification of SA-β-gal positive cells. Values are the mean +/- S.D. of three independent experiments. At least 20 different fields were analyzed for each experimental point.

4.6 PATZ1 inhibits cell migration and invasion in papillary and anaplastic thyroid cancer cells

Cell migration and invasiveness are key features of cancer cells responsible for tumor progression and metastasis (Bravo-Cordero et al. 2012). To analyze whether PATZ1 re-expression affects the migratory and invasive capabilities in PTC- and ATC-derived cell lines, a transwell migration and invasion assays have been performed. Specifically, the migration has been analyzed by a Transwell assay using the Boyden chamber composed of a polycarbonate membrane with pores of 8μm in size. The cells, plated in serum-free medium, were analyzed 24 hours later for their ability to have crossed the membrane attracted by the serum placed below, on the bottom of the plate. For each 200X field the migrated cells were counted.

The results of this migration assay were concordant for all the three cellular systems: indeed TPC-1/PATZ1, BC-PAP/PATZ1 and FRO/PATZ1 clones showed a drastic reduction in their migration capability compared to controls (Fig. 12). Then, to analyze whether the presence of PATZ1 could interfere also with the cell invasiveness, we conducted a similar assay through the Boyden chamber in the presence of Matrigel, a mixture of gelatin protein that mimics the extracellular. Also in the presence of Matrigel, TPC-1/PATZ1 and FRO/PATZ1 cells showed a lower invasive capacity than control cells. BC-PAP cells were not able to invade at the experimental conditions used.

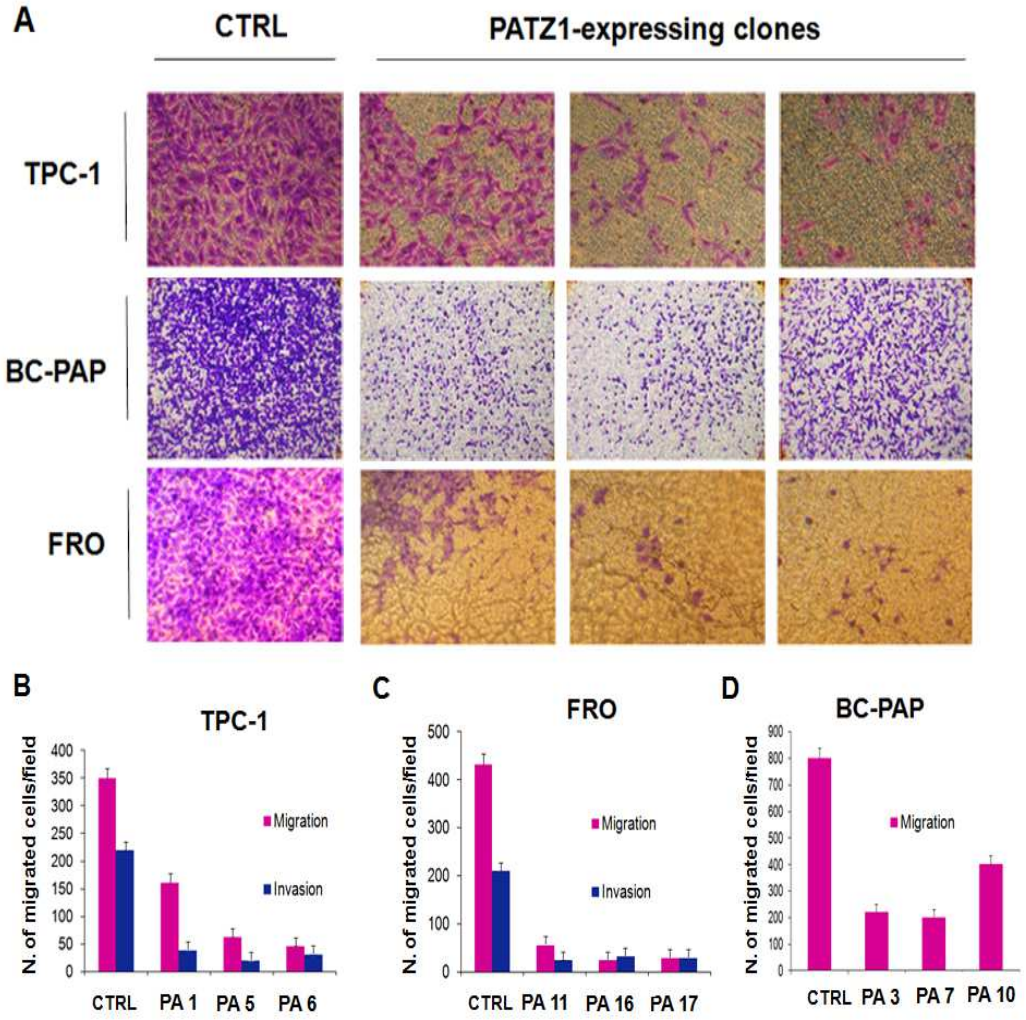

Figure 12. *PATZ1* inhibits cell migration and invasion in TPC-1, BC-PAP and FRO cells. A, transwell assays performed on different stably expressing PATZ1 cell clones of TPC1 (PA 1, PA 5, PA 6), BC-PAP (PA 3, PA 7, PA 10) and FRO (PA 11, PA 16, PA 17) compared to control cells expressing the empty vector (CTRL). Representative images are reported. B, C, D, the graphs show the mean values of three independent transwell or invasive assays by counting the number of cells that have migrated underneath the Boyden chamber in absence (purple bars) or in presence (blue bars) of matrigel.

4.7 PATZ1 expression in anaplastic thyroid cancer cells inhibits tumorigenicity *in vitro and in vivo*

In order to confirm the hypothesis that PATZ1 may have a tumor-suppressor function in thyroid cells, the transformed phenotype of the tumorigenic ATC-derived FRO cells was analyzed both *in vitro* and *in vivo*. *In vitro,* the tumorigenicity has been tested with a soft agar assay, a common method to monitor anchorage-independent growth, by measuring cell proliferation in a semisolid culture medium. As shown in Fig. 13 (Panels A-B), FRO/PATZ1 clones were not able to grow in soft agar differently from the parental cell line expressing the backbone vector. To confirm *in vivo* the loss of the tumorigenic potential in FRO cells mediated by *PATZ1* re-expression, FRO/PATZ1 and control cells were subcutaneously inoculated in athymic mice (on the right and left side, respectively, of the same mouse), and tumor dimensions were measured every day to analyze their growth rate. When a tumor reached a diameter of 1500 mm, the mouse was sacrificed, and the tumors of both sides removed, weighted and frozen or embedded into paraffin. Consistent with the *in vitro* results, the growth rate of tumors developed from FRO/PATZ1 cells was significantly inhibited compared to those originated from control cells (Fig. 13, panel C-D).

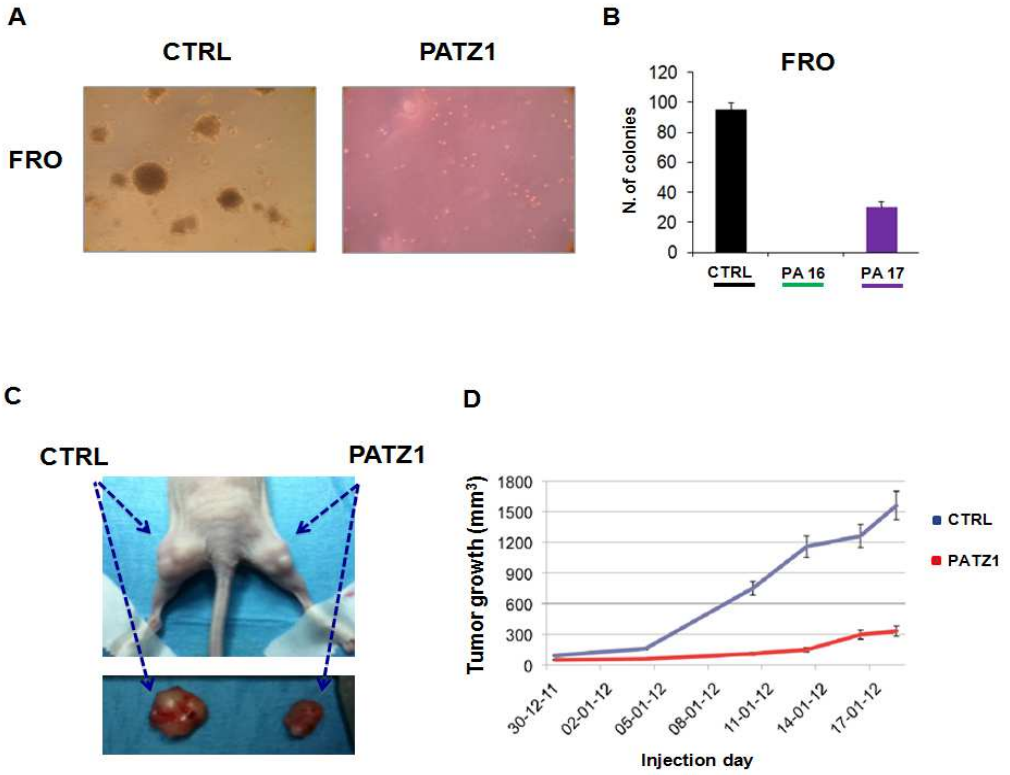

Figure 13. PATZ1 expression blocks tumorigenesis of FRO cells *in vitro* and *in vivo.* A, representative images of growth in soft agar of FRO clones expressing PATZ1 or the empty vector (CTRL). B, colonies with a diameter greater than 20 μm were counted after 2 weeks. C, D *In vivo* tumorigenic assay: inoculation of FRO cells expressing the empty vector (CTRL) or PATZ1 in athymic nude mice. C, A representative mouse and its derived xenografts. D, Tumor growth curves in cohorts of 10 mice. Mean values ± SD.

Subsequently, the tumors removed and embedded into paraffin were processed and examined for morphologic characterization by hematoxylin and eosin (H&E) staining in collaboration with the research group of Doctor G. Chiappetta at the Istituto dei Tumori di Napoli. Interestingly, as shown in Fig. 14, some tissues derived from tumors developed in athymic mice injected with FRO/PATZ1 cells, displayed features of epithelial differentiation. Conversely, tumors generated in athymic mice injected with FRO control cells, showed a disorganized and solid growth pattern.

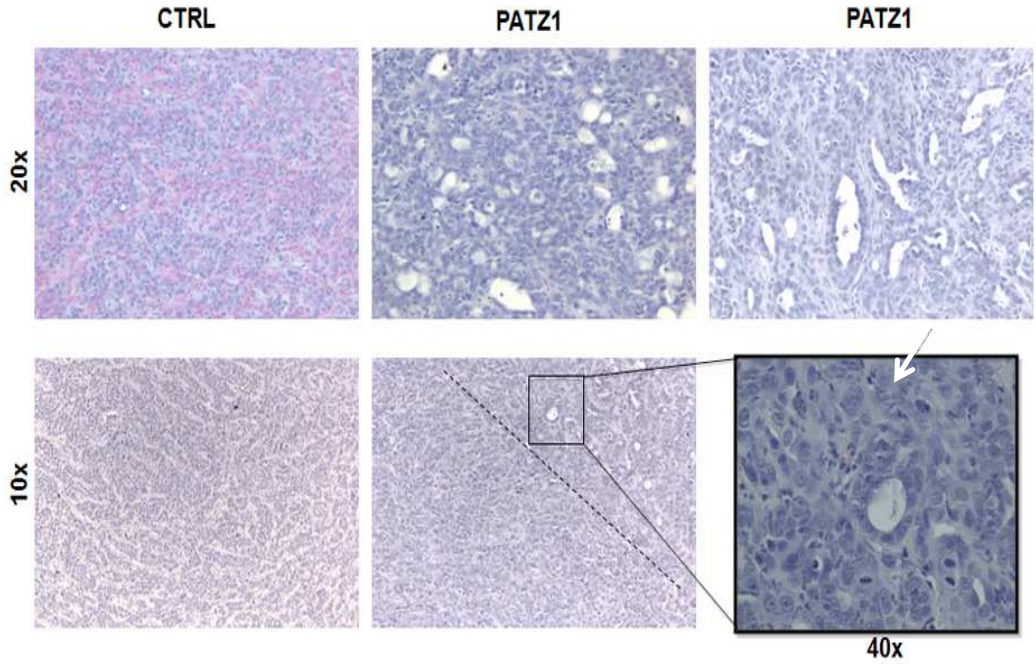

Figure 14. H&E staining of tumors developed in athymic mice. Representative images of tumors tissue derived from athymic mice injected with FRO/PATZ1(PATZ1) or control cells (CTRL). The tumors developed from FRO/PATZ1 cells showed features of a more differentiated morphology respect to those originated from control cells. In the same FRO/PATZ1 xenograft is possible to see the coexistence of both a disorganized solid pattern, similar to xenografts from CRTL cells (left side of the dotted line), and features of epithelial differentiation represented by follicular-like structures (indicated by the arrow in the outset).

Consistently, while FRO/CTRL cells expressed E-cadherin at low levels, suggesting a mesenchymal phenotype, FRO/PATZ1 cells strongly expressed E-cadherin as detected by Western blot, pointing to an epithelial differentiation through PATZ1 re-expression (Fig. 15). These data support the hypothesis that PATZ1 may have a tumor-suppressor function in thyroid cells.

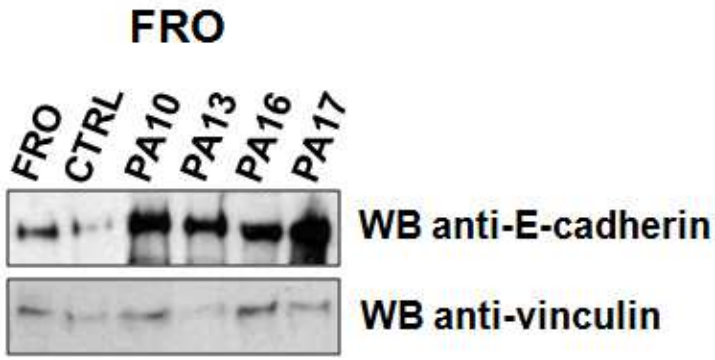

Figure 15. Expression of E-cadherin in FRO/PATZ1clones. Western Blot analysis of E-cadherin in 4 FRO/PATZ1 cell clones (PA10, PA13, PA16, PA17) compared to FRO cell line not transfected (FRO) or a clone transfected with the empty vector (CTRL).

4.8 *BAX*, *PUMA* and *PERP* are *up*-regulated in PATZ1-transfected FRO cells

To investigate the molecular mechanisms by which PATZ1 exerts its tumor suppressor role in thyroid carcinogenesis, since it is a transcriptional regulator, we looked for the genes specifically regulated by it. By in silico analysis through the TraFaC homology Server (Jegga et al., 2002), we found a number of genes with putative binding sites for PATZ1. Among them we focused on some p53-regulated genes, including *PUMA* and *PERP,* which could explain the role of PATZ1 in the thyroid cell transformation and in particular in the mechanisms of apoptosis and migration. Moreover, we decided to focus our attention also on another p53-regulated and proapoptotic gene, *BAX*, because our recent unpublished data showed the regulation of *BAX* promoter activity by PATZ1 in HEK293 and SAOS-2 cells. Therefore, we evaluated whether PATZ1 regulates the expression of these genes in FRO cells, in which, as I showed before, we observed that the restoration of PATZ1 expression is able to induce apoptosis. To this aim RNA was extracted from FRO/PATZ1 clones and their controls, and qRT-PCR was performed. As shown in Fig. 15, PATZ1 re-expression up-regulates *BAX*, *PUMA* and *PERP* mRNA levels in these cells, thus suggesting a positive role for PATZ1 in the transcriptional expression of these genes (Fig. 16).

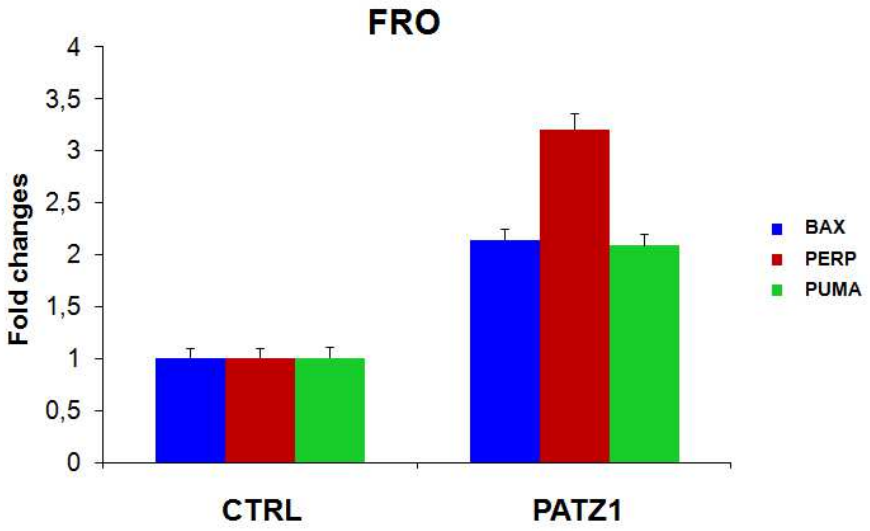

Figure 16. Up-regulation of *BAX, PERP* and *PUMA* gene expression in FRO/PATZ1clones. qRT-PCR results showing the significant increase of *BAX*, *PERP* and *PUMA* expression in FRO clones expressing PATZ1 compared to controls (CTRL).

4.9 *BAX, PUMA* and *PERP* gene expression depends upon the presence of PATZ1

To support the hypothesis of a role for PATZ1 in *BAX*, *PUMA* and *PERP* gene expression regulation, we analyzed *BAX*, *PUMA* and *PERP* expression in PATZ1-knockout mice, previously generated in our laboratory. In particular we compared *BAX*, *PUMA* and *PERP* mRNA levels in *PATZ1* (+/+), (+/-) and (-/-) MEFs. As shown in Fig. 17, the expression of these genes is significantly changed in both Patz1 (+/-) and Patz1 (-/-) MEFs compared to wild-type controls. In particular, *BAX* and *PUMA* are down-regulated, confirming *PATZ1* as an activator of their expression. Conversely, *PERP* is up-regulated, suggesting PATZ1 as an inhibitor of *PERP* expression, which is in contrast with what we observed in thyroid cells. This difference may be due to the different cellular context as PATZ1 may act as an architectural transcription factor and its action may mainly depend on its interactors, which may differ from cell to cell. It is noteworthy that in Patz1 +/- and Patz1 -/- cells the expression levels of *BAX*, *PERP* and *PUMA* were

undistinguishable, indicating that down-regulation of PATZ1 expression has the same effect as loss of PATZ1 expression on their transcriptional regulation.

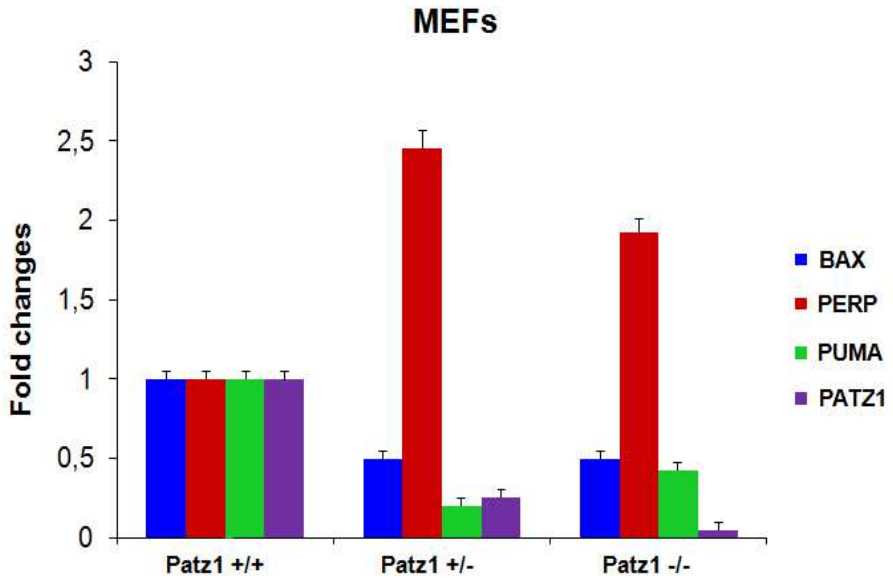

Figure 17. Down-regulation of *BAX* and *PUMA* expression, and up-regulation of *PERP* expression in Patz1-knockout MEFs. qRT-PCR results showing decrease of *BAX* and *PUMA*, and the increase of *PERP* expression in MEFs heterozygous (+/-) and homozygous (-/-) for a Patz1-null mutation.

4.10 PATZ1 binds to the promoters of *BAX*, *PUMA* and *PERP*

To evaluate whether the role played by PATZ1 in the regulation of *BAX*, *PUMA* and *PERP* gene expression depends on a direct binding of PATZ1 to their promoter regions, we performed ChIP assays. HEK293 cells were transiently transfected with HA-tagged-PATZ1, crosslinked and immunoprecipitated with anti-HA or non specific IgG antibodies as control. Immunoprecipitation of chromatin was then analyzed by quantitative PCR, using primers spanning the -250/-530 region of *BAX* and the -950/-700 region of *PERP*. Occupancy of these promoter regions by *PATZ1* was clearly detectable in anti-HA precipitated chromatin. No precipitation was observed with IgG precipitates (Fig. 18, Panel A). The binding of PATZ1 to *PUMA* promoter was evaluated by electrophoresis

mobility shift assay (EMSA), analyzing a region spanning nucleotides from -50/-24 which contains two putative PATZ1 binding sites and one p53 consensus sequence. As shown in Fig. 18, panel B, a PATZ1-recombinant peptide (spanning from aa 259 to aa 367) was able to bind the ^{32}P-end-labelled double strand *PUMA* promoter oligonucleotide. Binding specificity was demostrated by competition experiments showing loss of binding with the addition of a 200-fold molar excess of unlabelled *PUMA* promoter oligonucleotide.

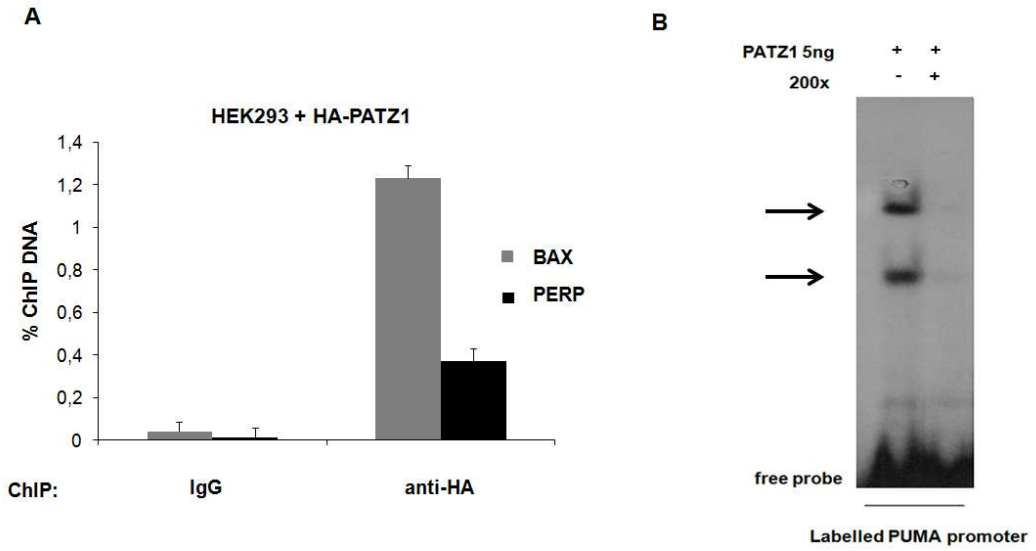

Figure 18. Binding of PATZ1 on *BAX*, *PERP* and *PUMA* promoters. A, ChIP assay on HEK293 transfected with HA-tagged-PATZ1. After transfection cells were crosslinked and immunoprecipitated using anti-HA antibody. As an immunoprecipitation control non specific IgG was used. B, EMSA performed with a radiolabelled oligonucleotide spanning from -50 to -24 of the human PUMA promoter incubated with 5 ng of a recombinant PATZ1 peptide. The arrows indicate the PATZ1/DNA complexes. To assess the specificity of the binding, the reaction mixture was preincubated with a 200X-fold excess of unlabelled oligonucleotide used as competitor.

4.11 PATZ1 correlates with PERP expression in human thyroid tumors

In order to verify whether PATZ1 down-regulation inversely correlates with BAX, PERP and PUMA expression in human thyroid cancer, we started to analyze

PATZ1 and PERP protein expression, by immunohistochemistry, in a few human paraffin embedded thyroid tumors representing different histological types compared to the normal thyroid gland. We found a positive correlation between PATZ1 and PERP expression, especially in ATC samples. Indeed, as shown in Fig.19, both PATZ1 and PERP are expressed in the normal thyroid, while in ATC PATZ1 and PERP expression was completely absent. These preliminary data need to be validated by further experiments increasing the number of samples in order to get a statistical significance.

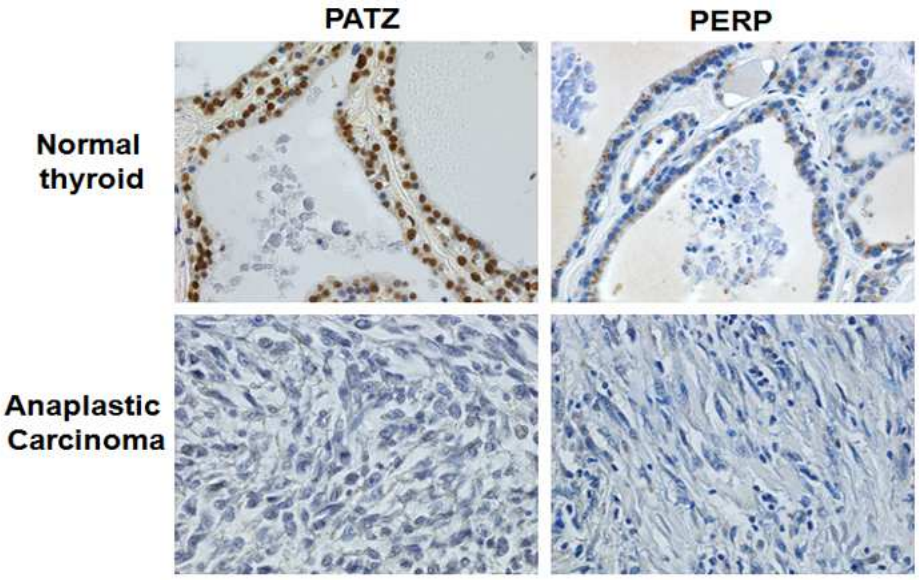

Figure 19. PATZ1 correlates with PERP expression. Representative IHC images showing the PATZ1 and PERP expression in normal thyroid and Anaplastic carcinoma (40X).

5. DISCUSSION AND CONCLUSIONS

The expression of POZ/BTB and AT-hook-containing zinc finger protein 1 (PATZ1) is frequently de-regulated in human cancer but the molecular basis of PATZ1 role in cancer still remains to be elucidated, and it is still debated if PATZ1 is a tumor suppressor or an oncogene. In a previous work we demonstrated that PATZ1 acts as a tumor suppressor in lymphomagenesis by inhibiting BCL6 expression. Moreover, the analysis of PATZ1 knock-out mice, carried out in our laboratory, provided a strong effort to the tumor-suppressor hypothesis, since PATZ1 knock-out mice spontaneously develop tumors, including BCL6-expressing Non-Hodgkin lymphomas, sarcomas, hepatocellular carcinomas and rare lung adenocarcinomas (Pero et al. 2012). To further investigate the role of PATZ1 in neoplastic transformation we decided to focus on thyroid tumors. Thyroid cancer is one of the most frequent malignancies of the endocrine system. It is a good model of multi-step carcinogenesis since it includes a wide spectrum of lesions with different phenotypic characteristics, biological behaviors and grades of malignity, but the mechanisms of pathogenesis are still far from being completely elucidated. So far, several oncogenes have been demonstrated to be involved in human thyroid carcinomas, particularly in the papillary histotype, but little is known with regard to tumor suppressor genes. In addition, about 20-25% of thyroid carcinomas seem not to present mutations or expression changes of well known oncogenes. Therefore, other mechanisms such as up- or down-regulation of some genes may have an important role in thyroid carcinogenesis. The results reported in the present study seem to support a role for *PATZ1* gene as a tumor suppressor in human thyroid carcinogenesis. Indeed, the analysis of *PATZ1* gene performed by qRT-PCR in a large number of thyroid carcinoma samples and thyroid carcinoma–derived cell lines, demonstrated that *PATZ1* is strongly down-regulated in most thyroid tumors compared with normal thyroids, and that its expression is inversely correlated with both malignancy and degree of de-differentiation. A severe reduction of *PATZ1* mRNA was observed in follicular carcinomas (FTC), in which the average down-regulation value was -20 fold changes, and anaplastic carcinomas (ATC), with a negative fold change up to 33,3, with respect to normal thyroid gland. Interesting results were obtained when PATZ1 protein expression was analyzed by immunohistochemistry. We found that in human thyroid carcinomas PATZ1 protein not only is downregulated but also presents a different localization. Indeed, in all normal thyroid tissues PATZ1 was strongly expressed only in the nucleus; in all differentiated carcinomas (both papillary and follicular) PATZ1 was present both in the nucleus and in the cytoplasm, while in undifferentiated carcinomas (poorly differentiated and anaplastic) more than 50% of the PATZ1 protein was localized in the cytoplasm. Moreover, in 62,5% of anaplastic carcinomas PATZ1 expression was completely

absent. Presently, we have no data that allow us to understand whether this new cellular localization PATZ1 can play an active role or whether it just stucks there in a state of inactivity. However, it has been recently demonstrated an interaction between PATZ1 and the RIα subunit of PKA under the proliferative stimulus induced by the cAMP (Yang et al, 2009); as a result of this interaction, PATZ1 is sequestered in the cytoplasm, losing the ability to regulate target genes, therefore supporting its role as a tumor suppressor.

To determine whether PATZ1 may contribute to thyroid carcinogenesis, we restored PATZ1 expression, by stable transfection, in two representative cell lines of papillary thyroid carcinoma (TPC-1 and BC-PAP) and two representative of anaplastic thyroid carcinoma (FB1 and FRO), selected specific clones of each cell lines re-expressing PATZ1, and characterized their growth and transformed properties. The first step has been the analysis of proliferation and survival of clones expressing PATZ1 compared to control cells. The cell division (proliferation) is a physiological process that occurs in almost all tissues. Normally, the balance between proliferation and programmed cell death, usually apoptosis, is strictly maintained by adjusting both processes to ensure tissues homeostasis. Mutations that lead to cancer, lead to impairment of these orderly processes, destroying their regulatory programs (Fearon et al. 1990). Therefore, the analysis of these cellular processes (proliferation and survival) was crucial to understand whether PATZ1 is involved in mechanisms underlying the pathogenesis of neoplasia. To this aim, we performed colony assays, growth curves and cell viability assays. On selected clones of TPC-1/ PATZ1 and control cells we showed no differences in growth and survival, suggesting that in this cell line PATZ1 does not have a role in these processes, generally associated with the early stages of tumor development. Conversely, colony assays and growth curves performed in BC-PAP/PATZ1 and FRO/PATZ1 clones showed a significant decreased proliferation capacity that, only in the case of FRO/PATZ1 transfectants, was accompanied by a significant increase in cell death compared to controls. To understand whether a mechanism of apoptosis was responsible of the low survival of these cells, we performed DNA-ladder assay. Apoptosis is an ordered and orchestrated cellular process that occurs in physiological and pathological conditions. The down-regulation of a tumor suppressor gene can result in reduced apoptosis and enhanced tumor growth and development (Wong SY 2011). The assay showed no differences in TPC1/PATZ1 and BC-PAP/PATZ1 clones compared to their control, whereas strong DNA-laddering was observed in FRO/PATZ1 cells compared to controls, indicating that a mechanism of apoptosis is responsible for the low survival of these cells. Further studies are necessary to understand the decreased growth rate of BC-PAP cells re-expressing PATZ1 looking at the different phases of the cell cycle by fluorocitometric assays. These

assays will also be performed in FRO/PATZ1 cells, to analyze if the decreased cell growth may be due to a proliferative defect, other than the induction of apoptosis.

Very striking results were obtained from senescence assays. Cellular senescence is an irreversible state of cell proliferation arrest, which can be caused by diverse factors, such as telomere shortening or dysfunction, oncogenic activation, chromatin perturbation, DNA damage, oxidative or inflammatory stresses, irradiation and so on (Collado et al. 2006). A large body of evidence suggests that the activation of various oncogenes induces an increase of senescence in cell lines, accompanied by a reduction in the expression and activity of tumor suppressor genes such as p53 and p16. This phenomenon may be a mechanism of protection of cells against neoplastic transformation (Campisi et al. 2007; Serrano et al. 1997). TPC-1 and FRO cells re-expressing PATZ1 showed a reduction in the β-galactosidase activity compared to controls, while both BC-PAP/PATZ1 transfectants and controls not showed positive staining for β-galactosidase. However, it has already demostrated that the parental BC-PAP cells displayed a very minimal β-galactosidase activity (Nowicki et al. 2011). The result obtained with TPC1/PATZ1 and FRO/PATZ1 clones is consistent with our recent data, showing that *PATZ1* (-/-) embryonic fibroblasts (MEFs) enter into premature cellular senescence (Valentino et al. 2012), and with previous data showing growth inhibition and accelerated senescence in human umbilical vascular endothelial cells (HUVECs) interfered for PATZ1 expression (Cho et al. 2011), thus confirming an anti-senescent role for PATZ1. This role of PATZ1 is apparently in contrast with its tumor suppressor function, since senescence is one of the main barriers to tumor progression. However, previous data showed that a tumor suppressor gene can inhibit senescence and simultaneously block other functions related to the development and/or progression of the tumor (Pan et al. 2011).

In this work we also demonstrated an inhibitory effect of PATZ1 re-expression on cell migration and invasiveness. Cell migration and invasiveness are key features of cancer cells responsible for tumor progression and metastasis (Bravo-Cordero et al. 2012). The process that leads cancer cells to migrate from the tumor site of origin to other sites begins with an epithelial-mesenchymal transition (EMT), a process during which cells undergo drastic changes, such as the alteration of the cell-cell and cell-extracellular matrix adhesion, the remodeling of the cytoskeleton and various molecular processes (Ylmaz and Christofori 2010). All the thyroid cell lines re-expressing PATZ1, TPC-1, BC-PAP and FRO showed a drastic reduction in their migration and invasiveness capability compared to controls. Moreover, PATZ1 expression in tumorigenic FRO cells inhibits both tumorigenicity *in vitro* and *in vivo.* Indeed**,** FRO re-expressing PATZ1 are not able to grow in soft agar, and inhibits tumors growth when injected into athymic mice, thus supporting a tumour suppressor role for PATZ1 in thyroid carcinogenesis.

Interestingly, some tumor tissues derived from FRO/PATZ1 cells injected in athymic mice, displayed features of epithelial differentiation, while tumors arisen starting from FRO control cells injected in athymic mice, showed a disorganized and solid growth pattern, suggesting a role of PATZ1 in negatively regulating the EMT and the tumor progression. Consistently, while FRO and FRO/CTRL cells expressed E-cadherin at low levels, suggesting a mesenchymal phenotype, PATZ1-transfected cells strongly expressed E-cadherin as detected by Western blot, pointing to an epithelial differentiation through PATZ1.

Thus, PATZ expression *in vitro* affected several hallmarks of malignancy, including anchorage-independent proliferation, survival, EMT and invasion. Therefore, we suggest that the loss of *PATZ1* expression exerts a functional role in the pathogenesis of thyroid cancer, and they are consistent with a specific role of PATZ1 in the signaling pathways involved in cell survival and metastatic progression. In particular, we hypothesize that down-regulation of PATZ expression could be an expedient of the cancer cells to escape apoptosis and go towards the epithelial-mesenchimal transition (EMT), which allows the cells to acquire the ability to migrate.

To dissect the molecular pathways that involves PATZ in both cell survival and metastatic progression, since PATZ is a transcriptional regulator, we looked for the genes directly regulated by it, which could explain the role of PATZ in the thyroid cell transformation. Among the genes with putative binding sites for PATZ1, we focused on some p53-regulated genes. After its activation, p53 is able to regulate various processes, such as cell cycle arrest, DNA repair, apoptosis, senescence, EMT, migration, invasiveness and metastasis (Zilfou et al. 2009). Under physiological conditions, p53 inhibits, directly or indirectly, repressors of the E-Cadherin protein, such as SLUG, TWIST and Snail. Otherwise, a loss of expression or function of p53, or the presence of a p53 mutant, determines the activation of such repressors; thereby is observed a decrease in the expression of E-Cadherin and a consequent loss of cell-cell junctions (Muller et al. 2011).

In this work we demonstrated that PATZ1 binds to the promoter regions of the p53-regulated genes *BAX*, *PUMA* and *PERP*. In FRO/PATZ1 cells all these genes were up-regulated, suggesting a positive role of PATZ1 on their expression. In another cell systems, such as MEFs, wild-type or knockout for the PATZ1 gene, we found again a positive role of PATZ1 on *BAX* and *PUMA* expression, being them down-regulated in PATZ1-KO cells, whereas *PERP* was down-regulated, suggesting a negative role of PATZ in its transcription. This difference may be due to the different cellular context, since PATZ1 likely acts as an architectural transcription factor and its activity mainly may depend on its interactors.

BAX, PUMA and PERP are down-stream effectors of p53 involved in apoptosis and, as far as PERP is concerned, also in cell motility and migration. There are already some evidences suggesting that PATZ1 and p53 are functionally

related. Indeed, other members of the POZ/BTB domain-containing protein family (HIC1, PLZF, BACH1, NAC-1 and BCL6) have been linked directly or indirectly to the p53 regulation (Kelly et al. 2006). Moreover, it has been recently shown that PATZ1 inhibits endothelial cell senescence through a p53 dependent pathway. In particular, Cho et al. have demonstrated that in HUVEC cells PATZ1 knockdown decreased cell proliferation and accelerates senescence unlike p53 knockdown cells; further, PATZ1 increased p53 protein levels in p16 knockdown cells (Cho et al. 2011). Therefore, we speculate that PATZ1 is present in the same complex with p53 on the promoter regions of *BAX*, *PUMA* and *PERP* and may exert its tumor-suppressor role cooperating with p53. This hypotesis is supported by our findings showing that PATZ1 and p53 interacts each other and that PATZ1 is able to cooperate with p53 in the transcriptional activation of *BAX* promoter. (Palmieri et al., manuscript in preparation). To verify our hypothesis, next experiments will investigate whether PATZ1 occupies *BAX*, *PERP* and *PUMA* promoter regions together with p53 and whether PATZ1 acts on *PERP* and *PUMA* promoters exactly as it does on *BAX* promoter. Moreover, we will confirm the ChIP data in FRO cells, and eventually in other thyroid cancer cells, expressing PATZ1, to ensure that the proposed mechanism of PATZ is active in the thyroid system. Furthemore, we will perform Elettroforetic Mobility Shift Assays (EMSA) in order to confirm the binding of PATZ1 to *BAX* and *PERP* promoters and, using mutated probes, identify the nucleotides important for this binding. Interestingly, we also planned to verify whether PATZ1 down-regulation inversely correlates with BAX, PERP and PUMA expression in human thyroid cancer samples at both mRNA and protein levels by qRT-PCR and immunohistochemistry analysis. Preliminary immunohistochemical data showed a positive correlation between PATZ1 and PERP expression in some anaplastic thyroid samples compared to normal thyroid samples, but further analysis, increasing the number of samples, are needed to validate these data.

In conclusion, in this study we demonstrated a role for PATZ1 as a tumor suppressor in human thyroid carcinogenesis. Our data indicated that the reduced PATZ1 gene expression is associated with a malignant phenotype of thyroid neoplasias and its delocalizzation into the cytoplasm may be an expedient of the neoplastic cell to inactivate its function. On the contrary, if re-expressed, PATZ1 is able to induce apoptosis, to inhibit cell migration and invasiveness and block tumorigenesis *in vitro* and *in vivo*, thus allowing a regression in neoplastic transformation. Moreover, we propose that the apoptosis induction, observed in FRO cells following PATZ1 expression, could be due to the induction of *BAX*, *PUMA* and/or *PERP* expression. Likewise, the inhibition of FRO cells migration may be due to induction of *PERP* expression.

From this study we envisage for the future a role for PATZ1 as a new diagnostic and/or prognostic factor of thyroid cancer, and figure out the up-regulation of PATZ1 expression as a therapeutic approach for advanced stages of cancer.

6. ACNOWLEDGEMENTS

I acknowledge with gratitude Prof. Massimo Santoro, coordinator of the Molecular Oncology and Endocrinology Doctorate Program, for the beautiful opportunity that gave me to work at the Dipartimento di Medicina Molecolare e Biotecnologie Mediche of the Università degli Studi di Napoli Federico II.

A special thank goes to my supervisor Dr. Monica Fedele for having encouraged my interest in research and whose passion and enthusiasm I had the privilege to appreciate since I started taking part of her group.

I wish to present my sincere thank to Prof. Alfredo Fusco who gave me the opportunity to work in his group since when I was an undergraduate student. His great knowledge of oncology, his enthusiasm and his kindness are really unique.

I also thank Prof. Carlo Croce for a very pleasant work experience and for the kind hospitality of his laboratory at the Ohio State University.

I would like to thank Dr. Gennaro Chiappetta's group of Istituto Nazionale dei Tumori, Fondazione "G. Pascale" of Naples for their great collaboration with human thyroid carcinoma samples.

I thank all my collegues and friends of "LAB1", Floriana, Francesco, Mara, Raffaele, Marco, Mariagrazia, Nicola and all the others of LAB2, LAB3 and LAB4 for their support, the scientific and moral help, but especially for the kind moments together.

My thank goes to Dr. Dario Palmieri that has been my first guide in my scientific way. I miss him and I never forget his teachings and advices.

A special thank is for my colleague and friend Michela that faced this and other works with me shoulder-to shoulder. I thank her for the great technical and scientific support and because without her I feel lost!

I thank my friends Mara, Valentina, Costantina, Francesca and Nunzio for their wonderful friendship, for precious and stimulating suggestions and because they close to me in good and bad times. ("Francesca thank you for all time you wasted with my thesis!").

Finally I want to express my special grateful to my family, my dad, my mom, my sisters Antonia and Valentina for their continuous teachings and encouragement and because they are my greatest love!

7. REFERENCES

Ain KB. Anaplastic thyroid carcinoma: a therapeutic challenge. Seminars in Surgical Oncology 1999 16 64–69.

Amsel AD, Rathaus M, Kronman N, Cohen HY. Regulation of the proapoptotic factor Bax by Ku70-dependent deubiquitylation. Pnas 2008;105(13):5117-22.

Attardi LD, Reczek EE, Cosmas C, Demicco EG, McCurrach ME, Lowe SW, Jacks T. PERP, an apoptosis-associated target of p53, is a novel member of the PMP-22/gas3 family. Genes Dev. 2000 Mar 15;14(6):704-18.

Beaudry VG, Jiang D, Dusek RL, Park EJ, Knezevich S, Ridd K, Vogel H, Bastian BC, Attardi LD. Loss of the p53/p63 regulated desmosomal protein Perp promotes tumorigenesis. PLoS Genet. 2010 Oct 21;6(10):e1001168.

Bilic I, Koesters C, Unger B, Sekimata M, Hertweck A, Maschek R, Wilson CB, Ellmeier W. Negative regulation of CD8 expression via Cd8 enhancer-mediated recruitment of the zinc finger protein MAZR. Nat Immunol 2006; 7:392-400.

Bravo-Cordero JJ, Hodgson L, condeelis J. Directed cell invasion and migration during metastasis. Curr Opin Cell Biol 2012; 24(2):277-83.

Burrow AA, Williams LE, Pierce LC, Wang YH. Over half of breakpoints in gene pairs involved in cancer-specific recurrent translocations are mapped to human chromosomal fragile sites. BMC Genomics 2009;10:59.

Campisi J, d'Adda di Fagagna F. Cellular senescence: when bad things happen to good cells. Nat Rev Mol Cell Biol. 2007;8(9):729-40.

Carcangiu, M. L., Zampi, G. & Rosai, J. Poorly differentiated (‘insular’) thyroid carcinoma. A reinterpretation of Langhans’ ‘wuchernde Struma’. Am. J. Surg. Pathol. 1984; 8, 655–668.

Cho JH, Kim MJ, Kim KJ, Kim JR.;POZ/BTB and AT-hook-containing zinc finger protein 1 (PATZ1) inhibits endothelial cell senescence through a p53 dependent pathway. Cell Death Differ 2012;19(4):703-12.

Choy EY, Siu K, Kok K, Lung RW, Tsang CM, To K, et al. An Epstein–Barr virus-encoded microRNA targets PUMA to promote host cell survival. J Exp Med 2008;205:2551–2560.

Ciampi R, Knauf JA, Kerler R, Gandhi M, Zhu Z, Nikiforova MN, Rabes HM, Fagin JA &Nikiforov YE. Oncogenic AKAP9-BRAF fusion is a novel mechanism of MAPK pathway activation in thyroid cancer. Journal of Clinical Investigation 2005; 115 94–101.

Collado M, Serrano M. The power and the promise of oncogene-induced senescence markers. Nat Rev Cancer. 2006; 6(6):472-6.

Costoya JA. Functional analysis of the role of POK transcriptional repressors. Brief Funct Genomic Proteomic. 2007;6(1):8-18.

DeLellis RA, Lloyd RV, Heitz PU & Eng C. Thyroid and parathyroid tumours. In World Health Organization. Classification of Tumours. Pathology and Genetics of Tumours of Endocrine Organs. 2004. pp 51–56. Lyon, France: IARC Press.

Dobashi Y, Sakamoto A, Sugimura H, Mernyei M, Mori M, Oyama T, Machinami R. Overexpression of p53 as a possible prognostic factor in human thyroid carcinoma. Am J Surg Pathol. 1993;17(4):375-81.

Donghi R, Longoni A, Pilotti S, Michieli P, Della Porta G & Pierotti MA . Gene p53 mutations are restricted to poorly differentiated and undifferentiated carcinomas of the thyroid gland Journal of Clinical Investigation 1993; 91: 1753–1760.

Dusek RL, Bascom JL, Vogel H, Baron S, Borowsky AD, Bissell MJ, Attardi LD. Deficiency of the p53/p63 target Perp alters mammary gland homeostasis and promotes cancer. Breast Cancer Res. 2012 Apr 20;14(2):R65.

Esposito F, Boscia F, Gigantino V, Tornincasa M, Fusco A, Franco R, Chieffi P.The high-mobility group A1-estrogen receptor β nuclear interaction is impaired in human testicular seminomas. J Cell Physiol. 2012 Dec;227(12):3749-55.

Fagin JA, Matsuo K, Karmakar A, Chen DL, Tang SH & Koeffler HP. High prevalence of mutations of the p53 gene in poorly differentiated human thyroid carcinomas. Journal of Clinical Investigation 1993; 91:179–184.

Farmer G, Bargonetti J, Zhu H, Friedman P, Prywes R, Prives C. Wild-type p53 activates transcription in vitro. Nature 1992; 358-83-6.

Fearon ER, Vogelstein B. A genetic model for colorectal tumorigenesis. Cell 1990 61 (5): 759–67.

Fedele M, Benvenuto G, Pero R, Majello B, Battista S, Lembo F, Vollono E, Day PM, Santoro M, Lania L, Bruni CB, Fusco A and Chiariotti L. A novel member of the BTB/POZ family, PATZ, associates with the RNF4 RING finger protein and acts as a transcriptional repressor. J Biol Chem 2000; 275:7894-7901.

Fedele M, Franco R, Salvatore G, Paronetto MP, Barbagallo F, Pero R, Chiariotti L, Sette C, Tramontano D, Chieffi G, Fusco A, Chieffi P.PATZ1 gene has a critical role in the spermatogenesis and testicular tumours. J. Pathol. 2008; 215:39-47.

Fernandez PC, Frank SR, Wang L, Schroeder M, Liu S, Greene J. Genomic targets of the human c-Myc protein. Genes Dev 2003;17:1115–1129.

Foulkes WD, Ragoussis J, Stamp GW, Allan GJ, Trowsdale J. Frequent loss of heterozygosity on chromosome 6 in human ovarian carcinoma. Br J Cancer 1993;67(3):551-9.

Frasca F, Rustighi A, Malaguarnera R, Altamura S, Vigneri P, Del Sal G, Giancotti V, Pezzino V, Vigneri R, Manfioletti G. HMGA1 inhibits the function of p53 family members in thyroid cancer cells. Cancer Res. 2006;66(6):2980-9.

Grieco M, Santoro M, Berlingieri MT, Melillo RM, Donghi R, Bongarzone I, Pierotti MA, Della Porta G, Fusco A & Vecchio G. PTC is a novel rearranged form of the ret proto-oncogene and is frequently detected in vivo in human thyroid papillary carcinomas. Cell 1990;60 557–563.

Hayakawa J, Mittal S, Wang Y, Korkmaz KS, Adamson E, English C, et al. Identification of promoters bound by c-Jun/ATF2 during rapid large-scale gene activation following genotoxic stress. Mol Cell 2004;16:521–535.

Hermann S, Sturm I, Mrozek A, Klosterhalfen B, Hauptmann S, Dorken B, Daniel PT. Bax expression in benign and malignant thyroid tumors: disregulation of wild-type P53 is associated with high Bax and p21 expression in thyroid carcinoma. Int J Cancer. 2001; 92:805-11.

Hershko T, Ginsberg D. Up-regulation of Bcl-2 homology 3 (BH3)-only proteins by E2F1 mediates apoptosis. J Biol Chem 2004;279:8627–8634.

Hickman JA. Apoptosis and tumourigenesis. Curr Opin Genet Dev. 2002;12(1):67-72.

Hoffseth LJ, Hussain SP, Harris CC. p53: 25 years after discovery. Trends Pharmacol Sci 2004; 25: 177-81.

Huynh KD, Bardwell VJ. The BCL-6 POZ domain and other POZ domains interact with the co-repressors N-CoR and SMRT. Oncogene 1998; 17:2473–2484.

ItoT, SeyamaT, Mizuno T, TsuyamaN,Hayashi T, HayashiY, Dohi K, Nakamura N & Akiyama M. Unique association of p53 mutations with undifferentiated but not with differentiated carcinomas of the thyroid gland. Cancer Research 1992; 52:1369–1371.

Kelly KF, Daniel JM. POZ for effect—POZ-ZF transcription factors in cancer and development. Trends Cell Biol 2006;16:578–87.

Kimura ET, Nikiforova MN, Zhu Z, Knauf JA, Nikiforov YE & Fagin JA. High prevalence of BRAF mutations in thyroid cancer: genetic evidence for constitutive activation of the RET/PTC-RAS-BRAF signaling pathway in papillary thyroid carcinoma. Cancer Research 63:1454–1457.

Kobayashi A, Yamagiwa H, Hoshino H, Muto A, Sato K, Morita M, Hayashi N, Yamamoto M, Igarashi K. A combinatorial code for gene expression generated by transcription factor Bach2 and MAZR (MAZ-related factor) through the BTB/POZ domain. Mol Cell Biol 2000; 20:1733-1746.

Kondo T, Ezzat S & Asa SL. Pathogenetic mechanisms in thyroid follicular-cell neoplasia. Nature Reviews Cancer 2006; 6: 292–306.

Kroll TG, Sarraf P, Pecciarini L, Chen CJ, Mueller E, Spiegelman BM & Fletcher JA. PAX8–PPARgamma1 fusion oncogene in human thyroid carcinoma. Science 2000; 289:1357–1360.

Levine AJ. P53, the cellular gatekeeper for growh and division. Cell 1997; 88:323-31.

Lindsten T, Ross AJ, King A, Zong WX, Rathmell JC, Shiels HA, Ulrich E, Waymire KG, Mahar P, Frauwirth K, Chen Y, Wei M, Eng VM, Adelman DM, Simon MC, Ma A, Golden JA, Evan G, Korsmeyer SJ, MacGregor GR, Thompson CB. The combined functions of proapoptotic Bcl-2 family members bak and bax are essential for normal development of multiple tissues. Mol Cell. 2000;6(6):1389-99.

Livak KJ, Schmittgen TD. Analysis of relative gene expression data using real-time quantitative PCR and the 2(-Delta Delta C(T)) Method. Methods. 2001; 25(4):402–408.

Malaguarnera R, Vella V, Vigneri R, Frasca F. p53 family proteins in thyroid cancer. Endocr Relat Cancer. 2007;14(1):43-25.

Mastrangelo T, Modena P, Tornielli S, Bullrich F, Testi, MA, Mezzelani A, Radice P, Azzarelli A, Pilotti S, Croce CM, Pierotti MA, Sozzi G. A novel zinc finger gene is fused to EWS in small round cell tumor. Oncogene 2000; 19:3799-37804.

Melino G, Bernassola F, Ranalli M, Yee K, Zong WX, Corazzari M, et al. p73 Induces apoptosis via PUMA transactivation and Bax mitochondrial translocation. J Biol Chem 2004;279:8076–8083.

Morii E, Oboki K, Kataoka TR, Igarashi K, Kitamura Y. Interaction and cooperation of mi transcription factor (MITF) and myc-associated zinc-finger protein-related factor (MAZR) for trascription of mouse mast cell protease 6 gene. J Biol Chem 2002; 277:8566-8571.

Millikin D, Meese E, Vogelstein B, Witkowski C, Trent J. Loss of heterozygosity for loci on the long arm of chromosome 6 in human malignant melanoma. Cancer Res. 1991;51(20):5449-53.

Moretti F, Farsetti A, Soddu S, Misiti S, Crescenzi M, Filetti S, Andreoli M, Sacchi A, Pontecorvi A. p53 re-expression inhibits proliferation and restores differentiation of human thyroid anaplastic carcinoma cells. Oncogene 1997;14(6):729-40.

Muller PA, Vousden KH, Norman JC. p53 and its mutants in tumor cell migration and invasion. J Cell Biol. 2011;192(2):209-18.

Murray-Zmijewski F, Lane DP, Bourdon JC. p53/p63/p73 isoforms: an orchestra of isoforms to harmonise cell differentiation and response to stress. Cell Death Differ. 2006;13(6):962-72.

Namba H, Rubin SA & Fagin JA. Point mutations of ras oncogenes are an early event in thyroid tumorigenesis. Molecular Endocrinology 1990;4:1474–1479.

Nakano K, Vousden KH. PUMA, a novel proapoptotic gene, is induced by p53. Mol Cell. 2001 Mar;7(3):683-94.

Nikiforov YE. RET/PTC rearrangement in thyroid tumors. Endocrine Pathology 2002;13: 3–16.

Nikiforov YE, Nikiforova MN. Molecular genetics and diagnosis of thyroid cancer. Nat Rev Endocrinol. 2011;7(10):569-80.

Nishida T, Nakao K, Hamaji M, Nakahara MA, Tsujimoto M Overexpression of p53 protein and DNA content are important biologic prognostic factors for thyroid cancer. Surgery 1996;119(5):568-75.

Nowicki TS, Zhao H, Darzynkiewicz Z, Moscatello A, Shin E, Schantz S, Tiwari RK, Geliebter J. Downregulation of uPAR inhibits migration, invasion, proliferation, FAK/PI3K/Akt signaling and inducessenescence in papillary thyroid carcinoma cells. Cell Cicle 2011;10(1):100-7..

Noviello C, Courjal F, Theillet C.Loss of heterozygosity on the long arm of chromosome 6 in breast cancer: possibly four regions of deletion. Clin Cancer Res. 1996;2(9):1601-6.

Olivier M, Hollstein M, Hainaut P. TP53 mutations in human cancers: origins, consequences, and clinical use. Cold Spring Harb Perspect Biol. 2010;2(1):a001008.

Oren M. Decision making by p53: life, death and cancer. Cell Death Differ 2003; 10:431-42

Paes JE, Ringel MD. Dysregulation of the phosphatidylinositol 3-kinase pathway in thyroid neoplasia. Endocrinol Metab Clin North Am 2008 Jun;37(2):375-87.

Pallante P, Visone R, Croce CM & Fusco A. Deregulation of microRNA expression in follicular cell-derived human thyroid carcinomas. Endocrine Releated Cancer 2010; 17: F91- F104.

Pan J, Zhong J, Gan LH, Chen SJ, Jin HC, Wang X, Wang LJ. Klotho, an anti-senescence related gene, is frequently inactivated through promoter hypermethylation in colorectal cancer. Tumour Biol 2011; 32:729–735.

Pero R, Lembo F, Palmieri EA, Vitiello C, Fedele M, Fusco A, Bruni CB, Chiariotti L. PATZ attenuates the RNF4-mediated enhancement of androgen receptor-dependent transcription. J Biol Chem 2002; 277:3280-3285.

Pero R, Palmieri D, Angrisano T, Valentino T, Federico A, Franco R, Lembo F, Klein-Szanto AJ, Del Vecchio L, Montanaro D, Keller S, Arra C, Papadopoulou V, Wagner SD, Croce CM, Fusco A, Chiaretti L, Fedele M. POZ-, AT-HOOK-, and zinc fingercontaining protein(PATZ) interacts with human oncogene B cell lymphoma 6 (BCL6) and is required for its negative autoregulation. J Biol Chem 2012; 287(22):18308-17.

Powell G., Wang X, Allard BL, Sahin M, Wang XL, Hay ID, Hiddinga HJ, Deshpande SS, Kroll TG, Grebe SK, Eberhardt NL, McIver B. The PAX8/PPARgamma fusion oncoprotein transforms immortalized human thyrocytes through a mechanism probably involving wild-type PPARgamma inhibition. Oncogene 2004; 23: 3634-3641.

Pierantoni GM, Rinaldo C, Mottolese M, Di Benedetto A, Esposito F, Soddu S, Fusco A. High-mobility group A1 inhibits p53 by cytoplasmic relocalization of its proapoptotic activator HIPK2. J Clin Invest. 2007;117(3):693-702.

Pollina L, Pacini F, Fontanini G, Vignati S, Bevilacqua G, Basolo F. bcl-2, p53 and proliferating cell nuclear antigen expression is related to the degree of differentiation in thyroid carcinomas. Br J Cancer. 1996;73(2):139-43.

Qiao L, Han SI, Fang Y, Park JS, Gupta S, Gilfor D, et al. Bile acid regulation of C/EBPbeta, CREB, and c-Jun function, via the extracellular signal-regulated kinase and c-Jun NH2-terminal kinase pathways, modulates the apoptotic response of hepatocytes. Mol Cell Biol 2003;23:3052–3066.

Reeves R. Molecular biology of HMGA proteins: hubs of nuclear function. Gene. 2001;277(1-2):63-81.

Renault TT, Manon S. Bax: Addressed to kill. Biochimie 2011;93(9):1379- 91.

Rocco JW, Leong CO, Kuperwasser N, DeYoung MP, Ellisen LW. p63 mediates survival in squamous cell carcinoma by suppression of p73-dependent apoptosis. Cancer Cell 2006;9:45–56.

Serrano M, Lin AW, McCurrach ME, Beach D, Lowe SW. Oncogenic ras provokes premature cell senescence associated with accumulation of p53 and p16INK4a. Cell. 1997; 88(5):593-602.

Soares P, Cameselle-Teijeiro J, Sobrinho-Simões M. Immunohistochemical detection of p53 in differentiated, poorly differentiated and undifferentiated carcinomas of the thyroid. Histopathology 1994;24(3):205-10.

Soussi T, Beroud C. Assessing TP53 status in human tumors to evaluate clinical outcome. Nat Rev Cancer 2001; 1:233-40.

Stogios PJ, Downs GS, Jauhal J, et al. Sequence and structural analysis of BTB proteins. Genome Biology 2005;6:R82.

Sakaguchi S, Hombauer M, Bilic I, Naoe Y, Schebesta A, Taniuchi I, Ellmeier W. The zinc-finger protein MAZR is part of the transcription factor network that controls the CD4 versus CD8 lineage fate of double-positive thymocytes. Nat Immunol 2010; 11:442-448.

Santoro M, Carlomagno F, Melillo RM & Fusco A . Dysfunction of the RET receptor in human cancer. Cellular and Molecular Life Sciences 2004;61: 2954–2964.

Soares P, Trovisco V, Rocha AS, Lima J, Castro P, Preto A, Ma´ximo V, Botelho T, Seruca R & Sobrinho-Simo˜es M. BRAF rearrangements are alternative events in the etiopathogenesis of PTC. Oncogene 2003; 22:4578–4580.

Tallini G. Poorly differentiated thyroid carcinoma. Are we there yet? Endocr Pathol. 2011; 22(4):190-4.

Tian X, Sun D, Zhang Y, Zhao S, Xiong H, Fang J. Zinc finger protein 278, a potential oncogene in human colorectal cancer. Acta Biochim Biophys Sin (Shanghai) 2008; 40:289- 296.

Tritz R, Mueller BM, Hickey MJ, Lin AH, Gomez GG, Hadwiger P, Sah DW, Muldoon L, Neuwelt EA, Kruse CA. siRNA Down-regulation of the PATZ1 Gene in Human Glioma Cells Increases Their Sensitivity to Apoptotic Stimuli. Cancer Ther 2008; 6:865-876.

Trovisco V., Soares P, Preto A, de Castro IV, Lima J, Castro P, Máximo V, Botelho T, Moreira S, Meireles AM, Magalhães J, Abrosimov A, Cameselle-Teijeiro J, Sobrinho- Simões M. Type and prevalence of BRAF mutations are closely associated with papillary thyroid carcinoma histotype and patients' age but not with tumour aggressiveness. Virchows Arch. 2005; 446: 589–595.

Valentino T, Palmieri D, Vitiello M, Simeone A, Palma G, Arra C, Chieffi P, Chiariotti L, Fusco A, Fedele M. Embryonic defects and growth alteration in mice with homozygous disruption of the Patz1 gene. J Cell Physiol 2013;228(3):646-53.

van der Laan B. F., Freeman J. L., Tsang R. W. & Asa S. L. The association of welldifferentiated thyroid carcinoma with insular or anaplastic thyroid carcinoma: evidence for dedifferentiation in tumor progression. Endocr. Pathol. 1993; 4, 215–221.

Vasko VV, Gaudart J, Allasia C, Savchenko V, Di Cristofaro J, Saji M, Ringel MD & De Micco C. Thyroid follicular adenomas may display features of follicular carcinoma and follicular variant of papillary carcinoma. European Journal of Endocrinology 2004; 151: 779–786.

Venter JC, Adams MD, Myers EW, et al. The sequence of the human genome. Science 2001;291:1304–51.

Vogelstein B, Kinzler KW. Cancer genes and the pathways they control. Nat Med 2004;10:789–799.

Vousden KH, Lu. Live or let die: the cell's response to p53. Nat Rev Cancer 2002; 2:594-604.

Yang WL, Ravatn R, Kudoh K, Alabanza L, Chin KV. Interaction of the regulatory subunit of the cAMP-dependent protein kinase with PATZ1 (ZNF278). Biochem Biophys Res Commun 2010; 391:1318-1323.

Yau T, Lo CY, Epstein RJ, Lam AK, Wan KY & Lang BH. Treatment outcomes in anaplastic thyroid carcinoma: survival improvement in young patients with localized disease treated by combination of surgery and radiotherapy. Annals of Surgical Oncology 2008;15: 2500–2505.

Yilmaz, M., and *Christofori*, G. (*2010*). Mechanisms of motility in metastasizing cells. Mol Cancer Res, 8(5), 629-42

Yu J and Zhang L. PUMA, a potent killer with or without p53 Oncogene. December 2008 ; 27(Suppl 1): S71–S83.

Yu J, Zhang L. The transcriptional targets of p53 in apoptosis control. Biochem Biophys Res Commun 2005;331:851–858.

Xing, M. BRAF mutation in thyroid cancer. Endocr. Relat. Cancer 2005; 12: 245–262.

Wong R SY. Apoptosis in cancer: from pathogenesis to treatment. *Journal of Experimental & Clinical Cancer Research* 2011; 30:87.

Wu WS, Heinrichs S, Xu D, Garrison SP, Zambetti GP, Adams JM, et al. Slug antagonizes p53- mediated apoptosis of hematopoietic progenitors by repressing puma. Cell 2005;123:641–653.

Zilfou JT, Lowe SW. Tumor suppressive functions of p53. Cold Spring Harb Perspect Biol. 2009;1(5):a001883.

THE JOURNAL OF BIOLOGICAL CHEMISTRY VOL. 287, NO. 22, pp. 18308–18317, May 25, 2012

POZ-, AT-hook-, and Zinc Finger-containing Protein (PATZ) Interacts with Human Oncogene B Cell Lymphoma 6 (BCL6) and Is Required for Its Negative Autoregulation*

Received for publication, January 25, 2012, and in revised form, March 29, 2012 Published, JBC Papers in Press, April 9, 2012, DOI 10.1074/jbc.M112.346270

Raffaela Pero[‡], Dario Palmieri[‡§], Tiziana Angrisano[‡], Teresa Valentino[‡], Antonella Federico[‡], Renato Franco[¶], Francesca Lembo[‖], Andres J. Klein-Szanto[**], Luigi Del Vecchio[‡‡§§], Donatella Montanaro[§§], Simona Keller[‡§§], Claudio Arra[¶], Vasiliki Papadopoulou[¶¶], Simon D. Wagner[¶¶], Carlo M. Croce[§], Alfredo Fusco[‡], Lorenzo Chiariotti[‡‖1], and Monica Fedele[‡2]

*From the [‡]Dipartimento di Biologia e Patologia Cellulare e Molecolare and the Istituto di Endocrinologia ed Oncologia Sperimentale, Università di Napoli "Federico II" and Consiglio Nazionale delle Ricerche (CNR), 80131 Naples, Italy, the [§]Department of Molecular Virology, Immunology and Medical Genetics, Comprehensive Cancer Center, Ohio State University, Columbus, Ohio 43210, the [¶]Istituto Nazionale dei Tumori, Fondazione Pascale, 80131 Naples, Italy, the [‖]Dipartimento di Chimica Farmaceutica e Tossicologica, Università di Napoli "Federico II", 80131 Naples, Italy, the **Department of Pathology, Fox-Chase Cancer Center, Philadelphia, Pennsylvania 19111, the [‡‡]Dipartimento di Biochimica e Biotecnologie Mediche, Università di Napoli "Federico II", 80131 Naples, Italy, the [§§]CEINGE, Biotecnologie Avanzate, 80145 Naples, Italy, and the [¶¶]Department of Cancer Studies and Molecular Medicine, University of Leicester, Leicester LE1 7RH, United Kingdom*

Background: PATZ is a transcription factor, whose role in cancer is still under debate.
Results: PATZ interacts with BCL6 and negatively modulates its expression. Consistently, *Patz1* knockdown mice showed up-regulation of BCL6 expression and BCL6-dependent B cell neoplasias.
Conclusion: PATZ is a tumor suppressor that acts by cooperating with BCL6 in its negative autoregulation.
Significance: This work helps in understanding the pathology of BCL6-expressing lymphomas in which *BCL6* is not mutated.

The *PATZ1* gene encoding a POZ/AT-hook/Kruppel zinc finger (PATZ) transcription factor, is considered a cancer-related gene because of its loss or misexpression in human neoplasias. As for other POZ/domain and Kruppel zinc finger (POK) family members, the transcriptional activity of PATZ is due to the POZ-mediated oligomer formation, suggesting that it might be not a typical transactivator but an architectural transcription factor, thus functioning either as activator or as repressor depending on the presence of proteins able to interact with it. Therefore, to better elucidate PATZ function, we searched for its molecular partners. By yeast two-hybrid screenings, we found a specific interaction between PATZ and BCL6, a human oncogene that plays a key role in germinal center (GC) derived neoplasias. We demonstrate that PATZ and BCL6 interact in germinal center-derived B lymphoma cells, through the POZ domain of PATZ. Moreover, we show that PATZ is able to bind the BCL6 regulatory region, where BCL6 itself acts as a negative regulator, and to contribute to negatively modulate its activity. Consistently, disruption of one or both *Patz1* alleles in mice causes focal expansion of thymus B cells, in which BCL6 is up-regulated. This phenotype was almost completely rescued by crossing $Patz1^{+/-}$ with $Bcl6^{+/-}$ mice, indicating a key role for Bcl6 expression in its development. Finally, a significant number of *Patz1* knock-out mice (both heterozygous and homozygous) also develop BCL6-expressing lymphomas. Therefore, the disruption of one or both *Patz1* alleles may favor lymphomagenesis by activating the BCL6 pathway.

The *PATZ1* gene encodes four main alternative proteins ranging from 537 to 687 amino acids that contain an N-terminal POZ domain, one or two AT-hooks in the central region, and four to six C2H2 zinc finger motifs at the C terminus (1–3). Both the AT-hooks and the POZ domain are characteristic of protein factors involved in gene transcription by interacting with a number of other protein factors. Indeed, PATZ protein, also known as MAZR, ZNF278, or ZSG, is a transcriptional regulatory factor that may function either as activator or as repressor depending upon the cellular context; it has been reported to either activate or repress c-Myc (1, 2), to activate mast cell protease 6 (4), and to repress androgen receptor (5) and CD8 (6) genes.

Different functional and genetic evidences suggest that PATZ might be directly involved in human tumors. Indeed, *PATZ1* is rearranged and deleted in small round cell sarcoma (3), and the chromosomal region where it is located (22q12) is in the human fragile site FRA22B, which suffers loss of heterozygosity in tumors (7). Increased expression of *PATZ1* mRNA has been observed in human malignant neoplasias, including colorectal (8), breast (9), and testicular (10) tumors. Moreover, PATZ knockdown by siRNA either blocks the growth or induces apoptosis of cell lines derived from colorectal cancer or gliomas, respectively (8, 11). However, in testicular tumors alone, PATZ protein expression has been analyzed,

* This work was supported by Associazione Italiana per la Ricerca sul Cancro Grant IG 5728 (to M. F.).
[1] To whom correspondence may be addressed: Dipartimento di Biologia e Patologia Cellulare e Molecolare, Università degli Studi di Napoli "Federico II", via Pansini, 5, 80131 Naples, Italy. Tel.: 39-0817462056; E-mail: chiariot@unina.it.
[2] To whom correspondence may be addressed: Istituto di Endocrinologia ed Oncologia Sperimentale (IEOS) del CNR, via S. Pansini, 5, 80131, Napoli, Italy. Tel.: 39-0817463054; Fax: 39-0817463749; E-mail: mfedele@unina.it.

demonstrating that it was mislocalized to cytoplasm (10, 12). Therefore, although *PATZ1* is strongly suggested to be a cancer-related gene, its role as tumor suppressor or oncogene is still controversial.

In the present study, starting from a yeast two-hybrid screening using *PATZ1* full-length cDNA as bait, we demonstrate that PATZ associates with BCL6,[3] a protein that shares with PATZ the N-terminal POZ domain, responsible for such association, and is involved in B and T cell development and lymphomagenesis (13–15, 38). We show that PATZ participates in BCL6 function by enhancing its activity of transcriptional repressor on BCL6 promoter in GC-derived lymphoma B cells. We also show that the knock-down of PATZ in mice causes BCL6-expressing thymus B cell hyperplasias (that eventually lead to B cell lymphomas), in which BCL6 is critical for their onset. The development of BCL6-expressing lymphomas in *Patz1* knock-down mice indicates a potential haploinsufficient tumor suppressor role for the *PATZ1* gene, whose disruption may lead to the lymphomas by activating the BCL6 pathway.

EXPERIMENTAL PROCEDURES

Two-hybrid Analysis—Two-hybrid screens were performed in yeast using full-length *PATZ1* (isoform 4) cDNA as a bait. Human heart and placenta cDNA libraries (Clontech) were simultaneously analyzed. A total of about 2×10^6 clones were tested for each library, and the specificity of interaction was assessed as described previously (16).

Plasmids—Full-length and truncated (devoid of the BTB/POZ domain) cDNAs for the human PATZ protein (isoform 4), Myc-tagged at their 3′-end, were subcloned into the XbaI-HindIII sites of the pcDNA3.1 plasmid (Invitrogen). The cDNA for the human BCL6 protein was subcloned into the EcoRI site of the pCEFL-HA vector (17), in-frame with the upstream HA tag. The BCL6i-luc reporter construct was obtained by cloning the −4.9 to +2.0-kb fragment of the BCL6 promoter into the pGL3Basic vector as described previously (18).

Protein Extraction, Immunoprecipitation, and Immunoblot Analysis—Tissues and cells were lysed in buffer containing 1% Nonidet P-40, 1 mmol/liter EDTA, 50 mmol/liter Tris-HCl (pH 7.5), and 150 mmol/liter NaCl supplemented with Complete protease inhibitors (Roche Applied Science). Total proteins were immunoprecipitated, in the presence or absence of 100 ng/ml ethidium bromide, as described previously (19), or they were directly resolved in a 10% polyacrylamide gel under denaturing conditions and transferred to nitrocellulose filters for Western blot analyses. Membranes were blocked with 5% BSA in TBS and incubated with the primary antibodies. The antibodies used were: anti-HA (sc-805), anti-Myc (sc-40), anti-BCL6 (sc-858), anti-tubulin (sc-5546), anti-vinculin (sc-7649) (Santa Cruz Biotechnology, Santa Cruz, CA), and anti-PATZ (polyclonal antibody raised against a conserved peptide recognizing all PATZ isoforms of mouse and human origin).

Cell Cultures and Transcriptional Activity Assays—Raji cells, originally derived from a Burkitt lymphoma, were cultured in RPMI 1640 medium adjusted to contain 1.5 g/liter sodium bicarbonate, 4.5 g/liter glucose, 10 mM HEPES, 1.0 mM sodium pyruvate, penicillin/streptomycin (Invitrogen/Life Technologies Italia, Monza, Italy), and 10% FBS (JRH Biosciences, Lenexa, KS). They were transfected by using the Amaxa Nucleofector kit V (Lonza, Cologne, Germany) following the manufacturer's instructions. COS-1 cells were cultured in DMEM with 10% FBS (JRH Biosciences). They were transfected using Lipofectamine Plus reagents (Invitrogen/Life Technologies Italia) according to the manufacturer's instructions and harvested 42 h after transfection. Cell lysates were extracted as described below and analyzed for luciferase activity. For transcriptional activity assays, a total of 2×10^6 cells (Raji) were seeded into each well of a 12-well plate and transiently transfected with 4 μg of BCL6i-luc, 5 μg of HA-BCL6, and 0.25–0.5 μg of PATZ-Myc, together with 1 μg of *Renilla* and various amounts of the backbone vectors to keep the total DNA concentration constant. Transfection efficiency, normalized for *Renilla* expression, was assayed with the Dual-Luciferase system (Promega Corp., Madison, WI). All transfection experiments were repeated at least three times. Aliquots of the same lysates were resolved by SDS-PAGE, transferred to nitrocellulose, and immunoblotted with anti-BCL6, anti-PATZ, and anti-vinculin antibodies, as above described.

Chromatin Immunoprecipitation—Chromatin immunoprecipitation (ChIP) of Raji cells ($\sim 3 \times 10^7$) or chopped spleens ($\sim$1 mg) from *Patz1*$^{+/+}$, *Patz1*$^{+/-}$, and *Patz1*$^{-/-}$ mice was carried out with an acetyl-histone H3 immunoprecipitation assay kit (Upstate Biotech Millipore, Lake Placid, NY) according to the manufacturer's instructions (19). The antibodies used are described above. Input DNA and immunoprecipitated DNA were analyzed by standard PCR for the presence of *BCL6* exon 1 and lipoprotein lipase *(LPL)* promoter sequences using the following primers: BCL6 exon 1, forward, 5′-CTCTTACTCGCCTCTCTAAC-3′; BCL6 exon 1, reverse, 5′-CGGCGGCAGCAACAGCAATAATCAC-3′; LPL pr, forward, 5′-ACCAAAGTGTCAAGGGCAAC-3′; and LPL pr, reverse, 5′-ATTCCCTAAACCCAGCATCC-3′.

We also used real-time quantitative PCR to amplify the *BCL6* exon 1, as described below. Primers specific for the glyceraldehyde-3-phosphate dehydrogenase (*GAPDH*) gene were used for normalization of real-time quantitative PCR data. The following primers were used: qBcl6 exon 1, forward, 5′-TAACACCACAAACTTGCAAAAGG-3′; qBcl6 exon 1, reverse, 5′-CTCCTCGAGCTAAATACACAAAAG-3′; qGapdh pr, forward, 5′-TGAGTCCTATCCTGGGAACCATCA-3′; qGapdh pr, reverse, 5′-TTTGAAATGTGCACGCACCAAGCG-3′.

Generation of Patz1-Knock-out Mice—The *Patz1* gene targeting vector was derived from a λΦXII phage library of a 129SvJ mouse strain (Stratagene, La Jolla, CA). It was designed to delete a 2317-bp PstI-XhoI fragment, including the start codon, the coding regions for the POZ domain, the AT-hook, and the first four zinc fingers. It was constructed by subcloning the 5′-flanking region (the SpeI-PstI 3-kb fragment), the *neo* cassette, and the 3′-flanking region (the XhoI-XbaI 3.2-kb fragment) into the Bluescript plasmid (Stratagene) that contained a PacI digestion site inserted at a distance from the multicloning site. The targeting vector was linearized with PacI before electroporation into embryonic stem (ES) cells (Incyte Genomics,

[3] The abbreviations used are: BCL6, B cell lymphoma 6 protein; BCL, B type lymphoma; GC, germinal center; ES, embryonic stem.

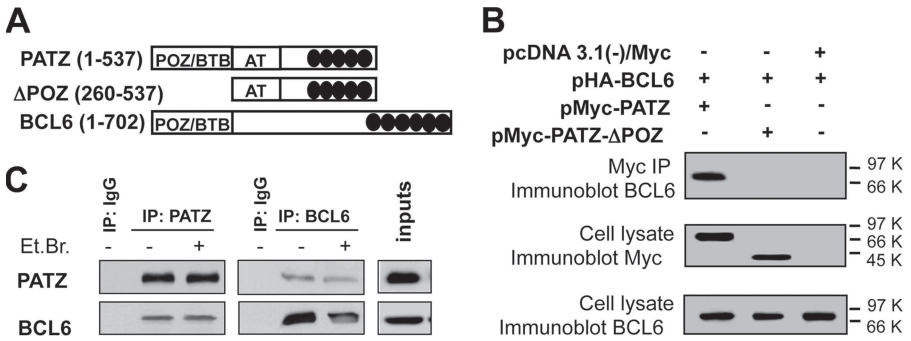

FIGURE 1. **Interaction between PATZ and BCL6.** *A*, schematic representation of portions of PATZ and BCL6 encoded by the transfected expression vectors. *AT*, AT-hook domain; *black ovals*, zinc finger motifs. *B*, co-immunoprecipitation (*IP*) of transfected PATZ-Myc, PATZ-ΔPOZ-Myc, and HA-BCL6 proteins in COS-1 cells. *C*, reciprocal co-immunoprecipitation of endogenous PATZ and BCL6 in Raji cells. Immunoprecipitation in the presence of EtBr was performed to control that it was not mediated by contaminating DNA. Immunoprecipitation with nonspecific IgG was carried out as a control for the specificity of the interaction.

Palo Alto, CA). Among 700 G418-resistant ES clones examined, 10 (1.4%) underwent homologous recombination. Two correctly targeted ES cell lines were injected into C57Bl/6J blastocysts. Both ES cell lines gave rise to germ line chimeras that were backcrossed to C57Bl/6J females to obtain *Patz1* heterozygous offspring. For Southern blot analysis, tail DNA samples were digested with StuI and probed with an external 5′ genomic fragment that would detect 9.3- or 8-kb fragments, corresponding to the wild-type and mutant alleles, respectively. The mice were maintained under specific pathogen-free conditions, and all studies were conducted in accordance with Italian regulations for experimentations on animals.

Isolation of mRNA and Quantitative RT-PCR—Total RNA was extracted using TRI-reagent solution (Sigma) according to the manufacturer's protocol, treated with DNase I (Invitrogen/Life Technologies Italia), and reverse-transcribed using random hexanucleotides as primers and MuLV reverse transcriptase (PerkinElmer Life Sciences) following the manufacturer's instructions. For quantitative RT-PCR, each reaction was performed three times in triplicate using the SYBR Green PCR master mix (Applied Biosystems, Foster City, CA) under the following conditions: 10 min at 95 °C followed by 40 cycles (15 s at 95 °C and 1 min at 60 °C). Subsequently, a dissociation curve was run to verify amplification specificity. The $2^{-\Delta\Delta CT}$ method was used to calculate relative expression levels (20). Primers specific for the glucose-6-phosphate dehydrogenase (*G6PD*) gene were used for normalization of real-time quantitative PCR data. The following primers were used: Patz, forward, 5′-GAGCTTCCCCGAGCTCAT-3′; Patz, reverse, 5′-CAGATCTCGATGACCGACCT-3′; G6pd, forward, 5′-CAGCGGCAACTAAACTCAGA-3′; G6pd, reverse, 5′-TTCCCTCAGGATCCCACAC-3′.

Histology and Immunohistochemistry—Dissected tissues were fixed in 10% formalin and embedded in paraffin by standard procedures. Mounted sections (5 μm thick) were stained with hematoxylin and eosin or incubated in a 750-watt microwave oven for 15 min in EDTA (10 mM, ph 8.0) and processed for immunohistochemistry using the avidin-biotin-peroxidase LSAB+ kit (Dako, Glostrup, Denmark). Endogenous peroxidase was quenched by incubation in 0.1% sodium azide with 0.3% hydrogen peroxide for 30 min at room temperature. Nonspecific binding was blocked by incubation with nonimmune serum. The antisera were directed toward B220 (RA3-6B2; SouthernBiotech, Birmingham, AL), CD3 (ab5690; Abcam, Cambridge, UK), CD79a (ab3121; Abcam), BCL6 (sc-858; Santa Cruz Biotechnology), and PATZ (described above).

IgH Gene Rearrangement Analysis—Genomic DNA was isolated from tumor masses or normal tissues from control mice, and Southern blotting was performed with the ^{32}P-labeled DNA probe PJ3 representing the J_H4 region of the IgH locus (21). A 1.3-kb Pst-1 fragment from the *Gapdh* gene was used for loading control.

Analysis of Lymphocyte Cell Surface Antigens—Spleens and thymi removed from mice were dissociated into single cells and stained for FACS analysis on a FACSCalibur flow cytometer (BD Biosciences, Buccinasco, Italy) as described previously (22). All the antibodies used were obtained from Pharmingen.

Statistical Analyses—Kaplan-Meyer survival curves were used to analyze the percentage of tumor-free mice. Differences were analyzed by the log rank test. The one-way analysis of variance followed by Tukey's multiple comparison test was used to compare groups of experiments. The statistical significant difference was considered when the p value was <0.05.

RESULTS

PATZ Interacts with BCL6—To identify PATZ interacting proteins, two-hybrid screenings of human heart and placenta pretransformed libraries were performed. A total of 87 positive clones (61 and 26 from heart and placenta, respectively) were isolated. Fourteen clones from heart and two from placenta libraries contained most of the coding sequence of the *BCL6* gene (data not shown). To confirm the interaction between PATZ and BCL6 in mammalian cells, co-immunoprecipitation experiments were performed. To this aim, total cell extracts from COS-1 cells transiently transfected with constructs encoding Myc-tagged PATZ, Myc-tagged PATZ-ΔPOZ (devoid of the BTB/POZ domain), and HA-tagged BCL6 (Fig. 1*A*) were subjected to immunoprecipitation using anti-Myc antibody. As shown in Fig. 1*B*, co-precipitation of the BCL6 protein was observed when constructs for BCL6 and full-length PATZ were co-transfected, and not when BCL6 was transfected together with PATZ-ΔPOZ or with the backbone vector. Therefore, PATZ and BCL6 form a complex in mammalian cells, and the POZ domain of PATZ is necessary for such interaction.

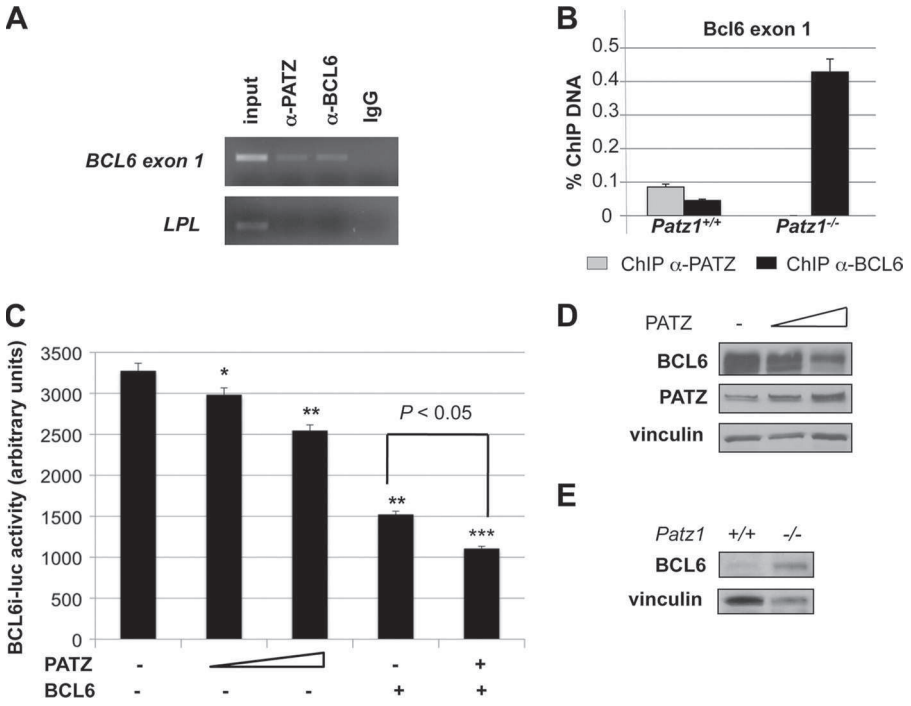

FIGURE 2. **Role of PATZ on BCL6 promoter.** *A*, ChIP analysis performed on Raji cells using specific anti-PATZ and anti-BCL6 polyclonal antibodies to detect the endogenous *in vivo* binding of PATZ and BCL6 to exon 1 of BCL6. The recovered DNA was used as a template for PCR with primers that specifically amplify exon 1 of *BCL6* or the promoter region of the *LPL* gene (negative control). *input* indicates PCR products with chromosomal DNA without immunoprecipitation. Nonspecific IgG was used as a negative control. *B*, ChIP assay, revealed by quantitative PCR, on spleens from *Patz1*$^{+/+}$ and *Patz1*$^{-/-}$ mice to detect the binding of PATZ and BCL6 proteins to exon 1 of *Bcl6* DNA. The percentage of immunoprecipitated DNA with respect to the input is reported. *C*, luciferase activity of the BCL6 promoter (−4.9 to +2.0 kb) in Raji cells. Where indicated, 0.25 and 0.5 μg of PATZ and/or 5 μg of BCL6 expression vectors were co-transfected with the BCL6i-luc plasmid. Where required, backbone vectors were also transfected to reach the same total amount of DNA for each experimental point. Data express mean ± S.D. of three independent experiments. *Asterisks* indicate the statistical results of a multiple comparison test *versus* promoter basic activity. *, $p < 0.05$; **, $p < 0.01$, ***, $p < 0.001$. *D*, representative Western blot analysis to detect BCL6 expression in Raji cells transfected or not with increasing amounts of PATZ expression plasmid, as in *C*. As a control for equal loading, the same blot was incubated with antibodies against vinculin. *E*, Western blot analysis of BCL6 expression in mouse embryonic fibroblasts from Patz1$^{+/+}$ and Patz1$^{-/-}$ mice. Vinculin has been analyzed as a loading control.

Next, to ensure that the interaction between PATZ and BCL6 takes place in a physiological context, endogenous PATZ and BCL6 were co-immunoprecipitated in Raji cells, deriving from a Burkitt lymphoma, which is a GC-derived lymphoma expressing both proteins. The result, shown in Fig. 1*C*, further demonstrates that PATZ and BCL6 interact *in vivo*.

PATZ Is Involved in BCL6 Negative Autoregulation—To study the functional consequences of the interaction between PATZ and BCL6, we investigated whether PATZ and BCL6 associate on a BCL6 endogenous target promoter. Previous experiments demonstrated that the *BCL6* gene contains two non-STAT6 functional BCL6 binding sites located within exon 1 (23). Thus, we examined whether PATZ could bind exon 1 of the *BCL6* gene *in vivo*. Endogenous PATZ and BCL6 bind to exon 1 of *BCL6*, as determined by ChIP experiments in Raji cells (Fig. 2*A*). This result was further confirmed *in vivo* using mouse spleens, a tissue that harbors GC cells, where both PATZ and BCL6 proteins were immunoprecipitated on BCL6 exon 1 (Fig. 2*B*). Interestingly, BCL6 binding to its own promoter was enhanced (Fig. 2*B*) in spleens lacking PATZ (obtained from *Patz1* knock-out mice described below). The absence of immunoprecipitated PATZ in Patz1-null tissues confirmed the binding of PATZ to BCL6 exon 1 observed in the wild-type mice.

It is known that BCL6, by binding to its exon 1 and recruiting the distal *cis*-acting factor ZEB1, represses its own transcription, thus establishing a circuit of negative autoregulation (23, 24). To further investigate the role of PATZ in such a function of BCL6, we used a reporter construct driving luciferase gene expression under control of a BCL6 genomic sequence of 6.9 kb, including the ZEB1-responsive element, exon 1, and 1.5 kb of intron 1 (BCL6i-luc) (18). Raji cells were co-transfected with BCL6i-luc and plasmids expressing PATZ, BCL6, or both proteins (Fig. 2*C*). As expected, BCL6 expression resulted in down-regulation of the BCL6 promoter activity. A similar, but less strong, activity was also achieved by PATZ, leading to a dose-dependent repression of this BCL6 promoter region. Interestingly, PATZ and BCL6 co-transfection resulted in the enhancement of the BCL6-dependent repression (Fig. 2*C*). Western blot analysis of Raji cells transfected or not with increasing amounts of PATZ expression plasmid, as in Fig. 2*C*, confirmed the negative dose-dependent effect of PATZ on BCL6 expression (Fig. 2*D*). To finally assess the dependence of BCL6 expression from PATZ, we analyzed, by Western blot, the BCL6 protein levels in mouse embryonic fibroblasts from Patz1$^{+/+}$ and Patz1$^{-/-}$ mice (described below). As shown in Fig. 2*E*, Patz1-null mouse embryonic fibroblasts showed a significant increase in BCL6 expression, which confirms the negative regulatory role of PATZ on it.

Disruption of Mouse Patz1 Gene Causes Thymus B Cell Expansion, Which Eventually Leads to B Cell Lymphomas—To gain insights into the physiological role of PATZ *in vivo*, a targeting vector was designed to knock out the mouse *Patz1* gene

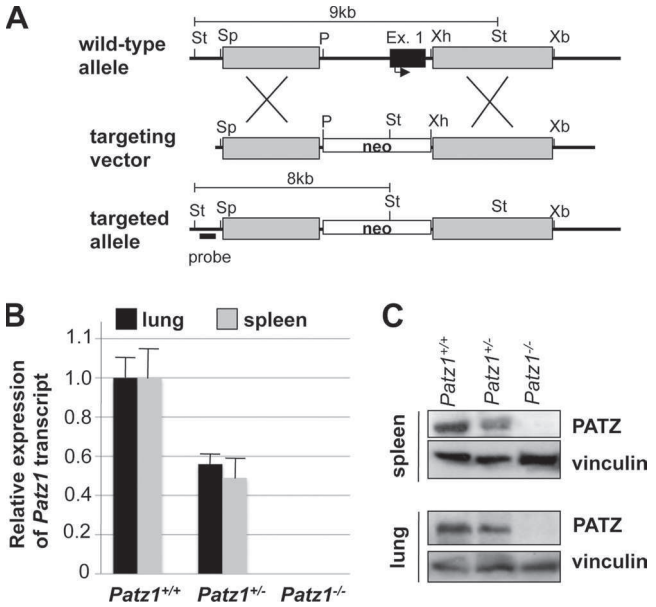

FIGURE 3. **Generation of *Patz1* knock-out mice.** *A*, schematic representation of the wild-type and mutant alleles and the targeting vector. *St*, StuI; *Sp*, SpeI; *P*, PstI; *Ex.*, exon; *Xb*, XbaI. *B* and *C*, quantitative RT-PCR (*B*) and Western blot analysis (*C*) in tissues from *Patz1*$^{+/+}$, *Patz1*$^{+/-}$, and *Patz1*$^{-/-}$ mice, to detect PATZ expression and confirm its knock-out at both RNA and protein levels. Data express mean ± S.D. of three independent experiments.

by homologous recombination in ES cells (Fig. 3*A*). Inactivation of the *Patz1* allele was verified by analyzing *Patz1* expression in adult tissues using quantitative RT-PCR and Western blot (Fig. 3, *B* and *C*). As expected, *Patz1* mRNA and protein were undetectable in homozygous mutants, whereas they were present at about half-levels in heterozygous as compared with wild-type controls. Heterozygous mice were viable and fertile, but heterozygous intercrosses produced viable homozygous mutants at non-Mendelian frequencies. Indeed, the large majority of homozygous mutants (about 75% on average) died prenatally due to developmental defects in the cardiac outflow tract.[4] Here we focused on some phenotypes, observed in adult mice (both heterozygous and homozygous for the *Patz1*-null mutation), which can be due to an impaired regulation of the *BCL6* gene.

By 2–3 months of age, with a similar frequency (75%), Patz1$^{+/-}$ and Patz1$^{-/-}$ mice develop thymus hyperplasias characterized by focal expansion of an intramedullary B cell population (Fig. 4*A*). B cells are the minority cell type (0.82 ± 0.50%) in the thymus of wild-type animals, as confirmed by FACS analysis in a cohort of 20 animals, but significantly increase to an average of 5.94 ± 4.42 ($p < 0.05$) in an equal number of *Patz1*$^{+/-}$ mice (Fig. 4*B*). A similar increase of B cells was also observed in Patz1$^{-/-}$, where, for the limited number of available animals, we could only do a qualitative analysis (data not shown). To exclude that this B cell expansion could be due to formation of intrathymic reactive B cell follicles possibly induced by an altered CD4 helper *versus* cytotoxic subset ratio (25), we analyzed CD4+ and CD8+ lymphocyte populations by FACS in *Patz1*$^{+/-}$ thymi showing B cell hyperplasia, without finding any differences in comparison with wild-type controls (data not shown). Interestingly, in 4 out of 75 Patz1$^{+/-}$ mice sacrificed at an advanced age (17–22 months old), we also found thymus B cell lymphomas, characterized by large cells with marked cell-to-cell variation in size and shape and abundant pale cytoplasm, which were diagnosed as diffuse large B cell lymphomas by our pathologists (Fig. 4*C* and data not shown).

Thymus B Cell Lesions in Patz1 Knock-out Mice Are Dependent on Bcl6 Expression—Pathological thymus B cells are considered to originate from the GC (26). Accordingly, focal expression of BCL6 was detected in *Patz1*-knock-out thymus lesions (either hyperplasia or lymphomas) but was absent in the wild-type controls (Fig. 5*A*). Western blot analyses on thymus tissues from *Patz1*$^{+/-}$ mice confirmed the expression of BCL6, which was absent in *Patz1*$^{+/+}$ controls (Fig. 5*B*). Up-regulation of BCL6 in these cells is consistent with the role of PATZ in BCL6 autoregulation (see above), which leads us to suggest that decreased or null levels of PATZ causes up-regulation of BCL6 expression, which in turn could be responsible for the thymus pathological phenotype. To validate our hypothesis of a role for increased BCL6 expression in the development of certain phenotypes in *Patz1* knock-out mice, we crossed *Patz1*$^{+/-}$ with *Bcl6*$^{+/-}$ mice (27) to generate double mutants. *Patz1*$^{-/-}$;*Bcl6*$^{+/+}$, *Patz1*$^{+/+}$;*Bcl6*$^{-/-}$, and *Patz1*$^{-/-}$;*Bcl6*$^{-/-}$ mice died during embryogenesis. However, because we observed the thymus phenotype in *Patz1* heterozygous mice, we analyzed the alterations present in *Patz1*$^{+/-}$;*Bcl6*$^{+/+}$ mice and compared them with the double heterozygous *Patz1/Bcl6* mutants.

Cohorts of 10 *Patz1*$^{+/-}$;*Bcl6*$^{+/+}$ and 10 *Patz1*$^{+/-}$;*Bcl6*$^{+/-}$ mice were equally distributed by gender and sacrificed at 12 months of age. Their thymus was analyzed by histological, immunohistochemical, and FACS assays. As shown in Fig. 5*C*, where representative FACS analyses are shown, 100% of the *Patz1*$^{+/-}$;*Bcl6*$^{+/-}$ mice analyzed did not show any significant thymus B cell expansion as compared with the *Patz1*$^{+/-}$;*Bcl6*$^{+/+}$ controls. Immunohistochemical analyses confirmed this result in 80% of the cases, whereas in the remaining 20% of double heterozygous mice, an aberrant thymus B cell hyperplasia was observed, but it was strongly reduced as compared with that observed in *Patz1*$^{+/-}$;*Bcl6*$^{+/+}$ mice (Fig. 5*D*). These results confirm a key role for the up-regulation of BCL6 in the pathological thymus phenotype of *Patz1* knock-out mice.

Increased Tumorigenesis in Patz1 Knock-out Mice—Although initially healthy, many adult *Patz1*$^{+/-}$ and most of the few available *Patz1*$^{-/-}$ mice developed signs of morbidity and displayed visible tumors as they aged. As evident in the survival curves in Fig. 6*A*, *Patz1*$^{-/-}$ and *Patz1*$^{+/-}$ mice showed an increased incidence of neoplastic lesions at ~17 or 21 months of age, respectively. Only 12% of the *Patz1*$^{-/-}$ and 67% of the *Patz1*$^{+/-}$ animals were tumor-free at 20 months, in contrast to the 95% of wild-type mice that were tumor-free at the same age.

The histological analyses revealed that 43 of 75 (57%) *Patz1*$^{+/-}$ and 9 of 11 (82%) *Patz1*$^{-/-}$ mice developed malignant tumors, *versus* only 7 of 63 (11%) wild-type mice. *Patz1* knock-out tumors were mainly lymphomas, but hepatocellular carcinomas and rare sarcomas and lung adenocarcinomas were also detected. Wild-type animals developed lymphomas and

[4] T. Valentino, D. Palmieri, M. Vitiello, A. Simeone, G. Palma, C. Arra, P. Chieffi, L. Chiariotti, A. Fusco, and M. Fedele, manuscript submitted.

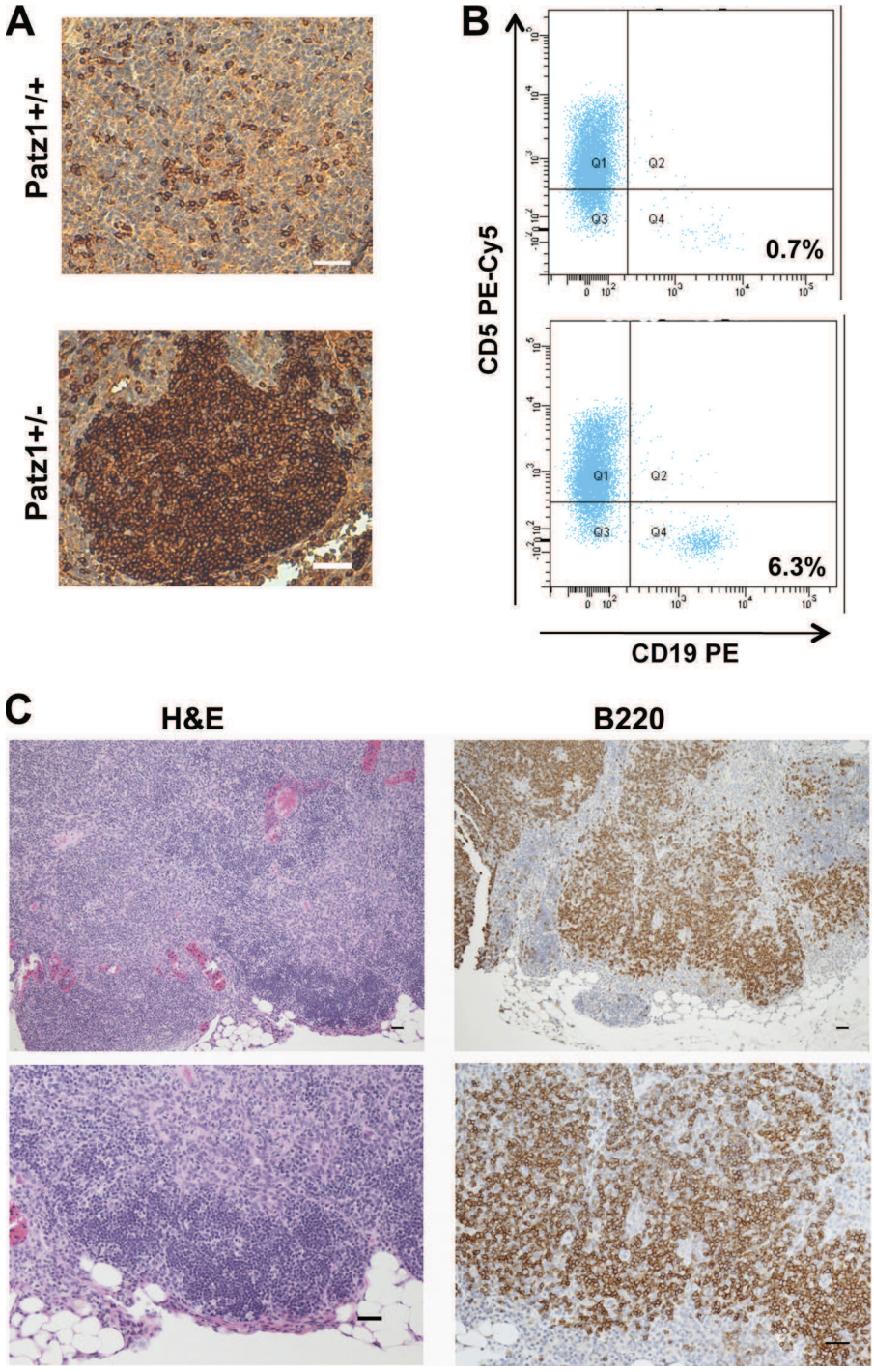

FIGURE 4. **Thymus neoplasias in *Patz1* knock-out mice.** *A*, immunohistochemical analysis in representative thymus sections of *Patz1*$^{+/+}$ and *Patz1*$^{+/-}$ mice. B220 staining shows the presence of a focal B cell hyperplasia in the medulla of the mutant sample, whereas only scattered B cells were present in the wild-type control. *Scale bars*, 100 μm. *B*, flow cytometry dot blots of the thymi showed in B stained with CD19 and CD5 antibodies. A distinct population of cells that positively stains with CD19-PE antibody in the *Patz1*$^{+/-}$ (*lower panel*) is evident. No appreciable CD19+ cell population was found in the wild-type control (*upper panel*). For each analysis, 10,000 events were counted. The relative percentage of CD19^{+} cells (B lymphocytes) was indicated in the *right-bottom corner* of each dot plot. *PE*, Phycoerythrin. *C*, representative sample of a thymus B cell lymphoma developed by a *Patz1*$^{+/-}$ mouse. *Left panels*, hematoxylin and eosin staining; *right panels*, immunostaining for B220. *Scale bars*, 100 μm.

one hepatocellular carcinoma (Fig. 6*B* and data not shown). Lymphomas from wild-type mice were all of the B cell lineage but did not show BCL6 expression nor PATZ down-regulation as compared with normal controls (data not shown).

To determine whether the tumors in Patz1$^{+/-}$ mice occurred via loss of heterozygosity or haploinsufficiency, PATZ protein expression and *Patz1* gene sequence were analyzed in the tumor tissues from *Patz1*$^{+/-}$ mice. Western blot (Fig. 6*C*) and immunohistochemical analysis (data not shown) revealed that PATZ was present in all of the tumors examined. Furthermore, sequence analysis of *Patz1* cDNA isolated from eight *Patz1*$^{+/-}$ tumors showed no mutation or rearrangement (data

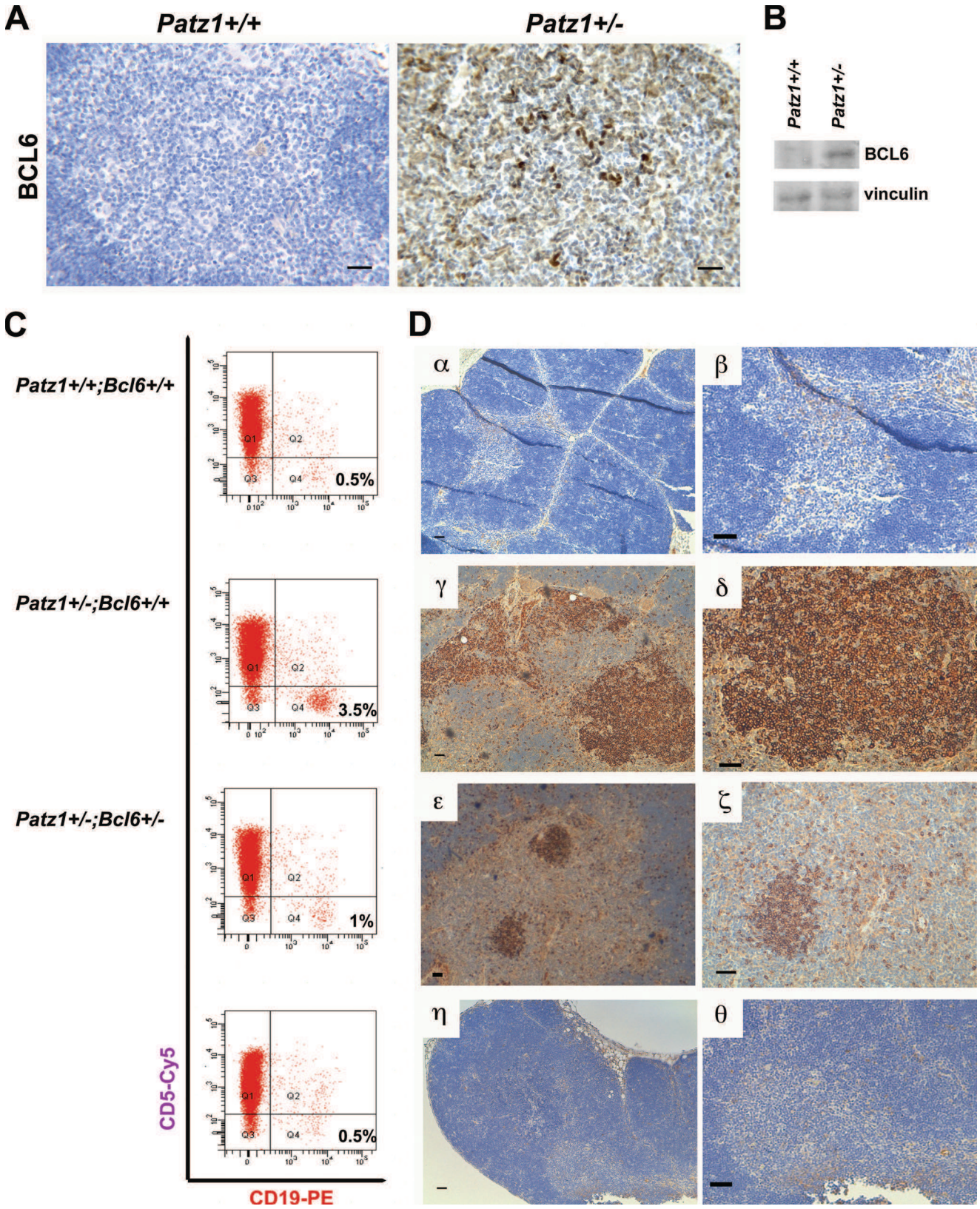

FIGURE 5. **Key role of BCL6 in thymus B cell expansion of *Patz1* knock-out mice.** *A*, immunohistochemical staining of BCL6 in representative thymus samples from *Patz1*$^{+/+}$ (*left panel*) and *Patz1*$^{+/-}$ (*right panel*) mice. *Scale bar*, 100 μm. *B*, Western blot analysis for BCL6 expression in a pool of three *Patz1*$^{+/+}$ and three *Patz1*$^{+/-}$ thymi. *C*, flow cytometry of representative thymi from *Patz1*$^{+/+}$;*Bcl6*$^{+/+}$, *Patz1*$^{+/-}$;*Bcl6*$^{+/+}$, and *Patz1*$^{+/-}$;*Bcl6*$^{+/-}$ mice. The thymocytes were double-stained for specific B (CD19) and T cell (CD5) surface antigens. For each analysis, 10,000 events were counted. The relative percentage of CD19^{+} cells (B lymphocytes) was indicated in the *right-bottom corner* of each dot plot. *CD19-PE*, CD19-Phycoerythrin staining. *D*, immunohistochemical analysis of the thymi shown in *C* to detect B cells (stained with anti-B220). Only scattered positive cells were detected in *Patz1*$^{+/+}$;*Bcl6*$^{+/+}$ (α,β) and most *Patz1*$^{+/-}$;*Bcl6*$^{+/-}$ thymi (η,θ). Large focal hyperplasias of B cells were detected in *Patz1*$^{+/-}$;*Bcl6*$^{+/+}$ (γ, δ) thymi, and small focal positivity was detected in some *Patz1*$^{+/-}$;*Bcl6*$^{+/-}$ thymi (ϵ, ζ). *Scale bars*, 100 μm.

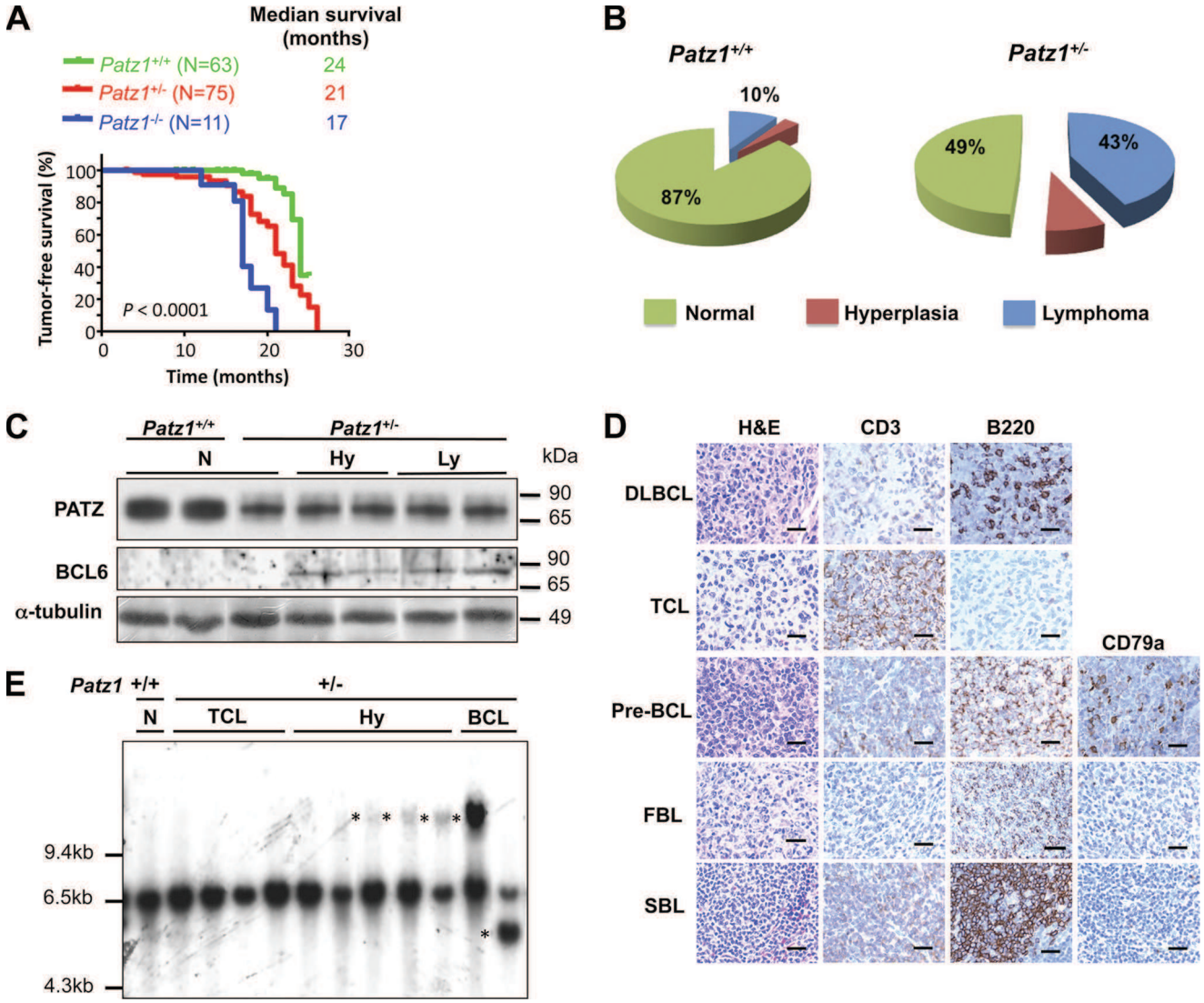

FIGURE 6. **Increased lymphomagenesis in Patz1 knock-out mice.** *A*, Kaplan-Meyer tumor incidence analysis of $Patz1^{+/+}$, $Patz1^{+/-}$, and $Patz1^{-/-}$ mice. Cohorts of 63 wild-type, 75 heterozygous, and 11 homozygous *Patz1* knock-out mice were monitored and harvested when they exhibited symptoms of disease. The curves were significantly different ($p < 0.0001$) as determined by log rank test. *B*, the lymphoid phenotype, as a function of the relative percentage, in mice homozygous and heterozygous for the *Patz1*-null mutation *versus* wild-type controls was plotted as pie charts. The number of mice analyzed for each genotype is the same as in *A*. *C*, Western blot analysis showing expression of BCL6 and PATZ in spleen samples from $Patz1^{+/+}$ and $Patz1^{+/-}$ mice. α-Tubulin expression was evaluated as a loading control. *N*, normal; *Hy*, hyperplasia; *Ly*, lymphoma. *D*, immunohistochemical staining for the phenotypic characterization of lymphomas in *Patz1* knock-out mice. Representative $Patz1^{+/-}$ spleen samples of all types of lymphomas observed are shown (for the percentage of each type, see under "Results"). Antibodies used for the staining are indicated on the *top*. *H&E*, hematoxylin and eosin staining; *DLBCL*, diffuse large cell B cell lymphoma; *TCL*, T cell lymphoma; *pre-BCL*, pre-B cell lymphoma; *FBL*, follicular B cell lymphoma; *SBL*, small B cell lymphoma. *Scale bars*, 100 μm. *E*, *IgH* gene rearrangements were analyzed by Southern blot on EcoRI-digested spleen DNA. Control (+/+) is the wild-type mouse with the genomic 6.5-kb fragment representing the gene in its germ line configuration. All hyperplastic (*Hy*) and B cell lymphoma samples from $Patz1^{+/-}$ mice, and normal spleen from a $Patz1^{-/-}$ mouse, show rearranged extra bands (*asterisks*). The histological diagnoses of the spleens are indicated above.

not shown). These results indicate that haploinsufficiency, rather than loss of heterozygosity, accounts for the tumor occurrence in $Patz1^{+/-}$ mice, thus suggesting *Patz1* as a haploinsufficient tumor suppressor gene.

Spleen lymphomas were the most representative malignant diseases in *Patz1* knock-out mice, and they were further characterized to determine the mechanism by which reduced *Patz1* expression induces such neoplasias. Tumor sections from $Patz1^{+/-}$ mice were stained with antibodies raised against T cell- and B cell-specific markers to determine the cell type of origin of the lymphoma. Interestingly, we found both B type and T type lymphomas with a prevalence of B (28%) *versus* T lymphomas (17%). The B type lymphoma (BCL) subtypes, as defined by Morse *et al.* (28), were as follows: (*a*) diffuse large B cell (16.8%), (*b*) follicular B cell (5.6%), (*c*) pre-B cell (2.8%), and (*d*) small B cell lymphomas (2.8%) (Fig. 6*D*). Flow cytometry analysis confirmed the immunohistochemical data (data not shown). To further characterize lymphoid neoplasias, *IgH* gene configuration was analyzed by Southern blot of EcoRI-digested spleen DNA from $Patz1^{+/+}$ and $Patz1^{+/-}$ mice using a probe representing the J_H4 region of the *IgH* locus (Fig. 6*E*). The 6.5-kb fragment represents the germ line configuration of the gene. All BCLs showed oligoclonal rearrangements of the germ line *IgH* joining region (Fig. 6*E*, *asterisks*). Interestingly, benign lymphoproliferative diseases often show aberrant V(D)J recombination at the *IgH* locus, suggesting that they may represent an

early stage in the development of BCLs. The same Southern blot was also probed for *gapdh*, which gave rise to a unique band for all loaded samples (data not shown). Both BCLs and lymphoproliferative diseases expressed BCL6, whereas it was not detectable in wild-type controls or normal spleens from *Patz1* knock-out mice (Fig. 6*C*), suggesting a key role for this oncoprotein in development of such neoplasias.

DISCUSSION

Previous studies suggest a cancer-related role for PATZ (3, 8–11), but the mechanisms by which PATZ is involved in the process of carcinogenesis are still controversial. Our data indicate that PATZ acts as a tumor suppressor in lymphomagenesis by inhibiting BCL6 expression. We first showed that PATZ and BCL6 bind to each other. This finding is consistent with the notion that POK proteins, such as PATZ and BCL6, commonly aggregate in large nuclear complexes by self-interaction, as heterodimers with other POK proteins and in association with unrelated partners, such as transcriptional corepressors, as a way to extend the repertoire of their target genes and/or the ways they act on their expression (29). BCL6 is the most commonly altered proto-oncogene in non-Hodgkin lymphomas, the majority of which derive from normal GC B cells (30). In fact, its sustained expression causes malignant transformation of GC B cells (31). Nearly half of human diffuse large B cell lymphomas, the most common form of non-Hodgkin lymphomas, express BCL6 constitutively, mainly as a consequence of *BCL6* gene rearrangements and activating point mutations that target the 5′ regulatory region of this gene (23, 24, 32, 33). However, different studies showed that *BCL6* expression in lymphoma is largely independent from the corresponding chromosomal alterations, suggesting that mechanisms other than gene rearrangements or mutations can deregulate its expression in lymphomas (34, 35). BCL6 expression is tightly regulated in a lineage- and developmental-stage-specific manner, and disruption of normal controls can contribute to lymphomagenesis (13, 14, 36). Transcription of the *BCL6* gene is negatively self-regulated by means of the interaction of two BCL6 binding sites within exon 1 of the gene and the BCL6 protein itself, which is a potent transcription repressor, and both chromosomal translocations and activating mutations allow lymphoma cells to bypass this negative autoregulation mechanism (23, 24). To date, a variety of corepressors have been described. Among them, the CtBP1 and ZEB1 transcriptional repressors are required for BCL6 autoregulation (18, 37). In a recent model, a repressive complex at the BCL6 locus that involves binding of transcription factors to both exon 1 and a distant *cis*-acting element (HSS-4.4) has been suggested to regulate BCL6 transcription. In this complex, ZEB1 and BCL6, which bind to distant sites, are linked through binding of the common corepressor CtBP1 (18). In the present study, we show that PATZ can bind *BCL6* exon 1 and negatively modulate *BCL6* promoter activity. Therefore, we speculate that PATZ can be one of the transcription factors involved in the complex and that, because of its ability to bind the minor groove of DNA via the AT-hooks, could be crucial for the bending of DNA required to put together distant *cis*-acting transcription factors. Because PATZ can interact and cooperate with BCL6, we can suggest that it acts together with BCL6 in its autoregulation. However, we cannot exclude that PATZ can also act without BCL6, thus contributing to keep BCL6 expression off when BCL6 is not expressed at all. Consistent with a role of PATZ in BCL6 negative regulation, we also show that mice carrying a null mutation of the *Patz1* gene develop an aberrant expansion of thymus B cells, in which BCL6 expression is up-regulated. We believe that this phenotype, which we demonstrated to be dependent on BCL6 expression, is also responsible for the development of BCLs that we observe in both thymi and spleens of Patz1 knock-out mice at a later age.

In conclusion, our data indicate a haploinsufficient tumor suppressor role for PATZ that would act in lymphomagenesis by down-regulating BCL6 expression.

Acknowledgments—We are grateful to Riccardo Dalla-Favera for providing us with the Bcl6$^{+/-}$ mice. We also thank Vincenzo Fidanza, Rosa Visone, Ivana De Martino, Ida Pellegrino, Michela Vitiello, Giosuè Scognamiglio, and Giuseppe Palma for helpful contributions under "Experimental Procedures" and animal care.

REFERENCES

1. Fedele, M., Benvenuto, G., Pero, R., Majello, B., Battista, S., Lembo, F., Vollono, E., Day, P. M., Santoro, M., Lania, L., Bruni, C. B., Fusco, A., and Chiariotti, L. (2000) A novel member of the BTB/POZ family, PATZ, associates with the RNF4 RING finger protein and acts as a transcriptional repressor. *J. Biol. Chem.* **275,** 7894–7901
2. Kobayashi, A., Yamagiwa, H., Hoshino, H., Muto, A., Sato, K., Morita, M., Hayashi, N., Yamamoto, M., and Igarashi, K. (2000) A combinatorial code for gene expression generated by transcription factor Bach2 and MAZR (MAZ-related factor) through the BTB/POZ domain. *Mol. Cell Biol.* **20,** 1733–1746
3. Mastrangelo, T., Modena, P., Tornielli, S., Bullrich, F., Testi, M. A., Mezzelani, A., Radice, P., Azzarelli, A., Pilotti, S., Croce, C. M., Pierotti, M. A., and Sozzi, G. (2000) A novel zinc finger gene is fused to EWS in small round cell tumor. *Oncogene* **19,** 3799–37804
4. Morii, E., Oboki, K., Kataoka, T. R., Igarashi, K., and Kitamura, Y. (2002) Interaction and cooperation of *mi* transcription factor (MITF) and myc-associated zinc-finger protein-related factor (MAZR) for transcription of mouse mast cell protease 6 gene. *J. Biol. Chem.* **277,** 8566–8571
5. Pero, R., Lembo, F., Palmieri, E. A., Vitiello, C., Fedele, M., Fusco, A., Bruni, C. B., and Chiariotti, L. (2002) PATZ attenuates the RNF4-mediated enhancement of androgen receptor-dependent transcription. *J. Biol. Chem.* **277,** 3280–3285
6. Bilic, I., Koesters, C., Unger, B., Sekimata, M., Hertweck, A., Maschek, R., Wilson, C. B., and Ellmeier, W. (2006) Negative regulation of CD8 expression via Cd8 enhancer-mediated recruitment of the zinc finger protein MAZR. *Nat. Immunol.* **7,** 392–400
7. Burrow, A. A., Williams, L. E., Pierce, L. C., and Wang, Y. H. (2009) Over half of breakpoints in gene pairs involved in cancer-specific recurrent translocations are mapped to human chromosomal fragile sites. *BMC Genomics* **10,** 59
8. Tian, X., Sun, D., Zhang, Y., Zhao, S., Xiong, H., and Fang, J. (2008) Zinc finger protein 278, a potential oncogene in human colorectal cancer. *Acta Biochim. Biophys. Sin.* **40,** 289–296
9. Yang, W. L., Ravatn, R., Kudoh, K., Alabanza, L., and Chin, K. V. (2010) Interaction of the regulatory subunit of the cAMP-dependent protein kinase with PATZ1 (ZNF278). *Biochem. Biophys. Res. Commun.* **391,** 1318–1323
10. Fedele, M., Franco, R., Salvatore, G., Paronetto, M. P., Barbagallo, F., Pero, R., Chiariotti, L., Sette, C., Tramontano, D., Chieffi, G., Fusco, A., and Chieffi, P. (2008) *PATZ1* gene has a critical role in the spermatogenesis and testicular tumors. *J. Pathol.* **215,** 39–47
11. Tritz, R., Mueller, B. M., Hickey, M. J., Lin, A. H., Gomez, G. G., Hadwiger,

P., Sah, D. W., Muldoon, L., Neuwelt, E. A., and Kruse, C. A. (2008) siRNA down-regulation of the PATZ1 Gene in human glioma cells increases their sensitivity to apoptotic stimuli. *Cancer Ther.* **6,** 865–876
12. Esposito, F., Boscia, F., Franco, R., Tornincasa, M., Fusco, A., Kitazawa, S., Looijenga, L. H., and Chieffi, P. (2011) Down-regulation of estrogen receptor-β associates with transcriptional co-regulator PATZ1 delocalization in human testicular seminomas. *J. Pathol.* **224,** 110–120
13. Pasqualucci, L., Bereschenko, O., Niu, H., Klein, U., Basso, K., Guglielmino, R., Cattoretti, G., and Dalla-Favera, R. (2003) Molecular pathogenesis of non-Hodgkin's lymphoma: the role of Bcl-6. *Leuk. Lymphoma* **44,** S5–S12
14. Ichii, H., Sakamoto, A., Kuroda, Y., and Tokuhisa, T. (2004) Bcl6 acts as an amplifier for the generation and proliferative capacity of central memory $CD8^+$ T cells. *J. Immunol.* **173,** 883–891
15. Cattoretti, G., Pasqualucci, L., Ballon, G., Tam, W., Nandula, S. V., Shen, Q., Mo, T., Murty, V. V., and Dalla-Favera, R. (2005) Deregulated BCL6 expression recapitulates the pathogenesis of human diffuse large B cell lymphomas in mice. *Cancer Cell* **7,** 445–455
16. Lembo, F., Pero, R., Angrisano, T., Vitiello, C., Iuliano, R., Bruni, C. B., and Chiariotti, L. (2003) MBDin, a novel MBD2-interacting protein, relieves MBD2 repression potential and reactivates transcription from methylated promoters. *Mol. Cell Biol.* **23,** 1656–1665
17. Melillo, R. M., Pierantoni, G. M., Scala, S., Battista, S., Fedele, M., Stella, A., De Biasio, M. C., Chiappetta, G., Fidanza, V., Condorelli, G., Santoro, M., Croce, C. M., Viglietto, G., and Fusco, A. (2001) Critical role of the HMGI(Y) proteins in adipocytic cell growth and differentiation. *Mol. Cell Biol.* **21,** 2485–2495
18. Papadopoulou, V., Postigo, A., Sánchez-Tilló, E., Porter, A. C., and Wagner, S. D. (2010) ZEB1 and CtBP form a repressive complex at a distal promoter element of the BCL6 locus. *Biochem. J.* **427,** 541–550
19. Fedele, M., Visone, R., De Martino, I., Troncone, G., Palmieri, D., Battista, S., Ciarmiello, A., Pallante, P., Arra, C., Melillo, R. M., Helin, K., Croce, C. M., and Fusco, A. (2006) HMGA2 induces pituitary tumorigenesis by enhancing E2F1 activity. *Cancer Cell* **9,** 459–471
20. Livak, K. J., and Schmittgen, T. (2001) Analysis of relative gene expression data using real-time quantitative PCR and the $2^{-\Delta\Delta^{CT}}$ method. *Methods* **25,** 402–408
21. Bichi, R., Shinton, S. A., Martin, E. S., Koval, A., Calin, G. A., Cesari, R., Russo, G., Hardy, R. R., and Croce, C. M. (2002) Human chronic lymphocytic leukemia modeled in mouse by targeted TCL1 expression. *Proc. Natl. Acad. Sci. U.S.A.* **99,** 6955–6960
22. Fedele, M., Fidanza, V., Battista, S., Pentimalli, F., Klein-Szanto, A. J., Visone, R., De Martino, I., Curcio, A., Morisco, C., Del Vecchio, L., Baldassarre, G., Arra, C., Viglietto, G., Indolfi, C., Croce, C. M., and Fusco, A. (2006) Haploinsufficiency of the *Hmga1* gene causes cardiac hypertrophy and myelo-lymphoproliferative disorders in mice. *Cancer Res.* **66,** 2536–2543
23. Wang, X., Li, Z., Naganuma, A., and Ye, B. H. (2002) Negative autoregulation of BCL-6 is bypassed by genetic alterations in diffuse large B cell lymphomas. *Proc. Natl. Acad. Sci. U.S.A.* **99,** 15018–15023
24. Pasqualucci, L., Migliazza, A., Basso, K., Houldsworth, J., Chaganti, R. S., and Dalla-Favera, R. (2003) Mutations of the *BCL6* proto-oncogene disrupt its negative autoregulation in diffuse large B-cell lymphoma. *Blood* **101,** 2914–2923
25. Sakaguchi, S., Hombauer, M., Bilic, I., Naoe, Y., Schebesta, A., Taniuchi, I., and Ellmeier, W. (2010) The zinc-finger protein MAZR is part of the transcription factor network that controls the CD4 *versus* CD8 lineage fate of double-positive thymocytes. *Nat. Immunol.* **11,** 442–448
26. Csernus, B., Timár, B., Fülöp, Z., Bognár, A., Szepesi, A., László, T., Jáksó, P., Warnke, R., Kopper, L., and Matolcsy, A. (2004) Mutational analysis of IgV_H and *BCL-6* genes suggests thymic B-cells origin of mediastinal (thymic) B-cell lymphoma. *Leuk. Lymphoma* **45,** 2105–2110
27. Ye, B. H., Cattoretti, G., Shen, Q., Zhang, J., Hawe, N., de Waard, R., Leung, C., Nouri-Shirazi, M., Orazi, A., Chaganti, R. S., Rothman, P., Stall, A. M., Pandolfi, P. P., and Dalla-Favera, R. (1997) The *BCL-6* proto-oncogene controls germinal-center formation and Th2-type inflammation. *Nat. Genet.* **16,** 161–170
28. Morse, H. C., 3rd, Anver, M. R., Fredrickson, T. N., Haines, D. C., Harris, A. W., Harris, N. L., Jaffe, E. S., Kogan, S. C., MacLennan, I. C., Pattengale, P. K., and Ward, J. M. (2002) Bethesda proposals for classification of lymphoid neoplasms in mice. *Blood* **100,** 246–258
29. Davies, J. M., Hawe, N., Kabarowski, J., Huang, Q. H., Zhu, J., Brand, N. J., Leprince, D., Dhordain, P., Cook, M., Morriss-Kay, G., and Zelent, A. (1999) Novel BTB/POZ domain zinc-finger protein, LRF, is a potential target of the *LAZ-3*/*BCL-6* oncogene. *Oncogene* **18,** 365–375
30. Fearon, D. T., Manders, P., and Wagner, S. D. (2001) Arrested differentiation, the self-renewing memory lymphocyte, and vaccination. *Science* **293,** 248–250
31. Ci, W., Polo, J. M., Cerchietti, L., Shaknovich, R., Wang, L., Yang, S. N., Ye, K., Farinha, P., Horsman, D. E., Gascoyne, R. D., Elemento, O., and Melnick, A. (2009) The BCL6 transcriptional program features repression of multiple oncogenes in primary B cells and is deregulated in DLBCL. *Blood* **113,** 5536–5548
32. Ye, B. H., Chaganti, S., Chang, C. C., Niu, H., Corradini, P., Chaganti, R. S., and Dalla-Favera, R. (1995) Chromosomal translocations cause deregulated BCL6 expression by promoter substitution in B cell lymphoma. *EMBO J.* **14,** 6209–6217
33. Lo Coco, F., Ye, B. H., Lista, F., Corradini, P., Offit, K., Knowles, D. M., Chaganti, R. S., and Dalla-Favera, R. (1994) Rearrangements of the *BCL6* gene in diffuse large cell non-Hodgkin's lymphoma. *Blood* **83,** 1757–1759
34. Muramatsu, M., Akasaka, T., Kadowaki, N., Ohno, H., Fukuhara, S., and Okuma, M. (1997) Rearrangement of the *BCL6* gene in B-cell lymphoid neoplasms. *Leukemia* **11,** 318–320
35. Skinnider, B. F., Horsman, D. E., Dupuis, B., and Gascoyne, R. D. (1999) Bcl-6 and Bcl-2 protein expression in diffuse large B-cell lymphoma and follicular lymphoma: correlation with 3q27 and 18q21 chromosomal abnormalities. *Hum. Pathol.* **30,** 803–808
36. Saito, M., Gao, J., Basso, K., Kitagawa, Y., Smith, P. M., Bhagat, G., Pernis, A., Pasqualucci, L., and Dalla-Favera, R. (2007) A signaling pathway mediating down-regulation of *BCL6* in germinal center B cells is blocked by *BCL6* gene alterations in B cell lymphoma. *Cancer Cell* **12,** 280–292
37. Mendez, L. M., Polo, J. M., Yu, J. J., Krupski, M., Ding, B. B., Melnick, A., Ye, B. H. (2008) CtBP is an essential corepressor for BCL6 autoregulation. *Mol. Cell Biol.* **28,** 2175–2186
38. Dent, A. L., Shaffer, A. L., Yu, X., Allman, D., and Staudt, L. M. (1997) Control of inflammation, cytokine expression, and germinal center formation by BCL-6. *Science* **276,** 589–592

Journal of Cellular Physiology

Embryonic Defects and Growth Alteration in Mice With Homozygous Disruption of the *Patz1* Gene

TERESA VALENTINO,[1] DARIO PALMIERI,[1] MICHELA VITIELLO,[1] ANTONIO SIMEONE,[2] GIUSEPPE PALMA,[3] CLAUDIO ARRA,[3] PAOLO CHIEFFI,[4] LORENZO CHIARIOTTI,[1,5] ALFREDO FUSCO,[1] AND MONICA FEDELE[1]*

[1]*Istituto di Endocrinologia ed Oncologia Sperimentale del CNR and Dipartimento di Biologia e Patologia Cellulare e Molecolare, Università di Napoli "Federico II", Naples, Italy*

[2]*CEINGE, Biotecnologie Avanzate, Naples, Italy*

[3]*Istituto dei Tumori di Napoli "Fondazione G. Pascale", Naples, Italy*

[4]*Dipartimento di Psicologia, II Università di Napoli, Caserta, Italy*

[5]*Dipartimento di Chimica Farmaceutica e Tossicologica, Università di Napoli "Federico II", Naples, Italy*

PATZ1 is an emerging cancer-related gene coding for a POZ/AT-hook/kruppel Zinc finger transcription factor, which is lost or misexpressed in human neoplasias. Here, we investigated its role in development exploring wild-type and Patz1-knockout mice during embryogenesis. We report that the *Patz1* gene is ubiquitously expressed at early stages of development and becomes more restricted at later stages, with high levels of expression in actively proliferating neuroblasts belonging to the ventricular zones of the central nervous system (CNS). The analysis of embryos in which *Patz1* was disrupted revealed the presence of severe defects in the CNS and in the cardiac outflow tract, which eventually lead to a pre-mature in utero death during late gestation or soon after birth. Moreover, the Patz1-null mice showed a general growth retardation, which was consistent with the slower growth rate and the increased susceptibility to senescence of Patz1$^{-/-}$ mouse embryonic fibroblasts (MEFs) compared to wild-type controls. Therefore, these results indicate a critical role of PATZ1 in the control of cell growth and embryonic development.

J. Cell. Physiol. 228: 646–653, 2013.

The *PATZ1* gene encodes four alternatively expressed proteins, ranging from 537 to 687 amino acids, that share a common modular structure consisting of a POZ domain, two AT-hooks and four to seven C2H2 Zinc fingers (Fedele et al., 2000; Kobayashi et al., 2000; Mastrangelo et al., 2000). According to these domains, PATZ is a member of the POK (POZ and Kruppel) family of transcriptional repressors (Costoya, 2007), but it may function either as activator or repressor depending upon the cellular context. Indeed, it has been reported to either activate or repress c-myc (Fedele et al., 2000; Kobayashi et al., 2000), to activate mast cell protease 6 (Morii et al., 2002) and FGF4 (Kobayashi et al., 2000), and to repress androgen receptor (Pero et al., 2002) and CD8 (Bilic et al., 2006) genes. Consistent with the CD8 regulation, it has been recently shown that PATZ is an important part of the transcription factor network that controls the CD4 versus CD8 lineage fate of double-positive thymocytes (Sakaguchi et al., 2010). Moreover, we have previously reported that PATZ has a critical role in the spermatogenesis, by regulating the apoptotic pathways in germ cells (Fedele et al., 2008).

Several studies suggest a role of PATZ in carcinogenesis. In fact, the *PATZ1* gene maps on the FRA22B fragile site, which suffers loss of heterozygosity in several solid tumors (Burrow et al., 2009), and it has been found rearranged with the *EWS* gene in a small round cell sarcoma, with the loss of heterozygosity of the wild-type *PATZ1* allele (Mastrangelo et al., 2000), suggesting a potential tumor suppressor role. However, an oncogenic role for *PATZ1* has also been suggested since it is overexpressed in some human malignant neoplasia, including colon (Tian et al., 2008), testicular (Fedele et al., 2008), and breast (Tritz et al., 2008) tumors. Consistently, PATZ down-regulation by siRNA either blocks the growth or induces apoptosis of cell lines derived from colorectal cancers or gliomas, respectively (Tian et al., 2008; Yang et al., 2010). PATZ was found mislocalized in testicular seminomas, teratomas, and embryonal carcinomas from the nucleus to the cytoplasm, suggesting that its function could be impaired in these tumors or, alternatively, that it may acquire some new cytoplasmic function that could contribute to neoplastic transformation (Fedele et al., 2008). Interestingly, it has been recently shown that such delocalization of PATZ in testicular seminomas depends on oestrogen receptor-β levels and the translocation from cytoplasm to the nucleus is mediated by cAMP (Esposito et al., 2011), as it was previously demonstrated in other cell

Conflict of interest: none to declare.

Additional supporting information may be found in the online version of this article.

Contract grant sponsor: AIRC;
Contract grant number: IG5728.

*Correspondence to: Monica Fedele, Istituto di Endocrinologia ed Oncologia Sperimentale (IEOS) del CNR, via S. Pansini, Napoli 5-80131, Italy. E-mail: mfedele@unina.it

Manuscript Received: 29 February 2012
Manuscript Accepted: 31 July 2012

Accepted manuscript online in Wiley Online Library (wileyonlinelibrary.com): 9 August 2012.
DOI: 10.1002/jcp.24174

systems, such as PC3M prostate carcinoma cells and normal fibroblasts (Tritz et al., 2008).

Since it is known that a large number of genes involved in embryonic development are either tumor suppressor or oncogenes (Dean, 1998), we focused on studying the role of PATZ during development. To this aim we first analyzed *Patz1* expression during normal mouse development. Then, we analyzed the phenotype of mouse embryos null for *Patz1* in comparison with wild-type (WT) controls. Finally, we examined the growth characteristics of Patz1$^{-/-}$ mice and their embryo-derived fibroblasts.

Materials and Methods

In situ hybridization

The probe used for this study was a 489 bp fragment carrying a portion of the mouse *Patz1* cDNA. The same fragment, cloned in the opposite orientation in pGem3Z, was used to obtain a sense probe which we used as a control of the specificity of hybridization. Probe synthesis and labeling was carried out as previously described (Chiappetta et al., 1996). Embryos of 8.5, 10.5, 12.5, 14.5, and 17.5 days post coitum (dpc), obtained from C57/Bl6 mice mated between 9 pm and 10 pm, were collected and classified according to the Theiler staging (Theiler, 1989). Three independent embryos for each stage have been analyzed. Tissue preparation, hybridization, and washes were carried out as previously described (Chiappetta et al., 1996). Ethical Committee approval was given in all instances.

Generation and genotyping of mutant mice

The *Patz1* gene targeting vector was derived from a λΦXII phage library of a 129SvJ mouse strain (Stratagene, La Jolla, CA). It was designed to delete a 2,317-bp *Pst*I–*Xho*I fragment, including the start codon, the coding regions for the POZ domain, the AT-hook and the first four zinc fingers (Supplementary Fig. 1). It was constructed by subcloning the 5′-flanking region (the *Spe*I–*Pst*I 3 kb fragment), the *neo* cassette and the 3′-flanking region (the *Xho*I–*Xba*I 3.2 kb fragment) into the Bluescript plasmid (Stratagene) that contained a *Pac*I digestion site inserted at a distance from the multi-cloning site (Pero et al., 2012). The targeting vector was linearized with *Pac*I before electroporation into embryonic stem (ES) cells (Incyte Genomics, Palo Alto, CA).

Two correctly targeted ES cell lines were injected into C57Bl/6J blastocysts. Both ES cell lines gave rise to germ line chimeras that were backcrossed to C57Bl/6J females in order to obtain *Patz1* heterozygous offspring. For Southern blot analysis, tail DNA samples were digested with *Stu*I and probed with an external 5′ genomic fragment that detects 9.3 or 8-kb fragments, corresponding to the WT and mutant alleles, respectively. All mice were maintained under standardized nonbarrier conditions in the Laboratory Animal Facility of Istituto dei Tumori di Napoli (Naples, Italy), and all studies were conducted in accordance with Italian regulations for experimentations on animals.

Histological analysis

For histological examination, the embryos were gently immersed in Bouin solution (picric acid, 37% formaldehyde, 100% acetic acid 15:5:1). Sections (6 μm thick) were stained with hematoxylin and eosin according to standard procedures.

MEF growth and BrdU-FACS analysis

Primary MEFs, obtained from 12.5-day-old embryos, were cultured at 37°C (5% CO_2) in Dulbecco's Modified Eagle's Medium (DMEM) containing 10% fetal bovine serum (Hyclone, Logan, UT) supplemented with penicillin/streptomycin. To determine the cell doubling time, each cell line (4×10^5 cells) was plated in 6-cm culture dishes and counted daily with a hemocytometer. MEFs in logarithmic growth were incubated for 2 h with 30 μM BrdU (Becton Dickinson, San Jose, CA) and then trypsinized and fixed in 70% ethanol for cell cycle analysis by FACS. After washing with PBS, cells were re-suspended in 250 μl of PBS and incubated with 250 μl of 4M HCl for 30 min at RT followed by two washes with PBS-Tween 0.1%. Subsequently, the cells were stained, first, with 20 μl anti-BrdU-FITC (Becton Dickinson) for 1h at RT in the dark, and then washed twice with PBS-Tween 0.1% and re-stained with 5 μg/ml propidium iodide containing RNase (20 μg/ml), for 20 min at RT in the dark, and analyzed with a FACScan flow cytometer (Becton Dickinson) interfaced with a Hewlett-Packard computer (Palo Alto, CA). Gating excluded cell debris and fixation artifacts, and the G1, S, and G2/M populations were quantified using CellQuest software. In each experiment, a similar number of events was analyzed.

Senescence associated-β-galactosidase assay

Cells (4×10^4), plated 24 h before the assay, were washed twice with PBS and immersed in fixation buffer [2% (w/v) formaldehyde, 0.2% (w/v) glutaraldehyde in PBS] for 7 min. After three additional PBS washes, the cells were stained overnight in staining solution (40 mM citric acid/sodium phosphate pH 6.0, 150 mM NaCl, 2.0 mM $MgCl_2$, 1 mg/ml X-gal) at 37°C without CO_2 to avoid modification of the PH. The next day, the stained solution was replaced with PBS, and all of the cells in at least 24 fields of view were counted under the light microscope.

RNA extraction and qRT-PCR

Total RNA was extracted using TRI-reagent solution (Sigma, St Louis, MO) according to the manufacturer's protocol, treated with DNAse I (Invitrogen/Life Technologies Italia, Monza, Italy), and reverse-transcribed using random hexanucleotides as primers and MuLV reverse transcriptase (Perkin-Elmer, Waltham, MA), following manufacturer's instructions. For quantitative RT-PCR each reaction was performed three times in triplicate using SYBR Green PCR Master Mix (Applied Biosystems, Foster City, CA), as previously described (Pero et al., 2012).

Protein extraction and immunoblot analysis

Protein extraction and Western blot analysis were carried out as previously described (Melillo et al., 2001). The antibodies used were as follows: anti-p27 (610241; Becton Dickinson), anti-vinculin (sc-7649; Santa Cruz Biotechnology, Santa Cruz, CA), anti-p21 (sc-397, Santa Cruz Biotechnology), anti-$p16^{Ink4a}$ (ab-54210; Abcam, Cambridge, UK), anti-cyclin D2 (sc-754; Santa Cruz Biotechnology), anti-$p19^{arf}$ (ab-80; Abcam), anti-cyclin E (sc-481; Santa Cruz Biotechnology), anti-p53 (sc-126; Santa Cruz Biotechnology), anti-cdk1 (Ab-1; Calbiochem, San Diego, CA), anti-cdk2 (sc-748; Santa Cruz Biotechnology), anti-cdk4 (sc-260; Santa Cruz Biotechnology), anti-cyclin A (sc-751; Santa Cruz Biotechnology), anti-HMGA1 (Melillo et al., 2001), and anti-HMGA2 (Fedele et al., 2006).

Statistics

The one-way ANOVA followed by Tukey's multiple comparison test was used to compare groups of experiments. The statistical significant difference was considered when *P*-value was <0.05.

Results

Developmental expression of *Patz1* gene

To define the temporal and spatial profile of *Patz1* expression, we performed an in situ hybridization analysis on mouse embryos between 8.5 and 17.5 days dpc, the period during which the most critical events of organogenesis take place. In general, the expression of *Patz1* gene was ubiquitous at early stages of development and became more restricted at later stages. Interestingly, *Patz1* was expressed at high levels in the central nervous system (CNS) becoming confined at later

stages to actively proliferating neuroblasts belonging to the ventricular zones (Figs. 1 and 2).

Early gestation (8.5–10.5 dpc). At 8.5 dpc *Patz1* transcripts were widely distributed in all embryonic tissues (Fig. 1, Panel A). At 9.5 dpc *Patz1* was still expressed in the majority of the embryonic tissues even though it was markedly transcribed along the CNS, throughout the branchial arches, in the otic vescicles and in stomach primordium (Fig. 1, Panels B and C). All the other tissues showed a reduced level of expression. At 10.5 dpc (Fig. 1, Panels D and E) *Patz1* mRNA was detected at high level in the differentiating spinal and cephalic ganglia. A lower expression was also detected through the limb buds, branchial arches, stomach and the epato-biliary primordium.

Midgestation (12.5–14.5 dpc) and late gestation (17.5 dpc). At 12.5 dpc *Patz1* transcripts were detected at high level in the cephalic and spinal ganglia as well as in the brain, hindbrain, and spinal cord (Fig. 2, Panels A and B). Their distribution along the CNS was not uniform and resulted more abundant in the proliferating neuroblasts belonging to the ventricular zones (Fig. 2, Panels A–D). Additional sites of strong expression were the olfactory and respiratory epithelium in the nasal pit (Fig. 2, Panels A and B), the retina (Fig. 2, Panel C), kidney (Fig. 2, Panel A), and Rathke's pouch (Fig. 2, Panel D). At 17.5 dpc *Patz1* was detected at high level along the CNS and in specific organs such as lung, liver, and kidney (Fig. 2, Panels E–G). In the CNS, its high expression appeared at this stage clearly confined to the actively proliferating neuroblasts in the periventricular neocortical neuroepithelium. Moreover, in the telencephalon it was expressed also in the cortical plate, in the hippocampus, and in the striatal neuroepithelium and subventricular zone (Fig. 2, Panels F and G). A high expression was also found in the thymus, thyroid, salivary glands (Fig. 2, Panels E and F), and in the tooth primordia (Fig. 2, Panel G).

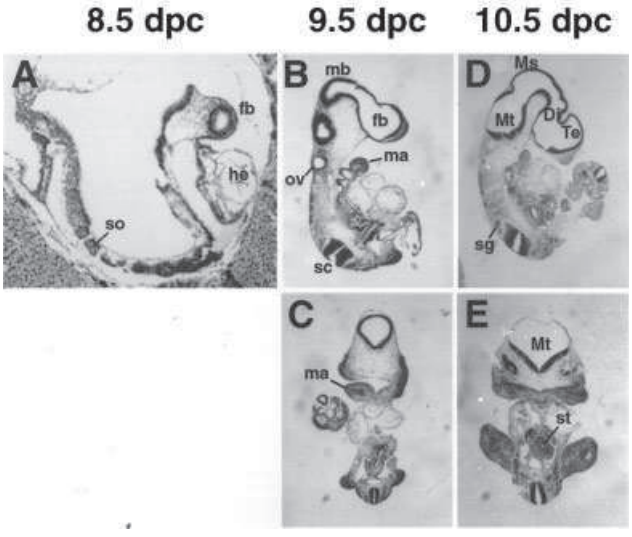

Fig. 1. Expression of the *Patz1* gene in early gestation. *Patz1* expression at 8.5 dpc (A), 9.5 dpc (B) and 10.5 dpc (D) in sagittal (A, B, D) and frontal (C, E) sections. Abbreviations stand as follows: fb and mb indicate the fore- and mid-brain, respectively; Te, Di, Ms, and Mt indicate the telencephalon, diencephalon, mesencephalon, and metencephalon, respectively; he, heart; sc, spinal cord; sg, spinal ganglia; so, somites; ov, otic vescicles; ma, mandibular arch; st, stomach.

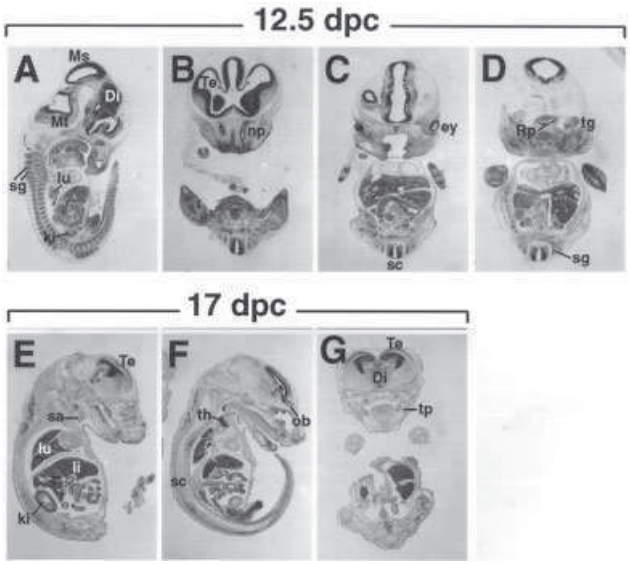

Fig. 2. Expression of the *Patz1* gene in mid- and late gestation. *Patz1* expression at 12.5 dpc (A–D) and 17 dpc (E–G) in sagittal (A, E, F) and frontal (B–D, G) sections. Abbreviations stand as in the previous figure plus: lu, lung; ki, kidney; np, nasal pit; ey, eye; Rp, rathke's pouch; tg, trigeminal ganglion; sa, salivary gland; li, liver; th, thymus; tp, tooth primordium.

Embryonic lethality and developmental defects in *Patz1*-null mice

To gain insights into the physiological role of Patz1 during development and adult life, we generated mice carrying a null mutation at the *Patz1* locus.

Mice heterozygous for the *Patz1* null allele appeared normal and were fertile. Homozygous mutant pups totaled only 4% of the newborn offspring from heterozygous intercrosses, instead of the expected 25%, indicating that most *Patz1*-null mice died during embryogenesis. Embryos from timed matings between heterozygotes were analyzed at different gestation stages (Table 1). Until 15.5 dpc all the embryos analyzed had beating hearts with no gross abnormalities except for a slight body size decrease in most of the homozygous mutant embryos (data not shown) and exencephaly in 4 out of 15 at 13.5 dpc (Fig. 3 and Supplementary Fig. 2A). Exencephaly is a cranial

TABLE 1. Embryonic lethality in Patz1$^{-/-}$ mice

	Litters	*Patz1*$^{+/+}$	*Patz1*$^{+/-}$	*Patz1*$^{-/-}$	Dead[a]	Readsorbed	Total
E8.5	2	4	11	5	0	0	20
E9.5	2	5	8	5	0	0	18
E10.5	2	2	10	3	0	0	15
E11.5	2	5	12	3	0	0	20
E12.5	5	5	10	9	0	4	24
E13.5	7	13	30	15	0	5	59
E14.5	2	4	9	3	0	2	16
E15.5	10	15	50	15	12 (80%)	10	80
E16.5	10	20	70	1	0	15	91
E18.5	10	10	40	0	—	20	50
3W[b]	24	50 (38%)	76 (58%)	5[c] (4%)	0	—	131

Embryos were isolated at the indicated time of gestation and analyzed for viability by observing heart beating. E, embryonic day; 3W, 3 weeks after birth.
[a]Percent of total *Patz1*$^{-/-}$ embryos given in parentheses.
[b]Percent of total pups given in parentheses.
[c]Growth retarded.

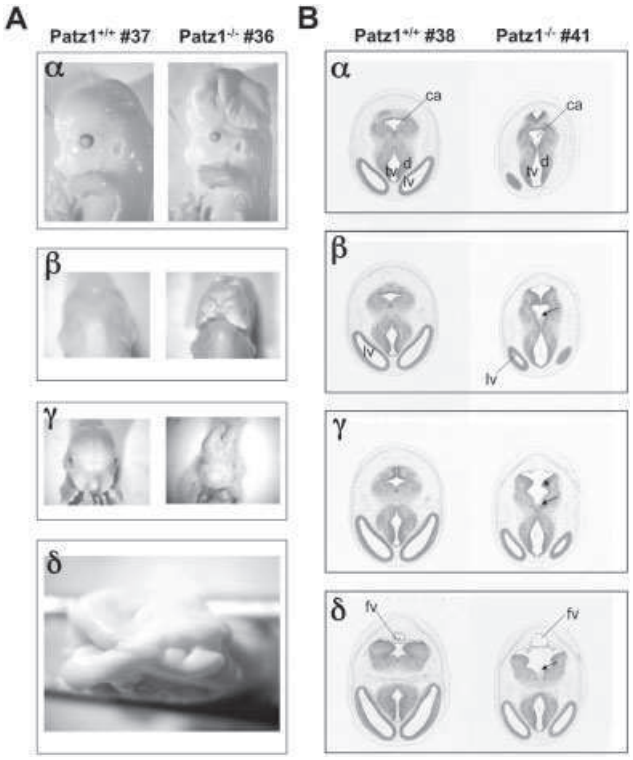

Fig. 3. CNS developmental defects in Patz1$^{-/-}$ embryos. A: Macroscopic comparison of a Patz1$^{-/-}$ embryo at 13.5 dpc with exencephaly (right side) with a normal WT embryo from the same littermate (left side). Lateral (α), dorsal (β), frontal (γ), and apical views (δ) are shown. B: Series of brain cross sections, progressively more caudal, of representative WT and Patz1$^{-/-}$ (without exencephaly) embryos at 13.5 dpc. For each panel, parallel sections are compared. Ca, cerebral aqueduct; d, diencephalon; tv, third ventricle; lv = lateral ventricle; fv, fourth ventricle; *, neuroepithelium of the isthmus; arrow indicates a tongue of cells projecting from the floor of the rhomboencephalon within the ventricular cavity.

neural tube defect, resulting from failed closure of the neural folds during neurulation. In the mouse, the neural tube initiates closure at 8.5 dpc, beginning at the cervical/hindbrain boundary. Two additional de novo closure sites occur at the caudal and rostral limits of the forebrain. Closure then spreads along the neural folds in the rostral and caudal directions. By 9.5 dpc, closure is normally complete (Juriloff et al., 1991). Differently from the WT controls, the Patz1$^{-/-}$ embryos with exencephaly (Fig. 3A and Supplementary Fig. 2A) had failure of closure of the anterior neuropore and severe malformation of the brain with the possible exception of the most caudal region of the hindbrain (caudal medulla oblongata). Histological examination of all the other 13.5 dpc homozygous mutant embryos with no exencephaly (11 out of 15) revealed some anomalies of brain development with a size and configuration roughly corresponding to 12.5–13 dpc. In particular, the brain of the mutants is smaller, the whole ventricular system is larger and, although the pattern of folding is preserved, the structures that bulge out such as the ganglionic eminence and the diencephalon are less pronounced (Fig. 3B and Supplementary Fig. 2B). Moreover, the thickness of the nervous tissue around the ventricular cavities is reduced overall, and it is particularly evident at the level of the telencephalon and diencephalon. The choroid plexus of the 4th ventricle is hypoplasic. The neuroepithelium of the isthmus and prospective cerebellum remains apart caudally (Fig. 3Bγ), although in more cranial sections the ventral part comes together (Fig. 3Bβ) and eventually fuses (Fig. 3Bα). Interestingly, in some mutant embryos (7 out of 15) a tongue of cells projects from the midline (median sulcus) of the floor of the rhomboencephalon within the ventricular cavity, extending rostrally to the region of the mesencephalon (arrows in Fig. 3B and Supplementary Fig. 2B).

Another anomaly, common to all the *Patz1*$^{-/-}$ embryos analyzed, is the origin of the aorta. In mutant embryos there is a clear malformation of the great vessels that exit the ventricular chambers of the heart. In contrast to WT embryos, where the descending aorta is located in the midline towards the left behind the esophagus (Fig. 4A, left), in 5 out of 15 mutant embryos the descending aorta is located towards the right of the midline (Fig. 4A, right). This suggests an origin from the right primitive dorsal aorta, in contrast to the normal development, in which the descending aorta originates from the left primitive dorsal aorta. From these histological sections it is not clear the real identity of the ascending aorta and pulmonary trunk. A possibility is that the identity of the two outflow trunks is the same as in the WT based on its relative position to each other. In this case, the ductus arteriosus assumes a left to right orientation, whereas the junction between the ascending aorta and the aortic arch is located on the right side. The course of the ascending aorta follows a ventral to dorsal direction with minimal displacement to the side. An alternative possibility is that the identity of the ascending aorta and pulmonary trunk is reversed in the mutant embryo, in such a way that the vessel occupying the position of the WT aorta is in reality the pulmonary trunk, and vice versa, the vessel that should be the pulmonary trunk is the ascending aorta. This malformation would be a transposition of the great vessels. In either case, the aortic arch would derive from the 4th right branchial arch artery and the ductus arteriosus from the 6th right branchial arch artery. In all the other mutants, the descending aorta is normally located in the left side of the esophagus but the aorta appears always ventral to the pulmonary trunk at its origin (Fig. 4B), suggesting outflow-tract (OFT) defects possibly including transposition or malposition of the great vessels. Consistent with these histological data, the cardiac OFT macroscopically analyzed in two agonizing newborn Patz1$^{-/-}$ pups appeared impaired by different types of vessels anomalies (Supplementary Fig. 3).

Growth retardation in *Patz1*-null mice

Almost all the *Patz1*$^{-/-}$ mice were 10–20% smaller than sex-matched littermate controls following weaning and these differences were kept almost unchanged throughout the whole of their lives (Fig. 5A,B). Similarly, their mean body weight was significantly lower than that of *Patz1*$^{+/+}$ mice in both sexes ($P < 0.01$), as depicted by the growth curves in Figure 5C. Conversely, the mean body weight of *Patz1*$^{+/-}$ mice did not differ from that of WT mice (Fig. 5C). To examine whether visceral organ size was proportional to the body weight we measured the wet weight of the heart, liver, spleen, kidney, and lung. The ratio of organ to body weight was consistently smaller in Patz1$^{-/-}$ mice as compared to WT mice (Fig. 5D).

Cell cycle profile alterations and premature senescence in *Patz1*-knockout MEFs

MEFs were prepared from *Patz1*$^{+/+}$, *Patz1*$^{+/-}$, and *Patz1*$^{-/-}$ embryos at 12.5 dpc. The growth properties of the MEFs were assessed at passage 4 by growth curves and cell-doubling time. As shown in Figure 6A–C, *Patz1*$^{-/-}$ MEFs grew significantly slower than their WT counterparts. Conversely, heterozygous *Patz1*-knockout MEFs grew significantly faster than WT MEFs.

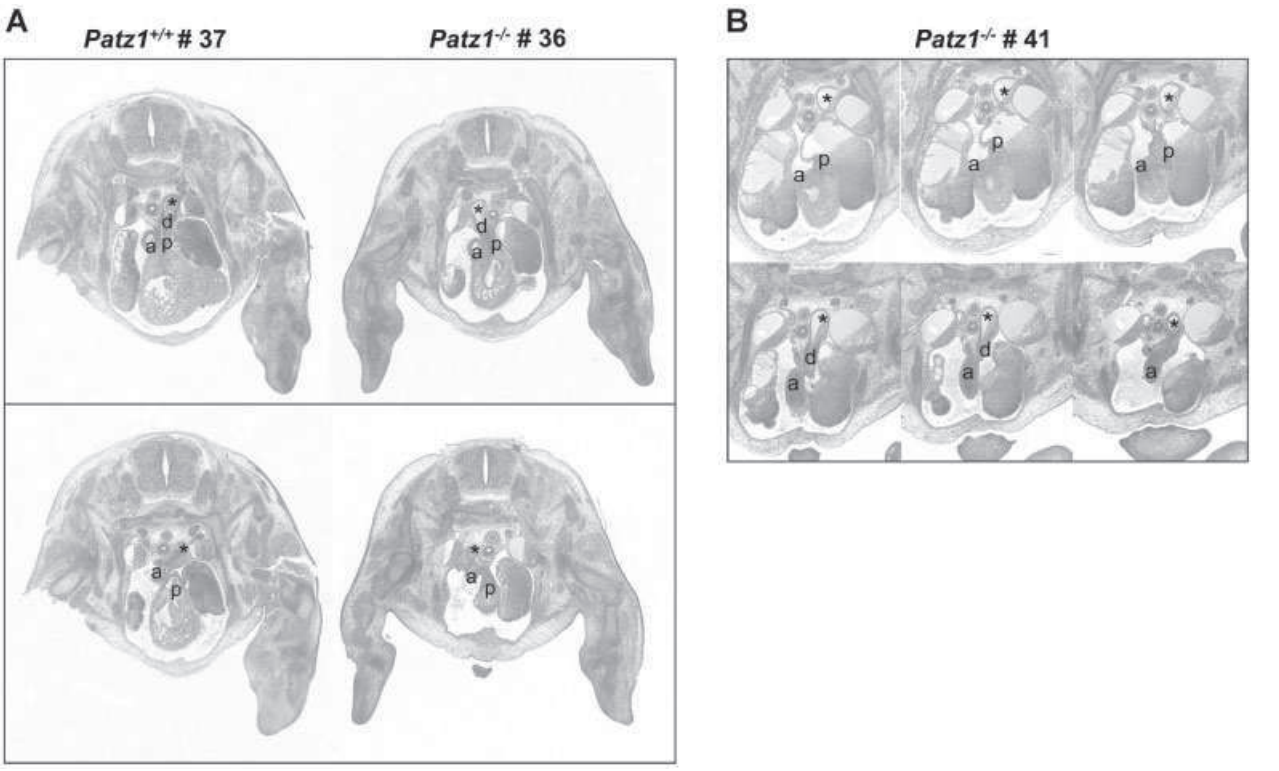

Fig. 4. Outflow-tract defects in Patz1$^{-/-}$ embryos. A: Cross sections, at the heart level, of representative WT and Patz1$^{-/-}$ embryos at 13.5 dpc. Parallel sections are aligned for comparison. B: Cross section, at the heart level, of a Patz1$^{-/-}$ embryo at 13.5 dpc different from that shown in A. All sections shown are progressively more cranial going from the top to the bottom (A) and for the left to the right (B). *, descending aorta and aortic arch; a, ascending aorta; p, pulmonary trunk; d, ductus arteriosus.

To determine whether the growth alterations observed in *Patz1*$^{-/-}$ and *Patz1*$^{+/-}$ MEFs were due to altered progression through the different phases of the cell cycle, proliferating MEFs in the logarithmic phase were analyzed by bromodeoxyuridine (BrdU) incorporation and flow cytometry. A drastic reduction in BrdU incorporation was observed in *Patz1*$^{-/-}$ compared to both WT and *Patz1*$^{+/-}$ cells, suggesting a significant decrease in S phase entrance in Patz1-null MEFs. Consistently, staining with propidium iodide for DNA content confirmed that the cell population in S phase was significantly decreased in *Patz1*$^{-/-}$ compared to both WT and heterozygous cells (Fig. 6D). Conversely, an increased number of *Patz1*$^{-/-}$ cells in both G0/G1 and G2/M has been observed compared to WT and *Patz1*$^{+/-}$ MEFs (Fig. 6D).

We next examined the susceptibility to senescence of the MEFs at different culture passages by measuring senescence-associated β-gal activity. As shown in Figure 6, Panels E and F, *Patz1*$^{-/-}$ MEFs entered into premature cellular senescence when they were cultured beyond seven passages.

To further investigate the mechanisms underlying the cell cycle profile alterations of *Patz1*-knockout MEFs, we examined the expression of cyclins, CDKs and CDK-inhibitor proteins in *Patz1*$^{+/+}$, *Patz1*$^{+/-}$, and *Patz1*$^{-/-}$ cells. Proteins involved in cell cycle activation, such as HMGA1 and HMGA2, were also examined. Consistent with the slow growth rates (Fig. 6A–C) and the increased susceptibility to senescence of *Patz1*$^{-/-}$ MEFs (Fig. 6E,F), an increased expression of cell cycle inhibitors, including p53, p21, p27, p16, and p19, was observed in *Patz1*$^{-/-}$ MEFs compared to their WT and heterozygous counterparts. Paradoxically, *Patz1*$^{-/-}$ cells also showed increased expression of various proteins involved in cell cycle activation, including cyclin D2, CDK4, Cyclin E, HMGA1, and HMGA2 (Fig. 6G). It is likely that conflicting signals could account for cell cycle arrest (hypermitogenic arrest) that might then induce premature senescence (Blagosklonny, 2003).

Collectively, these data suggest that cells devoid of two *Patz1* alleles enter the cell cycle more slowly than WT cells do, arrest in both G0/G1 and G2/M phases of the cell cycle and undergo premature cellular senescence. Conversely, heterozygous MEFs cells grow faster than WT controls but do not show significant differences in BrdU uptake and cell cycle profile, compared to WT cells.

Discussion

PATZ is an emerging cancer-related transcription factor, whose role in cancer pathogenesis is not clear, due to controversial reports supporting either a tumor suppressive or a tumor inducing activity (Mastrangelo et al., 2000; Fedele et al., 2008; Tian et al., 2008; Tritz et al., 2008; Yang et al., 2010; Pero et al., 2012). From the analysis of Patz1-null mice, we previously reported an important role for the *PATZ1* gene in testis development and spermatogenesis. Indeed, the lack of the *Patz1* gene led to increased apoptosis of the spermatocytes and total absence of spermatids and spermatozoa, with the subsequent loss of tubular structure and male infertility (Fedele et al., 2008). Consistent with these data, among the germ cells, PATZ1 is exclusively expressed in spermatogonia (Fedele et al., 2008), in which, as Plzf, another member of the POK family, it could regulate the maintaining of a stem cell pool (Buaas et al., 2004; Costoya et al., 2004). Also by generating Patz1-null mice, but focusing on T-cell development, it has been subsequently

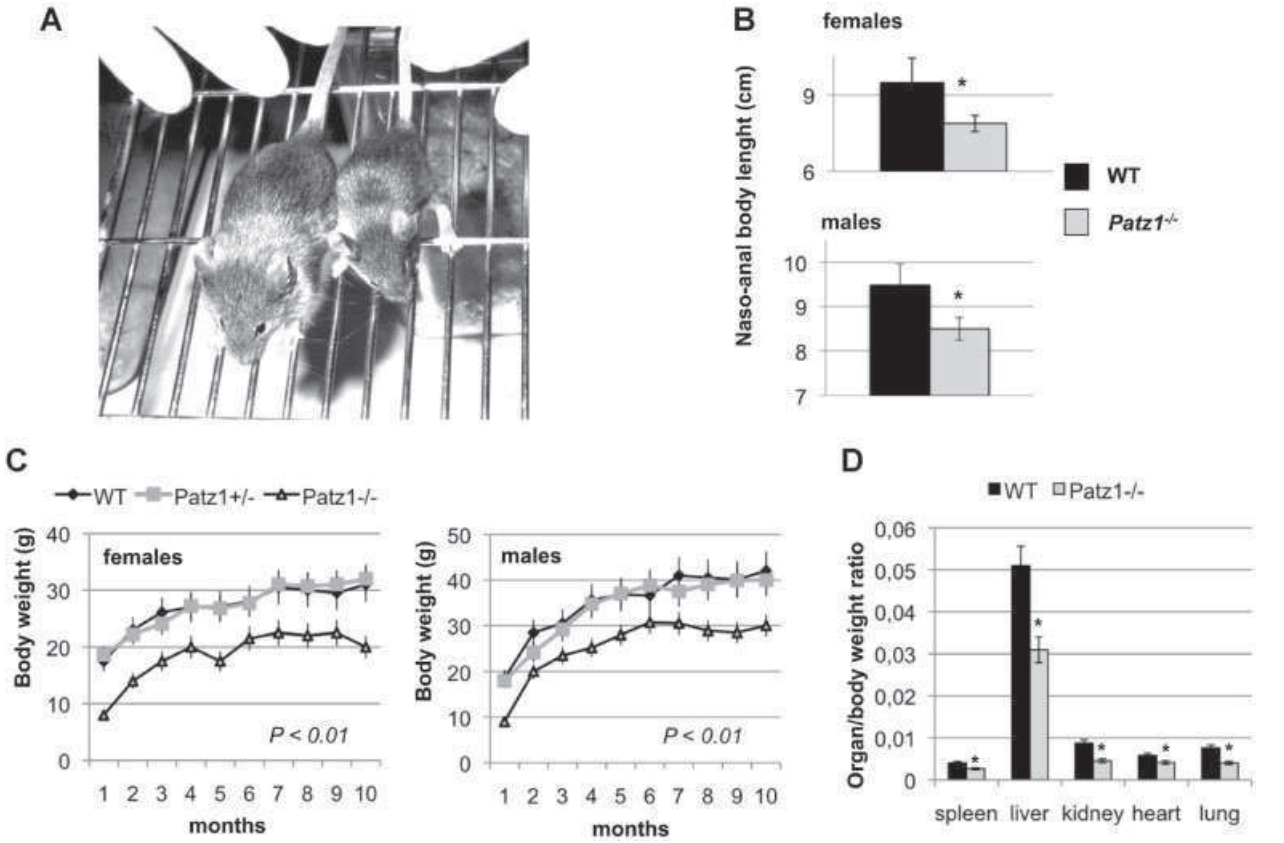

Fig. 5. Growth retardation of *Patz1*$^{-/-}$ mice. A: Gross appearance of a representative 1-year-old *Patz1*-null mouse (right) in comparison with a sex-matched wild-type sibling (left). B: Naso-anal length of cohorts of 10 mice, males or females, was measured at 12 months of age. Values are mean ± SD, $^{*}P < 0.05$. C: Body weights curves of cohorts of 10 WT, 10 *Patz1*$^{+/-}$ and 10 *Patz1*$^{-/-}$ female (left) and male (right) mice as a function of age. Value are mean ± SD. The curves of *Patz1*$^{-/-}$ mice were significantly lower than both *Patz1*$^{+/+}$ and *Patz1*$^{+/-}$ mice ($P < 0.01$), as calculated by ANOVA + Tukey test. D: Ratio of organ to body weight on mean values of four mice for each genotype above indicated. $^{*}P < 0.05$.

shown that PATZ regulates transcription of the *cd8* gene and is part of the transcription factor network that controls the fate of double positive thymocytes (Sakaguchi et al., 2010).

In the present work, we have more deeply studied the expression of PATZ during development, extending the analysis to the whole embryo. Interestingly, we found that it is widely expressed at high levels during embryogenesis, especially in the CNS, where it is clearly restricted to the actively proliferating neuroblasts in the periventricular neocortical neuroepithelium, in the telencephalic cortical plate, in the hippocampus, and in the striatal neuroepithelium and subventricular zone, suggesting the involvement of PATZ in CNS development, as then validated by the phenotype of *Patz1*$^{-/-}$ embryos. In fact, they show defects in the CNS with a clear reduction of periventricular cells. The critical role of PATZ in CNS development is consistent with previously published data reporting that PATZ is strongly expressed in the midbrain region (Kobayashi et al., 2000) and that it is one of the transcriptional factors that regulate a group of candidate genes for susceptibility to the fetal alcoholic syndrome, which is characterized by severe defects at the CNS (Lombard et al., 2007).

Interestingly, most of the CNS districts, where PATZ1 expression is confined at later stages of development, harbor embryonic neural stem cells (NSCs; Temple, 2003), once again suggesting a crucial role of PATZ1 in maintaining a stem cell pool. This is consistent with the reduction of the subventricular zone, which is one of the key neurogenic sites harboring the adult NSC niche (Doetsch, 2003), in Patz1-null embryos. It is noteworthy that in adult mammals, NSCs generate new neurons that are important for specific types of learning and memory (Yamasaki et al., 2007; Zhang et al., 2008). The control of adult NSC number and function is fundamental for preserving the stem cell pool and ensuring proper levels of neurogenesis throughout life. Indeed, decreased neurogenesis is implicated in the development of pre-mature aging and disorders in learning, memory, and cognition (Lemaire et al., 2000; Drapeau and Abrous, 2008; Kitamura et al., 2009). Therefore, the definition of the mechanisms underlying NSC maintaining may open the possibility of preventing the onset or progression of these disorders by therapeutically enhancing neurogenesis.

Another interesting phenotype, observed by the morphological analysis of *Patz1*$^{-/-}$ embryonic tissues at 12.5 dpc, and subsequently confirmed by macroscopic observations in newborn pups, was the altered positioning of the cardiac OFT. It is likely that these defects are responsible for the intrauterine or early neonatal death of most Patz1-null mice. In fact, the wrong positioning of the vessels that carry blood to and from the heart can cause birth asphyxia due to respiratory distress following the transition from placental to pulmonary-based breathing (Ranjit, 2000). Similar cardiovascular defects are reminiscent of common congenital heart defects, most of them known as DiGeorge syndrome, seen in human newborns.

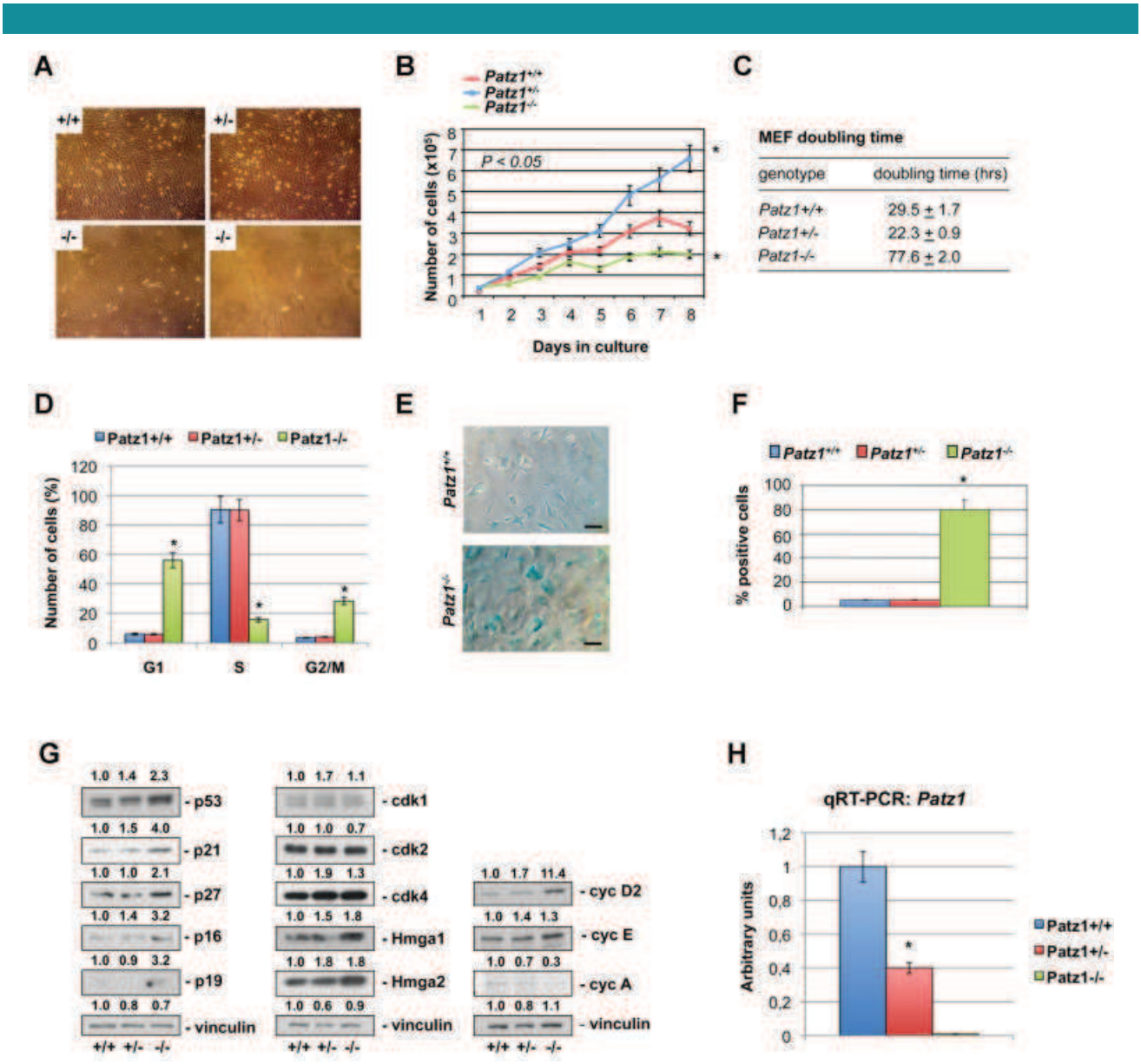

Fig. 6. Growth alterations in *Patz1*-knockout embryonic fibroblasts. A: MEFs were prepared from *Patz1*$^{+/+}$, *Patz1*$^{+/-}$, and *Patz1*$^{-/-}$ embryos at 12.5 dpc. At passage 4 their growth properties were examined in vitro. Representative clones from each genotype, as indicated in the figure, are shown 3 days after plating an equal number of cells from each. B: Growth curves of MEFs as described in (A). MEFs were plated equally and counted daily for 8 days. The values are the mean ± SE of three different cell clones (each originating from a different embryo) for each genotype. C: Cell-doubling time of MEFs as described in (A), calculated 4 days after plating. The values represent the mean ± SD of three different cell clones as described in (B). D: BrdU + Propidium iodide flow cytometry of asynchronous MEFs as described in (A). The percentage (expressed as mean ± SD) of cells in each phase of the cell cycle is indicated. E: Light microscopy of representative WT and homozygous *Patz1*-knockout MEFs stained for β-galactosidase activity at culture passage 8 (Scale bare: 10 μm). F: Quantification of the percent of cells positive for β-galactosidase activity (i.e., senescent cells) in *Patz1*$^{+/+}$, *Patz1*$^{+/-}$, and *Patz1*$^{-/-}$ MEFs is expressed as mean ± SD of three independent experiments. G: Expression of cell cycle and senescence regulators in representative MEFs from each genotype, as indicated on the bottom, was determined by Western blot. Relative expression levels, compared to WT cells and normalized with respect to vinculin, are indicated on the top of each panel. H: Relative *Patz1* expression in MEFs as in the previous panels, evaluated by qRT-PCR. Values are the mean ± SD of three independent experiments in three different clones for each genotype.

This disease has an incidence of 1 of 4,000 born and is caused by the alteration of several genes located in 22q11-22q12 (Schinke and Izumo, 2001). Since *PATZ1* is also located on chromosome 22q12, and many human newborns with aortic arch and/or OFT defects do not display characteristic mutations in well known genes associated to the DiGeorge syndrome (DGS), such as TBX1, *PATZ1* might be a good candidate among the genes responsible for some types of DGS. It is noteworthy, at this regard, that many experimental models of DSG focus on the cardiac neural crest cells, a unique subset of cells that migrate from the dorsal aspect of the neural tube to remodel the pharyngeal arch arteries and the septation of the cardiac OFT into two individual vessels: the pulmonary trunk and ascending aorta (Hutson and Kirby, 2007). Therefore, the two main pathological phenotypes observed in Patz1$^{-/-}$ embryos (neural tube and cardiac OFT defects) could be linked by a common pathological event in the neural crest cells.

The few mice Patz1$^{-/-}$ that survive to the birth harbor no or just slight cardiovascular defects (decrease in the diameter of a vessel), having a quite normal life expectancy, except for those which die prematurely for the onset of lymphomas (Pero et al., 2012). Interestingly, most of these adult mice are growth-retarded since they are 10–20% smaller and 40–50% lighter than their WT and *Patz1*$^{+/-}$ sex and age-matched controls. This phenotype is compatible with defects in the CNS development (Shanske et al., 1997). Nevertheless, the analysis of MEF growth properties suggest that this phenotype may be due, at least in part, to alterations in cell cycle progression and premature senescence. Indeed, cell cycle analysis of *Patz1*$^{-/-}$ MEFs shows arrest at or beyond the restriction point, in either G1 or G2 phase, which is compatible with a hypermitogenic arrest (Blagosklonny, 2003). Indeed, Patz1-null MEFs showed conflicting signals due to increased levels at the same time of both mitogenic cyclins and CDK inhibitors. This could conceivably create an oncogenic stress, which would be responsible for premature senescence (Serrano et al., 1997).

The results obtained on the Patz1-null MEFs are consistent with very recent data showing growth inhibition and accelerated senescence in human endothelial cells interfered for PATZ1 expression (Cho et al., 2011). Apparently, this anti-senescence function seems to conflict with the role of tumor suppressor that we envisaged for PATZ (Pero et al., 2012). However, the different cellular context may play a critical role in the effect of PATZ on cell fate. Moreover, a dual tumor suppressor/anti-senescence role has been previously reported for other genes (Pan et al., 2011). Indeed, differently from apoptosis that leads cells to death, senescence is a stable and metabolically active state, which in fibroblasts is associated with resistance to apoptosis caused by radiation (Yeo et al., 2000).

In conclusion, our findings in Patz1-knockout mice highlight the critical role that PATZ plays during neural and cardiac OFT development, deficiencies of which dramatically impact on embryonic development and postnatal growth. Moreover, they also indicate that *PATZ1* gene can affect cell-cycle decision, supporting its cancer-related function.

Acknowledgments

We thank Sara Sancho-Oliver from Frimorfo for embryos analysis, Francesco D'Agnello for technical assistance with artwork and Sabrina Battista for critically reviewing the article.

Literature Cited

Bilic I, Koesters C, Unger B, Sekimata M, Hertweck A, Maschek R, Wilson CB, Ellmeier W. 2006. Negative regulation of CD8 expression via Cd8 enhancer-mediated recruitment of the zinc finger protein MAZR. Nat Immunol 7:392–400.

Blagosklonny MV. 2003. Cell senescence and hypermitogenic arrest. EMBO Rep 4:358–362.

Buaas FW, Kirsh AL, Sharma M, McLeann DJ, Morris JL, Griswold MD, de Rooij DG, Braun RE. 2004. Plzf is required in adult male germ cells for stem cell self-renewal. Nat Genet 36:647–652.

Burrow AA, Williams LE, Pierce LC, Wang YH. 2009. Over half of breakpoints in gene pairs involved in cancer-specific recurrent translocations are mapped to human chromosomal fragile sites. BMC Genomics 10:59.

Chiappetta G, Avantaggiato V, Visconti R, Fedele M, Battista S, Trapasso F, Merciai BM, Fidanza V, Giancotti V, Santoro M, Simeone A, Fusco A. 1996. High level expression of the HMGI (Y) gene during embryonic development. Oncogene 13:2439–2446.

Cho JH, Kim MJ, Kim KJ, Kim JR. 2012. POZ/BTB and AT-hook-containing zinc finger protein 1 (PATZ1) inhibits endothelial cell senescence through a p53 dependent pathway. Cell Death Differ 19:703–712.

Costoya JA. 2007. Functional analysis of the role of POK transcriptional repressors. Brief Funct Genomic Proteomic 6:8–18.

Costoya JA, Hobbs RM, Barna M, Cattoretti G, Manova K, Sukhwani M, Orwig KE, Wolgemuth DJ, Pandolfi PP. 2004. Essential role of Plzf in maintenance of spermatogonial stem cells. Nat Genet 36:653–659.

Dean M. 1998. Cancer as a complex developmental disorder—Nineteenth Cornelius P. Rhoads Memorial Award Lecture. Cancer Res 58:5633–5636.

Doetsch F. 2003. A niche for adult neural stem cells. Curr Opin Genet Dev 13:543–550.

Drapeau E, Abrous DN. 2008. Stem cell review series: Role of neurogenesis in age-related memory disorders. Aging Cell 7:569–589.

Esposito F, Boscia F, Franco R, Tornincasa M, Fusco A, Kitazawa S, Looijenga LH, Chieffi P. 2011. Down-regulation of oestrogen receptor-β associates with transcriptional co-regulator PATZ1 delocalization in human testicular seminomas. J Pathol 224: 110–120.

Fedele M, Benvenuto G, Pero R, Majello B, Battista S, Lembo F, Vollono E, Day PM, Santoro M, Lania L, Bruni CB, Fusco A, Chiariotti L. 2000. A novel member of the BTB/POZ family, PATZ, associates with the RNF4 RING finger protein and acts as a transcriptional repressor. J Biol Chem 275:7894–7901.

Fedele M, Visone R, De Martino I, Troncone G, Palmieri D, Battista S, Ciarmiello A, Pallante P, Arra C, Melillo RM, Helin K, Croce CM, Fusco A. 2006. HMGA2 induces pituitary tumorigenesis by enhancing E2F1 activity. Cancer Cell 9:459–471.

Fedele M, Franco R, Salvatore G, Paronetto MP, Barbagallo F, Pero R, Chiariotti L, Sette C, Tramontano D, Chieffi G, Fusco A, Chieffi P. 2008. PATZ1 gene has a critical role in the spermatogenesis and testicular tumours. J Pathol 215:39–47.

Hutson MR, Kirby ML. 2007. Model systems for the study of heart development and disease. Cardiac neural crest and conotruncal malformations. Semin Cell Dev Biol 18:101–110.

Juriloff DM, Harris MJ, Tom C, MacDonald KB. 1991. Normal mouse strains differ in the site of initiation of closure of the cranial neural tube. Teratology 44:225–233.

Kitamura T, Saitoh Y, Takashima N, Murayama A, Niibori Y, Ageta H, Sekiguchi M, Sugiyama H, Inokuchi K. 2009. Adult neurogenesis modulates the hippocampus-dependent period of associative fear memory. Cell 139:814–827.

Kobayashi A, Yamagiwa H, Hoshino H, Muto A, Sato K, Morita M, Hayashi N, Yamamoto M, Igarashi K. 2000. A combinatorial code for gene expression generated by transcription factor Bach2 and MAZR (MAZ-related factor) through the BTB/POZ domain. Mol Cell Biol 20:1733–1746.

Lemaire V, Koehl M, Le Moal M, Abrous DN. 2000. Prenatal stress produces learning deficits associated with an inhibition of neurogenesis in the hippocampus. Proc Natl Acad Sci USA 97:11032–11037.

Lombard Z, Tiffin N, Hofmann O, Bajic VB, Hide W, Ramsay M. 2007. Computational selection and prioritization of candidate genes for fetal alcohol syndrome. BMC Genomics 8:389.

Mastrangelo T, Modena P, Tornielli S, Bullrich F, Testi MA, Mezzelani A, Radice P, Azzarelli A, Pilotti S, Croce CM, Pierotti MA, Sozzi G. 2000. A novel zinc finger gene is fused to EWS in small round cell tumor. Oncogene 19:3799–37804.

Melillo RM, Pierantoni GM, Scala S, Battista S, Fedele M, Stella A, De Biasio MC, Chiappetta G, Fidanza V, Condorelli G, Santoro M, Croce CM, Viglietto G, Fusco A. 2001. Critical role of the HMGI(Y) proteins in adipocytic cell growth and differentiation. Mol Cell Biol 21:2485–2495.

Morii E, Oboki K, Kataoka TR, Igarashi K, Kitamura Y. 2002. Interaction and cooperation of mi transcription factor (MITF) and myc-associated zinc-finger protein-related factor (MAZR) for trascription of mouse mast cell protease 6 gene. J Biol Chem 277:8566–8571.

Pan J, Zhong J, Gan LH, Chen SJ, Jin HC, Wang X, Wang LJ. 2011. Klotho, an anti-senescence related gene, is frequently inactivated through promoter hypermethylation in colorectal cancer. Tumour Biol 32:729–735.

Pero R, Lembo F, Palmieri EA, Vitiello C, Fedele M, Fusco A, Bruni CB, Chiariotti L. 2002. PATZ attenuates the RNF4-mediated enhancement of androgen receptor-dependent transcription. J Biol Chem 277:3280–3285.

Pero R, Palmieri D, Angrisano T, Valentino T, Federico A, Franco R, Lembo F, Klein-Szanto AJ, Del Vecchio L, Montanaro D, Keller S, Arra C, Papadopoulou V, Wagner SD, Croce CM, Fusco A, Chiariotti L, Fedele M. 2012. POZ-, AT-hook-, and zinc finger-containing protein (PATZ) interacts with human oncogene B cell lymphoma 6 (BCL6) and is required for its negative autoregulation. J Biol Chem 287:18308–18317.

Ranjit MS. 2000. Cardiac abnormalities in birth asphyxia. Indian J Pediatr 67:529–532.

Sakaguchi S, Hombauer M, Bilic I, Naoe Y, Schebesta A, Taniuchi I, Ellmeier W. 2010. The zinc-finger protein MAZR is part of the transcription factor network that controls the CD4 versus CD8 lineage fate of double-positive thymocytes. Nat Immunol 11:442–448.

Schinke M, Izumo S. 2001. Deconstructing DiGeorge syndrome. Nat Genet 27:238–240.

Serrano M, Lin AW, McCurrach ME, Beach D, Lowe SW. 1997. Oncogenic ras provokes premature cell senescence associated with accumulation of p53 and p16INK4a. Cell 88:593–602.

Shanske A, Caride DG, Menasse-Palmer L, Bogdanow A, Marion RW. 1997. Central nervous system anomalies in Seckel syndrome: Report of a new family and review of the literature. Am J Med Genet 70:155–158.

Temple S. 2003. The development of neural stem cells. Nature 414:112–117.

Theiler K. 1989. The house mouse (atlas of embryonic development), ed. New York: Springer-Verlab.

Tian X, Sun D, Zhang Y, Zhao S, Xiong H, Fang J. 2008. Zinc finger protein 278, a potential oncogene in human colorectal cancer. Acta Biochim Biophys Sin (Shanghai) 40:289–296.

Tritz R, Mueller BM, Hickey MJ, Lin AH, Gomez GG, Hadwiger P, Sah DW, Muldoon L, Neuwelt EA, Kruse CA. 2008. siRNA down-regulation of the PATZ1 gene in human glioma cells increases their sensitivity to apoptotic stimuli. Cancer Ther 6:865–876.

Yamasaki TR, Blurton-Jones M, Morrissette DA, Kitazawa M, Oddo S, LaFerla FM. 2007. Neural stem cells improve memory in an inducible mouse model of neuronal loss. J Neurosci 27:11925–11933.

Yang WL, Ravatn R, Kudoh K, Alabanza L, Chin KV. 2010. Interaction of the regulatory subunit of the cAMP-dependent protein kinase with PATZ1 (ZNF278). Biochem Biophys Res Commun 391:1318–1323.

Yeo EJ, Hwang YC, Kang CM, Choy HE, Park SC. 2000. Reduction of UV-induced cell death in the human senescent fibroblasts. Mol Cell 10:415–422.

Zhang CL, Zou Y, He W, Gage FH, Evans RM. 2008. A role for adult TLX-positive neural stem cells in learning and behaviour. Nature 451:1004–1007.

Endocrine-Related Cancer (2009) **16** 483–490

Impairment of the p27^{kip1} function enhances thyroid carcinogenesis in *TRK-T1* transgenic mice

Monica Fedele[1,2], Dario Palmieri[2], Gennaro Chiappetta[3], Rosa Pasquinelli[3], Ivana De Martino[2], Claudio Arra[3], Giuseppe Palma[3], Teresa Valentino[2], Giovanna M Pierantoni[2], Giuseppe Viglietto[4], Jay L Rothstein[5], Massimo Santoro[2] and Alfredo Fusco[1,2,6]

[1]Istituto di Endocrinologia ed Oncologia Sperimentale del CNR, Via S. Pansini 5, 80131 Naples, Italy
[2]Dipartimento di Biologia e Patologia Cellulare e Molecolare, Università di Napoli 'Federico II', 80131 Naples, Italy
[3]Istituto dei Tumori di Napoli Fondazione 'G. Pascale', 80131 Naples, Italy
[4]Dipartimento di Medicina Sperimentale e Clinica, Università 'Magna Graecia', 88100 Catanzaro, Italy
[5]Inflammation Research, Amgen Inc., Seattle, Washington 98119, USA
[6]NOGEC (Naples Oncogenomic Center)-Ceinge, Biotecnologie Avanzate, 80131 Naples, Italy

(Correspondence should be addressed to A Fusco at Istituto di Endocrinologia ed Oncologia Sperimentale del CNR; Email: afusco@napoli.com)

Abstract

Impairment of the p27^{kip1} function, caused by a drastic reduction of its expression or cytoplasmic mislocalization, has been frequently observed in thyroid carcinomas. To understand the role of p27^{kip1} impairment in thyroid carcinogenesis, we investigated the consequences of the loss of p27^{kip1} expression in the context of a mouse modeling of papillary thyroid cancer, expressing the *TRK-T1* oncogene under the transcriptional control of thyroglobulin promoter. We found that double mutant mice homozygous for a *p27^{kip1}* null allele (*TRK-T1*/*p27$^{-/-}$*) display a higher incidence of papillary thyroid carcinomas, with a shorter latency period and increased proliferation index, compared with *p27^{kip1}* wild-type compounds (*TRK-T1*/*p27$^{+/+}$*). Consistently, double mutant mice heterozygous for a *p27^{kip1}* null allele (*TRK-T1*/*p27$^{+/-}$*) show an incidence of thyroid carcinomas that is intermediate between *TRK-T1*/*p27$^{-/-}$* and *TRK-T1*/*p27$^{+/+}$* mice. Therefore, our findings suggest a dose-dependent role of *p27^{kip1}* function in papillary thyroid cancer development.

Endocrine-Related Cancer (2009) **16** 483–490

Introduction

Thyroid tumors include a wide spectrum of lesions with different phenotypic characteristics and biological behavior: benign adenomas, differentiated carcinomas, and anaplastic carcinomas (Hedinger *et al*. 1989). Several genetic lesions have been already identified in human thyroid carcinomas. In fact, RET/PTC oncogenes have been found in about 20% of human papillary thyroid carcinomas (PTCs). They are chimeric genes generated by the fusion of the catalytic domain of the RET receptor tyrosine kinase with the N-terminal region encoded by heterologous genes. In the most prevalent variants, RET/PTC1 (Grieco *et al*. 1990) and RET/PTC3 (Santoro *et al*. 1994), the fusion occurs between *RET* and the *H4* (*D10S170*) or *RFG* (*Ele1/ARA70/Ncoa4*) genes respectively. *TRK-T* oncogenes have been detected in about 5% of PTCs. They are generated by structural rearrangements of the *NTRK1* (*TRKA*) gene, coding for the high affinity nerve growth factor (NGF) receptor. The *TRK-T1* and *TRK-T2* oncogenes are both generated by *NTRK1* fusion with the *TPR* gene. *NTRK1* and *TPR* are both located on human chromosome 1 (Greco *et al*. 1997). Recently, it has been demonstrated that specific point mutations in the activation segment of the BRAF kinase are present in about 40% of adult PTCs (Kimura *et al*. 2003). Furthermore, a novel oncogene, designated *AKAP9-BRAF*, deriving from the in-frame fusion of the first eight exons of the A-kinase anchor protein 9

DOI: 10.1677/ERC-08-0272

Online version via http://www.endocrinology-journals.org

(*AKAP9*) gene with the carboxyl-terminal encoding-region (exons 9–18) of *BRAF*, has been isolated from PTCs developed in irradiated patients after a short latency period (Ciampi *et al*. 2005). As far as *ras* genes are concerned, mutations of codon 61 of *N-RAS* (N2) were significantly more frequent in follicular tumors (19%) than in papillary cancers (5%). *H-RAS* mutations in codons 12/13 (H1) were found in 2–3% of all types of thyroid tumors, but *H-RAS* mutations in codon 61 (H2) were observed in only 1.4% of tumors (Vasko *et al*. 2003). *K-RAS* mutations in exon 1 were found more often in papillary carcinomas (De Micco 2003). The genetic lesions described above are mutually exclusive, since no tumors have been found bearing more than one of these lesions. *PAX8-PPAR-γ* rearrangements are frequent in follicular thyroid carcinomas (Kroll *et al*. 2000, Dwight *et al*. 2003), whereas impaired function of the *p53* tumor suppressor gene is a feature of anaplastic thyroid carcinomas (Donghi *et al*. 1993). It is interesting to observe that all these oncogenes identified in thyroid cancer activate a signaling pathway that results in an increased MAPK activity, according to which one specific signaling pathway that leads to MAPK activation plays a major role in the generation of PTC. However, other genetic lesions have also been reported in PTCs: decreased levels of PTEN and PTPRJ, a dual-specific phosphatase and a receptor type tyrosine phosphatase respectively (Bruni *et al*. 2000, Trapasso *et al*. 2000), and alterations of the $p27^{kip}$ protein function (Baldassarre *et al*. 1999) represent frequent features of thyroid malignancies.

$p27^{kip1}$ has classically been regarded as a cell-cycle inhibitor based on its potent inhibitory activity of cyclin E/cdk2 and the observation that its forced expression results in G1 arrest (Toyoshima & Hunter 1994). Low levels of the $p27^{kip1}$ protein have been frequently found in human carcinomas, and these low levels directly correlate with both a high histological tumor grade and a poor outcome (Lloyd *et al*. 1999). In several cases, the impairment of the p27 function is due to its cytoplasmic mislocalization induced by AKT activation (Viglietto *et al*. 2002, Motti *et al*. 2005, Chu *et al*. 2008). Also in thyroid malignant neoplasias, the impairment of the p27 function is very frequent: a reduction in $p27^{kip1}$ protein levels has been previously described in 10 out of 28 papillary carcinomas, 3 out of 9 follicular carcinomas, and 6 out of 8 anaplastic carcinomas. Moreover, 80% of $p27^{kip1}$-expressing tumors shows an uncommon cytoplasmic localization of $p27^{kip1}$ protein, associated with a high cdk2 activity (Baldassarre *et al*. 1999). Several components account for the reduced p27 protein levels in thyroid malignant neoplasias: both PTEN and PTPRJ, whose expression is drastically reduced in thyroid malignant neoplasias (Bruni *et al*. 2000, Trapasso *et al*. 2000), increase the stability of the p27 protein. Recent data show increased miR221 and 222 levels in PTCs that correlate with low levels of p27 (Visone *et al*. 2007). However, a causal link between p27 impairment and thyroid carcinogenesis has not been established yet.

The aim of the present work was to validate the role of the loss of p27 function in thyroid carcinogenesis crossing transgenic mice carrying the *TRK-T1* transgene under the control of the bovine thyroglobulin (TG) promoter (Russell *et al*. 2000) with mice carrying targeted germline deletions of one or two $p27^{kip1}$ alleles (Fero *et al*. 1996). Despite the limited involvement of the *NTRK* gene in human PTCs in comparison with *RET/PTC*, the TRK-T1 mouse model develops follicular hyperplasia and papillary carcinoma similarly to RET/PTCs mice (Jhiang *et al*. 1996, Santoro *et al*. 1996, Powell *et al*. 1998, Russell *et al*. 2000), thus representing a valid system in the study of thyroid carcinogenesis mechanisms. p27 null mice show a syndrome of multiorgan hyperplasia with features of gigantism and develop pituitary adenoma with high incidence, lung, gonadal, and intestinal tumors at an increased frequency compared with wild-type mice (Fero *et al*. 1996), but no thyroid tumors or anomalies. Here, we report that loss-of-function of $p27^{kip1}$ in mice with targeted overexpression of *TRK-T1* in thyroid cells increases the penetrance of thyroid cancer and shortens the latency period of tumor incidence.

Materials and methods

Mouse strains, handling, and genotyping

TRK-T1 transgenic mice in a B6C3F1 genetic background (Russell *et al*. 2000) were crossed with $p27^{kip1}$-null ($p27^{-/-}$) mice from a mixed C57BL/6J and 129 genetic background (from Dr M L Fero; Fero *et al*. 1996) to obtain $p27^{+/+}$, $p27^{+/-}$, and $p27^{-/-}$ mice containing the *TRK-T1* transgene (*TRK-T1*/$p27^{+/+}$, *TRK-T1*/$p27^{+/-}$, and *TRK-T1*/$p27^{-/-}$ respectively). The *TRK-T1* and $p27^{kip1}$ genotypes were analyzed by the PCR with genomic DNA isolated from ∼1 cm section of mouse tail. For $p27^{kip1}$ genotyping, the following PCR primers were used: p27-K3 (common) TGGAACCCTGTGCCATCTCTAT; p27 F-N (generates mutant fragment = 800 bp), CCTTCTATGG-CCTTCTTGACG; and p27-K5 (generates wild-type fragment = 900 bp), GAGCAGACGCCCAAGAAGC. The primer sequences for TRK-T1 were forward,

CACATCATCGAGAACCCACAA and reverse, GCTCATGCCAAAATCACCAAT, which generate a 550 bp product.

All mice were maintained under specific pathogen-free conditions in our Laboratory Animal Facility (Istituto dei Tumori di Napoli, Naples, Italy) and all studies were conducted in accordance with Italian regulations for experiments on animals.

Histological and immunohistochemical procedures

Cohorts of 40 *TRK-T1/p27*$^{+/+}$, 52 *TRK-T1/p27*$^{+/-}$, and 40 *TRK-T1/p27*$^{-/-}$ live mice, equally distributed between males and females, were examined for tumor formation by observation and palpation every week beginning 1 month after birth. They were killed at the gross appearance of a neck mass or at 20 months of age and thyroid was removed for pathological analysis. In parallel, cohorts of 18 mice for each of the above genotypes, equally distributed between males and females, were killed in a time window of 12–14 months of age and their thyroids histologically examined. Tissues were fixed by immersion for 24 h in Bouin's solution and embedded in paraffin using standard procedures. Sections (5 μm) were stained with hematoxylin and eosin using standard histological techniques. To determine the proliferative status, tumor sections were incubated with monoclonal antibody to Ki-67 (Dako, Milano, Italy) at a 1:15 dilution following microwave antigen retrieval with citrate buffer on an autostainer (Dako) using the LSAB + kit (Dako). The percentage of apoptotic cells in the same tumor sections was determined by terminal deoxynucleotidyl transferase-mediated dUTP nick end labeling (TUNEL) using the TdT-FragEL DNA fragmentation Detection Kit (Calbiochem, Beeston, Nottinghamshire, UK). Micrographs were taken on Kodak Ektachrome film with a photo Zeiss system.

Protein extraction and western blot analysis

Frozen pieces from normal and tumoral thyroid samples were resuspended in NIH lysis buffer (1% Nonidet P-40; 1 mM EDTA; 50 mM Tris–HCl (pH 8.0); 150 mM NaCl; 2 mM phenylmethylsulfonyl fluoride; 50 mM NaF; 10 mM Na_3V_4; 20 mM NaPP; 1.5 mM aprotinin). Tissue lysates were clarified by centrifugation at 10 000 ***g*** for 20 min at 4 °C. The supernatant was then used for immunoblotting. Western blotting was performed by standard procedures using the following primary antibodies: anti-p27 (sc-528; Santa Cruz, Heidelburg, Germany), anti-trk (sc-11; Santa Cruz), and anti-γ-tubulin (sc-8035; Santa Cruz). Briefly, the protein extracts were separated by SDS-PAGE and transferred to nitrocellulose membranes (BioRad). Membranes were blocked with 5% nonfat milk in TTBS (Tris-buffered saline containing Tween-20) and incubated with antibodies diluted in the same solution. Bound antibodies were detected by the appropriate HRP–conjugated secondary antibodies followed by enhanced chemiluminescence (Amersham).

Statistical analysis

Kaplan–Meyer survival curves were used to analyze the percentage of tumor-free mice in all groups examined during the 20 months of monitoring. Differences were analyzed by Logrank test. For the comparison of cases and controls within and across the groups, normal, hyperplastic or tumoral frequencies were calculated for all participants and compared using χ^2 analysis. Ki67 data are expressed as mean ± S.E.M. Differences were analyzed by Student's *t*-test. *P* values ≤ 0.05 were considered significant for all the above statistical assays.

Results

The onset of PTCs is accelerated in p27-null mice

Mice carrying the *TRK-T1* transgene under the control of the bovine TG promoter (Russell *et al*. 2000) were mated with mice carrying targeted germline deletions of one or two *p27*^{kip1} alleles (Fero *et al*. 1996). From the above intercross, mice of all the three genotypic combinations (*TRK-T1/p27*$^{+/+}$, *TRK-T1/p27*$^{+/-}$, and *TRK-T1/p27*$^{-/-}$) were obtained, and cohorts of 40 *TRK-T1/p27*$^{+/+}$, 52 *TRK-T1/p27*$^{+/-}$, and 40 *TRK-T1/p27*$^{-/-}$ plus 20 wild-type and 20 p27$^{-/-}$ mice were included in our study and monitored daily for the appearance of a thyroid phenotype. Each mouse was killed at the gross observation of a neck mass and within 20 months of age, all the remaining mice were killed. Histopathological analyses of each thyroid lobe were performed on thyroids of all mice. On the strength of criteria previously described (Russell *et al*. 2000), we classified all the specimens in three categories: normal, hyperplasia, and papillary carcinoma. As shown in Fig. 1, differently from normal thyroid characterized by regular monolayered follicles containing colloid (panel A), hyperplasia was characterized by increased follicular cellularity together with the presence of irregular or colloid-deficient follicles (panel B), whereas PTC was diagnosed on the presence of proliferation of follicular epithelial cells containing scant cytoplasm and papillae containing fibrovascular stalks (panel C). As shown in Fig. 2A, we found that *TRK-T1/p27*$^{-/-}$ develop PTCs more precociously

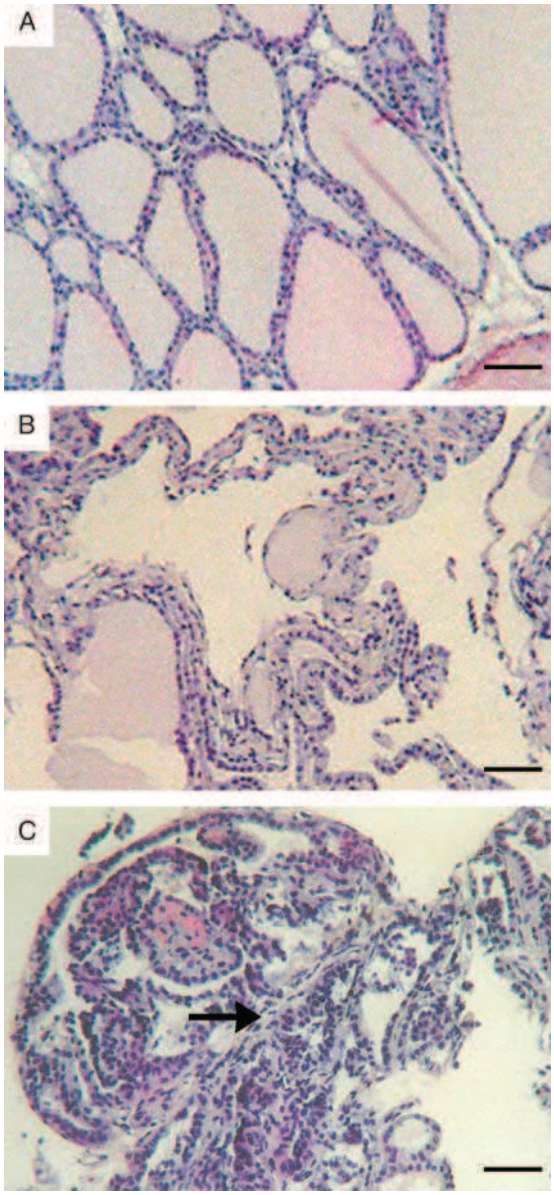

Figure 1 Histopathological features of normal, hyperplastic, and carcinomatous mouse thyroids. (A) Representative example of a normal thyroid as it appeared in a wild-type mouse. Uniform colloid-filled follicles, composed of a one cell thick layer of cuboidal epithelium are present. (B) Representative example of a hyperplastic thyroid lesion as it appeared in a *TRK-T1/p27*$^{+/-}$ mouse. Increased numbers of thyroid follicular epithelial cells surrounding large colloid-deficient follicles are present. (C) Representative example of PTC developed in a *TRK-T1/p27*$^{-/-}$ mouse. Follicular epithelial cells cluster together forming continuous sheets or papillae that surround a fibrovascular stalk. The arrow indicates a fibrovascular stalk in a papillary structure. Bar scale = 100 μm.

as compared with compound *TRK-T1/p27*$^{+/+}$ and *TRK-T1/p27*$^{+/-}$ mice. In particular, the comparison of tumor incidence curves (here representing the PTC-free mice) by Logrank test showed highly significant differences between *TRK-T1/p27*$^{-/-}$ and *TRK-T1/p27*$^{+/+}$ mice ($P < 0.0001$). Similarly, significant differences were found between *TRK-T1/p27*$^{+/-}$ and *TRK-T1/p27*$^{+/+}$ mice ($P = 0.0328$), as well as between *TRK-T1/p27*$^{-/-}$ and *TRK-T1/p27*$^{+/-}$ mice ($P = 0.0348$). No wild-type or p27$^{-/-}$ mice, lacking the *TRK-T1* transgene expression, develop PTCs by 20 months of age (Fig. 2A, dotted line).

p27 deficiency resulted in increased malignant thyroid transformation

On the basis of the histopathological results obtained from the above criteria on the thyroids of the mice killed in a time window of 12–14 months of age (18 mice for each genotype, equally distributed between males and females), we found significant pathological differences in both *TRK-T1/p27*$^{+/-}$ and *TRK-T1/p27*$^{-/-}$ mice compared with *TRK-T1/p27*$^{+/+}$. In particular, as summarized in Fig. 2B and analytically described in Supplementary Table 1, which can be viewed online at http://erc.endocrinology-journals.org/supplemental/, the total number of PTCs developed by *TRK-T1/p27*$^{-/-}$ mice was significantly higher than those observed in both compounds heterozygous for the *p27* null mutation ($P < 0.005$) and wild type ($P < 0.0005$). Interestingly, the carcinoma incidence in *TRK-T1/p27*$^{+/-}$ mice was statistically higher than in *TRK-T1/p27*$^{+/+}$ ($P < 0.01$), but intermediate between compound *p27*$^{-/-}$ and *p27*$^{+/+}$ mice, indicating a dose-dependency of p27 in TRK-induced tumor development (Fig. 2B). In addition, the data in Fig. 2B also show that *TRK-T1/p27*$^{+/-}$ and *TRK-T1/p27*$^{-/-}$ mice do not significantly differ from each other for the incidence of a normal phenotype, being in both of them significantly lower than in *TRK-T1/p27*$^{+/+}$ mice ($P < 0.0005$). Consequently, differently from *TRK-T1/p27*$^{-/-}$ mice ($P < 0.005$), compound mice heterozygous for the p27-null mutation show a high incidence of hyperplasias that likely represent a pre-malignant stage toward the development of PTCs, as suggested by the delayed onset of PTCs in *TRK-T1/p27*$^{+/-}$ compared with *TRK-T1/p27*$^{-/-}$ mice (Fig. 2A). No sex-related differences were observed (Supplementary Table 1). As a control, we also analyzed similar cohorts of wild-type and p27$^{-/-}$ mice finding no thyroid transformation in any of them (Fig. 2B and Supplementary Table 1).

Loss of p27 confers an increased proliferation rate to PTCs

Histological analyses of the PTCs arising in *TRK-T1/p27*$^{+/+}$, *TRK-T1/p27*$^{+/-}$, and *TRK-T1/p27*$^{-/-}$ mice did not show any significant differences and no

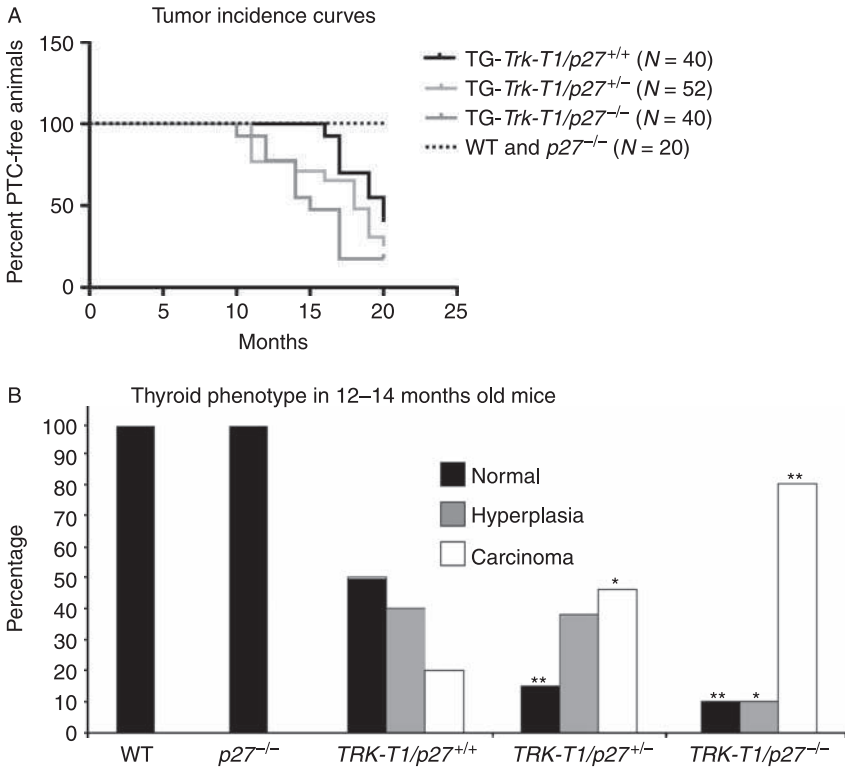

Figure 2 Deficiency of p27 alters cancer incidence of *TRK-T1* mice. (A) Kaplan–Meyer tumor incidence analysis of *TRK-T1* mice with different *p27* genotypes. Cohorts of at least 40 mice were monitored and harvested when they exhibited symptoms of disease. As assessed by Logrank test, the curves were significantly different ($P=0.0009$). Dotted line represents either wild-type or $p27^{-/-}$ mice. (B) The incidence of mice bearing normal, hyperplastic or cancerous thyroid was reported for each genotype, including negative controls, during a time-window of 12–14 months of age. Differences between two frequencies were statistically compared using χ^2 analysis. *$P<0.005$; **$P<0.0005$ versus *TRK-T1/p27*$^{+/+}$ controls.

abnormalities or tumor metastases in local cervical lymph nodes, peripheral lymph nodes or lungs were observed in any group (data not shown). Then, we analyzed in a comparative manner the proliferation index in PTCs developed by *TRK-T1* mice homozygous, heterozygous or wild type for the *p27* gene. The proliferation marker Ki67 was increased in PTC cells from both *TRK-T1/p27*$^{+/-}$ (23.5%$\pm$2.1) and *TRK-T1*$^{-/-}$ (25%$\pm$2) mice compared with *p27* wild-type compounds (9%$\pm$1.7; Fig. 3 and data not shown). Regardless of $p27^{kip1}$ dosage, Trk-induced PTCs contained a similar percentage of apoptotic cells (as determined by TUNEL analysis) as did normal thyroid tissues (data not shown). These findings indicate that loss of $p27^{kip1}$ enhances tumor growth by increasing the percentage of cycling cells (rather than the percentage of surviving cells) in the tumors.

Finally, to exclude the possibility that the loss of $p27^{kip1}$ may act on the transgene expression, leading to an increased mitogenic stimulus, thus assessing that the increased malignant phenotype is caused by the impairment of the p27 function, we have analyzed the transgene expression in PTCs from two mice for each genotypic combination. As shown in Fig. 4, no significant differences have been observed in TRK protein expression between *p27* null and *p27* wild-type mice. The expression of the p27 protein was also analyzed as control.

Discussion

Decreased expression and altered subcellular localization of p27 have been observed in thyroid cancers (Motti *et al*. 2005), but the functional relevance of this observation *in vivo* is not addressed yet. For this reason, we used a mouse experimental model of thyroid carcinogenesis to investigate *in vivo* the role of p27 inactivation in such neoplasm. In particular, we used transgenic mice for the *TRK-T1* gene, a well-described murine model of thyroid carcinogenesis (Russell *et al*. 2000), to investigate the relationship between the overexpression of the *TRK-T1* transgene and *p27*^{kip1} deletion in inducing thyroid carcinomas. Here, we report that the loss of $p27^{kip1}$

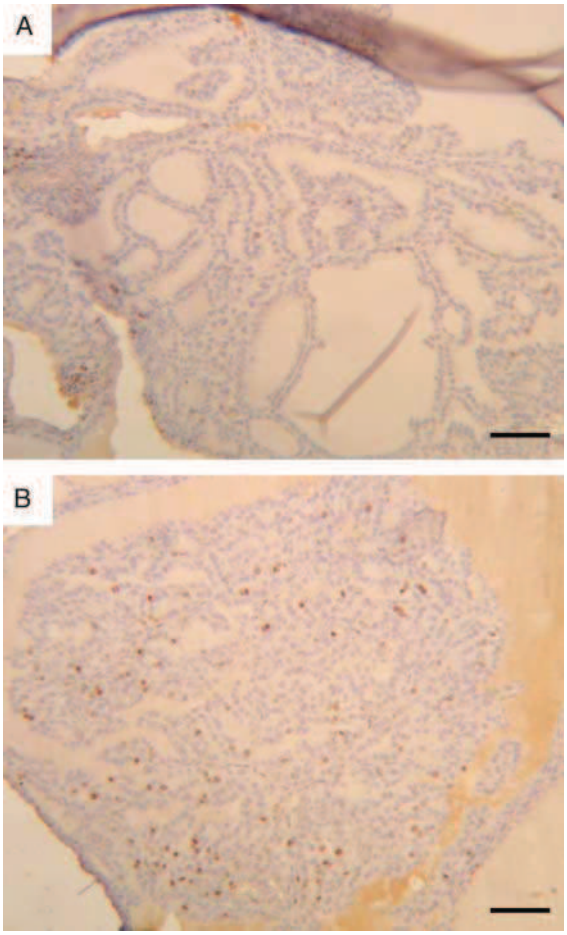

Figure 3 Ki67 staining of PTCs arising in *TRK-T1/p27*$^{+/+}$ and *TRK-T1/p27*$^{-/-}$ mutants. (A and B) Representative Ki67 immunostaining of PTCs occurring in *TRK-T1/p27*$^{+/+}$ and *TRK-T1/p27*$^{-/-}$ mice. A higher positivity is evident in the latter specimen (B) as better described in the text. Bar scale = 100 μm.

function increases the malignant phenotype of mice expressing the *TRK-T1* oncogene under the transcriptional control of TG promoter. Indeed, the *TRK-T1/p27*$^{-/-}$ mice show an increased number of carcinomas appearing with a shorter latency period compared with *TRK-T1/p27*$^{+/+}$ mice. The analysis of PTCs arising in *TRK-T1/p27*$^{-/-}$ mice shows an increased Ki67 positivity that indicates an increased proliferation rate in comparison with the PTCs arising in compound *p27* wild type. Conversely, *TRK-T1/p27*$^{+/-}$ mice show a phenotype that can be considered intermediate between *TRK-T1/p27*$^{-/-}$ and *TRK-T1/p27*$^{+/+}$ mice: their incidence of thyroid carcinomas was higher than *TRK-T1/p27*$^{+/+}$ mice, but lower than *TRK-T1/p27*$^{-/-}$ mice. Equally, *TRK-T1/p27*$^{+/-}$ mice have an incidence of PTCs that was earlier than *TRK-T1/p27*$^{+/+}$ mice, but significantly later than *TRK-T1/p27*$^{-/-}$ mice. Finally, PTCs developing in these mice show a proliferative index statistically increased compared with that shown by PTCs arising in *TRK-T1/p27*$^{+/+}$ mice, but lower than *TRK-T1/p27*$^{-/-}$ mice.

Interestingly, our results appear in contrast with those previously published regarding the *p27*-null mice carrying the *ErbB2/Neu* oncogene (*MMTV-neu/p27*$^{-/-}$; Muraoka *et al*. 2002). The mammary glands of these mice showed decreased proliferation, as well as markedly prolonged tumor latency, compared with *MMTV-neu/p27*$^{+/+}$ glands. Conversely, the *TRK-T1/p27*-null mice showed a great similarity with the *MMTV-neu/p27*$^{+/-}$ mice, whose mammary glands exhibited alveolar hyperplasia, enhanced proliferation, decreased apoptosis, and accelerated tumor formation compared with *MMTV-neu/p27*$^{+/+}$ mammary glands (Muraoka *et al*. 2002). It is likely that in *MMTV-neu/p27*$^{-/-}$ mice, the complete absence of the p27 protein leads to an impairment of cyclin D1/Cdk4 function, that makes these mice more resistant to transformation. Results very similar to those described for the *MMTV-neu/p27*$^{+/-}$ and *MMTV-neu/p27*$^{-/-}$ have also been described in a mouse model of prostate carcinogenesis (Gao *et al*. 2004): in p27 minus mice there is an inhibition of tumor progression, whereas the heterozygous compounds display enhanced prostate carcinogenesis. However, we must consider that p27 plays both a permissive and an inhibitory role in normal thyroid cell proliferation (Paternot *et al*. 2006), suggesting that also in carcinomas it can behave in both ways depending on the cellular context.

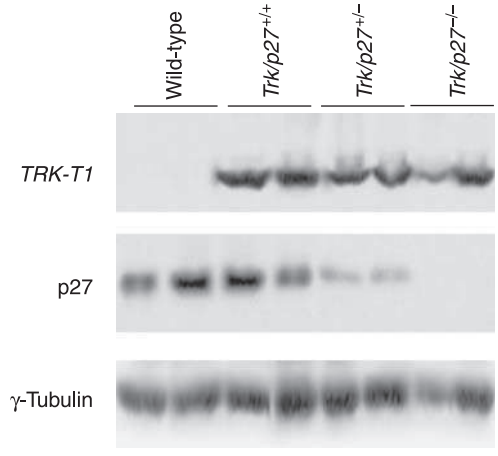

Figure 4 Western blot analyses on PTCs arising in *TRK-T1* mice with different *p27* genotypes. The proteins detected are indicated on the side. The γ-tubulin protein expression was analyzed as a loading control. Two normal thyroids from wild-type animals were also included as control.

Therefore, the results shown here demonstrate that loss of p27 has a role on thyroid tumor development and that *p27* behaves as a haploinsufficient tumor suppressor gene since even the loss of only one allele of *p27* is sufficient to confer a proliferative advantage to PTC growth.

Declaration of interest

We state that there does not exist any potential conflict of interest that could be perceived as prejudicing the impartiality of the research reported.

Funding

This work was supported by grants from the Associazione Italiana Ricerca sul Cancro (AIRC), the Ministero dell'Università e della Ricerca Scientifica e Tecnologica (MIUR), and the E.C. Contract GenRisk-T.

Acknowledgements

We are grateful to Matthew Fero for providing us of the $p27^{kip1}$ knockout mice, and Antonio Luciano and all the staff of the animal facility of the Istituto dei Tumori di Napoli for the mice housing and handling. We also thank the Associazione Partenopea per le Ricerche Oncologiche (APRO) and the NOGEC-Naples Oncogenomic Center for their support.

References

Baldassarre G, Belletti B, Bruni P, Boccia A, Trapasso F, Pentimalli F, Barone MV, Chiappetta G, Vento MT, Spiezia S *et al.* 1999 Overexpressed cyclin D3 contributes to retaining the growth inhibitor p27 in the cytoplasm of thyroid tumor cells. *Journal of Clinical Investigation* **104** 865–874.

Bruni P, Boccia A, Baldassarre G, Trapasso F, Santoro M, Chiappetta G, Fusco A & Viglietto G 2000 PTEN expression is reduced in a subset of sporadic thyroid carcinomas: evidence that PTEN-growth suppressing activity in thyroid cancer cells mediated by p27kip1. *Oncogene* **19** 3146–3155.

Chu IM, Hengst L & Slingerland JM 2008 The Cdk inhibitor p27 in human cancer: prognostic potential and relevance to anticancer therapy. *Nature Reviews. Cancer* **8** 253–267.

Ciampi R, Knauf JA, Kerler R, Gandhi M, Zhu Z, Nikiforova MN, Rabes HM, Fagin JA & Nikiforov YE 2005 Oncogenic AKAP9-BRAF fusion is a novel mechanism of MAPK pathway activation in thyroid cancer. *Journal of Clinical Investigation* **115** 94–101.

Donghi R, Longoni A, Pilotti S, Michieli P, Della Porta G & Pierotti MA 1993 Gene p53 mutations are restricted to poorly differentiated and undifferentiated carcinomas of the thyroid gland. *Journal of Clinical Investigation* **91** 1753–1760.

Dwight T, Thoppe SR, Foukakis T, Lui WO, Wallin G, Hoog A, Frisk T, Larsson C & Zedenius J 2003 Involvement of the PAX8/peroxisome proliferator-activated receptor gamma rearrangement in follicular thyroid tumors. *Journal of Clinical Endocrinology and Metabolism* **88** 4440–4445.

Fero ML, Rivkin M, Tasch M, Porter P, Carow CE, Firpo E, Polyak K, Tsai LH, Broudy V, Perlmutter RM *et al.* 1996 A syndrome of multiorgan hyperplasia with features of gigantism, tumorigenesis, and female sterility in p27(Kip1)-deficient mice. *Cell* **85** 733–744.

Gao H, Ouyang X, Banach-Petrosky W, Borowsky AD, Lin Y, Kim M, Lee H, Shin W-J, Cardiff RD, Shen MM *et al.* 2004 Combinatorial activities of Akt and B-Raf/Erk signaling in a mouse model of androgen-independent prostate cancer. *PNAS* **101** 17204–17209.

Greco A, Miranda C, Pagliardini S, Fusetti L, Bongarzone I & Pierotti MA 1997 Chromosome 1 rearrangements involving the genes TPR and NTRK1 produce structurally different thyroid-specific TRK oncogenes. *Genes, Chromosomes and Cancer* **19** 112–123.

Grieco M, Santoro M, Berlingieri MT, Melillo RM, Donghi R, Bongarzone I, Pierotti MA, Della Porta G, Fusco A & Vecchio G 1990 PTC is a novel rearranged form of the ret proto-oncogene and is frequently detected *in vivo* in human thyroid papillary carcinomas. *Cell* **60** 557–563.

Hedinger C, Williams ED & Sobin LH 1989 The WHO histological classification of thyroid tumors: a commentary on the second edition. *Cancer* **63** 908–911.

Jhiang SM, Sagartz JE, Tong Q, Parker-Thornburg J, Capen CC, Cho JY, Xing S & Ledent C 1996 Targeted expression of the ret/PTC1 oncogene induces papillary thyroid carcinomas. *Endocrinology* **137** 375–378.

Kimura ET, Nikiforova MN, Zhu Z, Knauf JA, Nikiforov YE & Fagin JA 2003 High prevalence of BRAF mutations in thyroid cancer: genetic evidence for constitutive activation of the RET/PTC-RAS-BRAF signaling pathway in papillary thyroid carcinoma. *Cancer Research* **63** 1454–1457.

Kroll TG, Sarraf P, Pecciarini L, Chen CJ, Mueller E, Spiegelman BM & Fletcher JA 2000 PAX8-PPAR-gamma1 fusion oncogene in human thyroid carcinoma. *Science* **289** 1357–1360.

Lloyd RV, Erickson LA, Jin L, Kulig E, Qian X, Cheville JC & Scheithauer BW 1999 p27kip1: a multifunctional cyclin-dependent kinase inhibitor with prognostic significance in human cancers. *American Journal of Pathology* **154** 313–323.

De Micco C 2003 Ras mutations in follicular variant of papillary thyroid carcinoma. *American Journal of Clinical Pathology* **120** 803.

Motti ML, Califano D, Troncone G, De Marco C, Migliaccio I, Palmieri E, Pezzullo L, Palombini L, Fusco A & Viglietto G 2005 Complex regulation of the cyclin-dependent kinase inhibitor p27kip1 in thyroid

cancer cells by the PI3K/AKT pathway: regulation of p27kip1 expression and localization. *American Journal of Pathology* **166** 737–749.

Muraoka RS, Lenferink AE, Law B, Hamilton E, Brantley DM, Roebuck LR & Arteaga CL 2002 ErbB2/Neu-induced, cyclin D1-dependent transformation is accelerated in p27-haploinsufficient mammary epithelial cells but impaired in p27-null cells. *Molecular and Cellular Biology* **22** 2204–2219.

Paternot S, Dumont JE & Roger PP 2006 Differential utilization of cyclin D1 and cyclin D3 in the distinct mitogenic stimulations by growth factors and TSH of human thyrocytes in primary culture. *Molecular Endocrinology* **20** 3279–3292.

Powell DJ Jr, Russell J, Nibu K, Li G, Rhee E, Liao M, Goldstein M, Keane WM, Santoro M, Fusco A *et al.* 1998 The RET/PTC3 oncogene: metastatic solid-type papillary carcinomas in murine thyroids. *Cancer Research* **58** 5523–5528.

Russell JP, Powell DJ, Cunnane M, Greco A, Portella G, Santoro M, Fusco A & Rothstein JL 2000 The TRK-T1 fusion protein induces neoplastic transformation of thyroid epithelium. *Oncogene* **19** 5729–5735.

Santoro M, Dathan NA, Berlingieri MT, Bongarzone I, Paulin C, Grieco M, Pierotti MA, Vecchio G & Fusco A 1994 Molecular characterization of RET/PTC3; a novel rearranged version of the RET proto-oncogene in a human thyroid papillary carcinoma. *Oncogene* **9** 509–516.

Santoro M, Chiappetta G, Cerrato A, Salvatore D, Zhang L, Manzo G, Picone A, Portella G, Santelli G, Vecchio G *et al.* 1996 Development of thyroid papillary carcinomas secondary to tissue-specific expression of the RET/PTC1 oncogene in transgenic mice. *Oncogene* **12** 1821–1826.

Toyoshima H & Hunter T 1994 p27, a novel inhibitor of G1 cyclin-Cdk protein kinase activity is related to p21. *Cell* **78** 67–74.

Trapasso F, Iuliano R, Boccia A, Stella A, Visconti R, Bruni P, Baldassarre G, Santoro M, Viglietto G & Fusco A 2000 Rat protein tyrosinephosphatase η suppresses the neoplastic phenotype of retrovirally-transformed thyroid cells through the stabilization of protein p27. *Molecular and Cellular Biology* **20** 9236–9246.

Vasko V, Ferrand M, Di Cristofaro J, Carayon P, Henry JF & de Micco C 2003 Specific pattern of RAS oncogene mutations in follicular thyroid tumors. *Journal of Clinical Endocrinology and Metabolism* **88** 2745–2752.

Viglietto G, Motti ML & Fusco A 2002 Understanding p27(kip1) deregulation in cancer: down-regulation or mislocalization. *Cell Cycle* **1** 394–400.

Visone R, Russo L, Pallante P, De Martino I, Ferraro A, Leone V, Borbone E, Petrocca F, Alder H, Croce CM *et al.* 2007 MicroRNAs (miR)-221 and miR-222, both overexpressed in human thyroid papillary carcinomas, regulate p27Kip1 protein levels and cell cycle. *Endocrine-Related Cancer* **14** 791–798.

EUROPEAN JOURNAL OF CANCER 47 (2011) 470–478

available at www.sciencedirect.com

ScienceDirect

journal homepage: www.ejconline.com

Expression of a truncated *Hmga1b* gene induces gigantism, lipomatosis and B-cell lymphomas in mice

Monica Fedele [a,f], *Rosa Visone* [a,b,f], *Ivana De Martino* [a], *Dario Palmieri* [a], *Teresa Valentino* [a], *Francesco Esposito* [a], *Andres Klein-Szanto* [c], *Claudio Arra* [d], *Andrea Ciarmiello* [d], *Carlo M. Croce* [b], *Alfredo Fusco* [a,e,*]

[a] *Istituto di Endocrinologia ed Oncologia Sperimentale del CNR c/o Dipartimento di Biologia e Patologia Cellulare e Molecolare, Università degli Studi di Napoli 'Federico II', 80131 Naples, Italy*

[b] *Division of Human Cancer Genetics, Comprehensive Cancer Center, Ohio State University, 43210 Columbus, OH, USA*

[c] *Experimental Histopathology, Fox-Chase Cancer Center, Philadelphia, PA, USA*

[d] *Istituto dei Tumori di Napoli Fondazione 'G. Pascale', 80131 Naples, Italy*

[e] *NOGEC (Naples Oncogenomic Center)-CEINGE, Biotecnologie Avanzate-Napoli, & SEMM, European School of Molecular Medicine, Naples Site, 80145 Naples, Italy*

ARTICLE INFO

Article history:
Received 3 June 2010
Received in revised form 23 September 2010
Accepted 30 September 2010
Available online 31 October 2010

Keywords:
Adipogenesis
Lymphoma
Experimental animal models
Oncogene
E2F1
High Mobility Group proteins

ABSTRACT

HMGA1 gene rearrangements have been frequently described in human lipomas. *In vitro* studies suggest that HMGA1 proteins have a negative role in the control of adipocyte cell growth, and that *HMGA1* gene truncation acts in a dominant-negative fashion. Therefore, to define better the role of the *HMGA1* alterations in the generation of human lipomas, we generated mice carrying an *Hmga1b* truncated (*Hmga1b/T*) gene. These mice develop a giant phenotype together with a drastic expansion of the retroperitoneal and subcutaneous white adipose tissue. We show that the activation of the E2F pathway likely accounts, at least in part, for this phenotype. Interestingly, the Hmga1b/T mice also develop B-cell lymphomas similar to that occurring in Hmga1-knockout mice, supporting a dominant-negative role of the Hmga1b/T mutant also *in vivo*.

1. Introduction

HMGA1 belongs to the *High Mobility Group A* (*HMGA*) gene family, which also includes the closely related *HMGA2* gene. The *HMGA1* gene codes, through alternative splicing, for two protein isoforms, HMGA1a and HMGA1b, which differ from each other for few aminoacids. The HMGA proteins are characterised by three DNA-binding domains containing short basic repeats, the so-called AT-hooks, capable of binding AT-rich sequences in the minor groove of the DNA, and an acidic carboxy-terminal tail that is believed to be important for protein–protein interactions.[1] They are non-histone chromatin-associated factors known as 'architectural transcription factors': by interacting with the transcription

* *Corresponding author:* Address: Istituto di Endocrinologia ed Oncologia Sperimentale (IEOS), Via Pansini 5, 80131 Napoli, Italy. Tel.: +39 081 67463602; fax: +39 081 2296674.
E-mail addresses: afusco@napoli.com, alfusco@unina.it (A. Fusco).
[f] Both authors contributed equally to the work.
0959-8049/$ - see front matter
doi:10.1016/j.ejca.2010.09.045

machinery they alter chromatin structure and thereby regulate, negatively or positively, the transcriptional activity of several genes.[2] Both *HMGA* genes are widely expressed during embryogenesis, but expression becomes more restricted as foetal development progresses and is absent or low in adult tissues,[3,4] except for the stem cell compartment. In fact, it has been recently shown that HMGA2 is highly expressed in foetal and young-adult stem cells, being required for the self-renewal of foetal and young-adult stem cells relative to old-adult stem cells by negatively regulating $p16^{In4a}$ and $p19^{Arf}$ expression in foetal and young-adult, but not old-adult stages.[5]

This protein family is implicated, through different mechanisms, in both benign and malignant neoplasias.[6] In fact, unrearranged HMGA overexpression is a feature of malignant tumours and is also causally related to neoplastic cell transformation, as demonstrated by the ability of HMGA1 and HMGA2 overexpression to transform cells in culture and induce tumours *in vivo*.[7,8] Conversely, rearrangements of *HMGA* genes, mainly the *HMGA2* gene, are a feature of most benign human mesenchymal tumours.[9]

Indeed, they are frequent in human benign neoplasias of mesenchymal origin, including lipomas, uterine leiomyomas, pulmonary chondroid hamartomas and others[9]; breakpoints in *HMGA2* preferentially cluster in the third large intron of the gene, resulting in deregulation of its expression, truncation or, more frequently, generation of fusion genes encoding chimeric transcripts containing the first three exons of *HMGA2* and ectopic sequences from other genes. Truncation of *HMGA2* with the loss of its carboxy-terminus, including the 3′ untranslated region (3′ UTR), seems to account for *HMGA2* gene overexpression in these tumours.[7,10,11] Indeed, 3′ UTR of *HMGA2* contains multiple target sites for let-7 microRNA, and therefore, its loss would result in the lack of the let-7 negative regulation of HMGA2.[12,13]

Rearrangements of *HMGA1* in various benign mesenchymal tumours consist of breakpoints located either upstream or downstream of the gene sequence, and molecular analyses of *HMGA1* transcripts revealed common deletions of the carboxy-terminal region and/or parts of the 3′ UTR.[14,15] The generation of transgenic mice overexpressing *HMGA1* and *HMGA2* genes confirmed an oncogenic role for these genes. In fact, transgenic mice carrying wild-type forms of either *Hmga2* or *Hmga1* develop NK/T-cell lymphomas and pituitary adenomas.[16,17] Conversely, the generation of knockout mice for the *Hmga1* gene revealed an unsuspected tumour-suppressor potential since they develop B-cell lymphomas and myelo-proliferative disorders.[18]

Several observations support a critical role for HMGA proteins in the development, and particularly, in the process of adipogenesis.[19] In fact, $Hmga2^{-/-}$ mice express a *pygmy* phenotype together with a drastic reduction (87%) in adipose tissue,[3] whereas transgenic animals overexpressing either wild-type or truncated Hmga2 show an opposite phenotype with a significant increase in weight and size, characterised by lipomas or abdominal/pelvic lipomatosis.[11,16,20] Moreover, the lack of Hmga2 expression prevents both diet- and gene-induced obesity.[21] Conversely, HMGA1 proteins exert a negative role on adipocytic cell growth.[22,23] In fact, *Hmga1* gene expression is induced in mouse 3T3-L1 fibroblasts, which rapidly differentiate to adipocytes upon treatment with several agents,[24] soon after differentiation.[22] Further, suppression of *Hmga1* or expression of a truncated *Hmga1b* (*Hmga1b/T*) gene, deprived of both the acidic tail and the 3′ UTR, dramatically increased growth rate and impaired adipocytic differentiation,[22,23] also suggesting that the Hmga1b/T mutant acts in a dominant-negative fashion.[23] Data obtained from our laboratory on Hmga1b-transgenic animal models, which do not develop lipomas, have so far supported this model.[17] To validate *in vivo* the putative lipomagenic activity of the *HMGA1b/T* gene, we generated transgenic mice carrying this mutant gene under transcriptional control of the cytomegalovirus promoter (Hmga1b/T mice). These mice are overgrown and accumulate abundant ectopic fat depots. Increased E2F activity has been detected in the transgenic mice compared to wild-type littermates, likely accounting, at least in part, for the phenotype of the Hmga1b/T mice. We also show that Hmga1b/T mice develop B-cell lymphomas with morphological, histological and molecular features similar to those observed in $Hmga1^{-/-}$ mice, again supporting the hypothesis of a dominant-negative role of HMGA1/T on the HMGA1 function.

2. Materials and methods

2.1. Generation of transgenic mice

The construct carrying the cDNA encoding the truncated form of the murine *Hmga1b* gene (pRc/CMV-*Hmga1*/T) was obtained by sub-cloning a 243-bp cDNA fragment (from +196 bp to +438 bp downstream the transcriptional starting site (TSS) of the mouse *hmga1b* cDNA) into the *HindIII* and *XbaI* sites of the expression vector pRc/CMV (Invitrogen), as previously described.[23] It was electroporated into ES AB2.2 cells,[25] and G418-resistant clones were selected and analysed by Southern blot hybridisation with a CMV promoter probe on genomic DNA digested with SspI (Fig. 1A). Seven positive clones were selected on the basis of the unique Southern band of 2000 bp corresponding to the expected length of the SspI fragment including the CMV-*Hmgab1*/T insert (asterisks in Fig. 1B). These clones were expanded and the expression of *Hmga1b/T* was evaluated by a semiquantitative RT-PCR assay, using a construct-specific primer set described in the following paragraph. The highest two *Hmga1b/T* expressing ES cell clones (asterisks in Fig. 1C) were microinjected into C57BL6/J mouse blastocysts and then transferred to pseudopregnant foster mothers (Thomas Jefferson University, Philadelphia, PA). Chimeric mice were crossed to wild-type C57BL6/J mice (Taconic Farm), and germ-line transmission of the transgene was checked by Southern blot analysis of tail DNA from agouti coat-coloured F1 offspring.

2.2. RT-PCR analyses

Tissues from transgenic animals were rapidly dissected, frozen on dry ice, and stored at –80 °C. Total RNA was extracted using TRI-reagent solution (Molecular Research Center, Cincinnati, OH) according to the manufacturer's protocol and treated with DNase I (Invitrogen). One micrograms of RNA was reverse transcribed using random exonucleotides as primers (100 mM) and MuLV reverse transcriptase (Applied

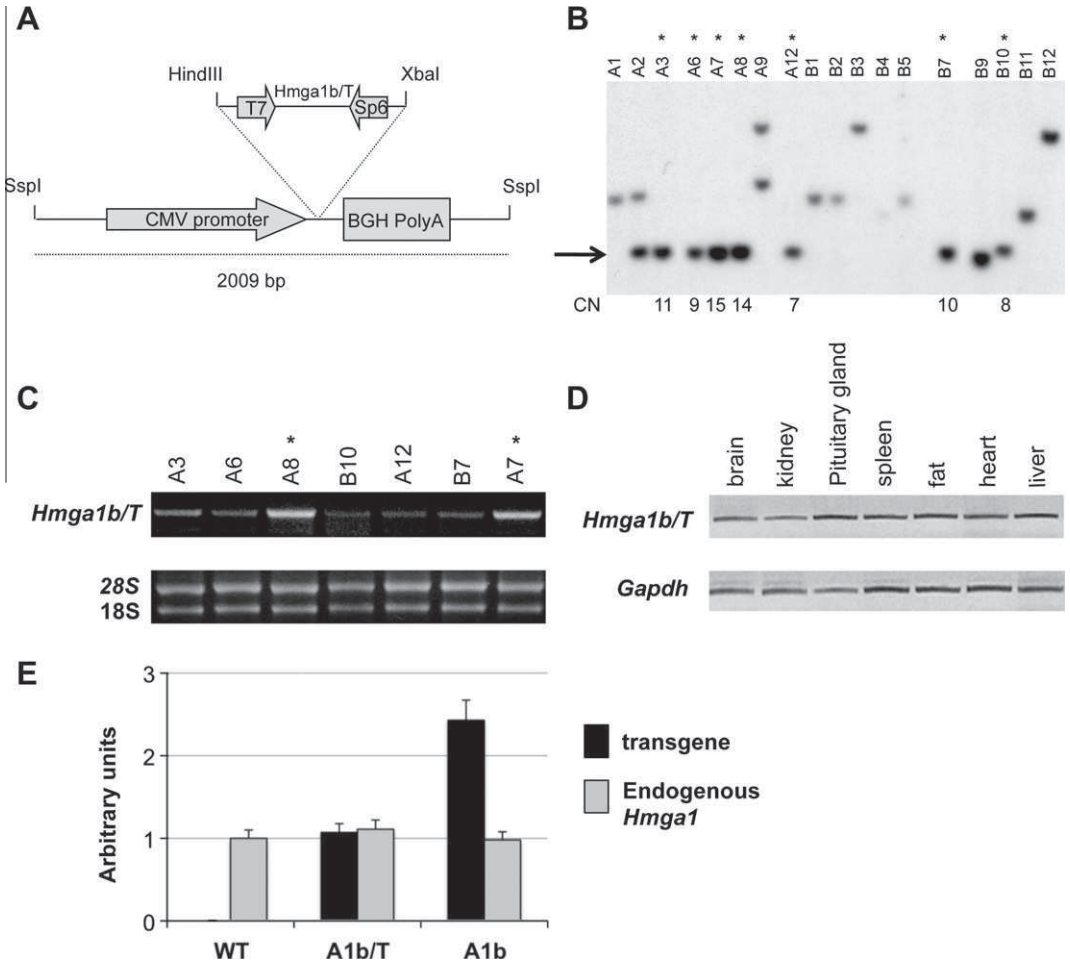

Fig. 1 – Generation of Hmga1b/T transgenic mice. Schematic representation of the CMV-Hmga1b/T transgene vector construction (A). Analysis, by Southern blot, of the integration of the CMV-Hmga1b/T transgene in ES cell clones. Asterisks = selected clones for further analyses and CN = copy number (B). RT-PCR analysis of the expression of the CMV-Hmga1b/T transgene in the selected ES cell clones. Asterisks = selected clones for blastocysts microinjection (C). RT-PCR analysis of the expression of the CMV-Hmga1b/T transgene in a panel of adult tissues from transgenic mice (D). Quantitative RT-PCR for the relative expression of the *Hmga1b/T* and *Hmga1b* transgenes in Hmga1b/T (A1b/T) and Hmga1b (A1b) mice, respectively. The relative expression of the two transgenes in comparison to the endogenous *Hmga1b* gene is also shown in the two trangenic mouse models. The data represent the mean values ± SD of two spleens from each mouse line performed in duplicate (E).

Biosystems). Five microlitres of cDNA were amplified as previously described.[11] Primers designed to amplify specifically the transcripts of the transgenic construct, as well as primers specific for the expressed enzyme glyceraldehyde 3-phosphate-dehydrogenase (GAPDH) that was used as an internal control of the amount of cDNA tested, and primers to amplify *V-preB* and *rag2* genes were previously described.[18,23]

2.3. *Quantitative RT-PCR*

Each reaction was performed in duplicate in a final volume of 20 μl using 10 μl of 2× Power SYBR Green PCR Master Mix (Applied Biosystems), 200 nM of each primer and 1 μl of each cDNA, using the following conditions: 10 min at 95 °C and then 45 cycles of 30 s at 95 °C and 1 min at 60 °C. At the end of the PCR run, a dissociation curve was constructed using a ramping temperature of 0.2 °C/s from 65 °C to 95 °C and a single melting point was obtained for each promoter. The $2^{-\Delta\Delta CT}$ method was used to calculate relative expression levels.[26] The following primer sequences were used: CMV-forward, 5′-tggcagtacatctacgtattagtcatc-3′; CMV-reverse, 5′-atccacgcccattgatgta-3′; hmga1-endog-forward, 5′-caagacccgggaaagtca-3′; hmga1-endog-reverse, 5′-cagaggactcctgggagatg-3′; cyclin E-forward, 5′-ctgagagatgagcactttctgc-3′; cyclin E-reverse, 5′-gagcttatagacttcgcacacct-3′; hprt-forward, 5-tcctcctcagaccgctttt-3′ and hprt-reverse, 5′-cctggttcatcatcgctaatc-3′.

2.4. *Protein extraction and Western blot*

Total protein lysates were obtained from transgenic (both normal and neoplastic) and wild-type spleens that had been homogenised in a solution containing 1% NP40, 1 mmol/l EDTA, 50 mmol/l Tris–HCl (pH 7.5) and 150 mmol/l NaCl, supplemented with complete protease inhibitors mixture

(Roche). Total proteins were separated by SDS–PAGE and transferred to nitrocellulose membrane. Membrane was blocked with 5% BSA in Tris Buffered Saline (TBS) and incubated with the specific primary antibodies (Ab) recognising the HMGA1 protein.[22] Bound Ab was detected by the appropriate secondary Ab, diluted in 5% nonfat milk in TBS solution containing 0.05% Tween 20 (TTBS), and revealed with an enhanced chemiluminescence system (Amersham Biosciences, Cologno Monzese, Italy).

2.5. MRI

Magnetic Resonance Imaging was performed at the 'Istituto dei Tumori di Napoli G. Pascale' on a 1.5-T magnet system using local receiver coils and an 8-cm field view. Coronal slices 3 mm thick were obtained with T1 weighting (TR/TE = 400/11 ms).

2.6. Plasmids, cell transfections and luciferase activity assay

The cyclin E-luciferase vector (cyclin E-luc) was generously provided by K. Helin (Biotech Research and Innovation Centre, University of Copenhagen, Denmark). Transfections for luciferase assays were carried out in 3T3-L1 mouse pre-adipocytes by using Lipofectamine 2000 method (Invitrogen), according to the manufacturer's instructions. A total of 2×10^5 cells were transiently transfected with 0.2 μg of cyclin E-luc and with 1 μg of each pCEFLHa-HMGA1,[22] pCEFLHa-HMGA1/T,[23] pCEFLHa-HMGA2 and pCEFLHa-HMGA2/T,[27] together with 0.5 μg of CMV-βgal and various amounts of the pCEFLHa plasmid (backbone vector) to keep the total DNA concentration constant. Cells were harvested 24 h post-transfection and lysates were analysed for luciferase activity. Transfection efficiency was normalised using the β-galactosidase activity. The assay was performed in duplicate and repeated in three independent experiments.

2.7. Electrophoretic mobility-shift assay

Protein/DNA-binding was determined by electrophoretic mobility-shift assay (EMSA) for E2F1 with protein extracts from wild-type and Hmgab1/T fat. Seven micrograms of each extract were pre-incubated in a buffer containing 20 mM Hepes pH 7.6, 1 mM $MgCl_2$, 0.1 mM EGTA, 0.02% NaN_3, 40 mM KCl, 10% glycerol and 1 μg of sonicated salmon sperm for 10 min at RT. Then, 2 μl of the radiolabelled oligonucleotide was added and the mixture was incubated for 20 min. For supershift analysis, pre-incubation was run for 30 min in ice in the presence of the specific antibody. The DNA-protein complexes were resolved on 4% non-denaturing acrylamide gels and visualised by autoradiography. The double-strand oligonucleotide used was the E2F1-responsive element (sc-2508, Santa Cruz Biotech, Santa Cruz, CA). The antibodies used for the supershift analysis were: anti-E2F1 (sc-193, Santa Cruz) and anti-Rb (sc-50, Santa Cruz).

2.8. Histological analysis and immunohistochemistry

For histological examination, dissected tissues were fixed by immersion in 10% formalin and embedded in paraffin. Mounted sections (5 μm thick) were stained with haematoxylin and eosin using routine procedures.

2.9. Analysis of splenocyte cell surface antigens

Spleens removed from mice were dissociated into single cells and RBCs were lysed by hypotonic shock using Tris–NH_4Cl buffer (NH_4Cl 0.14 M, Tris 0.017 M, pH 7.2). Cells were washed in PBS supplemented with 2% FCS, 0.2% sodium azide and labelled with FITC-, PE- and Cy5-conjugated appropriate antibodies for 30 min at 4 °C. Cells were then washed and analysed on FACS-Calibur flow cytometer (Becton Dickinson, Buccinasco, Italy). All the Abs used were obtained from Pharmingen/BD Biosciences (Buccinasco, Italy).

2.10. Statistics

The results are expressed as mean ± SD. For the comparison of statistical significance between two groups, Student's *t*-test was used. A P-value < 0.05 was considered statistically significant.

3. Results

3.1. Generation of transgenic mice with Hmga1b/T

An ES cell-mediated strategy has been used to generate transgenic mice, as previously described.[18] A truncated *Hmga1b* cDNA (*Hmga1b*/T), deprived of the COOH-terminal tail, under the transcriptional control of the CMV promoter (Fig. 1A) was transfected into the ES cells AB2.2. G418-resistant clones were selected and analysed by Southern blot hybridization with a CMV promoter probe (Fig. 1B). Seven positive clones were selected on the basis of the expected 2009 bp fragment recognised by the Southern blot assay (asterisks in Fig. 1B). The expression of the *Hmga1b/T* transgene was evaluated by RT-PCR. As shown in Fig. 1C, all selected clones expressed the transgene. The two clones with the highest levels of *Hmga1b/T* mRNA (asterisks in Fig. 1C) were microinjected into C57BL6/J mouse blastocysts, which were then transferred to pseudopregnant foster mothers. Several chimeric mice, identified by the mixed black/agouti coat colour, were obtained and crossed with wild-type C57BL6/J mice. Two independent Hmga1b/T strains, identified by Southern blot hybridization, were generated and examined. Both mouse lines showed the same phenotype. The *Hmga1b/T* expression was detected by RT-PCR in all the analysed tissues of transgenic animals (Fig. 1D), without any significant difference among them. Western blot analyses confirmed the expression of the Hmga1b/T protein in transgenic mice (data not shown). Expression of the *Hmga1b/T* transgene was compared to that of the *Hmga1b* transgene from Hmga1b/T and Hmga1b mice, previously generated in our laboratory,[16] respectively. The results, shown in Fig. 1E, indicate a higher expression of the transgene in Hmga1b mice then in Hmga1b/T mice. Moreover, we also show that the expression of the endogenous *Hmga1b* gene is not changed with respect to wild-type littermates in both transgenic mice models (Fig. 1E).

3.2. *Hmga1b/T mice exhibit a giant phenotype associated with abdominal/pelvic lipomatosis*

Most Hmga1b/T mice (derived from both lines) exhibited a giant and obese phenotype. At 12 months of age, 70% of them, both males and females, showed an average 10% increase in body length (naso-anal), compared to sex-matched wild-type littermates (Fig. 2B). The remaining 30% of Hmga1b/T mice was indistinguishable from the wild-types. Moreover, starting from the third month of age, both male and female transgenic mice revealed a significant increase of the body-weight growth curves compared to the controls (Fig. 2C and D). MRI of the transgenic and wild-type mice was performed to evaluate the extent of fat deposition and the presence of other abnormalities (Fig. 2A). Transgenic mice showed a drastic expansion of the abdominal and subcutaneous white adipose tissue. To confirm MRI results regarding fat mass, 14-month-old male and female mice were sacrified and three

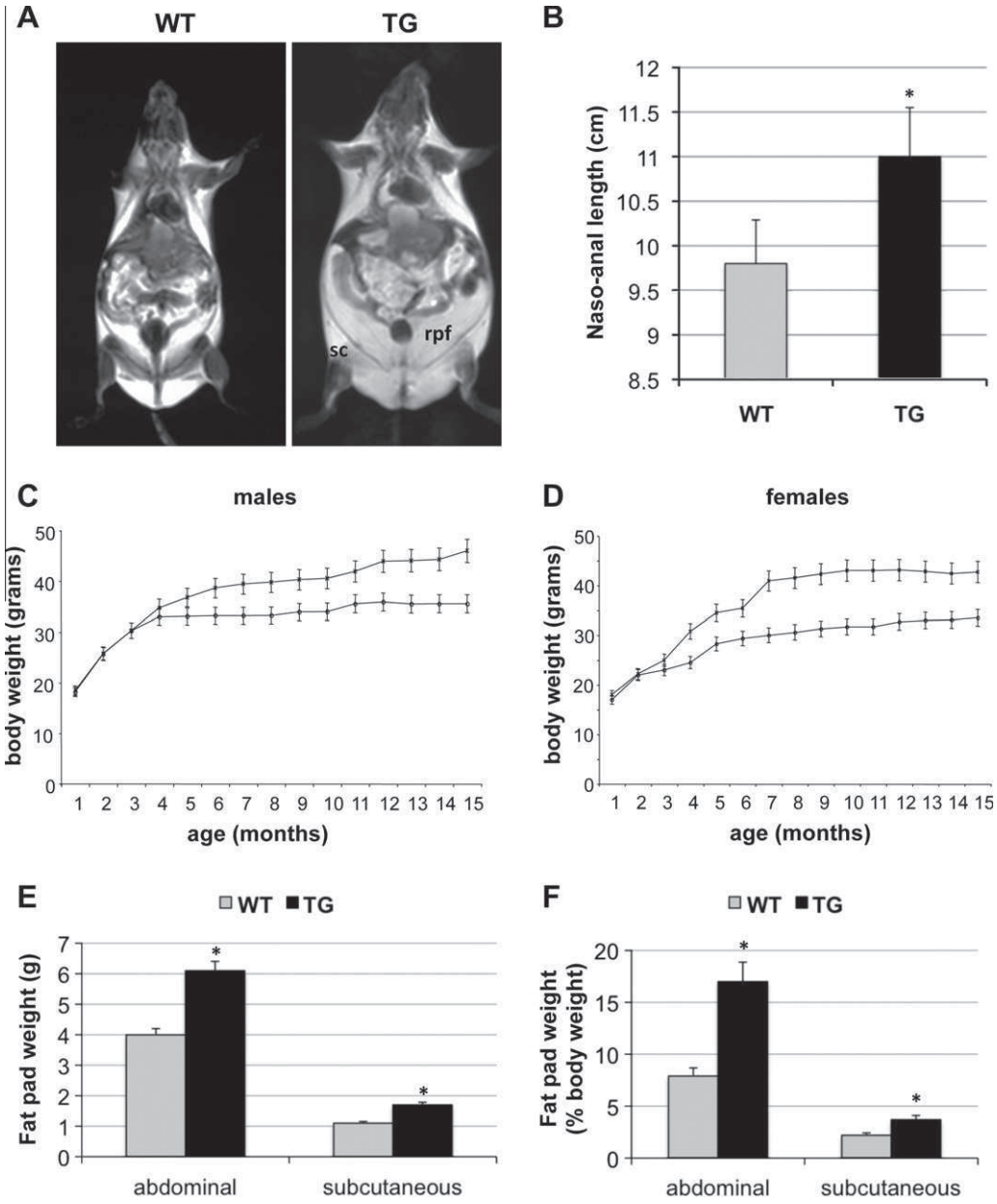

Fig. 2 – Hmga1b/T mice develop a giant and obese phenotype. MRI of representative one-year-old wild-type and Hmga1/T transgenic mice. A frontal section of each is shown. rpf = retroperitoneal fat and sf = subcutaneous fat (A). Naso-anal length of a cohort of 20 mice, equally distributed between males and females, was measured at 12 months of age and the mean values ± SD were plotted as histograms. *$P < 0.05$ (B). Increased weight of transgenic mice. Mean and 95% confidence intervals of weights of 10 wild-type (o) and 10 Hmga1b/T transgenic (×) male (C) and female (D) mice as a function of age. Weights of dissected fat pads in wild-type and Hmga1b/T mice. Abdominal fat includes gonadal, retroperitoneal and mesenteric fat pads; subcutaneous fat represents the inguinal fat pad. Values, expressed in grams (E) and % body weight (F) represent the means ± SD of 12-month-old male and female mice.

intra-abdominal fat pads (gonadal, retroperitoneal, and mesenteric) and one subcutaneous fat pad (inguinal, in the groin) were dissected and weighed. As shown in Fig. 2D and E, the absolute and relative weights of the abdominal and subcutaneous fat depots were increased in transgenic mice compared with that in wild-type controls. Histological examination of the abundant abdominal fat mass observed in Hmga1b/T mice showed an overall hypertrophy of the adipose tissue in the abdominal/pelvic area of these mice, consistent with a diagnosis of abdominal/pelvic lipomatosis.

3.3. *Enhanced E2F activity in Hmga1b/T mice*

Retinoblastoma proteins (pRB) are known to be critical in controlling cell cycle in most cell types, including adipocyte cells. They prevent the entry of cells into S phase by binding, and thereby inactivating the E2F transcription factors.[28] We have recently reported that HMGA2 activates E2F1 by binding pRB and displacing HDACs from the inhibitory complex recruited by pRB onto E2F-responsive elements.[27] A similar mechanism has also been demonstrated in 3T3-L1 adipocytic cells by HMGA1.[29] We have also previously shown that the truncated *Hmga1b* gene dramatically increased the growth rate of the 3T3-L1 cells and is able to enhance the free E2F (i.e. not complexed with pRB) DNA-binding activity highly.[23] Herein, we demonstrate that cyclin E promoter, a common E2F target, was significantly induced upon transfection of a truncated *Hmga1b* gene, similarly to what occurs for both wild-type and truncated *Hmga2* genes (Fig. 3A). Interestingly, a wild-type *Hmga1b* construct is not able to enhance cyclin E promoter (Fig. 3A), and this result is consistent with the phenotype of the *Hmga1b*-transgenic mice, which are not overgrown and do not gain weight compared to their wild-type littermates.[17] Next, we analysed the E2F activity in *Hmga1b/T* mice by EMSA assays with white adipose tissue (WAT) lysates from transgenic and wild-type animals. The results show an increase of the faster migrating complex, corresponding to the free E2F1-DNA-binding, in transgenic *versus* wild-type mice (Fig. 3B, lanes 1 and 4), confirming *in vivo* the capacity of the *Hmga1b/T* mutant to enhance E2F1 activity. Supershift analyses with antibodies directed against pRB and E2F1 confirmed the specificity of the protein-DNA complexes (Fig. 3B, lanes 2, 3, 5 and 6). In accordance with these data, cyclin E was found overexpressed in adipose tissue of these transgenic animals (Fig. 3C).

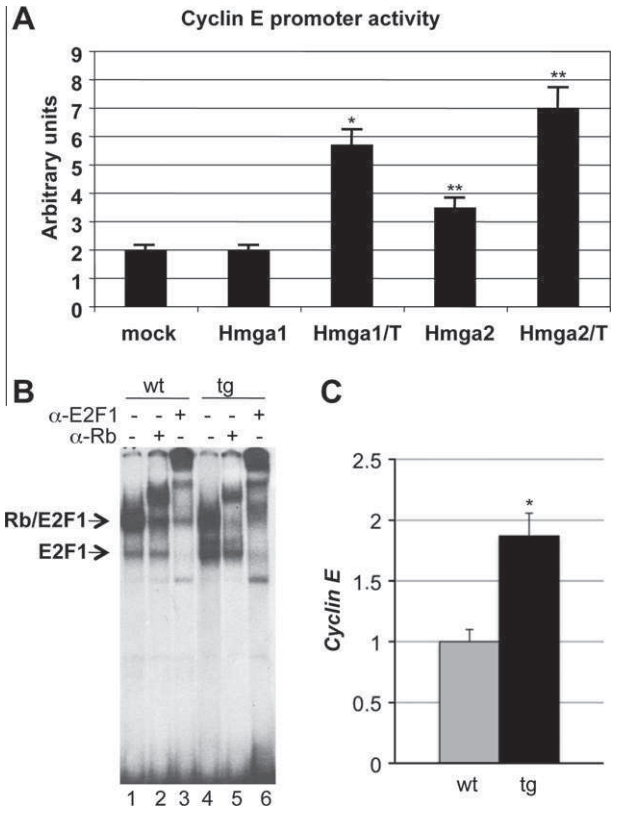

Fig. 3 – Hmga1b/T mutant protein enhances E2F1 activity. Cyclin E transactivation, by luciferase assay, in 3T3-L1 cells transfected with the indicated gene expression vectors or the backbone vector (mock). The data represent the mean values ± SD of three independent experiments performed in duplicate. *$P < 0.05$ and **$P < 0.001$ (A). EMSA of white adipose tissue extracts from wild-type (lanes 1–3) and Hmga1b/T transgenic mice (lanes 4–6) using an E2F-responsive element sequence (E2FRE) as a probe. Samples in lanes 2, 3, 5 and 6 were pre-incubated with the indicated antibodies before the addition of the probe. Supershifted bands confirmed the presence of E2F1 and pRB in the protein/DNA complexes as indicated on the left (B). qRT-PCR of white adipose tissue samples as in B to detect expression of cyclin E (C).

3.4. *Hmga1b/T mice develop B-cell lymphomas*

From 12 months of age, a high percentage (75%) of transgenic Hmga1b/T mice showed splenomegaly. This was histologically and cytologically diagnosed as B-type lymphoma (51%) (Fig. 4, Panels Aα and β, and C) or lymphoid/myeloid hyperplasia (24%) (Table 1). In a cohort of 37 transgenic mice, the B lymphoma subtypes, as defined by Morse et al.[30] were: 11 pre B-cell, 4 follicular B-cell, 3 diffuse large B-cell histiocyte-associated and 1 small B-cell lymphomas, as defined by immunohistochemical analysis with antibodies against specific B and T surface antigens and cytoplasmic proteins and further confirmed by flow cytometric analysis (data not shown). In most of the cases, lymphomas were also observed in other organs such as lymph nodes, liver (Fig. 4Aγ), biliary tract, prostate, pancreas, kidney, lung and thymus. We further characterised transgenic spleens by semiquantitative RT-PCR, looking at genes specifically altered in their expression. As shown in Fig. 4D, similarly to what we previously described for lymphomas developed by *Hmga1*-knockout mice,[18] Hmga1b/T splenocytes showed up-regulation of both *V-preB* and *Rag2* genes compared to wild-type controls. These results support a positive role of the *Hmga1b/T* mutant gene in B-cell expansion and strongly suggest its dominant-negative role, with respect to the wild-type Hmga1 protein, in the pathogenesis of this lymphoproliferative disease.

Finally, as summarised in Table 1, in our cohort of animals, analysed between the ages of 18 and 22 months, we also

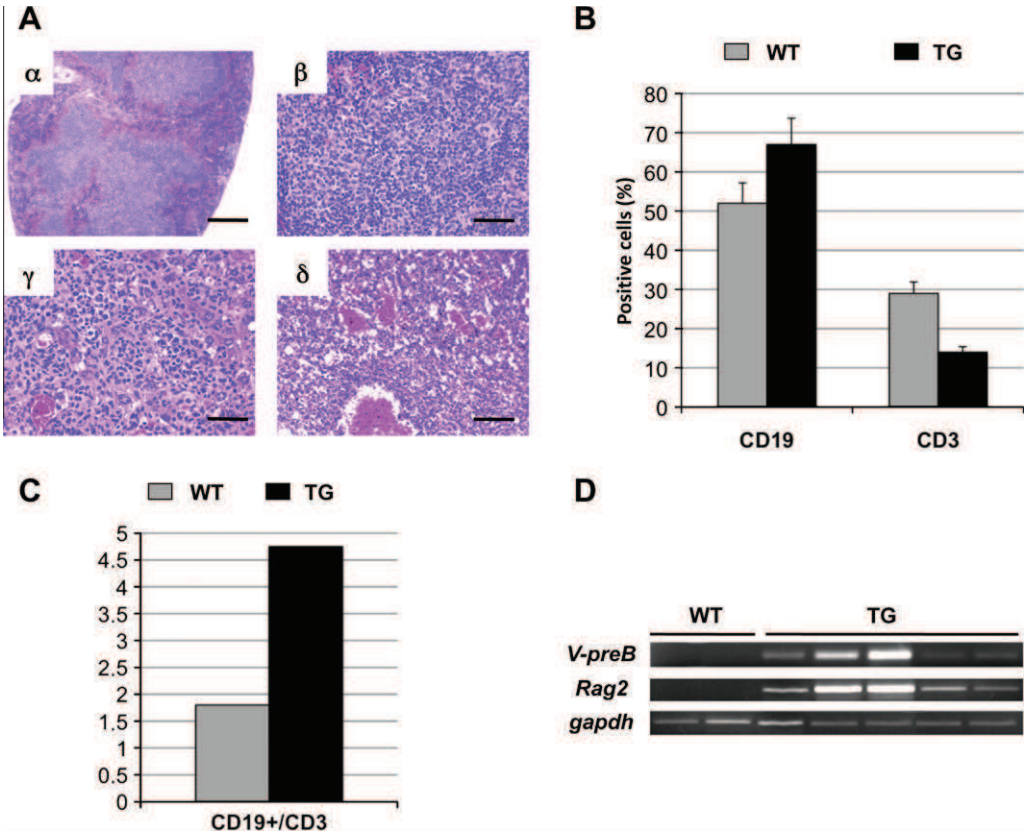

Fig. 4 – B-cell lymphomas in Hmga1/T mice. Histologic analyses of representative neoplasms developed by Hmga1b/T mice (A): spleen early lymphoma (α); higher magnification of sample shown in α (β); liver lymphoma (γ); hemangiosarcoma (δ). Scale bars: 100 μm (α), 50 μm (β, γ, δ). Analysis of B- and T-cell surface antigens by flow cytometry. The relative percentages of $CD19^+$ (B-lymphocytes) and $CD3^+$ (T-lymphocytes) cells were plotted as histograms, showing their changes in transgenic (TG) versus wild-type (WT) samples. The results represent the mean ± SE of seven different spleens for each genotype ($P < 0.05$) (B). The ratio between B- and T-cells has been represented to show the increase of the B-cell population in TG versus WT animals (C). RT-PCR analysis showing the expression of *V-preB* and *Rag2* genes in TG and WT spleens. Gapdh expression was evaluated as an internal control of RNA used (D).

Table 1 – Neoplastic lesions in Hmga1b/T transgenic mice.

Pathology	TG			WT		
	Females	Males	Total	Females	Males	Total
B-type lymphoma	13/19	6/18	19/37	2/16	1/16	3/32
Spleen lymphoid/myeloid hyperplasia	1/19	8/18	9/37	1/16	1/16	2/32
Heart hypertrophy	3/19	1/18	4/37	0/16	0/16	0/32
Spleen angiosarcoma	1/19	2/18	3/37	0/16	0/16	0/32
Lung adenocarcinoma	2/19	0/18	2/37	0/16	0/16	0/32
Lung adenoma	1/19	0/18	1/37	0/16	0/16	0/32
Uterine leiomyosarcoma	1/19	NA	1/19	0/16	NA	0/16
Endometrial hyperplasia	1/19	NA	1/19	0/16	NA	0/16
Mammary adenocarcinoma	1/19	0/18	1/37	0/16	0/16	0/32
Hepatocellular carcinoma	1/19	0/18	1/37	1/16	0/16	1/32
T-type lymphoma	0/19	1/18	1/37	0/16	0/16	0/32
Brain choroid papilloma	1/19	0/18	1/37	0/16	0/16	0/32

NA = not applicable.

found a certain number of other neoplastic lesions, including lung adenocarcinomas and spleen angiosarcomas (Fig. 4Aδ), further supporting the oncogenic potential of this mutant form of the *Hmga1* gene.

4. Discussion

Rearrangements of *HMGA1* by chromosomal aberrations of 6p21 have been frequently described in human benign

tumours of mesenchymal origin, including lipomas, uterine leiomyomas and pulmonary chondroid hamartomas.[6] The chromosomal breakpoints were located either upstream or downstream of the gene sequence, and sometimes within an 80 kb region surrounding *HMGA1*, but no intragenic rearrangements have ever been reported.[15] Therefore, it has been hypothesised that truncation of HMGA1 is not a pre-requisite to gain oncogenic potential. In contrast with this, we previously demonstrated the capacity of a construct expressing a truncated *Hmga1b* gene, devoid of the C-terminal tail (*Hmga1b/T*), to enhance proliferation of 3T3-L1 mouse fibroblasts.[23] A similar finding was obtained by blocking expression of *Hmga1*.[18] These data prompted us to hypothesise that the truncated Hmga1b mutant might have an oncogenic potential probably acting with a dominant-negative effect on the wild-type protein function. To validate this hypothesis we generated transgenic mice for the *Hmga1b/T* mutant gene. Characterisation of their phenotype confirmed the key role of the truncation of HMGA1 in the development of adipose tissue and in the acquisition of a neoplastic phenotype. Indeed, these mice are giant, obese and develop lymphomas of the same subtype developed by Hmga1-knockout mice,[18] once again suggesting a dominant-negative effect of this truncated form on wild-type HMGA1 proteins.

These mice represent one more wedge in the studies that independent groups have previously reported about Hmga1- and Hmga2-transgenic mice. Indeed, it has been reported that: (i) transgenic mice overexpressing either a wild-type or a truncated *Hmga2* cDNA, under two strong and essentially ubiquitous promoters, developed abdominal/pelvic lipomatosis and/or an abnormally high incidence of lipomas, NK-T/NK cell lymphomas and mixed growth hormone/prolactin cell pituitary adenomas[10,11,16,20]; (ii) transgenic mice with *Hmga1b* under control of the CMV promoter developed the same phenotype apart from the absence of lipomatosis[17]; (iii) transgenic mice that misexpressed full-length or truncated human HMGA2 transcript under control of the differentiated mesenchymal cell (adipocyte)-specific promoter of the adipocyte P2 (Fabp4) gene, produced neoplastic phenotype, including fibroadenomas of the breast and salivary gland adenomas[31]; and (iv) transgenic mice overexpressing *Hmga1a* flanked by the H-2K promoter and immunoglobulin intronic enhancer develop T-cell lymphoid malignancy and uterine sarcomas.[32,33]

Consistent with the behaviour of 3T3-L1 cells overexpressing the Hmga1b/T mutant,[23] mice expressing the *Hmga1b/T* transgene show enhanced E2F activity and accumulation of fat tissue, likely due to the enhanced adipocyte proliferation. This phenotype, not present in mice transgenic for the wild-type *Hmga1b* gene,[17] is quite similar to that observed in mice transgenic for either *Hmga2* or *Hmga2/T*.[11,16] Accordingly, in 3T3-L1 cells, overexpression of Hmga1b/T, Hmga2 and Hmga2/T but not Hmga1b is able to enhance the activity of an E2F-responsive element, such as cyclin E promoter. Moreover, differently from Hmga2-, Hmga2/T- and Hmga1b-transgenic mice, all the sharing the development of pituitary adenomas and T/NK lymphomas,[10,16,17] Hmga1b/T mice develop neither pituitary adenomas nor T- but B-type lymphomas, like Hmga1-knockout mice.[18]

Therefore, it appears that HMGA1b/T mutant has different biological effects in comparison to wild-type HMGA1b protein, depending on the cellular context. In adipocyte cells, even though both Hmga1b and Hmga1b/T are able to interact with pRB and displace HDAC1 from E2F1-responsive promoters,[27] only Hmga1b/T is able to enhance E2F1 activity, resulting in accumulation of fat tissue *in vivo*. Conversely, it appears that in lymphocytes Hmga1b/T has a dominant-negative effect on the endogenous Hmga1 protein. In fact, as for Hmga1$^{-/-}$ mice,[18] Hmga1b/T animals show higher levels of B-cell-specific genes and up-regulation of the *Rag2* gene expression compared with wild-type compounds, suggesting that B-cell lymphomas in Hmga1b/T mice may develop as a result of deficient T-cell function, as already hypothesised in Hmga1$^{-/-}$ mice.[18]

In conclusion, we validated *in vivo* the oncogenic role of the truncated *HMGA1* gene and its key role in the control of adipocyte proliferation. Moreover, our data indicate that HMGA1b/T might behave as a dominant-negative mutant in lymphocytic cells.

Conflict of interest statement

The authors declare that there is no conflict of interest that could be perceived as prejudicing the impartiality of the research reported.

Acknowledgements

This work was supported by grants from the Associazione Italiana Ricerca sul Cancro (AIRC) and the Ministero dell'Università e della Ricerca Scientifica e Tecnologica (MIUR).

We thank Ida Pellegrino and Michela Vitiello for their helpful contribution in some critical experiments, and the Associazione Partenopea per le Ricerche Oncologiche (APRO) for its support.

REFERENCES

1. Reeves R, Nissen MS. The A.T-DNA-binding domain of mammalian high mobility group I chromosomal proteins. A novel peptide motif for recognizing DNA structure. *J Biol Chem* 1990;**265**:8573–82.
2. Thanos D, Maniatis T. The high mobility group protein HMG I(Y) is required for NF-kappa B-dependent virus induction of the human IFN-beta gene. *Cell* 1992;**71**:777–89.
3. Zhou X, Benson KF, Ashar HR, Chada K. Mutation responsible for the mouse pygmy phenotype in the developmentally regulated factor HMGI-C. *Nature* 1995;**376**:771–4.
4. Chiappetta G, Avantaggiato V, Visconti R, et al. High level expression of the HMGI (Y) gene during embryonic development. *Oncogene* 1996;**13**:2439–46.
5. Nishino J, Kim I, Chada K, Morrison SJ. Hmga2 promotes neural stem cell self-renewal in young but not old mice by reducing p16^{Ink4a} and p19^{Arf} expression. *Cell* 2008;**135**:227–39.
6. Fusco A, Fedele M. Roles of HMGA proteins in cancer. *Nat Rev Cancer* 2007;**7**:899–910.

7. Fedele M, Berlingieri MT, Scala S, et al. Truncated and chimeric HMGI-C genes induce neoplastic transformation of NIH3T3 murine fibroblasts. *Oncogene* 1998;**17**:413–8.
8. Wood LJ, Maher JF, Bunton TE, Resar LM. The oncogenic properties of the HMG-I gene family. *Cancer Res* 2000;**60**:4256–61.
9. Hess JL. Chromosomal translocations in benign tumors: the HMGI proteins. *Am J Clin Pathol* 1998;**109**:251–61.
10. Baldassarre G, Fedele M, Battista S, et al. Onset of natural killer cell lymphomas in transgenic mice carrying a truncated HMGI-C gene by the chronic stimulation of the IL-2 and IL-15 pathway. *PNAS* 2001;**98**:7970–5.
11. Battista S, Fidanza V, Fedele M, et al. The expression of a truncated HMGI-C gene induces gigantism associated with lipomatosis. *Cancer Res* 1999;**59**:4793–7.
12. Lee YS, Dutta A. The tumor suppressor microRNA let-7 represses the HMGA2 oncogene. *Genes Dev* 2007;**21**:1025–30.
13. Mayr C, Hemann MT, Bartel DP. Disrupting the pairing between let-7 and Hmga2 enhances oncogenic transformation. *Science* 2007;**315**:1576–9.
14. Xiao S, Lux ML, Reeves R, Hudson TJ, Fletcher JA. HMGI(Y) activation by chromosome 6p21 rearrangements in multilineage mesenchymal cells from pulmonary hamartoma. *Am J Pathol* 1997;**150**:901–10.
15. Kazmierczak B, Dal Cin P, Wanschura S, et al. HMGIY is the target of 6p21.3 rearrangements in various benign mesenchymal tumors. *Genes Chrom Cancer* 1998;**23**:279–85.
16. Fedele M, Battista S, Kenyon L, et al. Overexpression of the HMGA2 gene in transgenic mice leads to the onset of pituitary adenomas. *Oncogene* 2002;**21**:3190–8.
17. Fedele M, Pentimalli F, Baldassarre G, et al. Transgenic mice overexpressing the wild-type form of the HMGA1 gene develop mixed growth hormone/prolactin cell pituitary adenomas and natural killer cell lymphomas. *Oncogene* 2005;**24**:3427–35.
18. Fedele M, Fidanza V, Battista S, et al. Haploinsufficiency of the Hmga1 gene causes cardiac hypertrophy and myelo-lymphoproliferative disorders in mice. *Cancer Res* 2006;**66**:2536–43.
19. Hock R, Furusawa T, Ueda T, Bustin M. HMG chromosomal proteins in development and disease. *Trends Cell Biol* 2007;**17**:72–9.
20. Arlotta P, Tai AK, Manfioletti G, et al. Transgenic mice expressing a truncated form of the high mobility group I-C protein develop adiposity and an abnormally high prevalence of lipomas. *J Biol Chem* 2000;**275**:14394–400.
21. Anand A, Chada K. In vivo modulation of Hmgic reduces obesity. *Nat Genet* 2000;**24**:377–80.
22. Melillo RM, Pierantoni GM, Scala S, et al. Critical role of the HMGI(Y) proteins in adipocytic cell growth and differentiation. *Mol Cell Biol* 2001;**21**:2485–95.
23. Pierantoni GM, Battista S, Pentimalli F, et al. A truncated HMGA1 gene induces proliferation of the 3T3-L1 pre-adipocytic cells: a model of human lipomas. *Carcinogenesis* 2003;**24**:1861–9.
24. Student AK, Hsu RY, Lane MD. Induction of fatty acid synthetase synthesis in differentiating 3T3-L1 preadipocytes. *J Biol Chem* 1980;**255**:4745–50.
25. Soriano P, Montgomery C, Geske R, Bradley A. Targeted disruption of the c-src proto-oncogene leads to osteopetrosis in mice. *Cell* 1991;**64**:693–702.
26. Livak KJ, Schmittgen T. Analysis of relative gene expression data using real-time quantitative PCR and the 2(–ΔΔC(T)) method. *Methods* 2001;**25**:402–8.
27. Fedele M, Visone R, De Martino I, et al. HMGA2 induces pituitary tumorigenesis by enhancing E2F1 activity. *Cancer Cell* 2006;**9**:459–71.
28. Helin K, Harlow E, Fattaey A. Inhibition of E2F-1 transactivation by direct binding of the retinoblastoma protein. *Mol Cell Biol* 1993;**13**:6501–8.
29. Esposito F, Pierantoni GM, Battista S, et al. Interaction between HMGA1 and retinoblastoma protein is required for adipocyte differentiation. *J Biol Chem* 2009;**284**:25993–6004.
30. Morse 3rd HC, Anver MR, Fredrickson TN, et al. Bethesda proposals for classification of lymphoid neoplasms in mice. *Blood* 2002;**100**:246–58.
31. Zaidi MR, Okada Y, Chada KK. Misexpression of full-length HMGA2 induces benign mesenchymal tumors in mice. *Cancer Res* 2006;**66**:7453–9.
32. Xu Y, Sumter TF, Bhattacharya R, et al. The HMG-I oncogene causes highly penetrant, aggressive lymphoid malignancy in transgenic mice and is overexpressed in human leukemia. *Cancer Res* 2004;**64**:3371–5.
33. Tesfaye A, Di Cello F, Hillion J, et al. HMGA1a up-regulates Cox-2 in uterine tumorigenesis. *Cancer Res* 2007;**67**:3998–4004.

Oncogene (2011) 1–12

www.nature.com/onc

ORIGINAL ARTICLE

HMGA proteins promote ATM expression and enhance cancer cell resistance to genotoxic agents

D Palmieri[1,3], T Valentino[1], D D'Angelo[1], I De Martino[1], I Postiglione[1], R Pacelli[2], CM Croce[3], M Fedele[1] and A Fusco[1,4]

[1]Dipartimento di Biologia e Patologia Cellulare e Molecolare c/o Istituto di Endocrinologia ed Oncologia Sperimentale del CNR, Facoltà di Medicina e Chirurgia di Napoli, Università degli Studi di Napoli "Federico II", Naples, Italy; [2]Istituto di Biostrutture e Bioimmagini del CNR, Naples, Italy; [3]Department of Molecular Virology, Immunology and Medical Genetics, Division of Human Cancer Genetics, Comprehensive Cancer Center, Ohio State University, Columbus, OH, USA and [4]NOGEC (Naples Oncogenomic Center)-CEINGE, Biotecnologie Avanzate, via Comunale Margherita, Naples, Italy

DNA-damaging therapies represent a keystone in cancer treatment. Unfortunately, many tumors often relapse because of a group of cancer cells, which are resistant to conventional therapies. High-mobility group A (HMGA) proteins has a key role in cell transformation, and their overexpression is a common feature of human malignant neoplasias, representing a poor prognostic index often correlated to anti-cancer drug resistance. Our previous results demonstrated that HMGA1 is a substrate of ataxia-telangiectasia mutated (ATM), the main cellular sensor of genotoxic stress. Here we also report thatHMGA2, the other member of the HMGA family, is a novel substrate of ATM. Interestingly, we found that HMGA proteins positively regulate *ATM* gene expression. Moreover, induction of ATM kinase activity by DNA-damaging agents enhances HMGA-dependent transcriptional activation of *ATM* promoter, suggesting that ATM expression is modulated by a DNA-damage- and HMGA-dependent positive feedback loop. Finally, inhibition of HMGA expression in mouse embryonic fibroblasts and in cancer cells strongly reduces ATM protein levels, impairing the cellular DNA-damage response and enhancing the sensitivity to DNA-damaging agents. These findings indicate this novel HMGA-ATM pathway as a new potential target to improve the effectiveness of conventional anti-neoplastic treatments on the genotoxic-drug resistant cancer cells.
Oncogene advance online publication, 21 February 2011; doi:10.1038/onc.2011.21

Keywords: HMGA; ATM; DNA repair

Introduction

The high-mobility group A (HMGA) protein family includes four members: HMGA1a, HMGA1b and HMGA1c (encoded by the *HMGA1* gene through alternative splicings) and HMGA2 (encoded by the *HMGA2* gene) (Johnson *et al*., 1989; Nagpal *et al*., 1999). HMGA proteins bind the minor groove of AT-rich DNA regions, through their amino-terminal DNA-binding domain, which consists of three short basic repeats, the so-called AT-hooks (Reeves and Nissen, 1990).

HMGAs are involved in several cellular processes such as gene and micro-RNA expression, chromatin and nucleosome remodeling, DNA replication, apoptosis and DNA repair (Wood *et al*., 2000; Reeves and Adair, 2005; Fusco and Fedele, 2007; Fedele and Fusco, 2010). HMGAs also has a causal role in cellular transformation (Wood *et al*., 2000), mainly through the regulation of expression of genes and micro-RNA involved in the control of cellular proliferation, invasion and apoptosis (Reeves and Adair, 2005; Fusco and Fedele, 2007; Fedele and Fusco, 2010).

Expression of both *HMGA* genes is restricted to the embryogenesis, resulting low or absent in normal adult tissues (Zhou *et al*., 1995; Chiappetta *et al*., 1996), while their overexpression is commonly found in almost all human malignant neoplasias, representing a poor prognostic marker correlated with the presence of metastasis, reduced survival and resistance to anti-cancer therapies (Fusco and Fedele, 2007; Fedele and Fusco, 2010).

We have previously shown that HMGA1 is a novel target of the ataxia-telangiectasia mutated (ATM) protein (Pentimalli *et al*., 2008), the main cellular sensor of DNA damage. Following the exposure to genotoxic agents, the serine/threonine kinase ATM directly and indirectly phosphorylates several substrates in order to orchestrate the cellular DNA-damage response (DDR), activating a signaling cascade which induces DNA repair, cell-cycle checkpoint activation and, eventually, apoptosis or senescence (Lavin, 2008). Interestingly, ATM-deficient cells display an increased sensitivity to genotoxic agents (Meyn *et al*., 1994; Savitsky *et al*., 1995; Kühne *et al*., 2004), and chemical inhibition of ATM induces cellular chemo- and radio-resistance (Sarkaria *et al*., 1998, 1999; Sarkaria and Eshleman 2001).

Correspondence: Professor A Fusco, Dipartimento di Biologia e Patologia Cellulare e Molecolare, Istituto di Oncologia ed Endocrinologia Sperimentale "G. Salvatore", Consiglio Nazionale delle Ricerche, via Pansini 5, 80131 Napoli, Italy.
E-mail: afusco@napoli.com
Received 23 September 2010; revised 12 January 2011; accepted 13 January 2011

In the present study, we demonstrate that HMGA2 also binds and is phosphorylated by ATM. Moreover, based on the widely described role of HMGAs in the regulation of gene expression (Reeves and Adair, 2005; Fusco and Fedele, 2007; Fedele and Fusco, 2010), we investigated their ability to bind and regulate the *ATM* gene promoter. Our results indicate that HMGAs positively regulate *ATM* expression and that ATM kinase activity on HMGA proteins can enhance their transcriptional activity on this promoter, activating a HMGA-dependent positive feedback loop in response to DNA damage. Accordingly, *Hmga1/2* double knock-out mouse embryonic fibroblasts (MEFs) display very low levels of ATM and an impaired DDR.

Finally, we report that block of HMGA expression in anaplastic thyroid cancer cells reduces cellular levels of ATM, impairs the DDR and enhances the cellular sensitivity to genotoxic agents such as ionizing radiations.

Results

HMGA2 interacts with and is phosphorylated by ATM

The carboxy-terminal domain of HMGA2 harbors a SQ motif (O'Neill *et al*., 2000) (serine 102/glutamine 103), which corresponds to the serine 88/glutamine 89 of HMGA1, phosphorylated by ATM (Pentimalli *et al*., 2008). Therefore, we investigated whether HMGA2 is also a novel target of ATM kinase activity (Figure1 and Supplementary Figure S1). For this purpose, we evaluated the ability of HMGA2 to interact with ATM transfecting HEK-293 cells with hemagglutinin (HA)-tagged-HMGA2 and FLAG-tagged-ATM expression vectors (Figure 1a). Cell extracts were immunoprecipitated with anti-FLAG antibody and immunoblotted with anti-HA antibody. Co-transfection of both HMGA2 and ATM resulted in co-immunoprecipitation of the two proteins. Conversely, HMGA2 was not immunoprecipitated by the anti-FLAG antibody when HA-HMGA2 expression vector was transfected alone. Co-immunoprecipitation experiments performed also in the presence of ethidium bromide demonstrated that the co-immunoprecipitation between HMGA2 and ATM did not depend on the contaminating DNA.

Moreover, we immunoprecipitated cell extracts from HEK-293 transfected with HA-HMGA2 expression vector alone using the anti-HA antibody, and immunoprecipitates were analyzed by western blot using anti-ATM antibody. As shown in Supplementary Figure S1, HA-HMGA2 was also able to interact with the endogenous ATM protein. Then, we verified that HMGA2, as HMGA1, is a novel substrate of ATM kinase activity in response to DNA damage. HEK-293 were transfected with HA-HMGA2 expression vector, and endogenous ATM kinase activity was induced by treating cells with 10 Gy of infrared (IR). Cells were collected 30 min after the treatment and total cell lysates were immunoprecipitated using antibodies raised against phospho-serine and phospho-threonine residues phosphorylated by ATM (Anti-P-Sub-ATM).

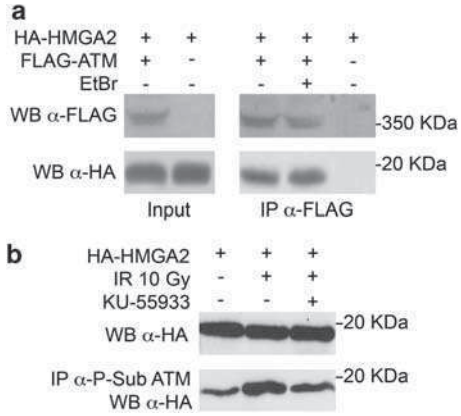

Figure 1 HMGA2 interacts with and is phosphorylated by ATM. (**a**) HEK-293 cells were transfected as indicated, and total cell extracts were immunoprecipitated using anti-FLAG antibody. Immunoprecipitated proteins were analyzed by western blot using anti-HA or anti-FLAG antibodies. Where indicated, ethidium bromide (EtBr) was added during immunoprecipitations. Cells transfected with the HA-HMGA2 vector alone were used as negative control. (**b**) HEK-293 cells transfected with the HA-HMGA2 vector were treated or not with a 10 Gy dose of IR and harvested after 30 min. Cell extracts were immunoprecipitated using the anti-P-Sub-ATM antibody. Inputs (upper panel) and immunoprecipitates (lower panel) were analyzed by western blot using anti-HA antibody. As a control of the specificity of phosphorylation, cells were also pre-treated with 10 μM KU-55933 for 1 h before the treatment with IR.

Immunoprecipitated ATM substrates were analyzed by immunoblot using anti-HA antibody, which revealed a band corresponding to the HA-HMGA2 protein (Figure 1b). Conversely, HA-HMGA2 was immunoprecipitated by the Anti-P-Sub-ATM also in cells not treated with IR. However, IR treatment significantly increased the amount of immunoprecipitated HA-HMGA2, and selective inhibition of ATM kinase activity, treating cells with 10 μM KU-55933, a specific inhibitor of ATM (Hickson *et al*., 2004), for 1 h before the IR exposure, abrogated the binding of Anti-P-Sub-ATM antibody to HA-HMGA2. These data indicate that HMGA2 is phosphorylated also in undamaged cells, but ATM activation have a key role in this phosphorylation following DNA-damaging agents exposure.

HMGA1 and HMGA2 positively regulate ATM expression

It is well known that HMGA proteins positively or negatively regulate the transcriptional activity of several genes (Fedele *et al*., 2001a, b; Fusco and Fedele, 2007; Fedele and Fusco, 2010). Therefore, we evaluated the possible role of HMGA proteins in the regulation of *ATM* expression (Figure 2). To this aim, we analyzed the expression levels of ATM mRNA and protein in MEFs lacking one or both *Hmga* genes (De Martino *et al*., manuscript in preparation). Expression levels of ATM are strongly influenced by the presence of HMGA proteins. In fact, ATM mRNA and total protein levels were strongly reduced in MEFs carrying one disrupted

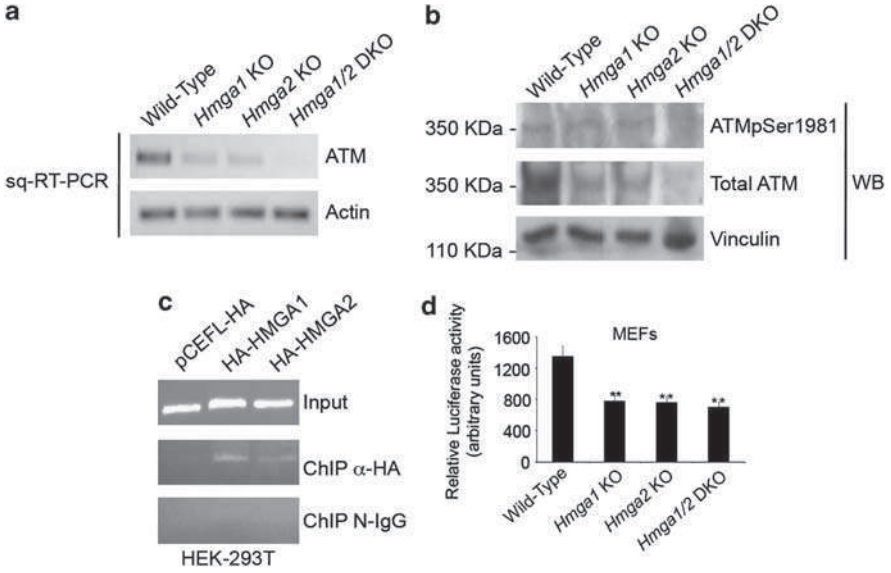

Figure 2 HMGA proteins positively regulate *ATM* expression. (**a**) sqRT–PCR on mRNA from MEFs of the indicated genotypes was used to assess *ATM* gene expression levels. Actin gene expression was evaluated to normalize RNA levels. (**b**) Total cell extracts from cells as in (**a**) were analyzed by western blot using the indicated antibodies. Vinculin was analyzed as loading control. (**c**) HEK-293T cells, transfected with the indicated vectors, were subjected to chromatin-immunoprecipitation using the anti-HA antibody. Normal rabbit IgGs (N-IgG) were used as immunoprecipitation negative control. Immunoprecipitates were analyzed by PCR using primers specific for human *ATM* promoter. (**d**) MEFs of the indicated genotypes were transfected with pLuc-ATM and luciferase activity was assessed. The data reported are the mean ± s.d. of three independent experiments performed in triplicate. **Significance values of $P<0.01$ relative to wild-type MEFs.

Hmga gene (*Hmga1* KO and *Hmga2* KO), and almost absent in double knock-out MEFs (*Hmga1/2* DKO) compared with wild-type controls, as demonstrated by semi-quantitative(sq)RT–PCR (Figure 2a) and western blot analysis (Figure 2b). Accordingly, reduced levels of active ATM, assessed using an antibody directed against its phophorylated serine 1981 (ATMser1981), were also observed in *Hmga1/2* double knock-out (DKO) MEFs compared with wild-type controls. The faint signal that is observed in wild-type and *Hmga1* or *Hmga2* single knock-out MEFs is likely due to the minimal ATM activation often observed in primary culture cells, particularly when grown in a typical cell culture incubator with 20% pO_2 (Parrinello *et al*., 2003). Moreover, we treated wild-type, *Hmga1* KO, *Hmga2* KO and *Hmga1/2* DKO MEFs with 5 Gy of IR to evaluate the activation of ATM using the anti-ATM-ser1981 antibody, and we found that ATM activation following the IR treatment was significantly decreased in *Hmga1*-KO and *Hmga2*-KO MEFs, and almost absent in *Hmga1/2*-DKO MEFs as shown in Supplementary Figure S2. These observations suggested that both HMGA proteins have a positive role in the control of *ATM* expression, leading us to further investigate a possible impairment of ATM-downstream pathways in *Hmga1/2* DKO MEFs.

To investigate whether HMGA proteins bind ATM promoter, we performed chromatin-immunoprecipitation experiments using both human HEK-293T (Figure 2c) and murine NIH-3T3 (Supplementary Figure S3) cells transiently transfected with either HA-HMGA1 or HA-HMGA2 expression vectors. Chromatin was immunoprecipitated using anti-HA or normal rabbit IgG antibodies. As shown in Figure 2c and Supplementary Figure S3, the ATM promoter was amplified only from the DNA recovered with anti-HA antibody in both 293T and NIH-3T3 cells transfected with HA-HMGA1 or HA-HMGA2, but not in cells transfected with the empty vector pCEFL-HA, used as a negative control. No amplification was obtained in the samples immunoprecipitated using normal rabbit IgG.

To better characterize the region of *ATM* promoter bound by HMGA proteins, we used different sets of PCR primers to amplify the DNA immunoprecipitated in the experiment described in Figure 2c. As shown in Supplementary Figure S4, we demonstrated that the main binding region by HMGA proteins on ATM promoter is located between −400 and −600 bp from the transcription start site of *ATM* gene. However, we found that HMGA1 was also able to bind the region located between −50 and −400 bp from the transcription start site, while HMGA2 binding was selective for the region −400 to −600 bp from the transcription start site. The specificity of the HMGA binding to ATM promoter was demonstrated as no amplification was observed using primers able to amplify the ATM promoter region between −800 and −1000 bp from the transcription start site.

To confirm the positive effect of HMGA proteins on the *ATM* promoter, we performed luciferase assays transfecting a construct expressing the luciferase reporter gene under the transcriptional control of the human *ATM* promoter (pLuc-ATM, region −512 to +9) (Berkovich and Ginsberg, 2003) along with HA-

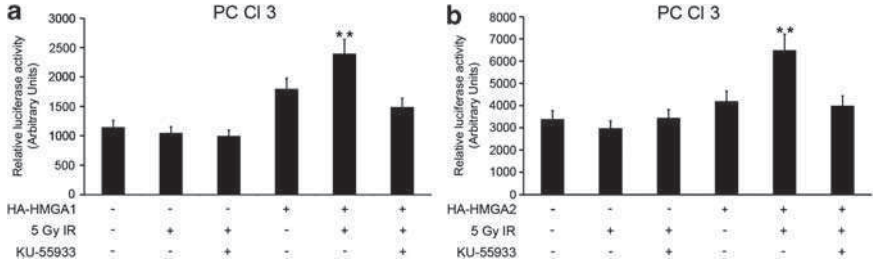

Figure 3 ATM kinase activity enhances HMGA-dependent *ATM* gene expression. PC Cl 3 cells were transfected with HA-HMGA1 (**a**) or HA-HMGA2 (**b**) vectors along with the luciferase reporter vector pLuc-ATM. Twenty-four hours after transfection, cells were treated or not with 10 μM KU-55933 for 1 h and then with 3 Gy of IR. Twenty-four hours later, luciferase activity was assessed. Data reported are the mean ± s.d. of three independent experiments performed in triplicate. **Significance values of $P<0.01$ relative to cells not treated with IR.

HMGA1 or HA-HMGA2 expression vectors or the empty vector (pCEFL-HA). As *ATM* promoter activity is dependent on the cellular context (Gueven *et al*., 2003), as well as HMGA protein transcriptional activity (Martinez Hoyos *et al*., 2004), therefore we performed luciferase assays in different cell lines, including HeLa, SAOS-2, NIH-3T3, MCF-7 and PC Cl 3 cells. As shown in Supplementary Figure S4, HA-HMGA1 has a positive effect on *ATM* promoter activity in MCF-7 (Supplementary Figure S5A) and SAOS-2 (Supplementary Figure S5B) cells while HA-HMGA2 activates *ATM* promoter in HeLa (Supplementary Figure S5C) and NIH-3T3 (Supplementary Figure S5D). Both HA-HMGA1 and HA-HMGA2 upregulate *ATM* promoter in PC Cl 3 cells, which express very low levels of endogenous HMGAs (Supplementary Figure S5E). Moreover, we also transfected PC Cl 3 cells with C-terminal deletion mutants of HA-HMGA1 (HA-HMGA1 (1–43)) and HA-HMGA2 (HA-HMGA2 (1–73)), as shown in Supplementary Figure S6, these mutants were unable to activate *ATM* promoter.

To confirm the results obtained with the previously shown cell lines, we transfected the pLuc-ATM reporter plasmid in wild-type, *Hmga1* KO, *Hmga2* KO and *Hmga1/2* DKO MEFs. Figure 2d shows that transcriptional activity of *ATM* promoter is strongly dependent on the presence of HMGA proteins. In fact, absence of HMGA1, HMGA2 or both HMGA proteins significantly reduces *ATM* promoter activity, accordingly with the results obtained from semi-quantitative RT–PCR and western blot experiments (Figures 2a and b).

Finally, we transfected the HA-HMGA1, HA-HMGA2 and their transcriptionally inactive deletion mutants HA-HMGA1 (1–43) and HA-HMGA2 (1–73) expression vectors in *Hmga1/2* DKO MEFs, and evaluated ATM mRNA levels by real time–PCR. As shown in Supplementary Figure S7, re-expression of the full-length HMGA proteins, but not the transcriptionally inactive mutants, rescued ATM expression.

Phosphorylation of HMGA proteins by ATM enhances their transcriptional activity on ATM *promoter*

ATM activation by DNA-damaging agents determines the phosphorylation of many substrates, in order to trigger an effective cellular response to the DNA damage (Lavin and Kozlov, 2007). Therefore, we hypothesized that ATM-dependent phosphorylation of HMGA1 and HMGA2 could have a role in the modulation of their function following the exposure to DNA-damaging agents. Then, we performed luciferase assays in PC Cl 3 cells transfected with HA-HMGA1 (Figure 3a) or HA-HMGA2 (Figure 3b) expression vectors along with the reporter construct pLuc-ATM, and assessed *ATM* promoter activity following the exposure to IR. Twenty-four hours after the transfection, cells were treated or not with 3 Gy of IR, in order to activate ATM kinase activity. As a specificity control, cells were also pre-incubated with KU-55933 for 1 h. As shown in Figures 3a and b, both IR and KU-55933 do not affect the transcriptional activity of *ATM* promoter in the absence of HMGA proteins, while IR enhanced HMGA-dependent upregulation of this promoter in cells transfected with either HA-HMGA1 or HA-HMGA2. Conversely, the KU-55933 prevents the IR-dependent increase of HMGA activity on *ATM* promoter, indicating that this effect depends on ATM.

MEFs null for both Hmga *genes display low levels of p21 mRNA and reduced phosphorylation of p53.*

Previous studies on Atm−/− MEFs have indicated a significant involvement of p53 and p21 in cellular defects dependent on the absence of ATM (Xu *et al*., 1996, 1998). In fact, following DNA damage, ATM phosphorylates p53 and enhances its transcriptional activity on several target promoters, such as p21 (Lavin and Kozlov 2007). Therefore, we first analyzed the levels of p53 phosphorylation on the residue (serine 15) that is phosphorylated by ATM (Canman *et al*., 1998). Accordingly to the reduced expression of ATM in *Hmga1/2* DKO MEFs, we found that the absence of HMGA proteins reduces the levels of p53-pSer15 (Figure 4a). Conversely, p53 phosphorylation levels in *Hmga1* KO MEFs are comparable to those observed in wild-type MEFs, while we observed a significant reduction of p53ser15 in *Hmga2* KO MEFs in comparison with wild-type MEFs. Moreover, the absence of both *Hmga* genes almost abolishes the levels of p21 mRNA (Figure 4a). However, *Hmga1* KO MEFs show a slight reduction of p21 mRNA, while *Hmga2* KO MEFs express p21 mRNA levels comparable to

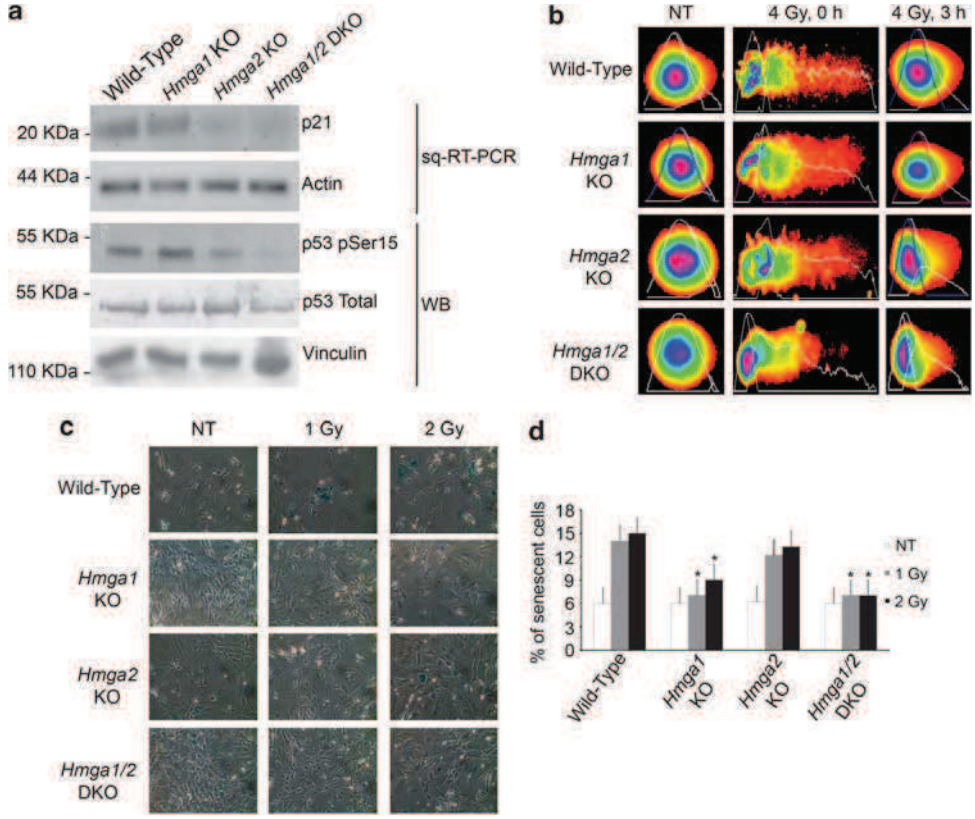

Figure 4 Altered ATM-downstream pathways and DNA-damage repair in MEFs lacking *Hmga* genes. (**a**) mRNA and protein extracts from MEFs of the indicated genotypes were analyzed by sqRT–PCR and western blot to evaluate p21 mRNA levels and p53 phosphorylation on serine 15 residue. Total p53 levels are also reported. Actin gene expression was evaluated to normalize RNA levels. Vinculin was evaluated as western blot loading control. (**b**) MEFs of the indicated genotypes, not exposed (NT) or exposed to 4 Gy of IR, were allowed to repair for 0 and 3 h and processed for comet assay. Comets were stained with SYBR Green, visualized by fluorescence microscopy and analyzed by COMET Score software. A representative comet for each experimental point is shown. (**c**) Early-passage MEFs of the indicated genotype were not treated (NT) or treated with different doses (1–2 Gy) of IR. Ninety-six hours after IR exposure, SA-β-gal-staining was performed and light microscope cell images were acquired. A representative image of each experimental point is reported. (**d**) Quantitative analysis of the experiment is shown in (**c**). The percentage of SA-β-gal positive cells is reported. Values are the mean ± s.d. of three independent experiments. At least 20 different fields were analyzed for each experimental point in each experiment. *Significance values of $P<0.01$ relative to wild-type MEFs.

Hmga1/2 DKO MEFs. These data clearly indicate that disruption of both *Hmga* genes drastically affects the ATM-dependent p53/p21 pathway, reducing p53 phosphorylation and p21 gene expression.

MEFs lacking Hmga *genes display an altered ability to repair DNA damage*

The data discussed above led us to investigate the biological effect of the HMGA proteins in DDR. To this aim, we analyzed the DNA-repair ability following IR exposure of MEFs lacking one or both *Hmga* genes. Wild-type, *Hmga1* KO, *Hmga2* KO and *Hmga1/2* DKO MEFs were either treated or not with 4 Gy of IR to induce DNA-double strand breaks (DSBs) and activate cellular DDR. Cells were harvested before or immediately after the treatment, or were allowed to repair DNA damage for 3 h. Then, we analyzed the amount of damaged DNA in each cell type by comet assay, evaluating the comet tail moment as a measure of the DNA damage. MEFs of all four genotypes display similar levels of DNA damage before and immediately after the treatment with IR compared with wild-type MEFs (Figure 4b and Supplementary Figure S8). However, after 3 h, wild-type and single knock-out MEFs almost completely recover the damage, while *Hmga1/2* DKO MEFs still show significant levels of damaged DNA (Figure 4b and Supplementary Figure S8). These observations suggest that absence of both HMGA proteins determines a significant impairment of the DNA-damage repair machinery, and reduced ATM levels might, at least in part, account for this phenotype. However, the presence of at least one of the two *Hmga* genes is sufficient to sustain the cellular DNA-damage repair.

Absence of HMGA proteins prevents stress-induced senescence

As previously described, ATM also have a key role in cellular senescence, following genotoxic stress (Crescenzi *et al*., 2008; d'Adda di Fagagna, 2008; Viale *et al*., 2009).

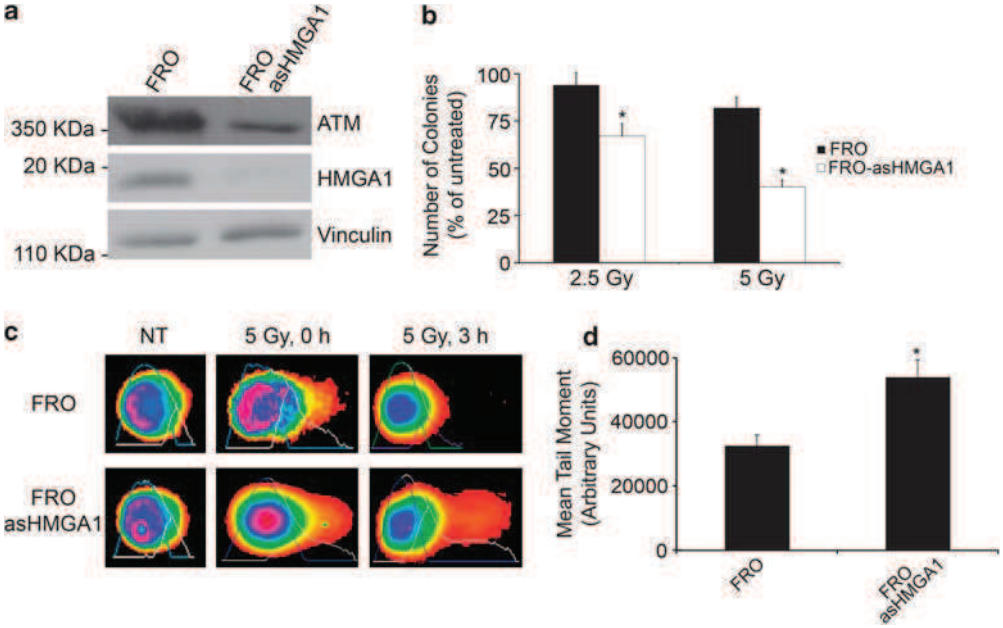

Figure 5 Downregulation of HMGA1 reduces ATM expression levels and enhances cancer cell sensitivity to DNA damage. (**a**) Western blot analysis of protein extracts from parental FRO cells and FRO-asHMGA1 cells, using the indicated antibodies. Vinculin was evaluated as loading control. (**b**) Clonogenic assay following IR exposure on FRO and FRO-asHMGA1 cells. Cells were not treated or treated with 2.5 or 5 Gy, cultured for 10 days and stained with crystal violet. Values are the mean ± s.d. of three independent experiments. *Significance values of $P<0.01$ relative to parental FRO cells. (**c**) Parental FRO and FRO-asHMGA1 were not treated (NT) or treated with 5 Gy of IR, allowed to repair for 0 and 3 h and processed for comet assay. Cells were stained with SYBR Green, visualized by fluorescence microscopy and then analyzed by COMET Score. A representative comet for each experimental point is shown. (**d**) Quantitative analysis of the experiment shown in (**c**) 3 h following the exposure to IR, using the COMET Score software. Mean tail moment values ± s.d. of three independent experiments are reported. At least 100 comets for experimental point were analyzed in each experiment. *Significance values of $P<0.01$ relative to mean tail moment of parental FRO cells.

Therefore, we decided to investigate whether absence of HMGA proteins could affect stress-induced senescence in early-passage MEFs. MEFs of all the four genotypes were treated with sub-lethal doses of IR (1–2 Gy) and senescence-associated β-galactosidase (SA-β-gal), a marker of cellular senescence, was assessed 72 h after the treatment (Figures 4c and d). As shown in Figures 4c and d, untreated MEFs, regardless of the genotype, show similar levels of SA-β-gal positive cells. Conversely, following IR exposure, we observed a significant increase in SA-β-gal positive cells only in wild-type and *Hmga2* KO MEFs, while *Hmga1* KO and *Hmga1/2* DKO MEFs were almost refractory to the stress-induced senescence. This result suggests that absence of both HMGA1 and HMGA2 prevents stress-induced senescence, likely because of the low cellular levels of ATM. Moreover, HMGA1 seems to be more involved than HMGA2 in this process, because only *Hmga1* KO, but not *Hmga2* KO cells, are resistant to stress-induced senescence.

Downregulation of HMGA1 protein enhances cancer cell sensitivity to DNA damage

An accumulating body of evidence indicates that inhibition of ATM kinase activity enhances cellular sensitivity to DNA-damaging agents (Jackson *et al*., 2009). These findings suggest that inhibition of HMGA proteins, affecting ATM expression, may result in the reduction of the ATM-mediated DDR and improvement of cell sensitivity to DNA-damaging agents. To validate this hypothesis, we analyzed the DDR of FRO (human thyroid anaplastic cancer cells, which express high levels of HMGA1 but not HMGA2) and FRO-asHMGA1 cells, that stably express an anti-HMGA1 antisense construct (Berlingieri *et al*., 2002).

As shown in Figure 5a, FRO-asHMGA1 display reduced levels of HMGA1 and of ATM protein compared with FRO parental cells. Accordingly, following the exposure of parental FRO and FRO-asHMGA1 to 5 Gy of IR, we found a reduced activation of ATM and its downstream pathways. In fact, IR treatment significantly increased ATMpSer1981, CHK2pThr68 and total p21 levels only in parental FRO but not in FRO-asHMGA1 cells, as shown by western blot analysis (Supplementary Figure S9).

Subsequently, we confirmed HMGA-dependent upregulation of ATM also in this cellular system. Indeed, we treated parental FRO and FRO-asHMGA1 cells with 5 Gy of IR and cells were then harvested at 72 h from the treatment to evaluate ATM mRNA levels by real time–PCR. As shown in Supplementary Figure S10, IR exposure increased ATM mRNA levels only in FRO but not in FRO-asHMGA1.

Then, we performed a clonogenic assay on FRO and FRO-asHMGA1 following the exposure to 2.5 or 5 Gy

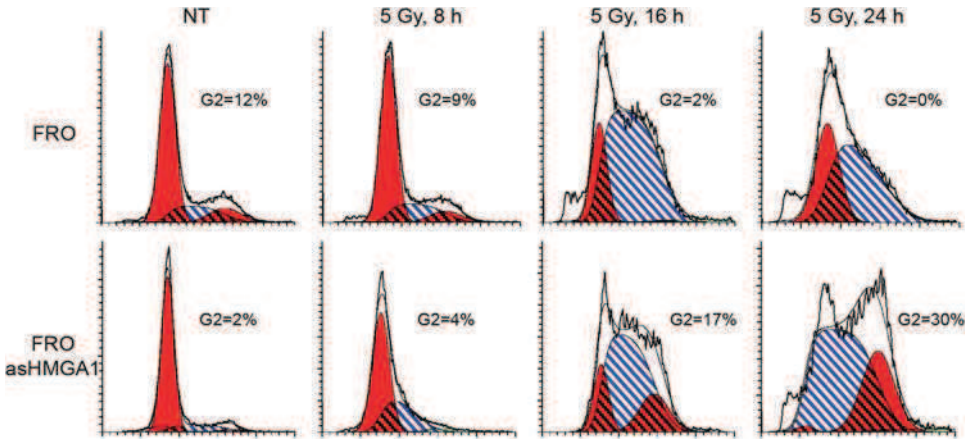

Figure 6 Downregulation of HMGA1 affects G1/S cell-cycle checkpoint in response to DNA damage. Cell-cycle analysis of parental FRO and FRO-as HMGA1. Cells were not treated (NT) or treated with 5 Gy of IR, harvested at the indicated time-points and analyzed by flow cytometry. Cells in G1 and in G2 phase of cell cycle are reported in red, cells in S phase are indicated with white and blue bars. Reported data are representative of three independent experiments.

of IR. Accordingly with their lower levels of ATM, FRO-asHMGA1 formed a much lower number of colonies, compared with parental FRO, following IR exposure (Figure 5b). Similar results were also obtained treating cells with different DNA-damaging agents such as UV-light (data not shown). This result suggests that inhibition of HMGA proteins expression affects cell proliferation and/or apoptosis following DNA damage.

To analyze the efficacy of the DNA-damage repair machinery in the absence of HMGA1, we performed a comet assay using parental FRO and FRO-asHMGA1 cells, treated or not with 5 Gy of IR. Cells were analyzed immediately or 3 h after the exposure to IR, and the tail moment of comets was analyzed. As shown in Figures 5c and d, we found significant differences in damaged DNA between wild-type FRO and FRO-asHMGA1 cells 3 h after the treatment with IR, while the amount of damaged DNA is almost comparable in untreated cells or immediately after the exposure to IR. These results indicate that, following the exposure to DNA-damaging agents, FRO-asHMGA1 activate a less effective DNA-repair machinery compared with wild-type FRO cells.

To further confirm that the reduced survival and DNA-repair ability of FRO-asHMGA1 cells following IR exposure was dependent on the lack of the transcriptional activation of ATM by HMGA1, we stably transfected FRO-asHMGA1 cells with the pFLAG-ATM expression vector (FRO-asHMGA1-ATM) or the pFLAG empty vector (FRO-asHMGA1-FLAG) (Supplementary Figure 11A). Then, we performed a clonogenic assay following the exposure to 5 Gy of IR on FRO-asHMGA1-ATM, FRO-asHMGA1-FLAG and parental FRO cells. As shown in Supplementary Figure S11B, the number of colonies formed by FRO and FRO-asHMGA1-ATM cells following the IR treatment was significantly higher compared with FRO-asHMGA1-FLAG cells. Moreover, we analyzed the DNA repair ability of FRO-asHMGA1-ATM cells by comet assay as previously described, following the exposure to 5 Gy of IR. Supplementary Figure S11C and S11D show that, 3 h after the IR treatment, the tail moment of FRO-asHMGA1-ATM cells was similar to parental FRO cells and significantly lower compared with FRO-asHMGA1-FLAG cells.

Next, we analyzed cell-cycle progression following IR exposure, in order to evaluate the ATM-dependent activation of cell-cycle checkpoints in response to DNA damage. Asynchronously growing FRO and FRO-asHMGA1 cells were harvested at different time-points following the exposure to 5 Gy of IR, fixed and stained with propidium iodide, and analyzed by flow cytometry. As shown in Figure 6, 16 and 24 h after IR treatment, parental FRO cells arrests cell-cycle progression in G1 and S phase more efficiently compared with FRO-asHMGA1. Accordingly, activation of the G1/S checkpoint following the exposure to UV-light was less efficient in FRO-asHMGA1 than in wild-type FRO cells (data not shown). These data suggest that abrogation of HMGA1 expression in cancer cells reduces the DDR, affecting the ATM-dependent activation of cell-cycle checkpoints. To focus our attention on G1/S and intra-S checkpoints, FRO and FRO-asHMGA1 were treated with 0.2 mg/ml of nocodazole following the exposure to 5 Gy of IR, in order to prevent cells from exiting G2/M phase and re-entering in G1. Wild-type FRO were also treated with 10 μM of KU-55933 to assess the effects of ATM inhibition. Cells were harvested 8 h after the nocodazole treatment, and analyzed by flow cytometry. As shown in Supplementary Figure S12, cell-cycle progression from G1 to G2 is significantly slower in FRO cells than in FRO cells treated with KU-55933 and FRO-asHMGA1 cells, following the treatment with IR and nocodazole. To better quantify the G1 checkpoint activation in FRO and FRO-asHMGA1 cells, we performed BrdU incorporation assays in these cells following IR exposure. Cells were synchronized in G1 phase by thymidine double block, then treated with 5 Gy of IR and released in complete medium containing 1 mM

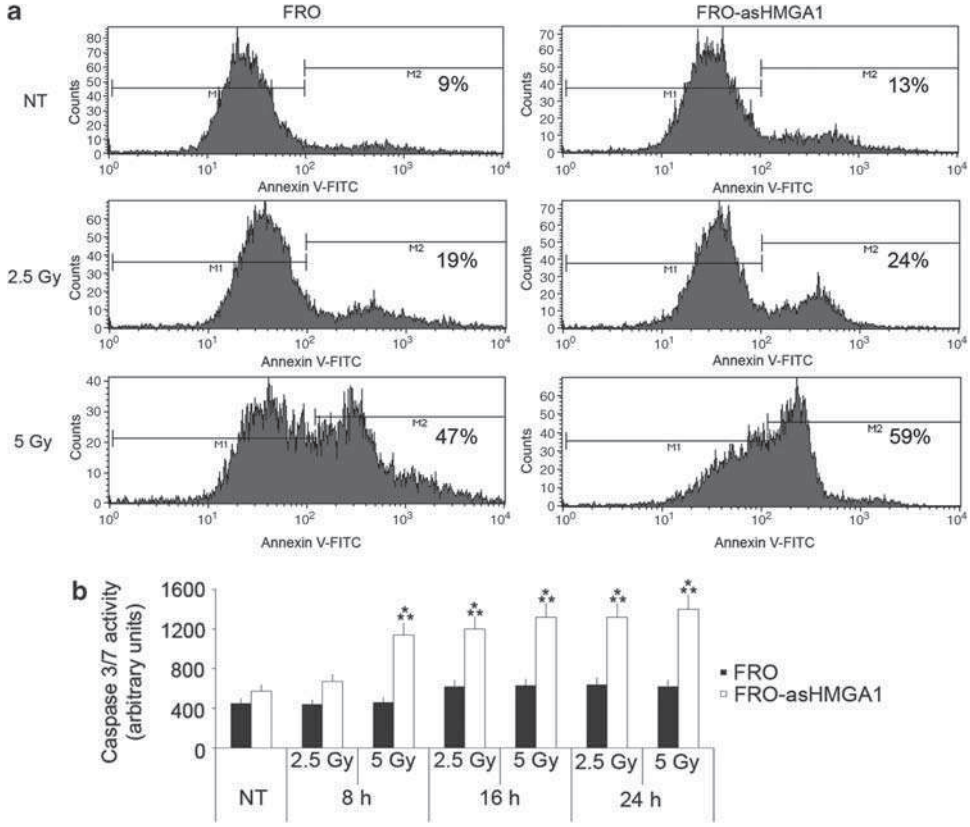

Figure 7 Downregulation of HMGA1 enhances DNA-damage-induced apoptosis. (**a**) Annexin-V staining of parental FRO and FRO-asHMGA1, not treated (NT) or treated with 2.5 and 5 Gy of IR. Cells were harvested 24 h after the exposure, stained using anti-annexin V antibody and analyzed by flow cytometry to quantify the amount of apoptotic, annexin-V positive cells (M2). Reported results are representative of three independent experiments. (**b**) Colorimetric caspase 3/7 activity assay, performed on FRO and FRO-asHMGA1 treated as in (**a**) and harvested at the indicated time-points. Values are the mean ± s.d. of three independent experiments performed in triplicate. *Significance values of $P<0.01$ relative to parental FRO cells. **Significance values of $P<0.01$ relative to untreated cells.

BrdU. Cells were harvested at different time-points and stained using an anti-BrdU antibody. BrdU incorporation was then evaluated by flow cytometry analysis. As shown in Supplementary Figure S13, BrdU incorporation was significantly higher in FRO-asHMGA1 compared with parental FRO cells after the IR treatment. These results further support the idea that block of HMGA1 expression in cancer cells prevents ATM induced G1/S checkpoint.

Then, we hypothesized that HMGA1, sustaining the expression levels of ATM, promotes the activation of G1/S checkpoint in response to DNA damage to slow down the cell-cycle progression in order to repair DNA and prevent DNA-damaging agents-induced apoptosis. To verify this hypothesis, we analyzed apoptotic markers such as annexin-V staining and caspase 3/7 activation in FRO and FRO-asHMGA1 cells, following IR treatment (Figure 7). Parental FRO and FRO-asHMGA1 cells were treated with 5 Gy of IR, harvested after 24 h, stained with anti-annexin-V fluorescent antibody and analyzed by flow cytometry. Annexin-V staining confirmed that FRO-asHMGA1 cells display a higher percentage of apoptotic cells already in untreated cells, compared with parental FRO (Figure 7a). However, following IR exposure, both FRO and FRO-asHMGA1 cells undergo apoptosis, but a significant higher percentage of annexin-V positive cells was found in FRO-asHMGA1 than in parental cells (Figure 7a). Consistently with this result, FRO-asHMGA1 cells display an increased basal caspase 3 and 7 activity compared with parental cells following the exposure to 2.5 and 5 Gy of IR (Figure 7b). However, 8 h after IR treatment, we observed a significant increase in caspase 3 and 7 activation, which increased until 24 h after the exposure only in FRO-asHMGA1 cells. Conversely, parental FRO cells show a slower and less intense activation of apoptotic pathways (Figure 7b). Therefore, these data clearly indicate that inhibition of HMGA expression in cancer cells effectively enhances DNA-damage-dependent apoptosis.

Discussion

HMGAs has a causal role in the process of carcinogenesis, and their overexpression is often correlated with resistance to conventional anti-cancer therapies and a poor prognosis (Fusco and Fedele, 2007). Previously, we reported that HMGA1 is a novel target of ATM following DNA damage (Pentimalli *et al*., 2008). Here,

we demonstrate that also HMGA2, the other member of HMGA family, interacts and is specifically phosphorylated by ATM following the exposure to IR, and that this phosphorylation can be prevented by chemical inhibition by ATM kinase activity.

Then, we investigated the potential role of HMGA proteins in the activation of *ATM* expression. Our results show that HMGA proteins bind and positively regulate the *ATM* promoter. Accordingly, MEFs null for *Hmga1* or *Hmga2* display reduced levels of ATM, compared with wild-type control, while the absence of both *Hmga* genes completely impairs ATM expression. As it has been widely demonstrated that HMGA1 and HMGA2 show overlapping functions (Fusco and Fedele, 2007), our results strongly suggest that HMGA proteins have an additive effect also in the regulation of *ATM* promoter.

Moreover, our data suggest that ATM activation by IR might trigger a positive feedback loop on its own promoter, which is dependent on the presence of HMGA proteins. In fact, luciferase, real time and western blot experiments performed in different cellular systems showed that, following IR exposure, *ATM* promoter activity and ATM mRNA and protein levels are enhanced in an ATM- and HMGA-dependent manner. However, the model that we hypothesize will require further studies in order to be clearly confirmed and clarified.

Absence of both *Hmga* genes results in the abrogation of the p53 phosphorylation on the serine 15 residue and of p21 expression, downstream targets of ATM. Conversely *Hmga1* KO MEFs did not show a reduction in the p53/p21 pathway, while *Hmga2* KO MEFs displayed reduced levels of p21 mRNA and p53ser15 compared with wild-type MEFs. The absence of *Hmga1*-dependent inhibition of p53 (Pierantoni *et al*., 2006; Pierantoni *et al*., 2007) may account for this difference between *Hmga1* and *Hmga2* single knock-out MEFs. Our results also indicate a key role for HMGA proteins in the cellular DDR. In fact, *Hmga1/2* DKO MEFs repair DNA less efficiently than wild-type MEFs following IR exposure. Moreover, we show that *Hmga1/2* DKO MEFs fail to undergo stress-induced senescence following IR treatment, further supporting the previously reported role of HMGA proteins in the process of cellular senescence (Narita *et al*., 2006). We hypothesize that reduced levels of ATM observed in *Hmga1/2* DKO cells may be, at least in part, responsible of this phenotype. However, it is very likely that HMGA1 and HMGA2 might differently affect ATM-downstream pathways and the DDR through the regulation of several other genes or transcription factors such as $p16^{INK4}$, p21 and p53.

Finally, inhibition of HMGA1 expression through antisense approach drastically decreases cellular levels of ATM in anaplastic thyroid cancer cells, resulting in increased sensitivity of these cells to DNA-damaging agents. In fact, block of HMGA1 enhances the pro-apoptotic effects of IR, and cell-cycle analysis following the exposure to DNA-damaging agents showed that absence of HMGA proteins affects the activation of the G1/S checkpoint. These findings further support the idea that abrogation of HMGAs results in the accumulation of DNA damages and in an enhanced sensitivity to DNA-damaging agents.

The data reported here suggest the hypothesis that HMGAs might enhance the cellular response to DNA damage, increasing ATM protein levels, and through their previously described anti-apoptotic activity (Pierantoni *et al*., 2007), could shift ATM signaling from cell death to cell survival and resistance to genotoxic drugs. However, further experiments are requested to be clearly confirmed and elucidated.

Our data present important clinical implications. As the depletion of HMGA proteins increases the sensitivity of cancer cells to radio- and chemo-therapeutic drugs, the block of the HMGA expression could represent a new therapeutic tool to reduce the resistance of cancer cells to genotoxic anti-cancer therapies. The differential expression of HMGA in neoplastic and normal cells should also allow for the specificity and low toxicity of such therapy. Moreover, as HMGA proteins are overexpressed in cancers of different origins, HMGA-based therapy should have a wide spectrum of anti-cancer applications.

Materials and methods

Chemicals and treatments

For γ-irradiation experiments, cells were irradiated by 6 MV X-ray of a linear accelerator with doses ranging from 0 to 10 Gy. For ATM inhibition experiments, cells were treated with KU-55933 (10 μM) for 1 h before the induction of ATM kinase activity.

Cell cultures, transfections and plasmids

HEK-293T, HEK-293, MCF-7, SAOS-2, HeLa and FRO cells were cultured in Dulbecco's modified eagle medium (DMEM) with 10% fetal bovine serum (FBS), L-glutamine and antibiotics (Invitrogen, Carlsbad, CA, USA). PC Cl 3 cells were grown as previously described (Fedele *et al*., 2001a, b). MEFs were established from 14.5 dpc embryos following standard procedures, and cultured in DMEM with 10% FBS, L-glutamine, antibiotics and 1% non-essential amino acids (Invitrogen). NIH-3T3 cells were grown in DMEM with 10% FCS and antibiotics. MEFs and FRO cells were transfected using Neon Electroporation System (Invitrogen) according to the manufacturer's instructions. All the other transfections were performed by using Lipofectamine 2000 (Invitrogen), as suggested by the manufacturer. The pCEFL-HA-HMGA1, pCEFL-HA-HMGA2, pCEFL-HA-HMGA1 (1–43) and pCEFL-HA-HMGA2 (1–73) vectors were previously described (Fedele *et al*., 2006; Pierantoni *et al*., 2001; Pentimalli *et al*., 2008). The anti-HMGA1 antisense construct was described elsewhere (Berlingieri *et al*., 2002). The pFLAG-ATM previously described (Bakkenist and Kastan, 2003) was kindly provided by Dr MB Kastan. The pLuc-ATM reporter plasmid was a kind gift of Dr D Ginsberg (Berkovich and Ginsberg, 2003). Stable clones (FRO-asHMGA1, FRO-as-HMGA1-FLAG and FRO-as-HMGA1-ATM) were generated by co-transfection of the indicated plasmids along with the pBabe-Puro vector, containing the puromycin resistance gene. Following the transfection, stable clones were selected

for puromycin resistance in medium containing 1 μg/ml of this antibiotic.

Immunoprecipitation and western blot
Protein extraction, western blots and immunoprecipitations were performed as previously described (Pentimalli *et al*., 2008). Antibodies used were anti-FLAG M2 (Sigma, St Louis, MO, USA), anti-HA Clone 12CA5 (Roche, Branford, CT, USA), anti-P-ATM-substrate (phospho-Ser/Thr antibody), anti-CHK2pThr68 (Cell Signalling Technology, Danvers, MA, USA), anti-ATM S1981p (Rockland, Philadelphia, PA, USA), anti-p53 DO-1, anti-p-p53 (Ser15), anti-ATM and anti-vinculin (7F9) (Santa Cruz, Santa Cruz, CA, USA). Anti-HMGA1 and anti-HMGA2 polyclonal antibodies were described elsewhere (Pierantoni *et al*., 2001; Fedele *et al*., 2006).

RNA extraction and semi-quantitative (sq)RT–PCR
Total RNA was isolated using TRI-reagent solution (Sigma) and treated with DNase (Invitrogen). Reverse transcription was performed according to standard procedures (Applied Biosystems, Foster City, CA, USA). cDNA was amplified by PCR using the following primers:.
mmuATM-F: 5′-ATTGGGATGCTGTTTTCAGG-3′
mmuATM-R: 5′-TAGCCTGGGTGCTCTTTTGT-3′
mmup21-F: 5′-TCCACAGCGATATCCAGACA-3′
mmup21-R: 5′-GGCACACTTTGCTCCTGTG-3′
mmuActin-F: 5′-TCAGAAGGACTCCTATGTGG-3′
mmuActin-R: 5′-CGCAGCTCATTGTAGAAGGT-3′

Quantitative real time–PCR
Total RNAs were treated with Dnase-I (Invitrogen) and reverse-transcribed using random hexanucleotides as primers and MuLV reverse transcriptase (Perkin-Elmer, Waltham, MA, USA), following manufacturer's instructions. Quantitative real time–PCR was performed with the SYBR Green PCR Master Mix (Applied Biosystems) under the following conditions: 10 min at 95 °C followed by 40 cycles (15 s at 95 °C and 1 min at 60 °C). Subsequently, a dissociation curve was run to verify amplification specificity. We used the 2^{-CT} method to calculate the relative expression levels (Livak and Schmittgen, 2001). All the experiments were performed three times in triplicate and the mean ± s.d. was reported. Primers specific for the glucose-6-phosphate dehydrogenase (G6PD) were used for normalization of real time–quantitative PCR data. The following primer sequences were used to amplify the indicated genes:
ATM-F: 5′-TCTCAAGCAGATGATCAAGAAGTT-3′
ATM-R: 5′-TGACTTTGAGACCTGCATCATT-3′
G6PD-F: 5′-CAGCGGCAACTAAACTCAGA-3′
G6PD-R: 5′-TTCCCTCAGGATCCCACAC-3′.

Luciferase assay
Cells were transfected with 1 μg of pLuc-ATM and with pCEFL-HA-HMGA1 or pCEFL-HA-HMGA2 expression vectors, together with 0.5-μg of pCMV-*Renilla*. Luciferase and *Renilla* activity were assessed with the Dual-Light Luciferase system (Promega, Fitchburg, WI, USA), 48 h after the transfection. The Luciferase activity was normalized for the *Renilla* activity. All the experiments were performed three times in triplicate and the mean ± s.d. was reported.

Chromatin-immunoprecipitation assay
Chromatin-immunoprecipitation assays were carried out with a chromatin-immunoprecipitation assay kit (Upstate Biotechnology, Lake Placid, NY, USA) according to manufacturer's instructions. Chromatin was sonicated on ice to an average length of about 400 bp with a Branson sonicator. Sonicated chromatin was then immunoprecipitated using anti-HA antibody (Santa Cruz) or normal rabbit IgG as negative control. Input and immunoprecipitated DNA were analyzed by PCR with AmpliTaq gold DNA polymerase (Applied Biosystems). Primers used were:
mmuATMprF: 5′-ATTGGGATGCTGTTTTCAGG-3′
mmuATMprR: 5′-TAGCCTGGGTGCTCTTTTGT-3′
hsaATMprF: 5′-AACACAGCGACAGCTCCTG-3′
hsaATMprR: 5′-AGTGACGACAGTTCCGAAGG-3′
hsaATMpr-1000F: 5′-GGGCTAGAAAACGTTCAAC-3′
hsaATMpr-800R: 5′-CTTTGTAGAGAGACCTTCCTG-3′
hsaATMpr-800F: 5′-CAGGAAGGTCTCTCTACAAAG-3′
hsaATMpr-600R: 5′-GGATTCGGAAGGAAAGTCAG-3′
hsaATMpr-600F: 5′-CTGACTTTCCTTCCGAATCC-3′
hsaATMpr-400R: 5′-GCCAAAGGTTTTCCCTTGG-3′
hsaATMpr-400F: 5′-CCAAGGGAAAACCTTTGGC-3′
hsaATMpr-200R: 5′-GTCGCTGTGTTTGCTTTAAC-3′
hsaATMpr-200F: 5′-GTTAAAGCAAACACAGCGAC-3′
hsaATMpr-50R: 5′-CAAGTCTGAGGACGGAAGTG-3′.

Comet assay
MEFs and FRO cells irradiated or not with 4 and 5 Gy of IR, respectively, were allowed to repair the DNA for 0 and 3 h in complete medium and then processed for the COMET assay (Trevigen, Helgerman, CT, USA) following manufacturer's instructions. Cell images were analyzed using COMET Score (TriTek, Annandale, VA, USA). Comet tail moment was used as the measure of DNA damage. In each experiment, 100 comets were measured per experimental point and the mean ± s.d. was reported.

Senescence assay
Early-passage MEFs were treated as described in results, and SA-β-gal activity was assessed by using Senescent Cells Staining kit (Sigma) following the manufacturer's instructions. Cells were analyzed with light microscopy to determine the percentage of senescent cells. At least 20 fields for each experimental point were analyzed. Reported values are the mean ± s.d. of three independent experiments.

Clonogenic assay
Cells were seeded at a density of 10^3 cells per 35-mm dish. After 1 day, cells were treated with different doses of IR. After 10 days, cells were stained with 500 mg/ml of crystal violet in 20% methanol, and resulting colonies were counted. The colony counts obtained were normalized for the untreated controls. The mean ± s.d. of three independent experiments performed in triplicate was reported.

Cell-cycle analysis
Twenty-four hours following the seeding, cells were exposed to 5 Gy of IR. Where indicated, cells were also treated with 0.2 mg/ml of nocodazole, following the IR treatment. Cells were harvested at different time-points, fixed with ice-cold 70% ethanol, treated with RNase-I (Invitrogen) and stained with 10 μg/ml of propidium iodide. Cells were sorted on a FACS-Calibur flow cytometer (Becton Dickinson, San Diego, CA, USA), and the results were analyzed with ModFit software, 3.2 version (Verity Software House). Experiments were performed in triplicate and representative cell-cycle profiles were reported.

BrdU incorporation analysis
Twenty-four hours following the seeding, cells were treated with 2 mM thymidine for 16 h, then washed twice with PBS and cultured for 8 h in complete medium. Cells were then treated again with 2 mM thymidine for 17 h, to synchronize them in G1 phase of the cell cycle. Following the thymidine double block, cells were treated with 5 Gy of IR, and then cultured in complete medium containing 1 mM BrdU and harvested at different time-points. Harvested cells were fixed and stained using the BrdU Flow Kit (BD Pharmingen, San Diego, CA, USA), according to the manufacturer's instructions. Stained cells were analyzed by flow cytometry, as described above. The assay was performed three times in triplicate and the mean ± s.d. was reported.

Apoptosis assays
Twenty-four hours after the seeding, FRO and FRO-asHMGA1 were untreated or exposed to 5 Gy of IR. Cells were then harvested after 24 h and stained with 10 μg/ml of propidium iodide and FITC-annexin-V antibody (BD Biosciences, San Diego, CA, USA), following manufacturer's instructions. Annexin-V-propidium iodide positive cells were analyzed using FACS-Calibur flow cytometer (Becton Dickinson). Experiments were performed in triplicate and representative annexin-V profiles were reported. Apoptosis was also quantified by measuring caspase 3 and 7 activation following the exposure to 2.5 or 5 Gy of IR, using Caspase-Glo 3/7 assay (Promega) according to the manufacturer's instructions on a Bio-Tek Synergy HT multi-detection microplate reader. The assay was performed three times in triplicate and the mean ± s.d. was reported.

Statistical analysis
Student's *t*-test was used to determine significance. All error bars represent the s.d. of the mean. Statistical significance for all the tests, assessed by calculating the *P*-value, was <0.01.

Conflict of interest

The authors declare no conflict of interest.

Acknowledgements

We thank V Costanzo for revision of the paper and I Pellegrino for technical support. We are grateful to MB Kastan for providing the pFLAG-ATM expression construct and to D Ginsberg for the pLuc-ATM reporter vector. This work was supported by grants from the Associazione Italiana Ricerca sul Cancro (AIRC). DP is recipient of a fellowship from Fondazione Italiana per la Ricerca sul Cancro (FIRC).

References

Bakkenist CJ, Kastan MB. (2003). DNA damage activates ATM through intermolecular autophosphorylation and dimer dissociation. *Nature* **421**: 499–506.

Berkovich E, Ginsberg D. (2003). ATM is a target for positive regulation by E2F-1. *Oncogene* **22**: 161–167.

Berlingieri MT, Pierantoni GM, Giancotti V, Santoro M, Fusco A. (2002). Thyroid cell transformation requires the expression of the HMGA1 proteins. *Oncogene* **21**: 2971–2980.

Canman CE, Lim DS, Cimprich KA, Taya Y, Tamai K, Sakaguchi K *et al*. (1998). Activation of the ATM kinase by ionizing radiation and phosphorylation of p53. *Science* **281**: 1677–1679.

Chiappetta G, Avantaggiato V, Visconti R, Fedele M, Battista S, Trapasso F *et al*. (1996). High level expression of the HMGI (Y) gene during embryonic development. *Oncogene* **13**: 2439–2446.

Crescenzi E, Palumbo G, de Boer J, Brady HJ. (2008). Ataxia telangiectasia mutated and p21CIP1 modulate cell survival of drug-induced senescent tumor cells: implications for chemotherapy. *Clin Cancer Res* **14**: 1877–1887.

d'Adda di Fagagna F. (2008). Living on a break: cellular senescence as a DNA-damage response. *Nat Rev Cancer* **8**: 512–522.

Fedele M, Battista S, Manfioletti G, Croce CM, Giancotti V, Fusco A. (2001a). Role of the high mobility group A proteins in human lipomas. *Carcinogenesis* **22**: 1583–1591.

Fedele M, Fusco A. (2010). HMGA and cancer. *Biochim Biophys Acta* **1799**: 48–54.

Fedele M, Pierantoni GM, Berlingieri MT, Battista S, Baldassarre G, Munshi N *et al*. (2001b). Overexpression of proteins HMGA1 induces cell cycle deregulation and apoptosis in normal rat thyroid cells. *Cancer Res* **61**: 4583–4590.

Fedele M, Visone R, De Martino I, Troncone G, Palmieri D, Battista S *et al*. (2006). HMGA2 induces pituitary tumorigenesis by enhancing E2F1 activity. *Cancer Cell* **9**: 459–471.

Fusco A, Fedele M. (2007). Roles of HMGA proteins in cancer. *Nat Rev Cancer* **7**: 899–910.

Gueven N, Keating K, Fukao T, Loeffler H, Kondo N, Rodemann HP *et al*. (2003). Site-directed mutagenesis of the ATM promoter: consequences for response to proliferation and ionizing radiation. *Genes Chromosomes Cancer* **38**: 157–167.

Hickson I, Zhao Y, Richardson CJ, Green SJ, Martin NM, Orr AI *et al*. (2004). Identification and characterization of a novel and specific inhibitor of the ataxia-telangiectasia mutated kinase ATM. *Cancer Res* **64**: 9152–9159.

Jackson SP. (2009). The DNA-damage response: new molecular insights and new approaches to cancer therapy. *Biochem Soc Trans* **37**: 483–494.

Johnson KR, Lehn DA, Reeves R. (1989). Alternative processing of mRNAs encoding mammalian chromosomal high-mobility-group proteins HMG-I and HMG-Y. *Mol Cell Biol* **9**: 2114–2123.

Kühne M, Riballo E, Rief N, Rothkamm K, Jeggo PA, Löbrich MA. (2004). Double-strand break repair defect in ATM-deficient cells contributes to radiosensitivity. *Cancer Res* **64**: 500–508.

Lavin MF. (2008). Ataxia-telangiectasia: from a rare disorder to a paradigm for cell signalling and cancer. *Nat Rev Mol Cell Biol* **9**: 759–769.

Lavin MF, Kozlov S. (2007). ATM activation. DNA damage response. *Cell Cycle* **6**: 931–942.

Livak KJ, Schmittgen TD. (2001). Analysis of relative gene expression data using real-time quantitative PCR and the 2(-Delta Delta C(T)) Method. *Methods* **25**: 402–408.

Martinez Hoyos J, Fedele M, Battista S, Pentimalli F, Kruhoffer M, Arra C *et al*. (2004). Identification of the genes up- and down-regulated by the high mobility group A1 (HMGA1) proteins: tissue specificity of the HMGA1-dependent gene regulation. *Cancer Res* **64**: 5728–5735.

Meyn MS, Strasfeld L, Allen C. (1994). Testing the role of p53 in the expression of genetic instability and apoptosis in ataxia-telangiectasia. *Int J Radiat Biol* **66**: S141–S149.

Nagpal S, Ghosn C, DiSepio D, Molina Y, Sutter M, Klein ES *et al*. (1999). Retinoid-dependent recruitment of a histone H1 displacement activity by retinoic acid receptor. *J Biol Chem* **274**: 22563–22568.

Narita M, Narita M, Krizhanovsky V, Nuñez S, Chicas A, Hearn SA *et al*. (2006). A novel role for high-mobility group a proteins

in cellular senescence and heterochromatin formation. *Cell* **126**: 503–514.

O'Neill T, Dwyer AJ, Ziv Y, Chan DW, Lees-Miller SP, Abraham RH *et al*. (2000). Utilization of oriented peptide libraries to identify substrate motifs selected by ATM. *J Biol Chem* **275**: 22719–22727.

Parrinello S, Samper E, Krtolica A, Goldstein J, Melov S, Campisi J. (2003). Oxygen sensitivity severely limits the replicative lifespan of murine fibroblasts. *Nat Cell Biol* **5**: 741–747.

Pentimalli F, Palmieri D, Pacelli R, Garbi C, Cesari R, Martin E *et al*. (2008). HMGA1 protein is a novel target of the ATM kinase. *Eur J Cancer* **44**: 2668–2679.

Pierantoni GM, Fedele M, Pentimalli F, Benvenuto G, Pero R, Viglietto G *et al*. (2001). High mobility group I (Y) proteins bind HIPK2, a serine-threonine kinase protein which inhibits cell growth. *Oncogene* **20**: 6132–6141.

Pierantoni GM, Rinaldo C, Esposito F, Mottolese M, Soddu S, Fusco A. (2006). High Mobility Group A1 (HMGA1) proteins interact with p53 and inhibit its apoptotic activity. *Cell Death Differ* **5**: 2045–2048.

Pierantoni GM, Rinaldo C, Mottolese M, Di Benedetto A, Esposito F, Soddu S *et al*. (2007). High-mobility group A1 inhibits p53 by cytoplasmic relocalization of its proapoptotic activator HIPK2. *J Clin Invest* **117**: 693–702.

Reeves R, Adair JE. (2005). Role of high mobility group (HMG) chromatin proteins in DNA repair. *DNA Repair (Amst)* **8**: 926–938.

Reeves R, Nissen MS. (1990). The A.T-DNA-binding domain of mammalian high mobility group I chromosomal proteins. A novel peptide motif for recognizing DNA structure. *J Biol Chem* **265**: 8573–8582.

Sarkaria JN, Busby EC, Tibbetts RS, Roos P, Taya Y, Karnitz LM *et al*. (1999). Inhibition of ATM and ATR kinase activities by the radiosensitizing agent, caffeine. *Cancer Res* **59**: 4375–4382.

Sarkaria JN, Eshleman JS. (2001). ATM as a target for novel radiosensitizers. *Semin Radiat Oncol* **11**: 316–327.

Sarkaria JN, Tibbetts RS, Busby EC, Kennedy AP, Hill DE, Abraham RT. (1998). Inhibition of phosphoinositide 3-kinase related kinases by the radiosensitizing agent wortmannin. *Cancer Res* **58**: 4375–4382.

Savitsky K, Bar-Shira A, Gilad S, Rotman G, Ziv Y, Vanagaite L *et al*. (1995). A single ataxia telangiectasia gene with a product similar to PI-3 kinase. *Science* **268**: 1749–1753.

Viale A, De Franco F, Orleth A, Cambiaghi V, Giuliani V, Bossi D *et al*. (2009). Cell-cycle restriction limits DNA damage and maintains self-renewal of leukaemia stem cells. *Nature* **457**: 51–56.

Wood LJ, Maher JF, Bunton TE, Resar LM. (2000). The oncogenic properties of the HMG-I gene family. *Cancer Res* **60**: 4256–4261.

Xu Y, Ashley T, Brainerd EE, Bronson RT, Meyn MS, Baltimore D. (1996). Targeted disruption of ATM leads to growth retardation, chromosomal fragmentation during meiosis, immune defects, and thymic lymphoma. *Genes Dev* **10**: 2411–2422.

Xu Y, Yang EM, Brugarolas J, Jacks T, Baltimore D. (1998). Involvement of p53 and p21 in cellular defects and tumorigenesis in Atm−/− mice. *Mol Cell Biol* **18**: 4385–4390.

Zhou X, Benson KF, Ashar HR, Chada K. (1995). Mutation responsible for the mouse pygmy phenotype in the developmentally regulated factor HMGI-C. *Nature* **376**: 771–774.

Supplementary Information accompanies the paper on the Oncogene website (http://www.nature.com/onc)

Oncogene (2011) 1–9

www.nature.com/onc

ORIGINAL ARTICLE

Downregulation of *HMGA*-targeting microRNAs has a critical role in human pituitary tumorigenesis

D Palmieri[1], D D'Angelo[1], T Valentino[1], I De Martino[1], A Ferraro[1,4], A Wierinckx[2], M Fedele[1], J Trouillas[3] and A Fusco[1,4]

[1]*Istituto di Endocrinologia ed Oncologia Sperimentale del CNR Dipartimento di Biologia e Patologia Cellulare e Molecolare Facoltà di Medicina e Chirurgia di Napoli, Università degli Studi di Napoli 'Federico II', Naples, Italy;* [2]*INSERM U1052, Centre de Recherche en Cancerologie de Lyon, Lyon, France and University Lyon, Lyon, France;* [3]*INSERM U1028, CNRS UMR 5292, Lyon Neuroscience Research Center, Neuro-oncology and Neuroinflammation team, Lyon, France and University Lyon1, Lyon, France and* [4]*NOGEC (Naples Oncogenomic Center)-CEINGE, Biotecnologie Avanzate-Napoli, & SEMM—European School of Molecular Medicine—Naples Site, Naples, Italy*

Previous studies have demonstrated that high mobility group A proteins have a critical role on the onset of human pituitary adenomas. Indeed, both high mobility group A (*HMGA*) genes are overexpressed in pituitary adenomas, and consistently transgenic mice overexpressing either the *Hmga1* or the *Hmga2* gene develop mixed growth hormone/prolactin (GH-PRL)-secreting pituitary adenomas. Trisomy of chromosome 12, where *HMGA2* is located, and/or amplification of the *HMGA2* gene locus account for the *HMGA2* overexpression in most human prolactinomas. Conversely, *HMGA1* overexpression is not associated to any rearrangement or amplification of the *HMGA1* locus. We have first identified micro RNAs (miRNAs) able to target both *HMGA1* and *HMGA2* messenger RNAs. Then, all of these miRNAs have been found downregulated in pituitary adenomas of different histotypes, compared with normal pituitary. Interestingly, their downregulation was also observed in nonfunctioning pituitary adenomas where *HMGA2* overexpression is not associated to any alteration of the *HMGA2* locus. Functional studies show that all these *HMGA*-targeting miRNAs inhibit the proliferation of the rat pituitary adenoma cell line GH3. Therefore, these results indicate that the downregulation of the miRNAs able to target the *HMGA* genes could contribute to increase HMGA protein levels in human pituitary adenomas, and then to pituitary tumorigenesis.
Oncogene advance online publication, 5 December 2011; doi:10.1038/onc.2011.557

Keywords: HMGA; pituitary adenoma; microRNA

Correspondence: Professor A Fusco, Istituto di Endocrinologia ed Oncologia Sperimentale del Consiglio Nazionale delle Ricerche, Via Pansini 5, Napoli 80131, Italy.
E-mail: alfusco@unina.it
Received 21 June 2011; revised 1 November 2011; accepted 2 November 2011

Introduction

Autoptic and radiological imaging studies have demonstrated that pituitary adenomas are very common in the general population, accounting for 10–15% of all intracranial tumors (Kovacs and Horvath, 1986; Monson, 2000; Daly *et al*., 2009; Melmed, 2011). Pituitary adenomas are clinically classified on the basis of their hormonal activity *in vivo*. Prolactin (PRL)-, gonadotropin (luteinizing hormone/follicle-stimulating hormone)- and growth hormone (GH)-secreting adenomas are the most frequent type of pituitary adenomas, whereas adenocorticotroph (ACTH (adrenocorticotropic hormone))- and tireotroph (TSH (thyroid-stimulating hormone))-secreting adenomas are very rare (Daly *et al*., 2006, 2009; Melmed, 2011). Moreover, about one-third of pituitary adenomas are not associated to hormone hypersecretion, and are classified as nonfunctioning pituitary adenomas (NFPA) (Daly *et al*., 2006, 2009; Fernandez *et al*., 2010). Commonly, both functioning and nonfunctioning adenomas are noninvasive, and their morbidity is mainly because of inappropriate secretion of pituitary hormones or symptoms of an intracranial mass, such as visual disturbance and headaches (Melmed, 2011).

Several studies indicate that high mobility group A (HMGA) proteins have a causal role in pituitary cell transformation. HMGAs are a family of small non-histone chromatin proteins that include four members, HMGA1a, HMGA1b, HMGA1c (encoded by the *HMGA1* gene through alternative splicings) and HMGA2 (encoded by the homonymous gene) (Johnson *et al*., 1989). HMGA proteins do not have transcriptional activity *per se*, however by interacting with the transcriptional machinery they alter the chromatin structure and, thereby, regulate, negatively or positively, the transcriptional activity of several genes and micro RNAs (miRNAs) (Thanos and Maniatis, 1992; Thanos *et al*., 1993; De Martino *et al*., 2009a).

HMGA expression is almost undetectable in differentiated adult tissues, whereas it is expressed highly during embryogenesis (Zhou *et al*., 1995; Chiappetta *et al*., 1996). Conversely, HMGA overexpression is

a constant feature of human malignant neoplasms, and rearrangements of the HMGA genes are frequently associated with human benign tumors of mesenchymal origin (Ashar *et al*., 1995; Schoenmakers *et al*., 1995; Fedele and Fusco, 2010). Several studies have demonstrated that HMGA proteins have a critical role in neoplastic transformation. In fact, blockage of HMGA synthesis prevents rat thyroid cell transformation by murine-transforming retroviruses (Berlingieri *et al*., 1995, 2002), and an adenovirus carrying the *HMGA1* gene in the antisense orientation induces apoptotic cell death in anaplastic human thyroid carcinoma cell lines, but not in normal thyroid cells (Scala *et al*., 2000). Moreover, transgenic mice overexpressing the *Hmga1* or the *Hmga2* gene under an ubiquitous promoter develop several malignant or benign neoplasias, including mixed GH/PRL pituitary adenomas (Baldassarre *et al*., 2001; Fedele *et al*., 2002, 2005). The involvement of the HMGA proteins also in human pituitary adenomas was further confirmed by the observed overexpression of both *HMGA* genes in these neoplasias (Finelli *et al*., 2002; Pierantoni *et al*., 2005; De Martino *et al*., 2009b; Wang *et al*., 2010). In the case of HMGA2, its overexpression is associated, in most of the PRL tumors, but less frequently in NFPAs, with gain of chromosome 12 (trisomy/tetrasomy), the most frequent cytogenetic alteration in PRL adenomas, and overrepresentation of the *HMGA2* locus (region 12q14-15) or structural rearrangements of chromosome 12 (Fedele *et al*., 2010). Conversely, no rearrangement or amplification of the *HMGA1* locus have been detected in pituitary adenomas, even though HMGA1 overexpression is a constant feature of these tumors (De Martino *et al*., 2009b; Wang *et al*., 2010).

Recent studies have shown that HMGA protein levels are regulated by miRNAs (Lee and Dutta, 2007; De Martino *et al*., 2009a), a class of small (19–25 nucleotides) noncoding RNAs involved in temporal and tissue-specific eukaryotic gene regulation (Lagos-Quintana *et al*., 2002) by binding the 3′-untranslated region (UTR) of target messenger RNAs (mRNAs) and inducing mRNA degradation or inhibition of its translation (Bartel, 2004; Calin and Croce, 2006). Indeed, the loss of HMGA2 3′-UTR, frequently detected in benign tumors of mesenchymal origin, results in the lack of inhibitory control of HMGA2 expression by different miRNAs (Hebert *et al*., 2007; Lee and Dutta, 2007), thereby leading to HMGA2 protein overexpression that accounts for cell transformation.

Therefore, the aim of our work has been to investigate whether HMGA1/2 overexpression occurring in human pituitary adenomas may be also dependent on altered expression of miRNAs that are able to target the *HMGA1/2* genes. The validation of such a hypothesis would account for the overexpression of the HMGA proteins in NFPAs, where modifications at the *HMGA2* locus are rarely observed, and in all the pituitary adenomas where the HMGA1 overexpression is associated neither to rearrangements nor to amplification of the *HMGA1* locus.

Starting from a bioinformatic approach using the miRo' web system (Laganà *et al*., 2009, http://ferrolab.dmi.unict.it/miro/), we identified and validated new miRNAs targeting highly evolutionarily conserved sequences of the 3′-UTR of *HMGA1* and *HMGA2* mRNAs. Then, we found a downregulated expression of these miRNAs, and other previously described *HMGA*-targeting miRNAs, in human pituitary adenomas in comparison with the normal pituitary gland. Finally, functional studies demonstrated that all the analyzed *HMGA*-targeting miRNAs inhibit the proliferation of a rat pituitary adenoma cell line, suggesting a critical role of their downregulation in pituitary tumorigenesis.

Results

Identification of HMGA-*targeting miRNAs*

In order to identify potentially conserved miRNAs being able to downmodulate the expression of both the HMGA proteins, we used the miRo' web system that includes Targetscan, Pictar and Miranda, and provides miRNA phenotype associations in humans (Laganà *et al*., 2009). This analysis identified miR-15ab, miR-16, miR-26ab, miR-196ab and Let-7a as potential *HMGA*-targeting miRNAs. Interestingly, the targeting sites of these *HMGA*-targeting miRNAs on the 3′-UTR of HMGA1 and HMGA2 are extremely conserved in human, mouse and rat. Moreover, it is noteworthy that these five miRNAs were associated by the web system to 57 cellular processes, including those in which HMGA proteins have been previously demonstrated to be involved, such as cell proliferation, differentiation, DNA-repair, chromatin modification and regulation of transcription (Fusco and Fedele, 2007; Fedele and Fusco, 2010). The direct targeting of HMGA1 by miR-16 (Kaddar *et al*., 2009), and of HMGA2 by Let-7a (Lee and Dutta, 2007) and miR196ab (De Martino *et al*., 2009a) was previously reported. Moreover, previous studies showed that miR-26a regulates HMGA2 expression (Lee *et al*., 2011). The targeting sites of miRo'-predicted miRNAs on *HMGA1* and *HMGA2* 3′-UTR are represented in Figure 1. Then, to validate that *HMGA1* and *HMGA2* were targets of the selected microRNAs, MEG-01 cells, which express significant levels of both HMGA1 and HMGA2 proteins, were transfected with miR-15a, miR-16, miR-26a, miR-196a2 and Let-7a synthetic precursors, and HMGA protein levels were evaluated after 72 h by western blotting (Figure 2a). As shown in Figure 2a, HMGA1 and HMGA2 protein levels were significantly reduced in cells transfected with each of the predicted miRNAs, in comparison with the cells transfected with the scrambled oligonucleotide. Interestingly, quantitative real-time (qRT)–PCR (qRT–PCR) experiments (Figure 2b) showed that both HMGA1 and HMGA2 mRNAs were reduced following the transfection of all the analyzed miRNAs (Figure 2b). Interestingly, Let-7a resulted the most efficient miRNA in the downregulation of both *HMGA1* and *HMGA2* mRNAs. Conversely, miR-196a2 and miR-15 showed the lowest

efficiency of downregulation of *HMGA1* and *HMGA2* mRNAs, respectively.

To validate the direct inhibition of HMGA proteins by these miRNAs, we used two pGL-3-CTRL vectors containing the *HMGA1* or *HMGA2* 3′-UTR cloned downstream the firefly luciferase gene. These reporter vectors were transfected in MEG-01 cells along with synthetic precursor of miR-15, miR-16, miR-26a, miR-196a2 and Let-7a, and luciferase activity was assessed 24 h after the transfection. As shown in Figures 2c and d, overexpression of all the predicted *HMGA*-targeting miRNAs significantly reduced luciferase activity, demonstrating that the inhibition of HMGA protein expression by these miRNAs was dependent on their direct binding to the 3′-UTR of *HMGA1* and *HMGA2*. Moreover, as our findings indicate that miR-15 was able to target both *HMGA* mRNAs, we also performed luciferase assays using pGL-3-CTRL vectors containing the *HMGA1* or *HMGA2* 3′-UTR where the miR-15 and miR-16 targeting sites were deleted. Our results show that both *HMGA1* and *HMGA2* 3′-UTR deletion mutants were not affected by miR-15 or miR-16 transfection (Supplementary Figure 1).

Taken together, our data clearly demonstrate that both HMGA proteins are direct targets of miR-15, miR-16, miR-26a, miR-196a2 and Let-7a.

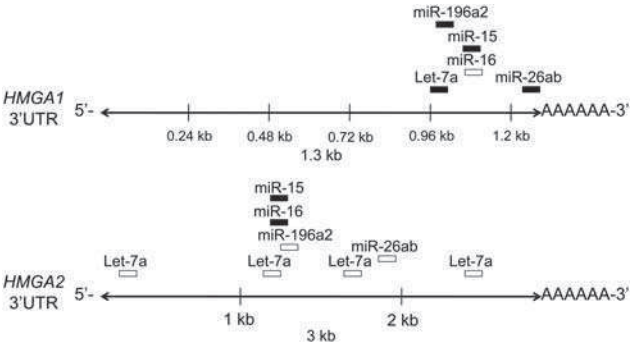

Figure 1 Binding sites of HMGA1/2-targeting miRNAs. Schematic representation of human *HMGA1* and *HMGA2* 3′UTR, and the relative position of the predicted binding sites for *HMGA*-targeting miRNAs, according to Targetscan. White and black bars indicate previously described and novel identified binding sites, respectively.

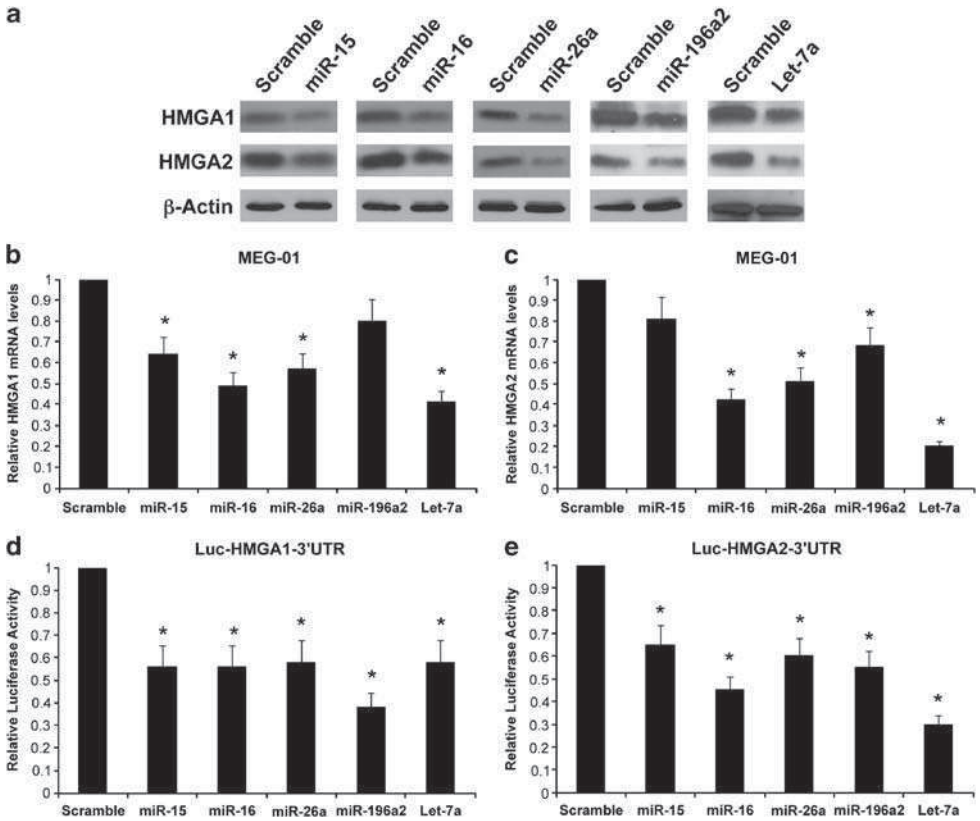

Figure 2 Direct inhibition of *HMGA1* and *HMGA2*s by *HMGA*-targeting miRNAs. (**a**) Western blot using anti-HMGA1 and HMGA2 antibodies on MEG-01 total cellular extracts previously transfected with the indicated synthetic miR precursor or scramble oligonucleotide. β-Actin was used for normalization. (**b**, **c**) qRT–PCR on total mRNA from MEG-01 cells transfected as in (**a**). HMGA1 (**b**) and HMGA2 (**c**) mRNA levels were normalized for endogenous G6PD levels. The mean ± s.d. of three independent experiments is reported. (**d**, **e**) Luciferase assay on MEG-01 cells co-transfected with the indicated Luc-*HMGA1*-3′UTR (**d**) or Luc-*HMGA2*-3′UTR (**e**), and pCMV renilla (**d**, **e**) reporter vectors along with the indicated synthetic miRNA precursors. Relative firefly luciferase activity levels were normalized for Renilla luciferase activity. The mean ± s.d. of three independent experiments performed in triplicate is reported. *$P<0.05$ compared with scramble transfected cells.

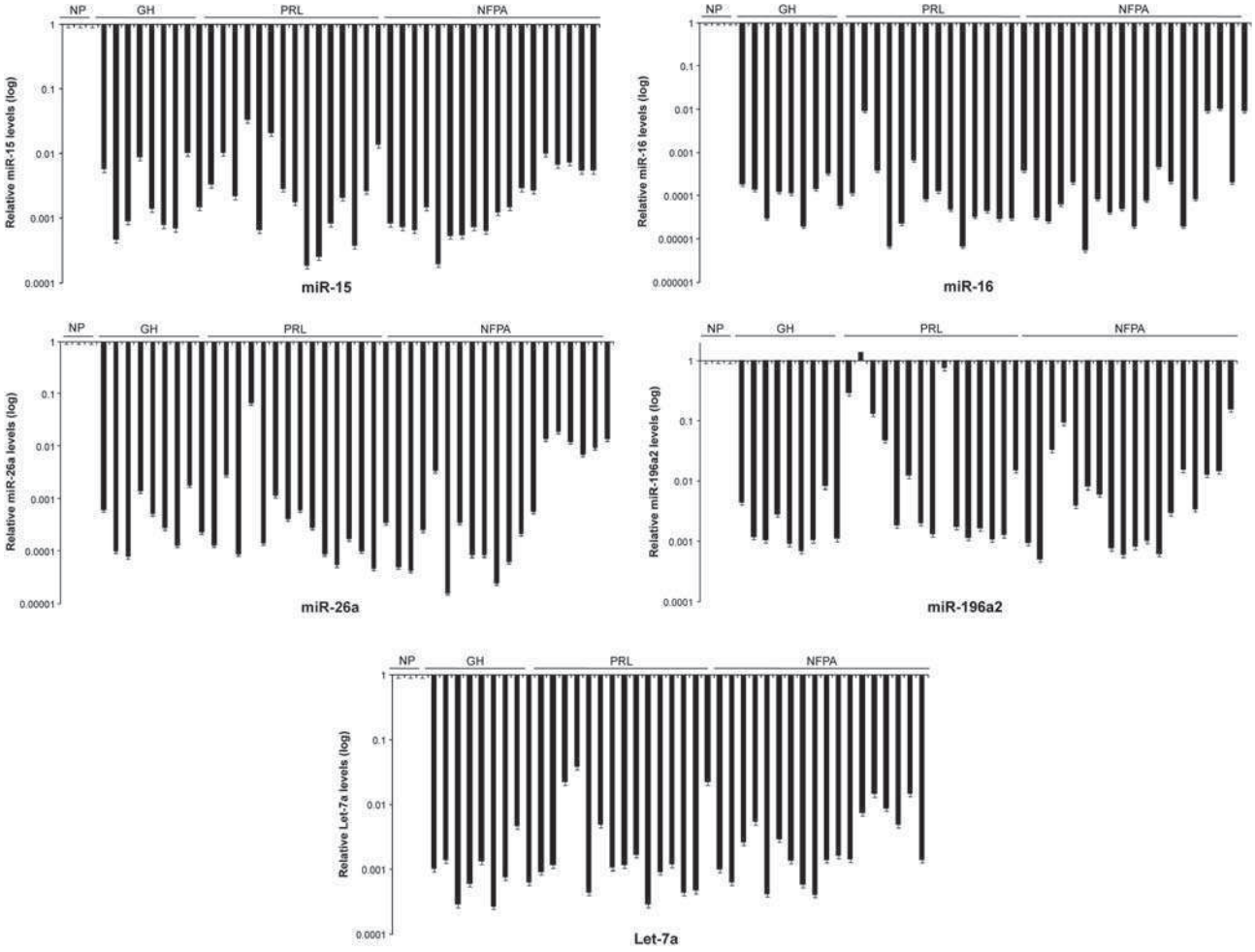

Figure 3 *HMGA*-targeting miRNAs downregulation in human pituitary adenomas. Quantification of *HMGA*-targeting miRNAs from human pituitary adenoma samples. Data reported are expressed in log scale, and mean ± s.d. is reported. RNU6 was used for normalization.

HMGA-*targeting miRNAs are downregulated in human pituitary adenomas*

Cytogenetic alterations accounting for the increased HMGA2 gene dosage have been frequently observed only in prolactinomas (Finelli *et al*., 2002) and in a subset of NFPA (Pierantoni *et al*., 2005), whereas neither rearrangement nor amplification of the *HMGA1* locus has been detected in human pituitary adenomas.

Then, the next step of our work was to analyze the expression of miR-15, miR-16, miR26a, miR-196a2 and Let-7a in a panel of 41 human pituitary adenomas, including 14 prolactinomas, 9 GH pituitary adenomas and 18 NFPA, by qRT–PCR. As shown in Figures 3a-e, all the selected *HMGA*-targeting miRNAs were drastically reduced in almost all the analyzed human pituitary adenomas, regardless of the histotype, when compared with the normal pituitary gland. Consistently, with the downregulation of these *HMGA*-targeting miRNAs that act also at mRNA level, an increase in the *HMGA1* and *HMGA2*-specific mRNAs was observed in all the analyzed pituitary adenomas. In fact, the analysis of the *HMGA1* and *HMGA2* expression in the same samples studied herein for miRNA expression has been already reported in another recent study from our group (De Martino *et al*., 2009b).

This result further suggests that reduced levels of *HMGA*-targeting miRNAs could represent a novel potential mechanism accounting, at least in part, for HMGA upregulation in human pituitary adenomas.

HMGA-*targeting miRNAs negatively regulate pituitary cell proliferation*

To investigate the functional role of *HMGA*-targeting miRNA downregulation in pituitary tumorigenesis, we determined the effects of the overexpression of these miRNAs on the cell growth of a GH/PRL rat pituitary cell line (GH3), which expresses high levels of HMGA1 but not of HMGA2.

The overexpression of *HMGA*-targeting miRNAs was achieved by transfecting different expression vectors (pMIRNA1) containing the precursor sequences of the miRNAs of our interest and the gene encoding the green fluorescent protein (GFP), in order to identify the efficiently transfected cells. As far as the expression

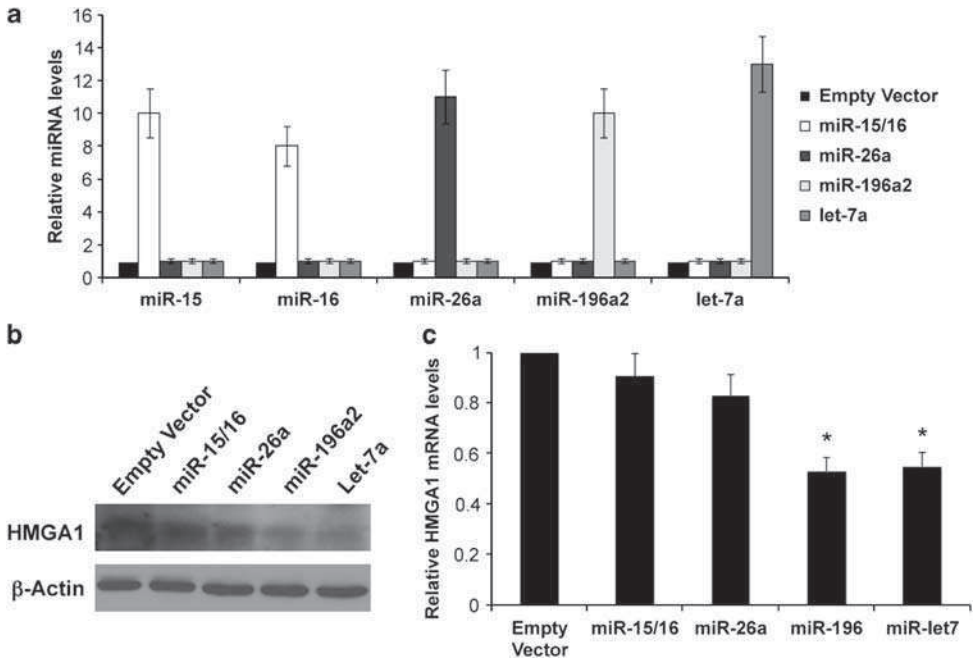

Figure 4 *HMGA*-targeting miRNAs affect HMGA expression in rat pituitary adenoma cells. (**a**) GH3 cells were transfected with the indicated pMIRNA1 miR-expression vectors and relative miRNA levels were analyzed by qRT–PCR. miRNA levels were normalized for endogenous RNU6 levels. The mean ± s.d. is reported. (**b**) Western blot analysis of HMGA1 protein levels in cells transfected as in (**a**). β-Actin was used for normalization. (**c**) qRT–PCR analysis of HMGA1 mRNA levels in cells transfected as in (**a**). mRNA levels were normalized for endogenous G6PD levels. The mean + s.d. of three independent experiments is reported. $*P<0.05$ compared with scramble transfected cells.

vector for miR-15 and miR-16 is concerned, we used a pMIRNA vector, which contains the entire miR-15-16 cluster. The expression levels of the analyzed miRNAs are reported in Figure 4a.

First, GH3 cells were transfected with the indicated miRNA expression vectors or the empty vector, and HMGA1 protein and mRNA levels were assessed by western blot and qRT–PCR. As shown in Figures 4b and c, overexpression of all the *HMGA*-targeting miRNAs reduced both HMGA1 protein and mRNA, compared with the empty vector-transfected cells.

Second, we analyzed the growth and the viability of GH3 cells following the overexpression of *HMGA*-targeting miRNAs. GH3 cells were transiently transfected with the synthetic precursors of miR-15, miR-16, miR-26a, miR-196a2 and Let-7a, and counted each day for 4 days. Figures 5a–d show that the growth rate of GH3 following the transfection of the *HMGA*-targeting miRNAs was lower compared with the cells transfected with the scrambled miRNA. Similar results were also obtained by transfecting synthetic precursors of miR-15, miR-16, miR-26a, miR-196a2 and Let-7a in MEG-01 cells (Supplementary Figure 2A). Moreover, GH3 cells were also transfected during the seeding in 96-wells, and cell viability was measured by XTT proliferation assay 24 and 72 h following the transfection. As shown in Figure 5e, GH3 cells overexpressing *HMGA*-targeting miRNAs displayed, at 72 h, a lower number of viable cells compared with the empty vector-transfected cells. Third, we performed a colony assay co-transfecting the pMIRNA miR-expression vectors or the corresponding empty vector in GH3 cells along with a pBABE-Puro plasmid, containing the puromycin-resistance gene. Cells were cultured in puromycin-containing medium, and 15 days after the transfection the number of GFP-positive colonies was counted. As shown in Figure 5f and Supplementary Figure 3, the transfection of each *HMGA*-targeting miRNA led to a drastic reduction of the number of colonies in comparison with the GH3 cells transfected with the empty vector. The same experiment was also performed co-transfecting the pMIRNA miR-expression vectors or the corresponding empty vector in MEG-01 cells. Interestingly, *HMGA*-targeting miRNAs reduced the colony formation ability also in this cellular context, even though the inhibitory effects were less drastic than those observed on pituitary GH3 cells (Supplementary Figure 2B).

These results indicate that *HMGA*-targeting miRNAs are able to impair cell growth, and that they have a critical role in the control of pituitary cell proliferation.

Discussion

Overexpression of HMGA proteins is a common feature of human pituitary tumors. Indeed, it has been shown that *HMGA2* gene is frequently amplified and overexpressed in human prolactinomas (Finelli *et al*., 2002) and, less often, in NFPAs (Pierantoni *et al*., 2005), and overexpression of the *HMGA1* gene has been constantly found in human pituitary adenomas (De Martino *et al*., 2009b; Fedele *et al*., 2010; Wang *et al*., 2010). Accordingly,

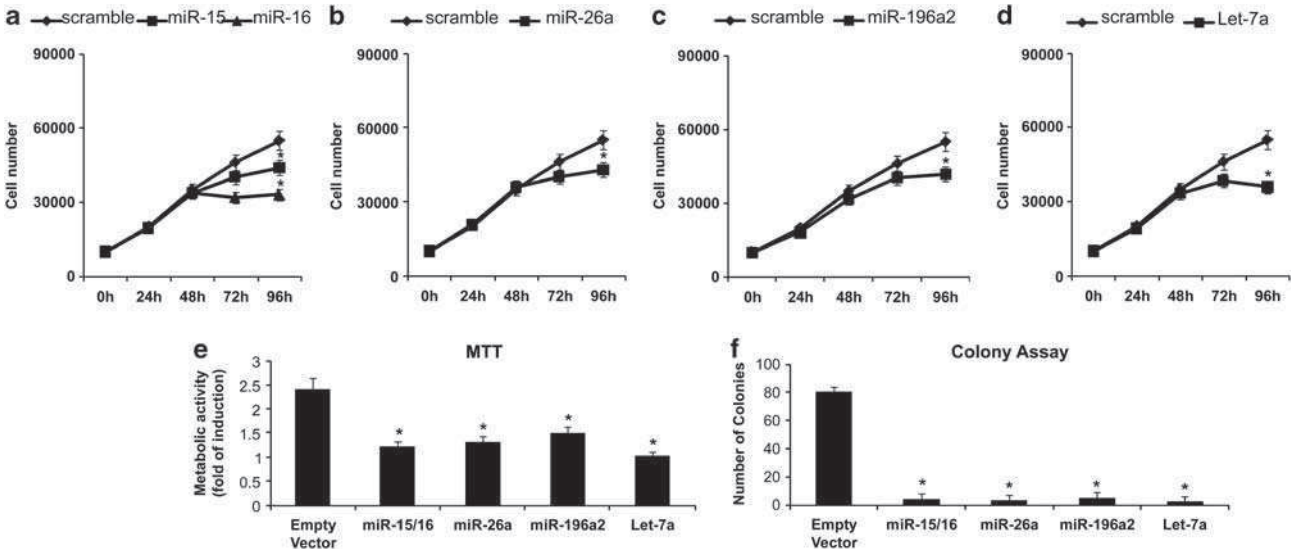

Figure 5 *HMGA*-targeting miRNAs negatively affect rat pituitary adenoma cell growth and viability. (**a**–**d**) GH3 cells were transiently transfected with synthetic miRNA precursor for miR-15 (**a**), miR-16 (**a**), miR-26a (**b**), miR-196a2 (**c**) and let-7a (**d**), and counted at different time points. The mean ± s.d. of three independent experiments is reported. *$P<0.05$ compared with scramble transfected cells. (**e**) MTT assay on GH3 cells transfected as in Figure 4, 72 h after the transfection. Metabolic activity at 24 h was used for normalization. The mean ± s.d. of three independent experiments is reported. *$P<0.05$ compared with empty vector transfected cells. (**f**) GH3 cells were transfected with the indicated pMIRNA miR-expression vectors or the empty vector, along with the pBABE-puro plasmid, and cultured in puromycin-containing medium for 15 days. Fluorescent colonies (> 30 cells) were counted. Data reported are the mean ± s.d. of three independent experiments performed in triplicate. *$P<0.05$ compared with empty vector transfected cells.

transgenic mice ubiquitously overexpressing *Hmga1, Hmga2* or the truncated form of *Hmga2* (*Hmga2/T*) spontaneously develop GH/PRL pituitary adenomas (Fedele *et al*., 2002, 2005), suggesting that both these genes might be considered as specific oncogenes for pituitary cell transformation (Fedele *et al*., 2010).

Several studies have widely explored the potential mechanisms of HMGA-dependent pituitary oncogenesis, and our group has demonstrated the involvement of HMGA proteins in the positive regulation of E2F1 activity (Fedele *et al*., 2006) and *Ccnb2* expression (De Martino *et al*., 2007) resulting in pituitary cell cycle dysregulation and development of pituitary adenomas. However, the so far identified cytogenetic alterations (gene amplifications, chromosome overrepresentation or formation of derivative chromosomes) affecting *HMGA1* and *HMGA2* loci or the chromosomes where *HMGA* genes are located have not been detected in all the human pituitary adenomas even though almost all of them overexpress the HMGA proteins. Therefore, in the present study, we propose that overexpression of HMGA1 and HMGA2 in pituitary tumors might be dependent on the downregulation of *HMGA*-targeting miRNAs. Indeed, by using the miRo' bioinformatic tool for the prediction of miRNA-targeting sites, we identified miR-15, miR-16, miR-26ab, miR-196ab and Let-7a targeting sites on the 3′-UTRs of both *HMGA1* and *HMGA2*.

The direct targeting of *HMGA1* by miR-16 (Kaddar *et al*., 2009), and of *HMGA2* by Let-7a (Lee and Dutta, 2007) and miR-196a2 (De Martino *et al*., 2009a) has been previously described. Moreover, reduced levels of HMGA2 upon miR-26a transfection were also observed (Lee *et al*., 2011). However, our present results clearly indicate that miR-16 is also able to directly target *HMGA2*, and that Let-7a and miR-196a2 target *HMGA1*. Finally, we first demonstrate the direct targeting of both *HMGA* genes by miR-26a and miR-15. It is noteworthy that all these *HMGA*-inhibiting miRNAs are able to affect the stability of the *HMGA1* and *HMGA2*-specific mRNAs.

Based on these findings, we analyzed the expression levels of *HMGA*-targeting miRNAs in a panel of 41 human pituitary adenomas including different histotypes. Our data show that all the analyzed miRNAs resulted strongly downregulated in all the samples analyzed, regardless of the pituitary tumor histotype, and their expression is inversely correlated with that of the *HMGA* genes.

These results are in agreement with previously published data indicating the downregulation of miR-15/16 (Bottoni *et al*., 2005) and of Let-7a (Qian *et al*., 2009) in human pituitary adenomas.

Transfection experiments demonstrated that *HMGA*-targeting miRs are able to reduce HMGA1 levels also in GH3, a rat GH/PRL pituitary cell line, and that all the analyzed *HMGA*-targeting miRNAs significantly reduced cell growth. These results were also confirmed by colony assay experiments showing that GH3 cells transfected with the *HMGA*-targeting miRNAs did not form colonies, unlike the empty vector-transfected cells, but remained in a single-cell state. These data suggest that *HMGA*-targeting miRNAs are able to negatively regulate the pituitary cell cycle progression through the downregulation, at least in part, of HMGA proteins, whose overexpression, as discussed above, results in pituitary cell cycle dysregulation.

These results present potential clinical implication, suggesting a new therapeutic approach for the most aggressive forms of pituitary adenomas based on the downregulation of HMGA proteins through the restoration of *HMGA*-targeting miRNAs. Moreover, as HMGA proteins have been found overexpressed in almost all human malignant neoplasias, where their abundance correlates with a poor prognosis (Fusco and Fedele, 2007), it is likely that downregulation of *HMGA*-targeting miRNAs might be also involved in the pathogenesis of several highly aggressive human malignancies, and, therefore, a miRNA-based abrogation of HMGA expression could represent a novel approach for the therapy of human neoplasias.

Materials and methods

Cell lines and transfections
MEG-01 were cultured in Rosewell Park Memorial Institute medium containing 10% fetal bovine serum supplemented with penicillin and streptomycin. GH3 cells were grown in Dulbecco's Modified Eagle medium containing 10% fetal bovine serum supplemented with penicillin and streptomycin. Cell lines were grown in a humidified atmosphere of 95% air and 5% CO2, at 37 °C. For transfection of miRNA oligonucleotides, cells were transfected with 50 nmol/ml pre-miR miRNA precursors or a control non-targeting scrambled oligonucleotides (Ambion, Austin, TX, USA) using siPORT neoFX Transfection Agent (Ambion). For pMIRNA1 expression vectors, cells were transfected using Lipofectamine 2000 (Invitrogen, Carlsbad, CA, USA), according to the manufacturer's instructions.

Plasmids and constructs
The 3′-UTR region of *HMGA2* gene, including binding sites for miR-15, miR16, miR26ab, miR-196a and let-7a was previously described (De Martino *et al*., 2009a). The 3′-UTR region of the *HMGA1* gene, including binding sites miR-15, miR16, miR26ab, miR-196a and let-7a was amplified by PCR from human genomic DNA by using the following primers:
3′-UTR-HMGA1-F 5′-GGCCTCTAGATTCCTCTGTTC ACAAACTAC-3′
3′-UTR-HMGA1-R 5′-GGCCTCTAGATTCAAGTAACT GCAAATAGG-3′
The amplified fragment was cloned into pGL3-Control Firefly luciferase vector (Promega, Fitchburg, WI, USA) at the XbaI site immediately downstream from the stop codon of luciferase. The Renilla luciferase vector (pRL-CMV) was purchased from Promega. MiRNA Precursor Constructs expressing the miR-15/16 cluster, miR-26a, miR-196a2 and let-7a under the transcriptional control of the CMV promoter and the GFP gene were purchased from SBI System Biosciences (Mountain View, CA, USA). HMGA1 and HMGA2 3′-UTR deletion mutants, where the miR-15/16 targeting sites were deleted, were generated by site-directed mutagenesis using the QuikChange II Site-Directed Mutagenesis Kits (Stratagene, Santa Clara, CA, USA), according to the manufacturer's instructions. Primers used were:
3′-UTR-HMGA1-MutF: 5′-CTTCGACATCCGTCATGC TACCAGCGCCA-3′
3′-UTR-HMGA1-MutR: 5′-TGGCGCTGGTAGCATGA CGGATGTCGAAG-3′
3′-UTR-HMGA2-MutF: 5′-AACGAATTTACAGTCTAGTA CTTATTACATACACAAGCAATGCAAGAAAAAAAC-3′
3′-UTR-HMGA2-MutR: 5′-GTTTTTTTCTTGCATTGCT TGTGTATGTAATAAGTACTAGACTGTAAATTCGTT-3′

Protein extraction, western blotting and antibodies
Cells were lysed in lysis buffer containing 1% NP40, 1 mM EDTA, 50 mM Tris–HCl (pH 7.5) and 150 mM NaCl, supplemented with complete protease inhibitors mixture (Roche, Branford, CT, USA). Total proteins were separated by SDS–polyacrylamide gel electrophoresis and transferred to nitrocellulose membranes (Amersham, Piscataway, NJ, USA). Membranes were blocked with 5% non-fat dry milk and incubated with anti-HMGA1 and anti-HMGA2 polyclonal antibodies, previously described (Pierantoni *et al*., 2001; Fedele *et al*., 2006).

Luciferase target assays
MEG-01 cells were co-transfected in 12-well plates with the modified firefly luciferase vectors described above, along with the Renilla luciferase reporter plasmid and the RNA oligonucleotides. Firefly and Renilla luciferase activities were measured 24 h after transfection with the Dual-Luciferase Reporter Assay System (Promega). Firefly activity was normalized to Renilla activity as the control of transfection efficiency. Data reported are the average + s.d. of three independent experiments performed in triplicate.

Tissue collection and RNA isolation
Pituitary adenomas were obtained from patients operated by E Jouanneau Service de Neurochirurgie U300, GHE Hospices Civils de Lyon. The tumors were selected from the pathological collection of one of us (JT). For each tumor, fragments were fixed in the Bouin–Holland fluid and embbeded in paraffine for pathological diagnosis, including immunocytochemistry. From the results of pituitary hormone immunoreactivity, the tumors were classified according to the WHO classification 2004 into GH-, PRL-, ACTH-, TSH- and gonadotropin-adenomas. Other fragments were immediately frozen and stored at −80 °C (Neurobiotec bank, Lyon, France). We declare that informed consent for the scientific use of biological material was obtained from all patients.

Total RNA isolation from human-pulverized tumors was performed with TRIzol reagent (Invitrogen) according to manufacturer's instructions. Three samples of total RNA from human normal pituitary glands obtained at autopsies were used as controls. The integrity of the RNA was assessed by denaturing agarose gel electrophoresis (virtual presence of sharp 28S and 18S bands).

Reverse transcription and (qRT–)PCR
Reverse trascription and qRT–PCR for mature miRNA was carried out according to manufacturer's instructions of the miScript System Kits (Qiagen, Valencia, CA, USA). Reactions contained miScript Primer Sets (Qiagen), specific for each analyzed miR and U6 (used to normalize RNA levels). qRT–PCR analysis for *HMGA1* and *HMGA2* gene expression was performed as already described (De Martino *et al*., 2009b). To calculate the relative expression levels we used the 2-ΔΔCT method (Livak and Schmittgen, 2001). Each reaction was carried out in triplicate and the average + s.d. was reported. Primers specific for the glucose-6-phosphate dehydrogenase (G6PD) were used for normalization of qRT–PCR data. The following primer sequences were used to amplify the indicated genes:
hsa-HMGA1-F 4′-CAACTCCAGGAAGGAAACCA-3′
hsa-HMGA1-R 5′-AGGACTCCTGCGAGATGC-3′
hsa-HMGA2-F 5′-TCCCTCTAAAGCAGCTCAAAA-3′
hsa-HMGA2-R 5′-ACTTGTTGTGGCCATTTCCT-3′
G6PD-F 5′-CAGCGGCAACTAAACTCAGA-3′
G6PD-R 5′-TTCCCTCAGGATCCCACAC-3′

Growth curves
Exponentially growing GH3 and MEG-01 cells were plated in 6-well plates and transfected with the indicated synthetic mircroRNA precursors. Cell numbers were determined in triplicate at daily intervals with a Burker hemocytometer chamber.

MTT cell proliferation assay
GH3 cells were transfected with 50 nmol/ml pre-miR miRNA precursor or a control non-targeting scrambled oligonucleotide (Ambion) using siPORT neoFX Transfection Agent (Ambion). At each time point, 20 µl of Promega's CellTiter 96 AQueous One Solution was dispensed into each well, and absorbance at 595 nm was measured to evaluate cell viability. Data reported are the average + s.d. of three independent experiments performed in triplicate.

Colony assay
Sub-confluent GH3 and MEG-01 cells were transfected with the above described miR expression vectors along with the pBabe-Puro plasmid, containing the puromycin-resistance gene, and selected by using 1 mg/ml puromycin. After 15 days, cells were stained with 500 mg/ml of crystal violet in 20% methanol, and resulting colonies were counted. The mean + s.d. of three independent experiments performed in triplicate was reported.

Statistical analysis
Student's *t*-test was used to determine the significance for all the quantitative experiments. All error bars represent the s.d. of the average. Statistical significance for all the tests, assessed by calculating the $P<0.05$.

Conflict of interest

The authors declare no conflict of interest.

Acknowledgements

This work was supported by grants from the Associazione Italiana Ricerca sul Cancro (AIRC). DP is recipient of a fellowship from Fondazione Italiana per la Ricerca sul Cancro (FIRC).

References

Ashar HR, Fejzo MS, Tkachenko A, Zhou X, Fletcher JA, Weremowicz S *et al*. (1995). Disruption of the architectural factor HMGI-C: DNA-binding AT hook motifs fused in lipomas to distinct transcriptional regulatory domains. *Cell* **82**: 57–65.

Baldassarre G, Fedele M, Battista S, Vecchione A, Klein-Szanto AJ, Santoro M *et al*. (2001). Onset of natural killer cell lymphomas in transgenic mice carrying a truncated HMGI-C gene by the chronic stimulation of the IL-2 and IL-15 pathway. *Proc Natl Acad Sci USA* **98**: 7970–7975.

Bartel DP. (2004). MicroRNAs: genomics, biogenesis, mechanism, and function. *Cell* **116**: 281–297.

Berlingieri MT, Manfioletti G, Santoro M, Bandiera A, Visconti R, Giancotti V *et al*. (1995). Inhibition of hmgi-c protein synthesis suppresses retrovirally induced neoplastic transformation of rat thyroid cells. *Mol Cell Biol* **15**: 1545–1553.

Berlingieri MT, Pierantoni GM, Giancotti V, Santoro M, Fusco A. (2002). Thyroid cell transformation requires the expression of the HMGA1 proteins. *Oncogene* **21**: 2971–2980.

Bottoni A, Piccin D, Tagliati F, Luchin A, Zatelli MC, degli Uberti EC. (2005). miR-15a and miR-16-1 down-regulation in pituitary adenomas. *J Cell Physiol* **204**: 280–285.

Calin GA, Croce CM. (2006). MicroRNA signatures in human cancers. *Nat Rev Cancer* **6**: 857–866.

Chiappetta G, Avantaggiato V, Visconti R, Fedele M, Battista S, Trapasso F *et al*. (1996). High level expression of the HMGI (Y) gene during embryonic development. *Oncogene* **13**: 2439–2446.

Daly AF, Rixhon M, Adam C, Dempegioti A, Tichomirowa MA, Beckers A. (2006). High prevalence of pituitary adenomas: a cross-sectional study in the province of Liege, Belgium. *J Clin Endocrinol Metab* **91**: 4769–4775.

Daly AF, Tichomirowa MA, Beckers A. (2009). The epidemiology and genetics of pituitary adenomas. *Best Pract Res Clin Endocrinol Metab* **23**: 543–554.

De Martino I, Visone R, Fedele M, Petrocca F, Palmieri D, Martinez Hoyos J *et al*. (2009a). Regulation of microRNA expression by HMGA1 proteins. *Oncogene* **28**: 1432–1442.

De Martino I, Visone R, Palmieri D, Cappabianca P, Chieffi P, Forzati F *et al*. (2007). The Mia/Cd-rap gene expression is downregulated by the high-mobility group A proteins in mouse pituitary adenomas. *Endocr Relat Cancer* **14**: 875–886.

De Martino I, Visone R, Wierinckx A, Palmieri D, Ferraro A, Cappabianca P *et al*. (2009b). HMGA proteins up-regulate CCNB2 gene in mouse and human pituitary adenomas. *Cancer Res* **69**: 1844–1850.

Fedele M, Battista S, Kenyon L, Baldassarre G, Fidanza V, Klein-Szanto AJP *et al*. (2002). Overexpression of the *HMGA2* gene in transgenic mice leads to the onset of pituitary adenomas. *Oncogene* **21**: 3190–3198.

Fedele M, Fusco A. (2010). HMGA and cancer. *Biochim Biophys Acta* **1799**: 48–54.

Fedele M, Palmieri D, Fusco A. (2010). HMGA2: a pituitary tumour subtype-specific oncogene? *Mol Cell Endocrinol* **326**: 19–24.

Fedele M, Pentimalli F, Baldassarre G, Battista S, Klein-Szanto AJP, Kenyon L *et al*. (2005). Transgenic mice overexpressing the wild-type form of the *HMGA1* gene develop mixed growth hormone/prolactin cell pituitary adenomas and natural killer cell lymphomas. *Oncogene* **24**: 3427–3435.

Fedele M, Visone R, De Martino I, Troncone G, Palmieri D, Battista S *et al*. (2006). HMGA2 induces pituitary tumorigenesis by enhancing E2F1 activity. *Cancer Cell* **9**: 459–471.

Fernandez A, Karavitaki N, Wass JA. (2010). Prevalence of pituitary adenomas: a community-based, cross-sectional study in Banbury (Oxfordshire, UK). *Clin Endocrinol (Oxf)* **72**: 377–382.

Finelli P, Pierantoni GM, Giardino D, Losa M, Rodeschini O, Fedele M *et al*. (2002). The high mobility group A2 gene is amplified and overexpressed in human prolactinomas. *Cancer Res* **62**: 2398–2405.

Fusco A, Fedele M. (2007). Roles of HMGA proteins in cancer. *Nat Rev Cancer* **7**: 899–910.

Hebert C, Norris K, Scheper MA, Nikitakis N, Sauk JJ. (2007). High mobility group A2 is a target for miRNA-98 in head and neck squamous cell carcinoma. *Mol Cancer* **6**: 5.

Johnson KR, Lehn DA, Reeves R. (1989). Alternative processing of mRNAs encoding mammalian chromosomal high-mobility-group proteins HMG-I and HMG-Y. *Mol Cell Biol* **5**: 2114–2123.

Kovacs K, Horvath E. (1986). Pathology of growth hormone-producing tumors of the human pituitary. *Semin Diagn Pathol* **3**: 18–33.

Kaddar T, Rouault JP, Chien WW, Chebel A, Gadoux M, Salles G *et al*. (2009). Two new miR-16 targets: caprin-1 and HMGA1, proteins implicated in cell proliferation. *Biol Cell* **101**: 511–524.

Lagos-Quintana M, Rauhut R, Yalcin A, Meyer J, Lendeckel W, Tuschl T. (2002). Identification of tissue-specific microRNAs from mouse. *Curr Biol* **12**: 735–739.

Laganà A, Forte S, Giudice A, Arena MR, Puglisi PL, Giugno R *et al*. (2009). miRò: a miRNA knowledge base. *Database (Oxford)* **2009**: bap008.

Lee S, Jung JW, Park SB, Roh K, Lee SY, Kim JH *et al*. (2011). Histone deacetylase regulates high mobility group A2-targeting microRNAs in human cord blood-derived multipotent stem cell aging. *Cell Mol Life Sci* **68**: 325–336.

Lee YS, Dutta A. (2007). The tumor suppressor microRNA let-7 represses the HMGA2 oncogene. *Genes Dev* **21**: 1025–1030.

Livak KJ, Schmittgen TD. (2001). Analysis of relative gene expression data using real-time quantitative PCR and the 2(-Delta Delta C(T)) Method. *Methods* **25**: 402–408.

Melmed S. (2011). Pathogenesis of pituitary tumors. *Nat Rev Endocrinol* **7**: 257–266.

Monson JP. (2000). The epidemiology of endocrine tumours. *Endocr Relat Cancer* **7**: 29–36.

Pierantoni GM, Fedele M, Pentimalli F, Benvenuto G, Pero R, Viglietto G *et al*. (2001). High mobility group I (Y) proteins bind HIPK2, a serine-threonine kinase protein which inhibits cell growth. *Oncogene* **20**: 6132–6141.

Pierantoni GM, Finelli P, Valtorta E, Giardino D, Rodeschini O, Esposito F *et al*. (2005). High-mobility group A2 gene expression is frequently induced in non-functioning pituitary adenomas (NFPAs), even in the absence of chromosome 12 polysomy. *Endocr Relat Cancer* **12**: 867–874.

Qian ZR, Asa SL, Siomi H, Siomi MC, Yoshimoto K, Yamada S *et al*. (2009). Overexpression of HMGA2 relates to reduction of the let-7 and its relationship to clinicopathological features in pituitary adenomas. *Mod Pathol* **22**: 431–441.

Scala S, Portella G, Fedele M, Chiappetta G, Fusco A. (2000). Adenovirus-mediated suppression of HMG I (Y) protein synthesis as potential therapy of human malignant neoplasias. *Proc Natl Acad Sci USA* **97**: 4256–4261.

Schoenmakers EF, Wanschura S, Mols R, Bullerdiek J, Van den Berghe H, Van de Ven WJ. (1995). Recurrent rearrangements in the high mobility group protein gene, HMGI-C, in benign mesenchymal tumours. *Nat Genet* **10**: 436–444.

Thanos D, Du W, Maniatis T. (1993). The high mobility group protein HMG I (Y) is an essential structural component of a virus-inducible enhancer complex. *Cold Spring Harb Symp Quant Biol* **58**: 73–81.

Thanos D, Maniatis T. (1992). The high mobility group protein HMG I (Y) is required for NF-kappa B-dependent virus induction of the human IFN-beta gene. *Cell* **71**: 777–789.

Wang EL, Qian ZR, Rahman MM, Yoshimoto K, Yamada S, Kudo E *et al*. (2010). Increased expression of HMGA1 correlates with tumour invasiveness and proliferation in human pituitary adenomas. *Histopathology* **56**: 501–509.

Zhou X, Benson KF, Ashar HR, Chada K. (1995). Mutation responsible for the mouse pygmy phenotype in the developmentally regulated factor HMGI-C. *Nature* **376**: 771–774.

Supplementary Information accompanies the paper on the Oncogene website (http://www.nature.com/onc)

Endocrine-Related Cancer (2012) **19** 123–135

PIT1 upregulation by HMGA proteins has a role in pituitary tumorigenesis

Dario Palmieri[1,2], Teresa Valentino[1,2], Ivana De Martino[1], Francesco Esposito[1,2], Paolo Cappabianca[3], Anne Wierinckx[4,5], Michela Vitiello[1,2], Gaetano Lombardi[6], Annamaria Colao[6], Jacqueline Trouillas[4,5], Giovanna Maria Pierantoni[1], Alfredo Fusco[1,2] and Monica Fedele[1,2]

[1]Dipartimento di Biologia e Patologia Cellulare e Molecolare, [2]Istituto di Endocrinologia ed Oncologia Sperimentale (IEOS) del Consiglio Nazionale delle Ricerche and [3]Dipartimento di Scienze Neurologiche, Divisione di Neurochirurgia, Università degli Studi di Napoli 'Federico II', via Pansini 5, 80131 Naples, Italy
[4]INSERM U1028; CNRS UMR5292; Lyon Neuroscience Research Center, Neuro-oncology and Neuro-inflammation Team, Lyon F-69372, France
[5]University Lyon1, F-69000 Lyon, France
[6]Dipartimento di Endocrinologia, Università degli Studi di Napoli 'Federico II', 80131 Naples, Italy

(Correspondence should be addressed to A Fusco; Email: alfusco@unina.it)

Abstract

We have previously demonstrated that HMGA1B and HMGA2 overexpression in mice induces the development of GH and prolactin (PRL) pituitary adenomas mainly by increasing E2F1 transcriptional activity. Interestingly, these adenomas showed very high expression levels of PIT1, a transcriptional factor that regulates the gene expression of *Gh*, *Prl*, *Ghrhr* and *Pit1* itself, playing a key role in pituitary gland development and physiology. Therefore, the aim of our study was to identify the role of *Pit1* overexpression in pituitary tumour development induced by HMGA1B and HMGA2. First, we demonstrated that HMGA1B and HMGA2 directly interact with both PIT1 and its gene promoter *in vivo*, and that these proteins positively regulate *Pit1* promoter activity, also co-operating with PIT1 itself. Subsequently, we showed, by colony-forming assays on two different pituitary adenoma cell lines, GH3 and αT3, that *Pit1* overexpression increases pituitary cell proliferation. Finally, the expression analysis of *HMGA1*, *HMGA2* and *PIT1* in human pituitary adenomas of different histological types revealed a direct correlation between *PIT1* and HMGA expression levels. Taken together, our data indicate a role of *Pit1* upregulation by HMGA proteins in pituitary tumours.

Endocrine-Related Cancer (2012) **19** 123–135

Introduction

Pituitary adenomas are one of the most frequent intracranial tumours with a prevalence of clinically apparent tumours close to one in 1000 of the general population and are the third most common intracranial tumour type after meningiomas and gliomas (Scheithauer *et al*. 2006). They are mostly non-metastatising monoclonal neoplasms arising from adenohypophyseal cells in the anterior pituitary, and exhibit a wide range of hormonal and proliferative activity. The most common types (about 50%) of pituitary adenomas are prolactinomas, while GH- or ACTH-secreting adenomas account for 20 and 10% of pituitary tumours respectively, and TSH-secreting adenomas are rare (1%) (Llyod *et al*. 2004). About one-third of pituitary adenomas are named non-functioning adenomas because they do not exhibit signs of hypersecretion or gonadotrophin adenomas related to FSH–LH immunoreactivity (Trouillas *et al*. 1986). They are usually large tumours diagnosed following local compressive effects on brain structures and cranial nerves.

Pituitary tumorigenesis is generally considered a model of the multi-step process of carcinogenesis, in which molecular genetic alterations represent the initialising event that transforms cells, and hormones and/or growth factors promote cell proliferation (Asa & Ezzat 2002). However, the molecular events leading

DOI: 10.1530/ERC-11-0135

Online version via http://www.endocrinology-journals.org

to pituitary tumour development are still unclear, since somatic mutations identified in other neoplasias, such as the *BRAF* and *RAS* genes, are rare events in pituitary adenomas (Lania *et al*. 2003, De Martino *et al*. 2007*a*). Activating mutations of *Gsα* (the so-called *gsp* mutations) are the most important somatic mutation in pituitary adenomas, being present in up to 40% of GH-secreting adenomas (Lyons *et al*. 1990). Mutations of *MEN1A*, the gene mutated in the MEN-1 syndrome, which includes pituitary adenomas, are uncommon in sporadic tumours (Zhuang *et al*. 1997, Schmidt *et al*. 1999). Similarly, other genes involved in familial pituitary adenomas, such the *AIP* gene, responsible for familial isolated pituitary adenomas, or the *CDKN1B* gene, mutated in the MEN-1-like syndrome MEN-4, have been found to be mutated in about 3% of sporadic GH-secreting adenoma or never in sporadic pituitary adenomas respectively (Occhi *et al*. 2010). However, epigenetic events, such as hypermethylation and/or microRNA-dependent impairment of protein translation, are likely to be responsible for the down-regulation of gene and/or protein expression associated with pituitary tumorigenesis (Amaral *et al*. 2009, Dudley *et al*. 2009, Tateno *et al*. 2010). Moreover, a parental-specific methylation pattern of the *Gsα* gene, responsible for a tissue-specific near-exclusive expression of Gsα from the maternal allele, is relaxed in the majority of GH-secreting pituitary adenomas negative for *gsp* (Hayward *et al*. 2001). Therefore, both genetic and epigenetic alterations appear to be involved in pituitary tumorigenesis. Our recent studies have identified a crucial role for the high-mobility group A (HMGA) proteins in pituitary tumour development (Fedele *et al*. 2002, 2005).

HMGA protein family includes four members, HMGA1A, HMGA1B and HMGA1C, splicing isoforms of the *HMGA1* gene, and HMGA2, encoded by the *HMGA2* gene (Fusco & Fedele 2007). They are small acidic non-histone nuclear factors that bind the minor groove of AT-rich DNA sequences through their amino-terminal region containing three short basic repeats, the so-called AT-hooks (Fusco & Fedele 2007). HMGA proteins do not have transcriptional activity *per se*, but regulate gene expression interacting with other transcription factors and modifying the structure of DNA, in order to modulate the formation of stereo-specific complexes on the promoter/enhancer regions of target genes (Thanos & Maniatis 1992, Falvo *et al*. 1995).

Both *HMGA* genes have a critical role during embryogenesis, when they are widely expressed, whereas their expression is absent or low in normal adult tissues (Zhou *et al*. 1995, Chiappetta *et al*. 1996). Conversely, they are frequently overexpressed in several human cancers including thyroid (Chiappetta *et al*. 1998, 2008), prostate (Tamimi *et al*. 1993, Winkler *et al*. 2007), cervix (Bandiera *et al*. 1998), colorectum (Fedele *et al*. 1996) and pancreas carcinoma (Abe *et al*. 2000, 2003), and several studies indicate that HMGA proteins are causally involved in tumour development (Fusco & Fedele 2007). In fact, overexpression of both *HMGA1* and *HMGA2* results in the transformation of rat1a fibroblast and human lymphoblastoid cells (Wood *et al*. 2000) while inhibition of their expression prevents thyroid transformation induced by mouse transforming retroviruses (Vallone *et al*. 1997) or induces apoptosis in two different thyroid anaplastic carcinoma cell lines (Scala *et al*. 2000).

Several data support a critical role for *HMGA2* (and probably for *HMGA1*) in the generation of human pituitary adenomas (Fedele *et al*. 2010). Indeed, *HMGA2* was found amplified and overexpressed in a large set of human prolactinomas (Finelli *et al*. 2002), and pituitary adenomas secreting prolactin (PRL) and GH developed in transgenic mice overexpressing HMGA1B or HMGA2 (Fedele *et al*. 2002, 2005). Our previous studies demonstrated that HMGA2 induces pituitary tumour development by enhancing E2F1 activity (Fedele *et al*. 2006). Indeed, following the interaction with the retinoblastoma protein pRB, HMGA2 displaces histone deacetylase 1 (HDAC1) from the pRB/E2F1 complex, increasing E2F1 acetylation and transcriptional activity. Consistently, functional loss of E2F1 activity (obtained by mating *Hmga2* transgenic and *E2f1* knockout mice) strongly reduced the incidence of pituitary tumours (Fedele *et al*. 2006). However, *Hmga2* mice still develop pituitary neoplasias also in an *E2f1* knockout background, although with a lower frequency and a less aggressive phenotype, suggesting that other molecular pathways may be involved in pituitary tumour development induced by HMGA overexpression. Recently, using a genechip microarray approach, we have shown that HMGA proteins can contribute to pituitary cell transformation through the transcriptional modulation of target genes, such as *Mia* (*Cd-rap*) (De Martino *et al*. 2007*b*) and *Ccnb2* (De Martino *et al*. 2009).

Our previous findings also showed a very abundant expression of *Pit1* (whose expression was not detectable in adult mouse pituitary) in pituitary adenomas from *Hmga1b* and *Hmga2* transgenic mice (Fedele *et al*. 2002, 2005). PIT1, also named GHF1, is a member of the POU transcription factor family (Delhase *et al*. 1996), and plays a key role in the specification, expansion and survival of three specific pituitary cell types (somatotropes, lactotropes and a subset of thyrotropes) during the development of the

anterior pituitary (Lefevre *et al*. 1987, Nelson *et al*. 1988, Li *et al*. 1990), and its transcriptional activity on many genes, such as *GH*, *PRL*, *TSHB*, *GHRHR* and *PIT1* itself, is crucial for pituitary gland physiology (Lefevre *et al*. 1987, Nelson *et al*. 1988, Chen *et al*. 1990, Li *et al*. 1990, McCormick *et al*. 1990). Moreover, *PIT1* is overexpressed in GH, PRL and TSH pituitary adenomas (Asa *et al*. 1993, Delhase *et al*. 1993, Friend *et al*. 1993, Pellegrini *et al*. 1994, Pellegrini-Bouiller *et al*. 1997).

The aim of the present study was to investigate the role of *Pit1* overexpression in the generation of pituitary adenomas in *Hmga1b* and *Hmga2* transgenic mice.

Here, we demonstrate that both HMGA1B and HMGA2 bind both PIT1 and PIT1-responsive DNA elements, thus positively modulating *Pit1* promoter activity. Functional studies show that *Pit1* overexpression enhances pituitary adenoma cell proliferation. Finally, a correlation was found between *PIT1* and *HMGA* overexpression in human pituitary adenomas, further supporting a role of HMGA-mediated *PIT1* overexpression in pituitary tumours.

Materials and methods

Plasmids, siRNAs, recombinant proteins and antibodies

Expression vector containing the V5-tagged full-length cDNA for *Pit1* sub-cloned in the pcDNA3.1/GS vector was purchased from Invitrogen. HA-tagged HMGA1B and HMGA2 expression plasmids were previously described (Fedele *et al*. 2001, 2006). The *PIT1* promoter construct, carrying the region −1321 to +15, related to the transcriptional start site, of the human *PIT1* gene fused to the luciferase cDNA (PIT-1-Luc), was a generous gift of Dr M Delhase (Brussels, Belgium). The pBABE-puro vector was previously described (Monaco *et al*. 2001). The siRNA anti-HMGA1 was purchased from Santa Cruz Biotechnology (Santa Cruz, CA, USA). GST- and His-HMGA1B and HMGA2 fusion proteins were expressed in *Escherichia coli* strain BL21 (DE3) and purified using glutathione sepharose or nickel beads as described previously (Baldassarre *et al*. 2001, Pierantoni *et al*. 2001). Full-length PIT1 protein, anti-HA (sc-805) and anti-PIT1 supershift antibodies (sc-442X) were purchased from Santa Cruz Biotechnology, whereas anti-V5 (R960-25) antibody was purchased from Invitrogen. Anti-HMGA1 and anti-HMGA2 antibodies were previously described (Fedele *et al*. 2006, Pierantoni *et al*. 2007).

Cell cultures and transfections

Human embryonic kidney (HEK) 293T, rat pituitary adenoma GH3 and mouse pituitary adenoma αT3 cells were cultured in DMEM supplemented with 10% FCS (GIBCO-BRL, Life Technologies). DNA was transfected by the calcium phosphate procedure, as described previously (Graham & Van der Eb 1973), in HEK293T, and by Lipofectamine 2000 (Invitrogen), according to the manufacturer's instructions, in GH3 and αT3 cells.

GST pull-down assay, protein extraction and co-immunoprecipitation

For *in vitro* protein–protein binding, 5 μg PIT1 recombinant protein were incubated with 5 μg resin conjugated to GST, GST-HMGA1B or GST-HMGA2 recombinant proteins. Reactions and analysis of the protein–protein interactions were performed as described previously (Pierantoni *et al*. 2001). A similar procedure was also applied to HEK293T cells transiently transfected with the Pit1-V5 expression vector. Briefly, 500 μg total protein extracts were incubated with 5 μg resin conjugated to GST, GST-HMGA1B or GST-HMGA2 recombinant proteins. The protein–protein complexes formed on the resin were pulled down by centrifugation. The resin was washed five times at 4 °C with 1 ml cold NETN buffer containing 0.1% NP-40, 1 mM EDTA, 50 mM Tris–HCl (pH 7.5), 150 mM NaCl, 20 mM pirophosphate, 0.2 μg aprotinin, 4 mM PMSF, 25 mM sodium fluoride, 10 mM activated sodium orthovanadate (Sigma) and a cocktail of protease inhibitors (Roche Applied Science).

Protein extracts were obtained by lysing cells and tissues in NETN buffer and then processed for co-immunoprecipitation as described previously (Pierantoni *et al*. 2001).

Electrophoretic mobility shift assay

Recombinant proteins (5 ng) were incubated for 15 min at RT in binding buffer (10 mM Tris–HCl, pH 7.5, 50 mM NaCl, 1 mM DTT, 2 μg BSA, 1 μg poly-dCdG) with a ^{32}P-end-labelled double-strand (DS) oligonucleotides (specific activity, 8000–20 000 c.p.m./fmol), corresponding to the PIT1 consensus (sc-2541; Santa Cruz Biotechnology) or to the same element mutated in the PIT1 binding site (sc-2542). Up to 400-fold excess of specific unlabelled competitor oligonucleotide was added as the control. Supershift analysis was carried out by incubating the reaction mix with 1 μg antibody for 30 min in ice. The DNA–protein complexes were resolved on 6%

non-denaturing acrylamide gels and visualised by exposure to autoradiographic films.

Chromatin immunoprecipitation

Chromatin immunoprecipitation (ChIP) was carried out with an acetyl-histone H3 immune precipitation assay kit (Upstate Biotechnology, Lake Placid, NY, USA) according to the manufacturer's instruction, as described previously (De Martino *et al*. 2009). Input and immunoprecipitated chromatin were analysed by PCR for the presence of the *Pit1* promoter sequence. PCR were performed with AmpliTaq gold DNA polymerase (Perkin–Elmer, Monza, Italy). Primers used to amplify the sequence of the *Pit1* promoter were 5′-GCACCAACCTATCATTAC-3′ (forward) and 5′-TGCTACTAACACAATTGC-3′ (reverse). PCR products were resolved on a 2% agarose gel, stained with ethidium bromide, and scanned using a Typhoon 9200 scanner. The intensity of the bands was quantified by densitometric analysis using ImageQuant software (GE Healthcare, Milan, Italy).

Luciferase and colony assays

For the luciferase assay, a total of 2×10^5 cells were seeded into each well of a six-well plate and transiently transfected with 1 μg PIT-1-Luc and with the indicated amounts of HA-HMGA1B and HA-HMGA2, together with 0.5 μg Renilla and various amounts of the backbone vector to keep the total DNA concentration constant. Transfection efficiency, normalised for the Renilla expression, was assayed with the dual luciferase system (Promega Corporation). All transfection experiments were repeated at least three times.

For the colony assay, GH3 and αT3 cells were seeded at a density of 2.5×10^6 per 10 mm dish. Two days after, the cells were transfected with 10 μg pcDNA3.1 or 10 μg pcDNA3.1/Pit1-V5 or 5 μg *Pit1* shRNA (Santa Cruz Biotechnology) or 5 μg scrambled shRNA (Santa Cruz Biotechnology) plus 2 μg pBABE-puro. After about 15 days of positive selection in puromycin, the cells were stained with 500 mg/ml crystal violet in 20% methanol, and the resulting colonies were counted.

Tissue samples

The human pituitary adenoma samples were obtained from 46 surgical excision biopsies, including 13 GH and 33 PRL adenomas) from patients of 'Federico II' University (Naples) and Neurosurgical Department (Pr Jouanneau E) of Hospices Civils de Lyon (France). One part of each pituitary adenoma was saved for routine histopathology evaluation, including immunohistochemistry with the systematic detection of GH, PRL, ACTH, TSH, FSH and LH, and the other one immediately frozen at −80 °C until the extraction of nucleic acids. Informed consent for the scientific use of biological material was obtained from all patients.

RNA extraction and real-time RT-PCR

Total RNA was extracted from tissues using TRI REAGENT (Molecular Research Center, Inc., Cincinnati, OH, USA) solution, according to the manufacturer's instructions. The RNA integrity was verified by denaturing agarose gel electrophoresis (virtual presence of sharp 28S and 18S bands) and spectrophotometry. One microgram of total RNA of each sample was reverse-transcribed with the QuantiTect Reverse Transcription (Qiagen) using an optimised blend of oligo-dT and random primers according to the manufacturer's instructions. To ensure that RNA samples were not contaminated with DNA, negative controls were obtained by performing the PCR on samples that were not reversed-transcribed but identically processed. Quantitative PCR was performed with the SYBR Green PCR Master Mix (Applied Biosystems, Foster City, CA, USA) as follows: 95 °C for 10 min and 40 cycles (95 °C for 15 s and 60 °C for 1 min). A dissociation curve was run after each PCR in order to verify amplification specificity. Each reaction was performed in duplicate. To calculate the relative expression levels, we used the $2^{-\Delta\Delta C_t}$ method (Livak & Schmittgen 2001).

Primer sequences are available upon request.

Statistical analyses

For the comparison between two groups of experiments, Student's *t*-test was used. Three or more groups of experiments were compared using the one-way ANOVA followed by Tukey's multiple comparison test. All results are expressed as mean ± S.D. The statistical significant difference was considered when P value was <0.05. Linear regression analysis was performed to determine the association of *PIT1* with *HMGA1* or *HMGA2* expression levels in human pituitary adenomas. The square of correlation coefficient (R^2) close to 1 was considered to be indicative of a significant direct correlation.

Results

HMGA proteins interact with PIT1

To investigate the role of HMGA proteins in the modulation of PIT1 function, we first hypothesised that HMGA proteins directly bind PIT1 protein. The finding

that other members of the POU transcription factor family, such as Oct-6 and Oct-2A, interact with HMGA proteins through their POU domain supports this hypothesis (Abdulkadir *et al*. 1995, Leger *et al*. 1995, Zwilling *et al*. 1995). Therefore, we performed a GST pull-down assay incubating the PIT1 recombinant protein with GST-HMGA1B or GST-HMGA2 fusion proteins. As shown in Fig. 1A, PIT1 was able to directly interact with both GST-HMGA1b and GST-HMGA2, but not with GST alone. To confirm this interaction in a cellular context, we transfected HEK293T cells with expression vectors containing the full-length cDNAs for PIT1, HMGA1b or HMGA2, fused to the V5 (Pit-1-V5) and HA (HA-HMGA1b and HA-HMGA2) tags respectively. Total cell extracts were immunoprecipitated with anti-V5 antibody and analysed by immunoblot with anti-HA antibody. As shown in Fig. 1B (left panels), HA-HMGA1b and HA-HMGA2 were immunoprecipitated by the anti-V5 antibody only when transfected along with Pit-1-V5. This result was confirmed by reverse co-immunoprecipitation carried out by immunoprecipitating with anti-HA antibody and analysing with anti-V5 antibody (Fig. 1B, right panels). The negative result obtained by blotting for the unrelated and endogenous E2F1 protein confirmed the specificity of the PIT1/HMGA interactions. Ethidium bromide was added to the immunoprecipitation reaction to prevent DNA-mediated interaction between proteins. Interestingly, cells co-transfected with PIT1 and each of the HMGA proteins show more abundant levels of HMGA proteins than those transfected with HMGA1b or HMGA2 alone (input in Fig. 1B, middle panels), suggesting that PIT1 can positively influence their expression. Western blot anti-V5 or anti-HA antibody, for samples immunoprecipitated with anti-V5 or anti-HA antibody respectively was performed to control the successful immunoprecipitation reactions (Fig. 1B).

Finally, to validate the HMGA/PIT1 interaction in the context of the pituitary tumours, we pulled down pituitary adenoma extracts from *Hmga1b* or *Hmga2* transgenic mice, where PIT1 is abundantly expressed (Fedele *et al*. 2002, 2005), from GST-HMGA1B or GST-HMGA2 beads. Figure 1C shows that both GST-HMGA1B and GST-HMGA2, but not GST, interacted with endogenous PIT1 protein in transgenic mouse tumours. These data demonstrate that HMGA proteins are direct molecular partners of PIT1 both *in vitro* and *in vivo*.

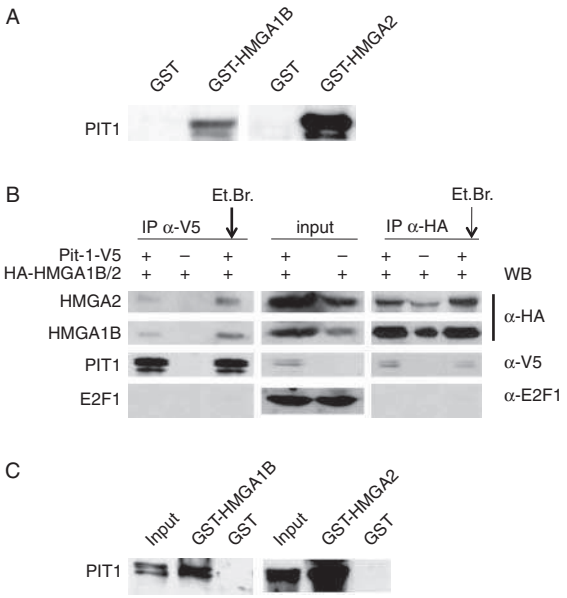

Figure 1 *In vitro* and *in vivo* interaction between PIT1 and HMGA proteins. (A) Recombinant PIT1 protein was incubated with immobilised GST-HMGA1B, GST-HMGA2 or GST alone in a GST pull-down assay. (B) HEK293T cells were transiently transfected with the Pit-1-V5, HA-HMGA1B and HA-HMGA2 expression plasmids where indicated. Protein extracts were immunoprecipitated (IP) with the anti-V5 or anti-HA, and probed with either anti-HA, anti-V5 or anti-E2F1 antibodies, as indicated on the right. Proteins detected are indicated on the left. Ethidium bromide was added to the IP reaction to make sure that the interaction was not mediated by any contaminating DNA. Western blot anti-V5 (lower panel) was done as a positive control of the IP reaction. Fifty micrograms of total cell extracts before IP were loaded as the control (input). (C) Protein extracts from pituitary adenoma tissues developed by *Hmga1b* (blot on the left) and *Hmga2* transgenic mice (blot on the right) were incubated with immobilised GST-HMGA1B, GST-HMGA2 or GST alone in a GST pull-down assay, and then probed with anti-PIT1 antibody.

HMGA proteins bind to and activate the *Pit1* promoter

PIT1 is able to directly regulate the expression of several genes with a key role in pituitary gland physiology such as *PRL*, *GH*, *GHRHR* and *PIT1* itself (Lefevre *et al*. 1987, Nelson *et al*. 1988, Chen *et al*. 1990, Li *et al*. 1990, McCormick *et al*. 1990). Since HMGA proteins physically interact with PIT1, we investigated whether this interaction may affect PIT1 activity. HMGA1B or HMGA2 recombinant proteins were incubated with a ^{32}P-end-labelled DS oligonucleotide corresponding to the consensus site recognised by PIT1 in an electrophoretic mobility shift assay (EMSA). As shown in Fig. 2A, both HMGA1B and HMGA2 were able to bind the PIT1 responsive element (Pit-1-RE) *in vitro*. The specificity of the binding was assessed using a 100- and 400-fold molar excess of the specific unlabelled DS oligonucleotide or a 100-fold molar excess of the same unlabelled, but single-strand (SS) oligonucleotide as specific and non-specific competitors respectively. Moreover, the

binding was also abolished pre-incubating the reaction mix with anti-HMGA1 and anti-HMGA2 antibodies, which, as reported previously (Martinez Hoyos *et al.* 2009), specifically displace HMGA proteins from their target DNA (data not shown). As shown in Fig. 2B, the binding of HMGA proteins to the Pit-1-RE does not interfere with the binding of PIT1 to the same oligonucleotide. Moreover, as shown by the absence of a slower migrating spot when both HMGA and PIT1 proteins are incubated with the probe, it appears that they do not form a unique complex, but independently bind the same DNA response element. We also used, as a control of specificity of the PIT1 binding, an oligonucleotide mutated in a key residue within the PIT1 consensus site, which was incapable of binding PIT1 (Fig. 2C, lane 1). Interestingly, this mutant oligonucleotide still binds HMGA1B with the same efficiency of the wild-type Pit-1-RE, whereas the binding to HMGA2 was highly compromised (Fig. 2C, lanes 2 and 3). Therefore, it is likely that HMGA1B and HMGA2 do not bind exactly to the same residues nearby the PIT1 consensus site.

Next, since one of the PIT1 targets is *Pit1* gene itself, we focused on the potential role of HMGA in PIT1-dependent *Pit1* gene regulation in pituitary adenomas. For this purpose, we first performed a ChIP assay in pituitary adenomas from *Hmga1b* or *Hmga2* transgenic mice. Chromatin was immunoprecipitated using specific anti-HMGA1 or anti-HMGA2 antibody, or IgG as the negative control, and analysed by PCR using primers specific for the mouse *Pit1* promoter. Figure 3A shows the *in vivo* binding of both *Hmga1* and *Hmga2* to the *Pit1* promoter, while no amplification was obtained in the negative control. Then, we investigated the functional effect of the physical interaction between HMGA proteins and PIT1 on the *PIT1* promoter activity by luciferase assays. HEK293T cells were transiently transfected with a reporter vector (PIT1-1-Luc), containing the luciferase gene under the control of the *PIT1* promoter, along with vectors coding for HA-HMGA1B, HA-HMGA2 or Pit-1-V5 proteins. As shown in Fig. 3B, only HA-HMGA2, but not HA-HMGA1B, was able to positively regulate the activity of the *PIT1* promoter. Moreover, a strong and significant cooperation between HMGA2 and PIT1 was observed ($P<0.001$), while HMGA1 only slightly but significantly increased the positive transcriptional effect of PIT1 on its promoter ($P<0.05$). To confirm these data in a pituitary context, we transiently transfected GH3 cells, derived from a rat pituitary PRL- and GH-secreting adenoma expressing high levels of endogenous PIT1 (Fig. 3D), with HMGA1B or HMGA2 expression vectors, along with the Pit-1-Luc

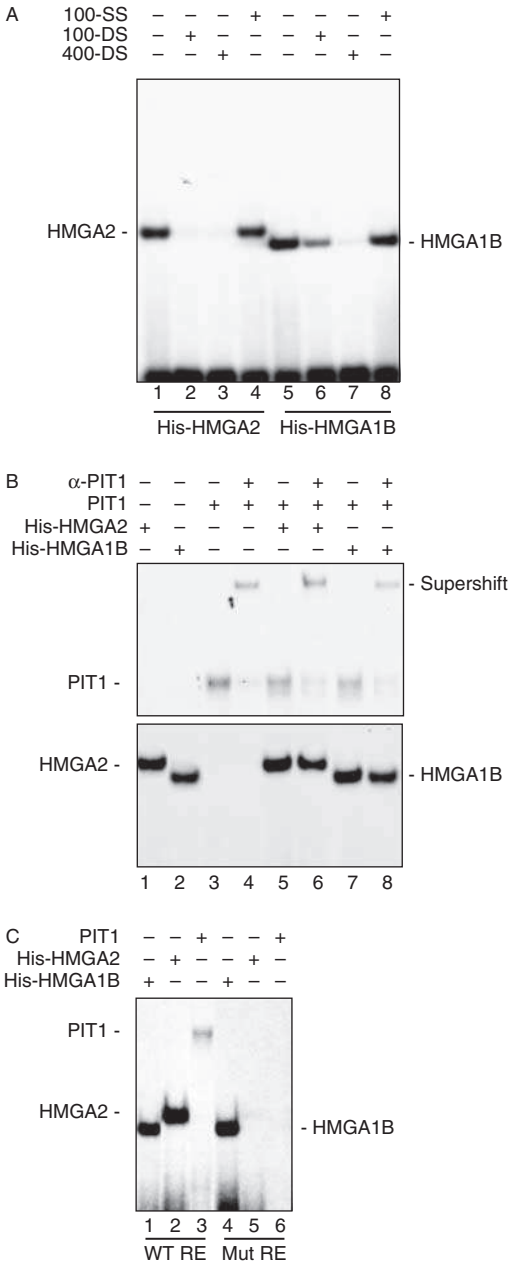

Figure 2 *In vitro* binding of HMGA proteins to the PIT1 consensus site. (A) Electrophoretic mobility shift assay (EMSA) performed with the radiolabelled PIT1 consensus site incubated with recombinant His-HMGA1B and His-HMGA2 as indicated. To assess the specificity of the binding, a 100- and 400-fold excess of unlabelled double-strand (DS) oligonucleotide was added as a specific competitor, and a 100-fold excess of unlabelled single-strand (SS) oligonucleotide was added as a non-specific competitor. (B) EMSA performed with the same oligonucleotide as in (A), incubated with recombinant PIT1, His-HMGA1B and His-HMGA2 as indicated. Supershift assay was performed with anti-PIT1 antibody where indicated. Two different autoradiographic exposure times were needed to allow a good view of both the binding of HMGA proteins and that of PIT1: upper panel, 18 h; lower panel, 1 h. (C) The same EMSA as in (B), but with an oligonucleotide mutated in the PIT1 consensus site.

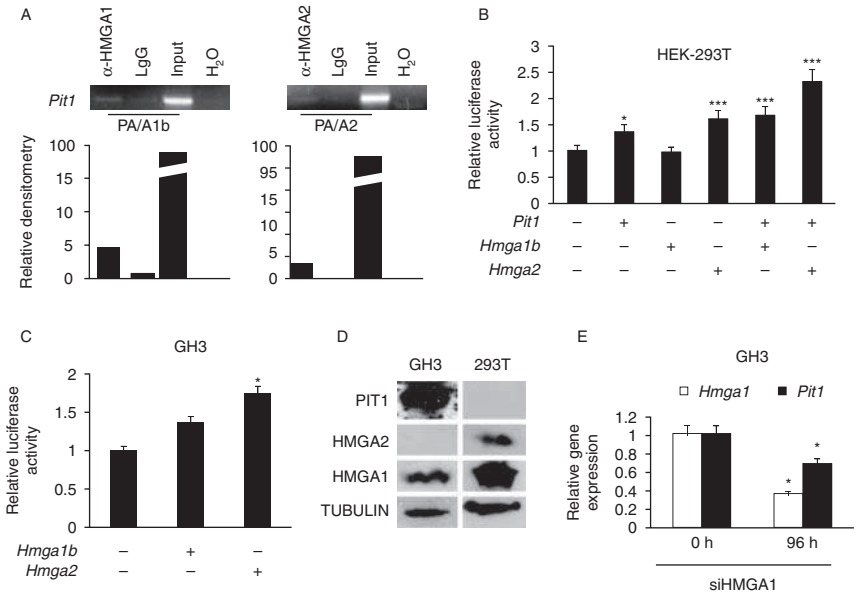

Figure 3 *In vivo* binding and activation by HMGA of the *PIT1* promoter. (A) Chromatin immunoprecipitation (ChIP) assay performed on pituitary adenomas from *Hmga1b* and *Hmga2* transgenic mice to detect the endogenous *in vivo* binding of HMGA proteins to the *Pit1* promoter gene, as indicated. As an immunoprecipitation control, IgG was used. *Input*, PCR products with genomic DNA without immunoprecipitation. All the PCR products were quantified with ImageQuant software and reported in the histograms below each band. (B and C) Luciferase activity (fold of activation vs promoter basic activity) of the *PIT1* promoter in HEK293T (B) and GH3 (C) cells. Where indicated, *PIT1* and/or either *Hmga1b* or *Hmga2*, or both, expression vectors were co-transfected with the PIT1-1-Luc plasmid. Data express mean ± S.D. of three independent experiments. Asterisks indicate the statistical results of a multiple comparison test vs promoter basic activity. $*P<0.05$; $***P<0.001$. (D) Western blot analysis to detect HMGA1, HMGA2 and PIT1 expression in GH3 and HEK293T cells. (E) qRT-PCR analysis of *Pit1* and *Hmga1* expression in GH3 cells interfered for HMGA1 with 100 nM of siHMGA1 for 96 h. The reported data (mean ± S.D. of three independent experiments) are normalised with respect to scrambled siRNA-treated cells. $*P<0.05$.

vector. As shown in Fig. 3C, HA-HMGA2 expression led to a significant increase in *Pit1* promoter activity, while only a slight but not significant increase was observed after the transfection of the HA-HMGA1B construct. These data clearly demonstrate that HMGA2 is able to positively regulate *PIT1* promoter activity in co-operation with PIT1, whereas they suggest that HMGA1 shows only a very weak effect on the regulation of *PIT1* gene expression. The abundant expression of HMGA1 in GH3 cells, in contrast to the total absence of HMGA2 expression (Fig. 3D), could probably account for the lack of a significant effect of HMGA1 transfection on *PIT1* promoter activity. To further evaluate the role of endogenous HMGA1 on *Pit1* expression in pituitary cells, *Pit1* expression was analysed in GH3 cells interfered for HMGA1, through an anti-HMGA1 siRNA, in comparison with GH3 cells treated with a scrambled siRNA. As shown in Fig. 3E, *Pit1* mRNA levels were significantly decreased in cells knocked down for HMGA1 compared with their scrambled-treated controls. Therefore, both HMGA1 and HMGA2 play a crucial role in the regulation of *Pit1* expression in GH3 cells.

Overexpression of *Pit1* increases the proliferation rate of pituitary adenoma cells

To evaluate the role of *Pit1* overexpression in cell proliferation in a pituitary context, we performed a colony-forming assay in GH3 cells. As shown in Fig. 4A, the number of colonies obtained, after puromycin selection, by transfection of a Pit1 expression vector, was significantly higher (a fourfold increase) compared with that obtained by transfecting the empty vector. Consistently, the knock-down of the endogenous PIT1 in GH3 cells caused a significant decrease in their growth in a colony-forming assay (data not shown). Similar results were obtained using a different pituitary cell type, such as the mouse gonadotroph cell line αT3. Indeed, as shown in Fig. 4B, *Pit1* overexpression caused a twofold increase in the number of colonies with respect to the backbone vector. Since αT3 cells do not express *Pit1* normally, we asked whether the exogenous expression of *Pit1* upregulates the classical PIT1 targets, such as *Gh* and *Ghrhr*. To answer this question, we performed RT-PCR analysis in αT3 cell clones stably expressing *Pit1*, with the result that *Gh* was not expressed in these

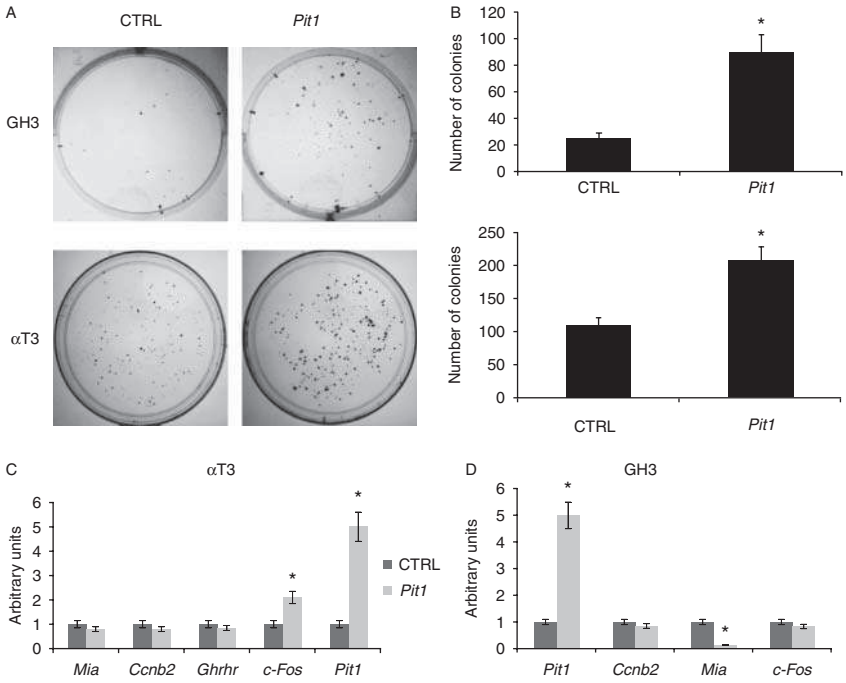

Figure 4 Effect of *Pit1* expression on pituitary adenoma cell proliferation. (A) Representative colony-forming assay performed on GH3 and αT3 cells transfected with a vector expressing *PIT1*. As a negative control, the empty vector (CTRL) was used. (B) The results of three colony-forming assays performed as in (A) were expressed as mean ± S.D. (C and D) qRT-PCR analysis of gene expression changes upon transfection of *Pit1* in αT3 (C) and GH3 (D) cells. The resulting mean ± S.D. of three independent experiments are reported. The genes analysed are indicated below the *x*-axis. *$P<0.05$.

cells (data not shown), and *Ghrhr* expression did not change significantly between parental and *Pit1*-transfected cells (Fig. 4C). Similarly, the expression of *Pit1* in these cell clones does not lead to a different expression, compared with the parental cells, of genes, such as *Ccnb2* and *Mia* (*Cd-rap*) (Fig. 4C), that are directly regulated by HMGA proteins in pituitary adenomas (De Martino *et al*. 2007*a*,*b*, 2009). Conversely, as reported for other cell systems (Gaiddon *et al*. 1999), the expression of *Pit1* in αT3 cells, but not in GH3 cells, leads to the upregulation of *c-Fos* (Fig. 4C and D). Surprisingly, overexpression of *Pit1* in GH3 cells inhibits the expression of *Mia* (*Cd-rap*) (Fig. 4D). These findings indicate that *Pit1* overexpression positively regulates pituitary cell proliferation through different mechanisms depending on the specific pituitary cellular context.

Positive correlation between *HMGA* and *PIT1* expression in human pituitary adenomas

Overexpression of *PIT1* is a common feature of GH-, PRL- and TSH-, but not of ACTH-, FSH-, LH- or non-functioning human pituitary adenomas (Pellegrini-Bouiller *et al*. 1997). Moreover, we have previously demonstrated that *HMGA1* and *HMGA2* expression levels are significantly increased in human pituitary adenomas compared with normal gland (De Martino *et al*. 2009). To evaluate whether there is a direct correlation between *HMGA1/2* and *PIT1* mRNA levels, we analysed a panel of 46 human pituitary adenomas (including 13 GH and 33 PRL adenomas) for the expression of *PIT1*, *HMGA1* and *HMGA2* mRNAs by quantitative RT-PCR. As shown in Fig. 5, a direct correlation between *PIT1* and *HMGA1* or *HMGA2* mRNA levels was observed. In fact, the correlation coefficients for the fold changes between adenomas and normal gland, calculated in both *PIT1* and *HMGA1*, as well as *PIT1* and *HMGA2* expression levels, were $R^2=0.82$ ($P<0.001$) and $R^2=0.61$ ($P<0.001$) respectively.

Discussion

Various studies support a critical role of HMGA proteins in the development of human pituitary adenomas (Finelli *et al*. 2002, De Martino *et al*. 2009, Qian *et al*. 2009, Wang *et al*. 2010). However, the mechanism by which they act in pituitary tumour development is still not completely known. We have previously demonstrated, using mouse models over-expressing HMGA2 and knockout for E2F1, that

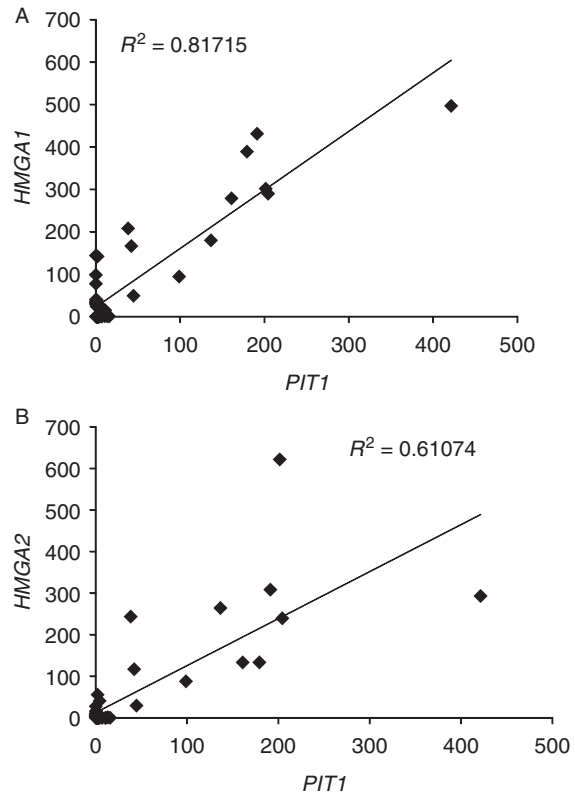

Figure 5 qRT-PCR analysis of *PIT1* mRNA in correlation with *HMGA1* and *HMGA2* expression in human pituitary adenomas. (A and B) Statistical analysis of the correlation between *PIT1* and *HMGA1* (A) or *HMGA2* (B) relative expression, as analysed by qRT-PCR, in pituitary adenomas vs normal gland. R^2, correlation coefficient.

induction of pituitary adenomas in *Hmga2* transgenic mice is mainly due to E2F1 activation (Fedele *et al.* 2006). Nevertheless, alternative pathways that may co-operate in the achievement of the full pituitary phenotype have been envisaged because of the incomplete rescue of the pituitary tumour phenotype in double *HMGA2/E2F1* mutants (Fedele *et al.* 2006). Analysing the gene expression profile of pituitary adenomas from *Hmga2* transgenic mice in comparison with normal pituitary glands from control mice (De Martino *et al.* 2007*b*), we identified *Mia* (*Cd-rap*) and *Ccnb2* genes as directly downregulated or upregulated respectively by both HMGA1 and HMGA2 proteins, and able to affect pituitary cell proliferation (De Martino *et al.* 2007*b*, 2009).

Here we report another mechanism, based on *Pit1* induction, by which HMGA overexpression may induce the development of pituitary adenomas. Indeed, we previously demonstrated that *Pit1* is expressed at high levels in pituitary adenomas developed by *Hmga* transgenic mice (Fedele *et al.* 2002, 2005), and here we show that HMGA proteins bind both PIT1 and PIT1-responsive DNA elements, thus positively modulating the PIT1 promoter activity, also synergistically co-operating with *Pit1*. Moreover, we demonstrated that *Pit1* overexpression drastically enhances (up to fourfold) pituitary cell proliferation by inducing the expression of *c-Fos* in gonadotroph cells or by inhibiting the expression of *Mia* (*Cd-rap*) in GH/PRL-secreting cells. Therefore, these results indicate a potential causal role of the aberrant *Pit1* expression in the cell biology of pituitary tumour.

We can envisage two different, but not mutually excluding, mechanisms by which HMGA-mediated *Pit1* upregulation may contribute to pituitary cell transformation:

a) HMGA overexpression may upregulate *Pit1* levels in pituitary adenoma cells of the *Pit1* lineage, enhancing their proliferation.
b) The enhancement of *Pit1* expression by HMGA during development might lead to abnormal growth of the embryonic cells secreting GH and PRL, which results in pituitary adenoma during adult life.

Interestingly, high expression levels of *PIT1* represent a constant feature of human pituitary GH, PRL and TSH adenomas (Asa *et al.* 1993, Delhase *et al.* 1993, Friend *et al.* 1993, Pellegrini *et al.* 1994, Pellegrini-Bouiller *et al.* 1997), and several previous studies suggested a potential role for *PIT1* in cell proliferation, the prevention of apoptotic death and the pathogenesis of pituitary tumours (Castrillo *et al.* 1991, Gaiddon *et al.* 1999, Salvatori *et al.* 2002, Pellegrini *et al.* 2006). In fact, microinjection of *Pit1* antisense sequences blocks cell growth in the GC somatotroph cell line (Castrillo *et al.* 1991) and dominant-negative mutants of *Pit1* reduce cell viability by decreasing the growth rate and inducing apoptosis via a caspase-independent pathway (Pellegrini *et al.* 2006). Moreover, PIT1 can also upregulate the expression of genes, such as *c-Fos* (Gaiddon *et al.* 1999) and *Ghrhr* (Salvatori *et al.* 2002), involved in cell proliferation. Interestingly, recent studies have identified an increased expression of PIT1 also in breast tumours (Ben-Batalla *et al.* 2010), suggesting a potential role of PIT1 in the proliferation of different cell types.

In conclusion, our data demonstrate that the high expression of *Pit1* in the pituitary adenomas of *Hmga* transgenic mice is induced by a positive regulation by HMGA proteins of *Pit1* transcription and support a role for *Pit1* overexpression in pituitary tumour.

Declaration of interest

The authors declare that there is no conflict of interest that could be perceived as prejudicing the impartiality of the research reported.

Funding

This work was supported by grants from Associazione Italiana Ricerca sul Cancro (AIRC), CNR (DG.RSTL. 030.001) and MIUR (PRIN 2008). D Palmieri and F Esposito are recipients of fellowships from Fondazione Italiana Ricerca sul Cancro (FIRC).

Acknowledgements

We thank Mireille Delhase for providing us the Pit-1 promoter plasmids, Angelo Ferraro for performing real-time PCR on human tissues and Luigi Di Guida for animal care.

References

Abdulkadir SA, Krishna S, Thanos D, Maniatis T, Strominger JL & Ono SJ 1995 Functional roles of the transcription factor Oct-2A and the high mobility group protein I/Y in HLA-DRA gene expression. *Journal of Experimental Medicine* **182** 487–500. (doi:10.1084/jem.182.2.487)

Abe N, Watanabe T, Masaki T, Mori T, Sugiyama M, Uchimura H, Fujioka Y, Chiappetta G, Fusco A & Atomi Y 2000 Pancreatic duct cell carcinomas express high levels of high mobility group I(Y) proteins. *Cancer Research* **60** 3117–3122.

Abe N, Watanabe T, Suzuki Y, Matsumoto N, Masaki T, Mori T, Sugiyama M, Chiappetta G, Fusco A & Atomi Y 2003 An increased high-mobility group A2 expression level is associated with malignant phenotype in pancreatic exocrine tissue. *British Journal of Cancer* **89** 2104–2109. (doi:10.1038/sj.bjc.6601391)

Amaral FC, Torres N, Saggioro F, Neder L, Machado HR, Silva WA Jr, Moreira AC & Castro M 2009 MicroRNAs differentially expressed in ACTH-secreting pituitary tumors. *Journal of Clinical Endocrinology and Metabolism* **94** 320–323. (doi:10.1210/jc.2008-1451)

Asa SL & Ezzat S 2002 The pathogenesis of pituitary tumours. *Nature Reviews. Cancer* **2** 836–849. (doi:10.1038/nrc926)

Asa SL, Puy LA, Lew AM, Sundmark VC & Elsholtz HP 1993 Cell type-specific expression of the pituitary transcription activator pit-1 in the human pituitary and pituitary adenomas. *Journal of Clinical Endocrinology and Metabolism* **77** 1275–1280. (doi:10.1210/jc.77.5.1275)

Baldassarre G, Fedele M, Battista S, Vecchione A, Klein-Szanto AJ, Santoro M, Waldmann TA, Azimi N, Croce CM & Fusco A 2001 Onset of natural killer cell lymphomas in transgenic mice carrying a truncated HMGI-C gene by the chronic stimulation of the IL-2 and IL-15 pathway. *PNAS* **98** 7970–7975. (doi:10.1073/pnas.141224998)

Bandiera A, Bonifacio D, Manfioletti G, Mantovani F, Rustighi A, Zanconati F, Fusco A, Di Bonito L & Giancotti V 1998 Expression of HMGI(Y) proteins in squamous intraepithelial and invasive lesions of the uterine cervix. *Cancer Research* **58** 426–431.

Ben-Batalla I, Seoane S, Garcia-Caballero T, Gallego R, Macia M, Gonzalez LO, Vizoso F & Perez-Fernandez R 2010 Deregulation of the Pit-1 transcription factor in human breast cancer cells promotes tumor growth and metastasis. *Journal of Clinical Investigation* **120** 4289–4302. (doi:10.1172/JCI42015)

Castrillo JL, Theill LE & Karin M 1991 Function of the homeodomain protein GHF1 in pituitary cell proliferation. *Science* **253** 197–199. (doi:10.1126/science.1677216)

Chen RP, Ingraham HA, Treacy MN, Albert VR, Wilson L & Rosenfeld MG 1990 Autoregulation of pit-1 gene expression mediated by two cis-active promoter elements. *Nature* **346** 583–586. (doi:10.1038/346583a0)

Chiappetta G, Avantaggiato V, Visconti R, Fedele M, Battista S, Trapasso F, Merciai BM, Fidanza V, Giancotti V, Santoro M *et al.* 1996 High level expression of the HMGI (Y) gene during embryonic development. *Oncogene* **13** 2439–2446.

Chiappetta G, Tallini G, De Biasio MC, Manfioletti G, Martinez-Tello FJ, Pentimalli F, de Nigris F, Mastro A, Botti G, Fedele M *et al.* 1998 Detection of high mobility group I HMGI(Y) protein in the diagnosis of thyroid tumors: HMGI(Y) expression represents a potential diagnostic indicator of carcinoma. *Cancer Research* **58** 4193–4198.

Chiappetta G, Ferraro A, Vuttariello E, Monaco M, Galdiero F, De Simone V, Califano D, Pallante P, Botti G, Pezzullo L *et al.* 2008 HMGA2 mRNA expression correlates with the malignant phenotype in human thyroid neoplasias. *European Journal of Cancer* **44** 1015–1021. (doi:10.1016/j.ejca.2008.02.039)

Delhase M, Vergagni P, Malur A, Trouillas J & Hooghe-Peters EL 1993 Pit-1/GHF-1 expression in pituitary adenomas: further analogy between human and rat SMtTW tumors. *Journal of Molecular Endocrinology* **11** 129–139. (doi:10.1677/jme.0.0110129)

Delhase M, Castrillo JL, de la Hoya M, Rajas F & Hooghe-Peters EL 1996 AP-1 and Oct-1 transcription factors down-regulate the expression of the human PIT1/GHF1 gene. *Journal of Biological Chemistry* **271** 32349–32358. (doi:10.1074/jbc.271.50.32349)

De Martino I, Fedele M, Palmieri D, Visone R, Cappabianca P, Wierinckx A, Trouillas J & Fusco A 2007*a* B-RAF mutations are a rare event in pituitary adenomas. *Journal of Endocrinological Investigation* **30** RC1–RC3.

De Martino I, Visone R, Palmieri D, Cappabianca P, Chieffi P, Forzati F, Barbieri A, Kruhoffer M, Lombardi G, Fusco A *et al.* 2007*b* The Mia/Cd-rap gene expression is down-regulated by the HMGA proteins in mouse pituitary adenomas. *Endocrine-Related Cancer* **14** 875–886. (doi:10.1677/ERC-07-0036)

De Martino I, Visone R, Wierinckx A, Palmieri D, Ferraro A, Cappabianca P, Chiappetta G, Forzati F, Lombardi G, Colao A *et al.* 2009 HMGA proteins up-regulate *CCNB2* gene in mouse and human pituitary adenomas. *Cancer Research* **69** 1844–1850. (doi:10.1158/0008-5472.CAN-08-4133)

Dudley KJ, Revill K, Clayton RN & Farrell WE 2009 Pituitary tumours: all silent on the epigenetics front. *Journal of Molecular Endocrinology* **42** 461–468. (doi:10.1677/JME-09-0009)

Falvo JV, Thanos D & Maniatis T 1995 Reversal of intrinsic DNA bends in the IFN beta gene enhancer by transcription factors and the architectural protein HMG I(Y). *Cell* **83** 1101–1111. (doi:10.1016/0092-8674(95)90137-X)

Fedele M, Bandiera A, Chiappetta G, Battista S, Viglietto G, Manfioletti G, Casamassimi A, Santoro M, Giancotti V & Fusco A 1996 Human colorectal carcinomas express high levels of high mobility group HMGI(Y) proteins. *Cancer Research* **56** 1896–1901.

Fedele M, Pierantoni GM, Berlingieri MT, Battista S, Baldassarre G, Munshi N, Dentice M, Thanos D, Santoro M, Viglietto G *et al.* 2001 Overexpression of proteins HMGA1 induces cell cycle deregulation and apoptosis in normal rat thyroid cells. *Cancer Research* **61** 4583–4590.

Fedele M, Battista S, Kenyon L, Baldassarre G, Fidanza V, Klein-Szanto AJ, Parlow AF, Visone R, Pierantoni GM, Outwater E *et al.* 2002 Overexpression of the *HMGA2* gene in transgenic mice leads to the onset of pituitary adenomas. *Oncogene* **21** 3190–3198. (doi:10.1038/sj.onc.1205428)

Fedele M, Pentimalli F, Baldassarre G, Battista S, Klein-Szanto AJ, Kenyon L, Visone R, De Martino I, Ciarmiello A, Arra C *et al.* 2005 Transgenic mice overexpressing the wild-type form of the HMGA1 gene develop mixed growth hormone/prolactin cell pituitary adenomas and natural killer cell lymphomas. *Oncogene* **24** 3427–3435. (doi:10.1038/sj.onc.1208501)

Fedele M, Visone R, De Martino I, Troncone G, Palmieri D, Battista S, Ciarmiello A, Pallante P, Arra C, Melillo RM *et al.* 2006 HMGA2 induces pituitary tumorigenesis by enhancing E2F1 activity. *Cancer Cell* **6** 459–471. (doi:10.1016/j.ccr.2006.04.024)

Fedele M, Palmieri D & Fusco A 2010 HMGA2: a pituitary tumour subtype-specific oncogene? *Molecular and Cellular Endocrinology* **326** 19–24. (doi:10.1016/j.mce.2010.03.019)

Finelli P, Pierantoni GM, Giardino D, Losa M, Rodeschini O, Fedele M, Valtorta E, Mortini P, Croce CM, Larizza L *et al.* 2002 The high mobility group A2 gene is amplified and overexpressed in human prolactinomas. *Cancer Research* **62** 2398–2405.

Friend KE, Chiou YK, Laws ER Jr, Lopes MB & Shupnik MA 1993 Pit-1 messenger ribonucleic acid is differentially expressed in human pituitary adenomas. *Journal of Clinical Endocrinology and Metabolism* **77** 1281–1286. (doi:10.1210/jc.77.5.1281)

Fusco A & Fedele M 2007 Roles of HMGA proteins in cancer. *Nature Reviews. Cancer* **7** 899–910. (doi:10.1038/nrc2271)

Gaiddon C, de Tapia M & Loeffler JP 1999 The tissue-specific transcription factor Pit-1/GHF-1 binds to the c-fos serum response element and activates c-fos transcription. *Molecular Endocrinology* **13** 742–751. (doi:10.1210/me.13.5.742)

Graham FL & van der Eb AJ 1973 Transformation of rat cells by DNA of human adenovirus 5. *Virology* **54** 536–539. (doi:10.1016/0042-6822(73)90163-3)

Hayward BE, Barlier A, Korbonits M, Grossman AB, Jacquet P, Enjalbert A & Bonthron DT 2001 Imprinting of the G(s)alpha gene GNAS1 in the pathogenesis of acromegaly. *Journal of Clinical Investigation* **107** R31–R36. (doi:10.1172/JCI11887)

Lania A, Mantovani G & Spada A 2003 Genetics of pituitary tumors: focus on G-protein mutations. *Experimental Biology and Medicine* **228** 1004–1017.

Lefevre C, Imagawa M, Dana S, Grindlay J, Bodner M & Karin M 1987 Tissue-specific expression of the human growth hormone gene is conferred in part by the binding of a specific trans-acting factor. *EMBO Journal* **6** 971–981.

Leger H, Sock E, Renner K, Grummt F & Wegner M 1995 Functional interaction between the POU domain protein Tst-1/Oct-6 and the high-mobility-group protein HMG-I/Y. *Molecular and Cellular Biology* **15** 3738–3747.

Li S, Crenshaw EB III, Rawson EJ, Simmons DM, Swanson LW & Rosenfeld MG 1990 Dwarf locus mutants lacking three pituitary cell types result from mutations in the POU-domain gene pit-1. *Nature* **347** 528–533. (doi:10.1038/347528a0)

Livak KJ & Schmittgen TD 2001 Analysis of relative gene expression data using real-time quantitative PCR and the 2(−Delta Delta *C*(T)). *Methods* **25** 402–408. (doi:10.1006/meth.2001.1262)

Llyod RV, Kovacs K, Young WF Jr, Farrell WE, Asa SL, Trouillas J, Kontogeorgos G, Sano T, Scheithauer BW & Horvath E 2004 Pituitary tumours: introduction. In chapter 1: tumours of the pituitary. In *World Health Organization Classification of Tumours-Pathology and Genetics of Tumours of Endocrine Organs*, pp 10–13. Eds RA DeLellis, RV Lloyd, PU Heitz & C Eng. Lyon: IARC Press.

Lyons J, Landis CA, Harsh G, Vallar L, Grünewald K, Feichtinger H, Duh QY, Clark OH, Kawasaki E, Bourne HR

et al. 1990 Two G protein oncogenes in human endocrine tumors. *Science* **249** 655–659. (doi:10.1126/science.2116665)

Martinez Hoyos J, Ferraro A, Sacchetti S, Keller S, De Martino I, Borbone E, Pallante P, Fedele M, Montanaro D, Esposito F *et al.* 2009 HAND1 gene expression is negatively regulated by the High Mobility Group A1 proteins and is drastically reduced in human thyroid carcinomas. *Oncogene* **28** 876–885. (doi:10.1038/onc.2008.438)

McCormick A, Brady H, Theill LE & Karin M 1990 Regulation of the pituitary-specific homeobox gene GHF1 by cell-autonomous and environmental cues. *Nature* **345** 829–832. (doi:10.1038/345829a0)

Monaco C, Visconti R, Barone MV, Pierantoni GM, Berlingieri MT, De Lorenzo C, Mineo A, Vecchio G, Fusco A & Santoro M 2001 The RFG oligomerization domain mediates kinase activation and re-localization of the RET/PTC3 oncoprotein to the plasma membrane. *Oncogene* **20** 599–608. (doi:10.1038/sj.onc.1204127)

Nelson C, Albert VR, Elsholtz HP, Lu LI & Rosenfeld MG 1988 Activation of cell-specific expression of rat growth hormone and prolactin genes by a common transcription factor. *Science* **239** 1400–1405. (doi:10.1126/science.2831625)

Occhi G, Trivellin G, Ceccato F, De Lazzari P, Giorgi G, Dematte S, Grimaldi F, Castello R, Davì MV, Arnaldi G *et al.* 2010 Prevalence of AIP mutations in a large series of sporadic Italian acromegalic patients and evaluation of CDKN1B status in acromegalic patients with multiple endocrine neoplasia. *European Journal of Endocrinology* **163** 369–376.

Pellegrini I, Barlier A, Gunz G, Figarella-Branger D, Enjalbert A, Grisoli F & Jaquet P 1994 Pit-1 gene expression in the human pituitary and pituitary adenomas. *Journal of Clinical Endocrinology and Metabolism* **79** 89–96. (doi:10.1210/jc.79.1.189)

Pellegrini I, Roche C, Quentien MH, Ferrand M, Gunz G, Thirion S, Bagnis C, Enjalbert A & Franc JL 2006 Involvement of the pituitary-specific transcription factor pit-1 in somatolactotrope cell growth and death: an approach using dominant-negative pit-1 mutants. *Molecular Endocrinology* **20** 3212–3227. (doi:10.1210/me.2006-0122)

Pellegrini-Bouiller I, Morange-Ramos I, Barlier A, Gunz G, Enjalbert A & Jaquet P 1997 Pit-1 gene expression in human pituitary adenomas. *Hormone Research* **47** 251–258. (doi:10.1159/000185472)

Pierantoni GM, Fedele M, Pentimalli F, Benvenuto G, Pero R, Viglietto G, Santoro M, Chiariotti L & Fusco A 2001 High mobility group I (Y) proteins bind HIPK2, a serine–threonine kinase protein which inhibits cell growth. *Oncogene* **20** 6132–6141. (doi:10.1038/sj.onc.1204635)

Pierantoni GM, Rinaldo C, Esposito F, Mottolese M, Soddu S & Fusco A 2007 High mobility group A1 (HMGA1) proteins interact with p53 and inhibit its apoptotic activity. *Cell Death & Differentiation* **13** 1554–1563. (doi:10.1038/sj.cdd.4401839)

Qian ZR, Asa SL, Siomi H, Siomi MC, Yoshimoto K, Yamada S, Wang EL, Rahman MM, Inoue H, Itakura M *et al.* 2009 Overexpression of HMGA2 relates to reduction of the let-7 and its relationship to clinicopathological features in pituitary adenomas. *Modern Pathology* **22** 431–441. (doi:10.1038/modpathol.2008.202)

Salvatori R, Fan X, Mullis PE, Haile A & Levine MA 2002 Decreased expression of the GHRH receptor gene due to a mutation in a Pit-1 binding site. *Molecular Endocrinology* **16** 450–458. (doi:10.1210/me.16.3.450)

Scala S, Portella G, Fedele M, Chiappetta G & Fusco A 2000 Adenovirus-mediated suppression of HMGI(Y) protein synthesis as potential therapy of human malignant neoplasias. *PNAS* **97** 4256–4261. (doi:10.1073/pnas.070029997)

Scheithauer BW, Gaffey TA, Lloyd RV, Sebo TJ, Kovacs KT, Horvath E, Yapicier O, Young WF Jr, Meyer FB, Kuroki T *et al.* 2006 Pathobiology of pituitary adenomas and carcinomas. *Neurosurgery* **59** 341–353. (doi:10.1227/01.NEU.0000223437.51435.6E)

Schmidt MC, Henke RT, Stangl AP, Meyer-Puttlitz B, Stoffel-Wagner B, Schramm J & von Deimling A 1999 Analysis of the MEN1 gene in sporadic pituitary adenomas. *Journal of Pathology* **188** 168–173.

Tamimi Y, van der Poel HG, Denyn MM, Umbas R, Karthaus HF, Debruyne FM & Schalken JA 1993 Increased expression of high mobility group protein I(Y) in high grade prostatic cancer determined by *in situ* hybridization. *Cancer Research* **53** 5512–5516.

Tateno T, Zhu X, Asa SL & Ezzat S 2010 Chromatin remodeling and histone modifications in pituitary tumors. *Molecular and Cellular Endocrinology* **326** 6670. (doi:10.1016/j.mce.2009.12.028)

Thanos D & Maniatis T 1992 The high mobility group protein HMG I(Y) is required for NF-kappa B-dependent virus induction of the human IFN-beta gene. *Cell* **71** 777–789. (doi:10.1016/0092-8674(92)90554-P)

Trouillas J, Girod C, Sassolas G & Claustrat B 1986 The human gonadotropic adenoma: pathological diagnosis and hormonal correlations in 26 tumors. *Seminars in Diagnostic Pathology* **3** 42–57.

Vallone D, Battista S, Pierantoni GM, Fedele M, Casalino L, Santoro M, Viglietto G, Fusco A & Verde P 1997 Neoplastic transformation of rat thyroid cells requires the junB and fra-1 gene induction which is dependent on the HMGI-C gene product. *EMBO Journal* **16** 5310–5321. (doi:10.1093/emboj/16.17.5310)

Wang EL, Qian ZR, Rahman MM, Yoshimoto K, Yamada S, Kudo E & Sano T 2010 Increased expression of HMGA1

correlates with tumour invasiveness and proliferation in human pituitary adenomas. *Histopathology* **56** 501–509. (doi:10.1111/j.1365-2559.2010.03495.x)

Winkler S, Murua Escobar H, Meyer B, Simon D, Eberle N, Baumgartner W, Loeschke S, Nolte I & Bullerdiek J 2007 HMGA2 expression in a canine model of prostate cancer. *Cancer Genetics and Cytogenetics* **177** 98–102. (doi:10.1016/j.cancergencyto.2007.06.008)

Wood LJ, Maher JF, Bunton TE & Resar LM 2000 The oncogenic properties of the HMG-I gene family. *Cancer Research* **60** 4256–4261.

Zhou X, Benson KF, Ashar HR & Chada K 1995 Mutation responsible for the mouse pygmy phenotype in the developmentally regulated factor HMGI-C. *Nature* **376** 771–774. (doi:10.1038/376771a0)

Zhuang Z, Ezzat SZ, Vortmeyer AO, Weil R, Oldfield EH, Park WS, Pack S, Huang S, Agarwal SK, Guru SC *et al.* 1997 Mutations of the MEN1 tumor suppressor gene in pituitary tumors. *Cancer Research* **57** 5446–5451.

Zwilling S, König H & Wirth T 1995 High mobility group protein 2 functionally interacts with the POU domains of octamer transcription factors. *EMBO Journal* **14** 1198–1208.

Received in final form 9 December 2011
Accepted 23 December 2011
Made available online as an Accepted Preprint
23 December 2011